PhD School of Pharmaceutical Sciences XXVI cycle

University of Naples "Federico II"

DESIGN, SYNTHESIS AND BIOLOGICAL EVALUATION OF SMALL MOLECULES AS MODULATORS OF HISTONE METHYLTRANSFERASES AND DEMETHYLASES

Doctoral Candidate: **Supervisor:**

Stefano Tomassi   **Prof. Ettore Novellino**

Department of Pharmacy

Faculty of Pharmacy

University of Naples "Federico II"

Supervisors

Professor Ettore Novellino Ph.D. (tutor and main supervisor)
Department of Pharmacy, University of Naples "Federico II",
Via Domenico Montesano, 49 - 80131 Naples, Italy.

Adjunct Professor Antonello Mai Ph.D. (external supervisor)
Department of Drug Chemistry and Technology, "Sapienza" University of Rome,
P.le Aldo Moro, 5 - 00185 - Rome, Italy.

Table of contents

A mio padre

Roberto Tomassi

1. INTRODUCTION

Eukaryotic organisms have developed elaborate cellular mechanisms to endow themselves with differential and cell-type specific expression of genes. Born nearly in 1997, Epigenetics, which literally means "upon genetics", refers to these mechanisms and can be defined as changes in state of genes functions and expressions ("on" versus "off") that are mitotically and/or meiotically heritable and do not entail a change in DNA sequence. This means that it concerns how eukaryotic DNA, and so *chromatin,* is distinctively accessed in cells during embryonic development and differentiation; and finally how the chromatin states are maintained/changed, not only during the normal life of a cell but from a generation of cells to an another one in multicellular organisms. The dynamic nature of the epigenetic state of cells thus offers a pre-ordered scheme for the development and the differentiation of organisms, moreover their changes empower cells of environmental plasticity enabling cellular reprogramming and responses to the changing outward conditions. Notwithstanding the notable precision of these mechanisms, mistakes may occur, and when not appropriately correct, they may lead to aberrant expression and/or silencing of critical downstream target genes, with far-reaching implication in the most fields of cell biology and human health, including: viral latency, somatic gene therapy, cloning and transgenic technologies, metabolic, cardiovascular and neurodegenerative diseases and remarkably in cancer.

For many years oncogenesys has been deemed the outcome of multistep processes involving irreversible genetic defects as gene mutations, deletions and chromosomical aberrations, leading to loss or gain of function of oncosuppressor genes and oncogenes, respectively. However, recent studies have underlined how these processes involved an imbalance of normal molecular signalling pathways that regulate the cellular proliferation and differentiation and how Epigenetics plays a pivotal role in the activation and/or repression of these programs during the normal cell cycle.

In the late '70 Lewis and Lewis elegantly showed how critical a fine-tuned epigenetic regulation for the functional development of an organism might be. Upon mutations of a set of genes on *drosophila melanogaster* (Polycomb genes), specific body segments of the

mutants assume the identity of a completely different, but otherwise normal, body segment. This is the case of adult animals having legs in the place of antennas.

The authors also investigated the biochemical mechanisms underlying the aberrant phenotypes and found that Polycomb (PC) mutations caused inappropriate reactivation of genes that should have been repressed and are responsible for segment identity. Their reactivation leads the body segments to assume new character (the antenna-leg transformation).

The Lewis and Lewis findings opened the way to new and more focused analysis on the chromatin on/off state, its modulators (or on/off switchers) and their implication on both normal and pathological conditions as neurological diseases, immunological disorders and several types of cancer. In particular numerous evidences link deregulated epigenetic networks to the loss of function and propagation of cancer cells and more in general to the development and also relapse of different tumours.

Reinstating a correct epigenetic regulation is a current therapeutic goal in cancer, the importance of which can be better understood considering the heterogenic and multiple nature of tumour cells. Several hypotheses exist accounting for this peculiarity, the most important being the *cancer stem cell hypothesis* and the *clonal evolution model*. The first hypothesis states that only a rare subset of cells (the so called "cancer stem cells" or CSCs) is responsible for the maintenance of the neoplasm. The cancer stem cells start the propagation and according to the clonal evolution model, lead to different clonal subset in which different genetic abnormalities are present. In this way the evolutionary pressure allows the sequential selection of the most aggressive subpopulations.

The propagation and renewal of the cancer stem cells could arise from an inappropriate reactivation of some developmental pathways, due to the ability of the tumour-propagating cells to hijacked cellular networks that control the normal behaviour of an adult stem cell. The reactivation of developmental pathways involves both genetic defects and epigenetic alterations, which might be responsible for the evolution of new cancer cell lineages by disrupting the expression of oncogenes and oncosuppressor genes that lies at the basis of a normal cell development and differentiation. The concrete possibility of completely reversing the aberrant epigenetic regulation by tackling down the biochemical mediators of chromatin remodelling with small molecules inhibitors has greatly focused the attention on

chromatin modifying enzymes as targets and promising clinical trials have boost both the academic and private epigenetic research programs. Unfortunately, the suitable set of enzymes to inhibit, in order to restore or shut down the expression of target genes, has been proved difficult to find. This is mainly due to the inner complexity of the rules dictating the chromatin state, where even small modifications of the proteins structure will correspond to critical changes on genes expression and functions. Chromatin modifications are generally of a covalent type, as acetylation and methylation. Several different families of specific enzymes exist, for the vast majority of them, inhibitors have been designed, synthesized and tested, some of which have also shown potent and selective activity both *in vitro* and *in vivo*. Anyway new and more potent compounds are needed to modulate different target activities and change specific patterns of covalent modifications to achieve the desired therapeutic goal. Several techniques generally adopted in the pharmaceutical research and development (R&D) have been applied to this scope. For example high throughput screening (HTS) in concert with bioinformatics techniques is responsible for early identifying most of the molecules currently tested. Moreover the number of currently HTS compatible biological assays is continuously increasing allowing a growing number of chemical scaffolds to be tested. Also the number of experimentally solved chromatin modifying enzymes crystal structure available in the protein data bank (PDB) is becoming bigger and bigger, constituting a valuable tool for computational and medicinal chemists to analyse and explore the physicochemical characteristic specific for a particular protein, gain insight in the relationship between its structure and function and make a set of rules necessary to build inhibitors not just more potent but also with a range of activity covering different enzymes at once. All these different approaches gathered together will likely lead to better "hits" and will help medicinal chemists in the lead optimization process.

2. EPIGENETIC AND CHROMATIN DYNAMICS

One of the striking aspects that emerges when we consider the inner organization of a mammalian cell, is how Nature solved the crucial matter of settling in a 1.7 metres long DNA strand into a 5-micrometre nucleus, in a form that not only allows it to be replicated through a relatively fast and accurate process, but that permits it to be read and then transcribed in a tissue-specific manner too, in a nutshell: *chromatin*.

Chromatin is a dynamic macromolecular complex consisting in DNA, histone and non-histone proteins and represents the form in which DNA is packed within a eukaryotic nucleus. It comprises a repetitive sequence of units, the *nucleosome*, composed of 146 base pairs of DNA wrapped, nearly twice, around 4 pairs of highly conserved core proteins, called *histones*: H2A, H2B, H3 and H4. Since a nucleosome based structure compacts DNA around seven fold, but eukaryotic cells need, and actually exhibit, an overall compaction of several thousand fold, it is glaring that *in vivo* only a relatively small fraction of DNA is under a simple nucleosomal organization, while the most of chromatin is further compacted in an highly order architecture[1]. Nucleosomes are still important in this higher order folding as they help the arrangement of DNA into the 30-nm fiber by the electrostatic neutralization among DNA spacer motifs and the linker histone H1, together with RNAs and non-histonic proteins.
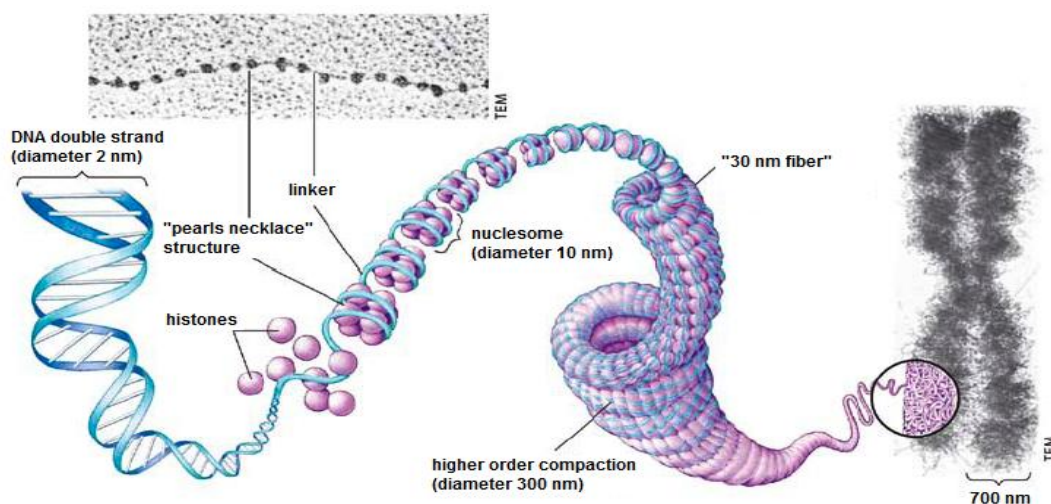
Figure 2.1. Chromatin architecture

Histones, the core components of the nucleosome, are basic proteins, they have a comparable overall structure, with a globular hydrophobic internal region, that represents

the platform whereby the DNA sequence is rolled up, and a flexible charged amino termini protruding out the nucleosome.
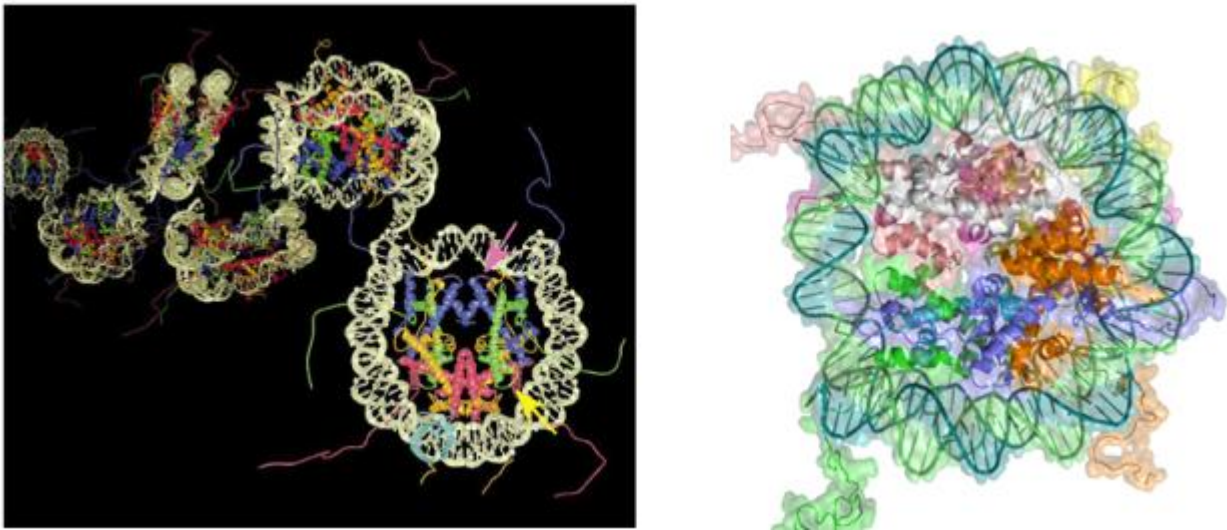
Figure 2.2. Detailed view of nucleosome structure

The amino terminal region, so called histone "*tail*", consists of ~25-30% of the mass of an individual histone and offers an exposed surface for protein-protein interaction. These tails are interested by a plenty of covalent reversible Post-Translational Modifications (PTMs), which are referred to as *epigenetic marks*, that can modify the overall structure of the nucleosome and eventually regulate the chromatine state acting as a "platform" for the recruitment of multi-protein complexes responsible of the transition from an open-access, and therefore transcriptionally active folding (euchromatine), to a close conformation or transcriptionally silent one (heterochromatine). Histone PTMs can therefore play key roles in DNA replication, repair, recombination and notably in genes transcription. Although, evaluating the complexity of genes expression as the result of an "on/off" dynamic, could appear too much simplistic, it should be considered that nucleosomes are not static entities and DNA can transiently unwrap and then rebind the histone template in a finely tuned way, depending on the varied epigenetic mark arrays that decorate the histones and also the DNA at the promoter and at the enhancer sequences. Genes can thus be accessed by transcriptional factors with different rates and strength; thereby, giving a motley phenotypic output.

After years of intense efforts in unrevealing the epigenetic modification patterns[2], comprehensive literature exhibits an elaborated repertoire of post-translational modifications affecting histone tails, among them: lysine acetylation/deacetylation, arginine/lysine methylation/demethylation, serine/threonine phosphorylation, ubiquitylation, ADP-ribosylation, SUMOylation and citrullination (demethylimination). These covalent reversible marks, together with the well-characterized DNA methylation of cytosines in the CpG islands, not only crosstalk with each others in a synergistic or antagonistic way but are not mutually exclusive, thereby establishing a tangled signalling network which can properly address the cell requirements.

Histone marks patterns effects are determined by proteins or protein complexes which are often divided into three functional families. The enzymes that insert histone marks (the "*writers*") like, for example, the histone acetyltransferases (HATs) and the histone methyltransferases (HMTs) add acetyl and methyl groups respectively; the proteins that recognize and then decrypt the epigenetic message (the "*readers*"), which generally possess effector domains like plant homeodomain (PHD), bromo, chromo, RING finger and tudor domains; finally the enzymes in charge of removing histone marks (the "*erasers*") as the histone deacetylases (HDACs) and histone demethylases (HDMs).

The writers/erasers-driven dynamics display different effects on chromatin states, depending on the type of modification. Lys acetylation correlates in general with transcription activation, while deacetylation usually leads to gene silencing. Differently, arginine/lysine methylation can be associated to transcription activation or repression depending on the distinct residue involved, and the type (symmetrical/asymmetrical) or the extension of methylation (mono-, di-, or tri-methylation), respectively. Given the wide-spread implications of chromatine state regulation not only in Epigenetics, but in oncology, developmental biology, stem cell fate and regenerative medicines too, the "writers", "readers" and "erasers" are essential targets to further deciphering the histone code (epigenome) and its role in human deseases.

3. HISTONE METHYLATION

Although phosphorylation remains by far the most elucidated PTMs, in recent years methyl groups started ascending into prominence as one of the major controlling elements in protein function since a remarkable variety of methylation and demethylation reactions take place at the side chains of distinct amino acids.

Methyltransferases are a huge family of proteins, indeed, it has been hypothesized that over 1% of mammalian genome encodes for this kind of enzymes[3], and they catalyze the addition of methyl groups to nitrogen, carbon, sulphur, and oxygen atoms of proteins, lipids, nucleic acids and small molecules too. These modifications originate a multitude of chemical interactions which involve histonic and non histonic proteins thus affecting a large number of regulatory pathways ranging from the epigenetic control of gene expression and transcription, modulation of the activity effector proteins and of transcription factors.[4] Within histone proteins, arginine and lysine residues are very abundant and highly post-translationally modified on their side chains, as they can generally undergo acetylation, methylation, ubiquitination, citrullination, SUMOylation and ADP-ribosylation reactions.

As far as methylation is concerned histone methyltrasferases (HMTs) enzymes catalyze methylation by removing a methyl group from the donor molecule *S*-Adenosyl-L-Methionine or *SAM* (AdoMet), thus generating a *S*-Adenosyl-L-Homocysteine or *SAH* (AdoHcy) as product, and transferring this methyl group on the guanidino and ϵ amino groups of arginine (R) and lysine (K) residues, respectively (Figure 3.1). Thus, HMTs are divided in two groups: the Histone Lysine Methyltransferases (HKMTs or KMTs) and the Protein Arginine Methyltransferases (PRMTs). As reported in a broad number of *in vitro* and cell based studies, both HKMTs and PRMTs are able to methylate only specific residues on their substrates, thus being capable of a *substrate selectivity*, but additionally they methylate this residues only to a distinct methylation state, which is referred to as *product specificity*. Indeed, PRMTs can mono- and then di-methylate arginines side chain in a symmetric or asymmetric fashion, while KMTs can mono-, di- and trimethylate the ϵ amino group of lysines.
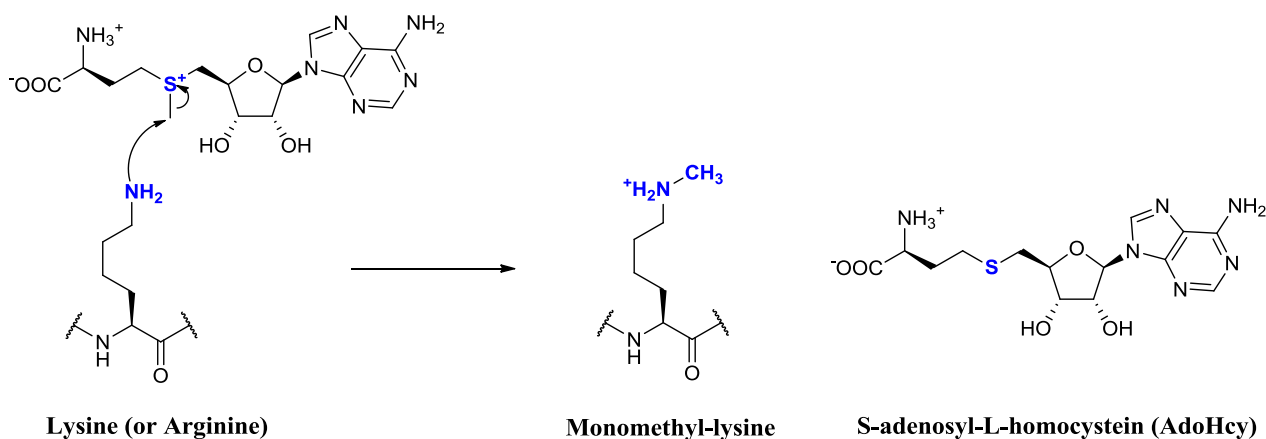
Figure 3.1. Proposed mechanism for lysine methylation by SAM

3.1 Protein Arginine Methyltransferases (PRMTs)

Arginine is a positively charged amino acid which is deemed unique as its guanidino group mediates for amino-aromatic interactions and can generate up to five potential hydrogen bonds with the counterpart acceptors in biological systems[5]. Consequently the addition of a methyl group not only prevents the formation of a potential hydrogen bond but imparts also bulkiness to arginine, influencing the protein-protein interactions both positively and negatively. Importantly, methylation does not neutralize the cationic charge of an arginine residue[6]. As a proof of concept for the far reaching implications of arginine methylation effects, it should be accounted for that arginine residues participate in a multitude of protein-protein interactions especially in protein-DNA complexes, where they are the main responsible of hydrogen bonding to the backbone phosphate groups and to thymine, adenine and guanine bases[7]; they can interact with flanking phosphate groups in specific RNA loops[8] and, moreover, owing to two H-bond interactions, arginine-aspartate dimers, are known to be especially stable in proteins[9].

In mammal cells, nine protein arginine methyltransferases (PRMTs), divided into three different classes, have been identified so far[10]. Type I (PRMT1, PRMT2, PRMT3, PRMT4/CARM1, PRMT6 and PRMT8) and Type II (PRMT5 and PRMT7) enzymes both catalyze the formation of monomethylarginine (MMA) as an intermediate, but while Type I enzymes facilitate the formation of ω-N^G,N^G-asymmetric dimethylarginine (ADMA),

Type II members lead to the formation ω-N^G,N^G-symmetric dimethylarginine (SDMA) (Figure 3.2).
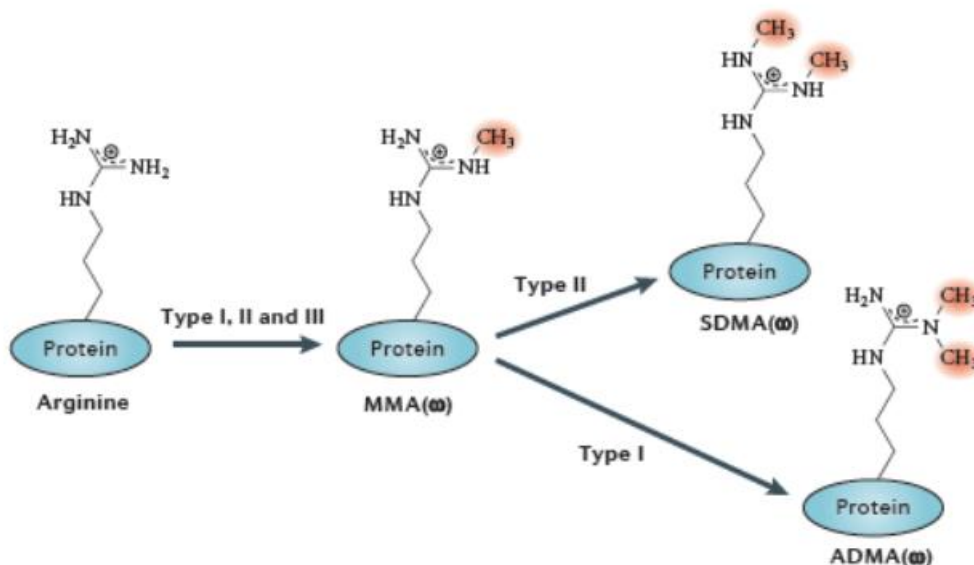
Figure 3.2. Types of methylation on arginine residues.
(Image courtesy of Yang Y. *et al* Nature review/Cancer 2013)

Upon certain substrates PRMT7 seems to generate only ω-N^G-monomethylation (MMA) arginines thus being classified as a Type III enzyme too; while PRMT9 activity has not been well characterized yet. To date, no enzymes forming both asymmetric and symmetric dimethylarginines have been identified[11].

PRMTs are ubiquitously expressed in most human cell types and tissues, even though they can also endow themselves with tissue specificity by alternative splicing[12], and with the unique exception of PRMT8, which is thought to be selectively expressed in brain neurons[13] and has the characteristic to be incorporated into plasma membrane via N-terminal myristoylation[14]. They are constitutively active and essential for existence since they take part at the early development of embryos, as ablation experiments of PRMT1 on dyes and PRMT4/CARM1 on mice have attested[15,16].

As far as the substrate recognition is concerned PRMTs generally methylate in correspondence of glycine- and arginine rich motifs[8,17] (GAR), and this is particular true for PRMT1, PRMT3 and PRMT6, but there are exceptions to this general rule. PRMT4 or CARM1 (*Co-activator Associated Arginine Methyltransferase 1*) exhibits an higher degree of specificity since it recognizes arginines flanking proline-, glycine- and methionine-rich (PGM) motifs-containing substrates[18] and does not interact with GAR motifs[19]. Instead,

PRMT5 simmetrically methylates arginines either within GAR and PGM motifs[20]. Once considered mostly active on RNA-binding proteins (RPBs), nowadays PRMTs are widely recognised as histone marks *writers* too, since they methylate arginine residues on H3 and H4. More recently proteins, like p53, P300/CBP, ERα, pRb, TAF10 and HIV tat have also shown to be PRMTs targets[21,22,23].

The different PRMT subfamilies are characterized by common structural features. Each of them harbours motifs of seven-β-strand, typical of methyltransferase family[24], as well as an additional "double E" and "THW" sequence motifs, which characterizes the specific subfamily[25].

Among PRMTs, only four crystal structures are currently available (rat PRMT1, rat PRMT3, yeast RMT1/hmt1 and CARM1/PRMT4), their core structures are proven similar and provide some insights into the mechanism of methylation process and substrate recognition. Structural evidences show that PRMTs are ring-like dimer, and their methyltransferase activity is strictly dependent from the dimerization[26,27,28,29]. Moreover, PRMTs (but also KMTs) have two binding regions: the substrate binding pocket and the cofactor binding site[30].

Once activated, these enzymes endow themselves with an ordered sequential bi-bi kinetic mechanism, in which SAM binds prior to the substrate[31]. The substrate binding pocket and the cofactor binding site, almost flanking each other, are joined by a narrow hydrophobic channel, large enough to allow the terminal amino group of the substrate to come within bonding distance of the cofactor (Figure 3.3). Two conserved residues (Glu-100 and Arg-54 in PRMT1) interact with the two ribose hydroxyls and carboxylate from SAM, respectively, placing the methylsulfonium group of the cofactor at the base of the channel where arginine side chain of the substrate raises. In the same manner two hydrogen bonds by other invariant glutamate residues (Glu-144 and Glu-153 of PRMT1) are established with the guanidinium side chain of the arginine substrate. These two H-bonds are critical interactions as they are supposed to concentrate the delocalized positive charge onto an only one nitrogen of the guanidinium group, leaving the lone pair of the other one available for the nucleofilic substitution (S_N2 mechanism) to the methylsulfonium group. After the methyl transfer, the proton elimination step is supposed to be by a His-Asp proton relay mechanism[25].
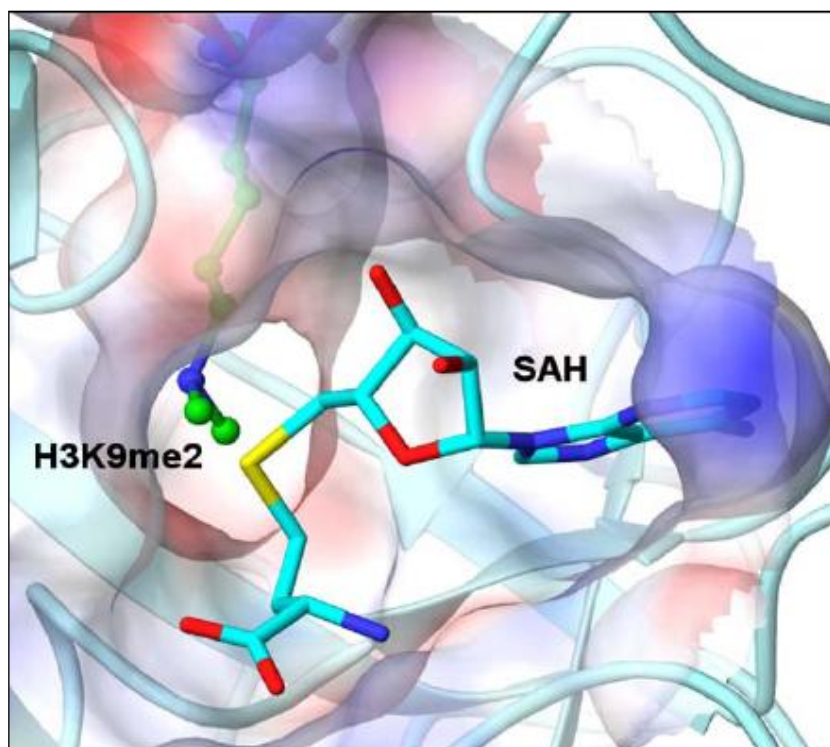
Figure 3.3. GLP-H3 co-crystal structure (PDB: 2RFI, H3K9me2 shown in green) with SAH (cyan) depicting the hydrofobic channel joining the substrate binding pocket and the cofactor binding site

As proof of concept for the importance of these two glutamate residues, *in vitro* data have shown that mutations of either, even to the closely related glutamine or aspartate, reduce the methyltransferase activity by >3000-fold and >10-fold, respectively[26]. Once methylation transfer has occurred, S-Adenosyl-Homocystein (SAH) is released, but mono-methylated arginine may still undergo to a second methylation, depending on the specific case, before leaving the substrate binding pocket[32,33].

PRMTs can methylate and modulate a large fraction of the proteome and their substrates take part into different cellular activities, among them: gene expression and transcription, mRNA splicing, nuclear/cytoplasmic shuttling, DNA repair and signal transduction.

As far as is known, tudor domain-containing proteins (TDRDs) are the unique PRMTs cellular effectors, since they are the only "*readers*" to recognise methylarginine motifs, not only on histones but on other proteins too[34]. Tudor domains may be subdivided into methylarginine- and methyl-lysine-binding groups and their selective recognition is essentially based on the different width of the aromatic cage, which harbours the aminoacidic residues: methylated arginines are narrower than lysine ones by virtue of the

planarity of the methylguanidinium group[35]. Being able to methylate arginines on histone *tails (*most frequent sites of histone arginine methylation are H3R2, H3R8, H3R17, H3R26 and H4R3), as well as on transcriptional factors and RNA polimerase, PRMTs directly play a notable role (as *writers*) in the epigenetic regulation of gene expression[11]; on the other hand as they methylate co-activators (e.g. p300, CBP and SRC3) they indirectly affect the epigenetic marks patterns by regulating the competences of these acetyltransferases. Owing to this "cloud" of methylation[11], TDRDs localize themselves on Transcriptional Start-Sites (TSSs) where they exert their control on genes transcription. The remarkable role of PRMTs not only in the epigenetic control of genes expression and transcription, but in different cellular pathways may be well exemplified by the activity of the best characterized PRMTs: PRMT1, PRMT4/CARM1 and PRMT5 (Figure 3.4).
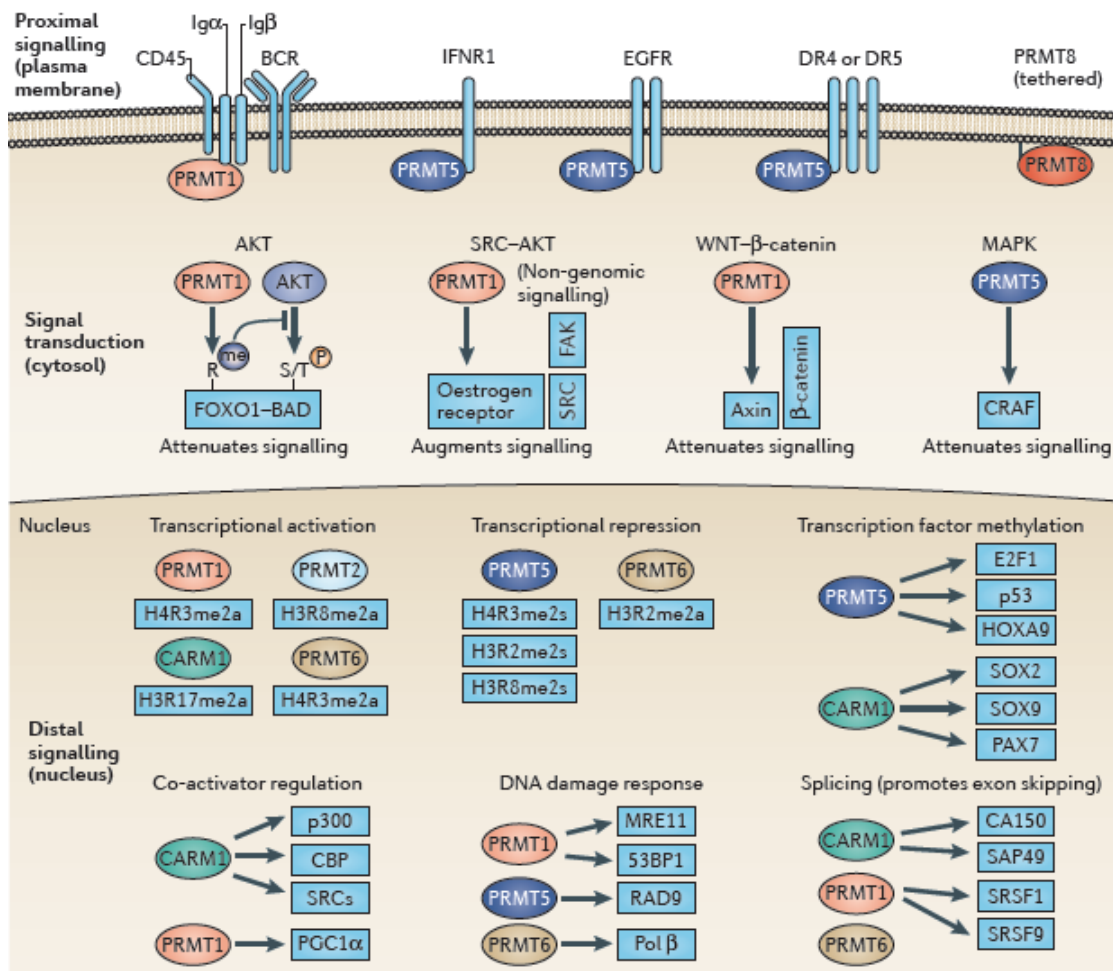
Figure 3.4. Cellular signalling processes in which arginine methylation has integral roles.
(Image courtesy of Yang Y. *et al* Nature review/Cancer 2013)

PRMT1 is the founding member of the arginine methyltransferase family and its activity accounts for more than 85% of the methylarginines among mammalians[36]. It selectively dimethylates arginine 3 on histone H4 in an asymmetrical manner (H4R3me2a), which is an epigenetic mark usually correlated with transcriptional activation[37,38] and that has been found associated with increasing prostate cancer grade and with the risk of the tumour recurrence[39]. H4R3me2a mark is recognised by TDRD3 (the former member of the tudor domain-containing proteins) which is probably the ultimate effector for the transcription activation, however the complete molecular pathways that lie behind this effect has not been elucidated yet[40]. The first evidence that PRMT1 plays a role in oncogenesis arose in studies demonstrating that mouse primary hematopoietic cells that are transduced with the MLL-EEN gene fusion product displayed enhanced self-renewal abilities and can form compact CFU-GEMM-like colonies in vitro[41]. Another study shed light on to the fact that PRMT1 mRNA levels have been reported to be higher in a panel of breast cancer cell lines than in normal controls.[42] A plenty of non histonic substrates of PRMT1 have been found so far, linking its aberrant activity to possible roles in cancer onset and progression. PRMT1 can methylated proteins involved in DNA repair pathway such as MRE11 (also known as MRE11A) and p53 binding protein 1 (53BP1) within their GAR motif and thus regulates its exonuclease activity on double-stranded DNA. Cells containing hypomethylated MRE11 displayed intra-S phase DNA damage checkpoint defects; likewise cells with hypomethylated 53BP1, which is involved in the early steps of detection and repair of damaged DNA, show alteration in the 53BP1 localization to damaged DNA and forms fewer γH2AX foci[43]. Another study has indicated that PRMT1 is associated with human telomerase, and in particular that telomeric repeat-binding factor 2 (TERF2) a component of the sheltering proteins which protects the telomeres, is a substrate of PRMT1[44].

Oestrogen receptor (ER) pathway is also a target of PRMT1, indeed it has been found that PRMT1 methylates ERα in the DNA-binding domain (R260), both *in vitro* and in cells, and oestrogen treatment of MCF7 cells rapidly increases this methylation. ERα methylation seems to influence the downstream activation of ERα effectors as it has been shown that the R260 methylation is required for the assembly of ERα with SRC and focal adhesion kinase (FAK), as proof of the concept the mutation of ERα-R260 to alanine or

results in the inability of oestrogen to activate AKT[45]. Hence PRMT1-mediated ERα methylation is a triggering process for the activation of the SRC–PI3K–FAK cascade and AKT, moreover hypermethylation of ERα in breast cancer might cause hyperactivation of this signalling pathway, thus affording survival advantage to tumour cells, even in the presence of anti-oestrogen drugs[46].

PRMT	Deregulation in cancers
PRMT1	Overexpressed and/or aberrantly spliced in breast, prostate, lung, colon and bladder cancer and leukemia
PRMT2	Overexpressed in breast cancer and correlated with ERα-positive status
PRMT3	Breast tumors may display higher levels of PRMT3 activity owing to DAL1 loss
CARM1	Overexpressed in breast, prostate and colorectal cancers
PRMT5	Overexpression or increase enzymatic activity observed in gastric, colorectal and lung cancer, and lymphoma and leukemia
PRMT6	Overexpressed in lung and bladder cancers
PRMT7	Gene expression meta-analysis identified PRMT7 as a candidate gene involved in breast cancer metastasis
PRMT8	Somatic mutations were found in ovarian, skin and large intestine cancers

Table 3.1. Aberration of PRMTs and cancer.

PRMT4/CARM1 (Co-activator-Associated-Arginine-Methyltransferase 1) was the first PRMT to be associated to the regulation of genes expression, its ability to methylate histonic arginines (H3R17me2a and H3R26me2a), which is correlated with transcriptional activation[5], provides a direct mean to insert into the epigenetic marks network. Moreover, being able to methylate the histone acetyltransferases (HATs) CREB-binding protein (CBP or CREBB) and p300, it indirectly controls their epigenetic output[47,48]. In general CARM1 mediated methylation of CBP leads to an increase of its activity. On the contrary the methylation of p300-R2142, in its C-terminal domain, inhibits the interaction with the

Glucocorticoid Receptor-Interacting Protein 1 (GRIP1), which is necessary for the cell cycle arrest in response to DNA damage, whereas the methylation of R754 in the KIX domain, lead to the induction of the cell cycle regulator p21[49]. It's nowadays well accepted that CARM1 levels are elevated in castration-resistant prostate cancer[50,51] and in aggressive breast tumours[52]. The aggressive breast tumours that overexpress CARM1 exhibits high levels of the oncogenic co-activator AIB1, which is a well established marker for breast cancer and associated with poor prognosis[53]. There is a functional synergism between CARM1 and AIB1 in breast cancer, indeed CARM1 methylates AIB1 and regulates its activity and stability, while CARM1 recruitment to ERα-regulated promoters relies on the presence of AIB1[54]. CARM1 also play important role in colon rectal cancer, through its positive modulation of WNT–β-catenin-driven transcription. Depletion of CARM1 expression in colorectal cancer cells suppresses clonal survival and anchorage-independent growth, supporting the clinical evidences showing that 75% of colorectal cancers have CARM1 overexpression[55].

PRMT5 is the major type II arginine methyltransferase, it was upfront recognised as a transcriptional repressor and it is in this framework that it has an oncogenic potential, owing to its capacity to induce tumour suppressor genes silencing[56]. Once recruited to the promoter it symmetrically dimethylates H3R8 (H3R8me2s) and H4R3 (H4R3me2s) which are two key repressive epigenetic marks[57,58]. Since, as previously mentioned, H4R3 is also the epigenetic site of action of PRMT1, which inserting a symmetrical dimethyl group induces a transcriptional activation; hence PRMT1 and PRMT5 exert a counteracting activity on gene expression just dimethylating H4R3 side chain with a different symmetry. PRMT5 cooperates and has been found in complex with different transcriptional factors such as BRG1 and hBRM[59], Blimp1[60], SNAIL[61] and E2F1[62] and seems to play a central role into the *epithelial-mesenchymal transition* (EMT) process. This process allows cancer cells to migrate and invade tissues much more efficiently, thus PRMT5 can be correlated with metastasis and therefore with tumour progression An characteristic feature of EMT is the loss of E-cadherin expression, which is repressed by the transcription factor SNAIL, which form a macromolecular complex with PRMT5 and AJUBA[63].

Programmed cell death protein 4 (PDCD4) is another substrate of PRMT5, it has been correlated with a positive outcome in different cancer types, even if there are exception to

this general evidence depicting PDCD4 as an oncogenic protein. In this concern PRMT5 seems to play a pivotal role into this switch of function, as it is able to methylate PDCD4 in its GAR motif at N terminus[64]. Moreover, PRMT5 has a regulatory role at two different nodes of the epidermal growth factor receptor (EGFR)–RAS–ERK signalling pathway. PRMT5 destabilizes CRAF (also known as RAF1) by methylation moreover EGFR is arginine methylated by PRMT5 at R1175, this aminoacidic modification doesn't seem to affect the ligand binding to EGFR, instead it enhances subsequent phosphorylation of Y1173 which in turn acts as a docking site for the SH2 domain of the phosphatase SHP1, thus dampening EGFR signalling[65].

Despite the fact that most of PRMTs are constitutively active proteins, suggesting that these enzymes have a basal activity that does not need any PTMs or modulation, mechanisms for fine-tuning their activity exist and can be ascribed into: PTMs, association with regulatory proteins, subcellular compartimentalization, factors that influence enzyme–substrate interactions and microRNAs interference (miRNAs). Below, only the most remarkable ones will be reported.

Post Translational Modifications (PTMs): albeit a few evidences currently report that PRMTs are influenced by PTMs, some studies addressing the crosstalk between phosphorylation and arginine methylation are arising[66,67]. For example, CARM1 (*Co-activator Associated Arginine Methyltransferase 1*) is prevented from binding the S-adenosyl-1-methionine cofactor (SAM) after being phosphorylated on S217 by a not yet identified kinase, thus blocking its methyltransferase activity[68,69]. Similarly, PRMT5 has been shown to be phosphorylated by a Janus Kinase 2 (JAK2) mutated form, (V617F), which is found constitutively active in most of patients with myeloproliferative neoplasms[70]. The phosphorylation affects the interaction with methylosome protein 50 (MEP50) and inhibits PRMT5 methyltransferase activity[71]. However PTMs not only can modulate methyltransferases activity directly, but can affect the sites of methylation and also the methylation itself by exerting an effect on PRMTs substrates, and thus creating a crosstalk between arginine methylation and the other epigenetic marks: histone H3 lysine 18 acetylation (H3K18ac) trigger the asymmetric dimethylation on H3R17me2 by CARM1[72,73]. Interestingly, histone 4 lysine 5 acetylation (H4K5ac) induces a shift from an asymmetrical to a symmetrical methylation of H4R3, by PRMT1 to PRMT5, respectively;

hence influencing the balance from an activating ADMA mark to a repressive SDMA mark at the H4R3 site[74].

Regulation proteins: binding of proteins with regulating factors is a very common tool used by cells to modulate their activity; in this concern PRMTs are not an exception. PRMT5 activity is strictly dependent by MEP50 interaction[75], as previously mentioned the tyrosine phosphorylation of PRMT5 by a mutant form of JAK2, deeply affects its interaction with MEP50 and therefore its activity. Another phosphorylation of MEP50 by the cyclin D1-cyclin-dependent kinase 4 (CDK4) complex further stimulates PRMT5 methyltransferase activity, prompting neoplastic growth *in vitro*[76]. Some binding factors can modulate the activity of the PRMT5-MEP50 complex itself, among them the SWI/SNF chromatin remodelling complex, which focuses the methyltransferase activity towards histonic substrates[77], or the histone-binding protein cooperator of PRMT5 (COPR5) which lead the MEP50-PRMT5 complex to methylate H4R3 rather H3R8[78].

As for PRMT1 activity, it is down-regulated by the orphan nuclear receptor TR3[79] and its activity is "switched off" by the BTG1-binding chromatin assembly factor 1 (CAF1) complex[80]. Interestingly, PRMT1 activity has been proposed to be enhanced by the heterodimerization with PRMT2[81].

miRNA regulation: this type of regulation has been found particularly relevant for PRMT5 mRNA levels since their 3'-untranslated regions have been supposed to be annealed by more than 50 miRNAs. Moreover, miRNAs like: miR-19a, miR-25, miR-32, miR-92, miR-92b and miR-96, are found downregulated in several lymphoid cancer cell lines[82]. PRMTs can also regulate the expression of miRNAs by themselves, regarding to this it has been proposed that PRMT1 and CARM1 could upregulate miRNAs levels in order to lower PRMT5 expression[83].

3.2 Histone Lysine Methyltransferases (HKMTs)

As previously mentioned protein methylation may occur also on lysines and specifically on the ε amino groups of their side chains. This covalent reversible modification is inserted by a distinct family of methyltransferases, called Protein Lysine Methyl Transferases (PKMTs). This enzymes are capable of a *substrate selectivity* being able to modify only

distinguishing lysinic residues of their substrates, and moreover of a *product specificity* being endowed to methylate these residues only to a characteristic state as mono- (me1), di- (me2) and trimethylated (me3).

As well as protein arginine methyltransferases, the PKMTs catalyze the methylation transfer using *SAM* or *S*-Adenosyl-L-Methionine (AdoMet) as cofactor and affording *SAH* or *S*-Adenosyl-L-Homocysteine (AdoHcy) and the methylated substrate as products.

More than 50 human lysine methyltransferases have been identified and characterized so far. According to structural and sequence criteria of their catalytic domain, these can be classified into two families: the DOT1-like (DOT1L) and the SET-domain-containing methyltransferases. To date only the DOT1L enzyme belongs to the former family, which is distinguished by the presence of seven-stranded *β*-sheet motif, which also structurally characterizes the PRMTs family[84]. Another aspect that makes DOT1L unique is the fact that it is the only methyltransferase catalyzing the methylation reaction of Lysine 79 on histone H3 (H3K79), which differs from the other lysines as it is located in the inner part of the nucleosomes. H3K79 methylation is a transcriptional activating histone mark playing pivotal roles in early embryonic development, and DOT1L has been found involved in MLL translocation effects in mixed lineage leukemia[85].

Most of the PKMTs belong to the SET-domain-containing protein subset which is in turn organized into five subfamilies according to their founding member: RIZ, SET1, SET2, SMYD3 and SUV39[86] (Figure 3.5).
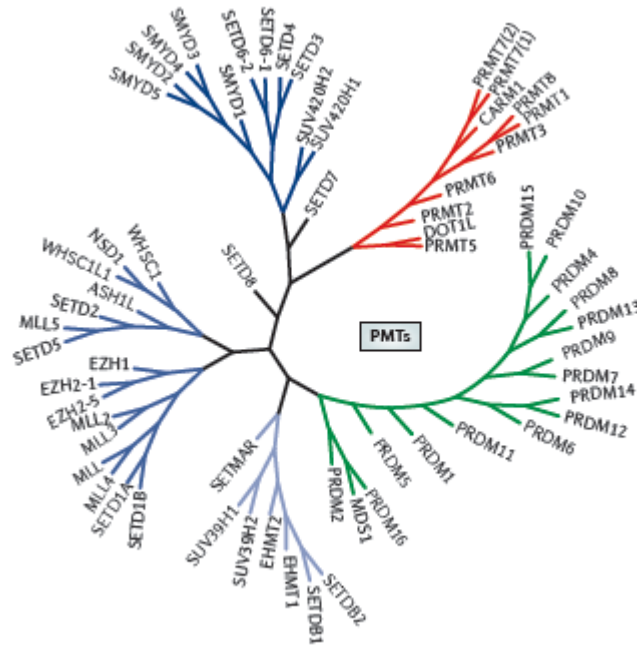
Figure 3.5. Phylogenetic tree of Protein Methyl Transferases (PMTs).
(Image courtesy of Arrowsmith C.H. *et al* Nature review/Drug discovery 2012)

The SET domain is a sequence of 130 amino-acids and it takes its name from the Drosophila genes Su(var)3-9, E(z) (Enhancer of zeste) and Tritorax where it was initially identified[87]. Structurally it's organised in a "thread-the-needle" folding, called *pseudo-knot*, characterized by the juxtaposition of two conserved peptides, in which one of the motif inserts into the loop created by the other one[88]. As for the PRMTs, within the SET domain the substrate and the cofactor bind in different sites, flanking each other, and meet at the core of the domain through a narrow hydrophobic channel, where the methyltransfer takes place. Albeit SET domain is the responsible for the methyltrasferase activity, the catalysis also relies on the simultaneous presence of other domains that act as "framework" for the recruitment of the substrate or other partners within large multiunit complexes or modulate the catalytic step, like for example in the Polycomb Repressive Complex 2 (PRC2), where the catalytic subunit EZH2 displays a methyltransferase activity only in complex with the non-catalytic partners EED and SUZ12. All these surrounding domains act like a bark around the SET sequence and can be divided into two subsets: the I-SET and post-SET motifs (respectively inserted within and *C*-terminal shifted respect to the SET domain) that participate to the substrate recognition and in a lesser extent to the cofactor binding; and the Pre-SET (cysteine-rich also referred to as a CXC domain),

MYND (between I-SET and SET) and CTD (C-terminal to Post-SET) domains, which are thought to be interfaces for the interaction with other proteins and DNA. The pre-SET motif, with its triangular Zn_3Cys_9 zinc cluster seems to play an important role also in the catalytic event[89]. According to this, distinct domains with different sequence and structure may decorate the SET fold in assorted combinations to obtain selective recruitment of interaction partners and therefore specific functions. Being involved in the substrate recognition, the I-SET and post-SET domain are always found in the SET methyltransferases. Even if the amino acidic sequence can change, the I-SET sequence has a overall conserved structural organization, while the Post-SET domain is more dynamic and can adopt different conformations.

As far as the substrate recognition is concerned, different mechanistic analysis has displayed that the Lys- and Arg-rich electropositive histone tails and the overall electronegative substrate-binding groove, spatially defined by pre-formed I-SET and the open folded Post-SET, initially interplay through a long range electrostatic interactions. Once this loose complex has been formed, SAM binding induces a partially folded Post-SET conformation which keeps close the PKMT and the substrate, allowing the sequence specific recognition to start. In this proposed model, the PKMT slides along the substrate peptide, with I-SET domain acting as a reading template. Once specific interactions have been established, the lysine substrate looses a proton to the solvent and fits into the hydrofobic channel. The loose complex thus turns into a catalytically competent conformation and the substrate peptide is further fasten by the Post-SET domain, which closes on it and shields the active site from the surrounding solvent. Owing to a tyrosine residue, the deprotonated ε-amino group of lysine substrate aligns its lone pair with the assailable methyl-sulfur bond, raising from the bottom of the channel, and methyltransfer takes place[90].

In all the available co-crystal structures with substrate peptides, an arginine side-chain, positioned one to four residues upstream or downstream in respect to the substrate lysine, makes wide-ranging interactions with a specific cleft of the I-SET domain. Both the shape and the position (relative to the substrate lysine) of this cleft and the structure of the active site are peculiar of each PKMTs and suggest that is theoretically possible to develop selective PKMTs inhibitors.

As previously stated SET-domain containing methyltransferases not only exhibit a substrate selectivity but also a product specificity. EZH2 has the greatest catalytic activity in mono-methylating the H3K27 but can achieve all three methylated states of this lysine, SET7/9 affords only monomethylated H3K4 (H3K4me1) after one round of catalysis, while G9a and GLP are either mono- and dimethyltransferases for H3K9 (H3K9me1/me2)[91]. This product specificity can be realized on the basis of structural and sequence explanations: the ability to mono-, di- and trimethylate lysine substrates seems to be correlated to a "tyrosine-phenylalanine switch" and in general to the steric crowding of the hydrophobic channel, since some PKMTs (Dim5, G9a) change their specificity following point mutations from tyrosine to phenylalanine, and vice versa, nearby the active site[92].

The protein lysine methyl transferases exert their activity mainly on histones even if other proteins have been identified as PKMTs substrates[93,94,95]. A extensive example may be represented by the tumour suppressor protein p53, also known as the "*genome guardian*", which can be targeted by different PKMTs with opposing cellular outcomes depending on the site of lysinic methylation: p53-responsive genes may be transcriptionally repressed after methylation at K370 by SMYD2[96] or on K382 by SETD8[97], while methylation of K372 by SET7/9 result in transcriptional activation[98]; p53 may be also inactivated because of the methylation on K373 by G9a and GLP[99].

Histones represent the main site of action of lysine methyltransferases which are therefore referred to as Histones Lysine Methyl-Transferases (HKMTs). As epigenetic "*writers*" they are correlated with both transcriptional activation and silencing, depending on the specific residue involved and on the extent of methylation, since lysine may be methylated up to three times. Nonetheless, generally methylation on H3K4, H3K36 and H3K79 is associated with activation of transcription whereas methylation at H3K9, H3K27 and H4K20 is correlated with transcriptional silencing[100]. Differently from the lysinic acetylation, whose transcription-activating mechanism is essentially based on the neutralization of the positive charge of the lysine side chains (which in turn interrupts the electrostatic interaction with phosphate groups of DNA backbone); lysine methylation doesn't affect the overall charge of the residues. Methyl groups rather seem acting as "*hubs*" for the recruitment of highly evolved methyl-lysine-binding proteins able to

distinguish distinct level of methylation and the surrounding amino acid sequence, especially along histone tails. The most remarkable biological consequences of the enhanced specificity of HKMTs in respect to HDACs is that each component of the former family of enzymes controls genes expression in a narrower group of cell types, being them normal or cancerous, thus proving to be more promising targets for drug development. In this concern a multitude of evidences draw attention to the wide spreading involvement of HKMTs in the human diseases related biochemical pathways including oncogenic transformation, inflammation, metabolic and neuropsychiatric disorders, finally in the handling of stem cells as tools for regenerative medicine[101].

HKMTs may contribute to the diseases development or maintenance by gaining aberrant activity due to mutations, altered expression or translocations that directly affect cellular genes expression, or being involved in altered upstream cellular signals.

In cancer, MLL1 (mixed –lineage leukemia 1) methyltransferase is subject of more than 50 chromosomal translocations, especially in human lymphoid and myeloid leukemias, where these are associated with very poor prognosis[102]. Despite the translocations are responsible for the loss of the carboxy-terminal SET domain, the N-terminal fusion proteins upregulate expression of several target genes including HoxA7, HoxA9 and the Hox factor MEIS1 that are important for proliferation and final differentiation of hematopoietic cells[103]. During normal hematopoiesis, expression of HoxA7, HoxA9 and HoxA10 promote stem cell self-renewal, and the downregulation of these genes correlates with terminal differentiation[104]. The inappropriate transcriptional activation seems to arise from the interplay with transcriptional elongation partners like AFF4, AFF1, AF9, and ENL, and with other epigenetic factors such as the methyltransferase DOT1-like protein (DOT1L). MLL-DOT1L and MLL-AF10 fusion proteins lead to the abnormal expression of leukemia-relevant genes, like Hox9A, and the transcriptional "prime" due by H3K79 instead of H3K4 methylation, respectively own of DOT1L and MLL1 methyltransferases, could be the prompting signal for oncogenic transformation in hematopoietic cells[105]. Other MLL fusion proteins can interact with factors that promote malignancy: MLL-AF9 fusion protein holds AF9 (also know MLLT3) capacity to recruit YEATs domain-containing 4 (YEATS4), which is upregulated in neuroblastoma and is required for the aberrant inactivation of p53[106].

Being composed of multipotent precursor cells interested by cellular differentiation and clonal expansion following a triggering stimulus (antigens), which then turn into specialized lymphocytes, the adaptive immune system shows all the hallmarks of a cellular process that can be regulated by epigenetic pathways. Though acetylation is the most firmly recognised histone modification playing important role in these mechanisms, the immune system regulation represents a new field of application of histone lysine methylation; in particular, G9A has been found to silence specific genes in the endotoxin shock through its H3K9 dimethylation[107].

SET-domain-containing protein 7 (SETD7) and Suppressor of Variegation 3-9 homolog 1 (SUV39H1), two other lysine methyltransferases, contribute to hyperglycaemic memory. Together with LSD1, they maintain the glucose response-related upregulation of p65 gene (a subunit of NF-kB), which is associated with diabetic vascular injury[108].

Modulation of epigenetic proteins find application also in the newest regenerative medicine, as they can direct the differentiation of embryonic stem cells and induce a pluripotent stem cellular state starting from somatic cells[109]. Small modulators of epigenetic proteins, including HDACs, PKMTs and Histone Lysine Demethylases (HDMs), when associated with biological techniques like transduction with transcription factors (OCT3, SOX2, MYC and KLF4), give the same cellular output, improve the reprogramming efficacy and avoid the risk of carcinogenesis. For example the G9A inhibitor BIX-01294 improves the stem cell reprogramming process in neural progenitors when in association with only OCT3 and KLF4[110].

3.2.1 Enhancer of Zeste Homologue 2 (EZH2)

Enhancer of Zeste Homologue 2 (EZH2 or KMT6A) is a SET-domain-dependent lysine methyltransferase whose main currently recognized activity is the sequential methylation (mono-, di- and trimethylation) of lysine 27 on histone 3 (H3K27). Some studies have displayed that EZH2 can insert also the H3K9me3 repressive mark but this point is still controversial[111]. Albeit all the different methylated state of H3K27 can exist at the same moment in a cell, the tri-methylated form is presently viewed as the predominant type that

mediate the biological function *in vivo*. Demethylated form of H3K27 is then regenerated by the subfamily of UTX and JMJD3 histone demethylases[112].

Mostly recognized as a repressive transcriptional histone mark, the methylation of H3K27 is an epigenetic mechanism for silencing genes normally involved in cellular development and differentiation and in the early steps of X-chromosome inactivation[113]. According to this, up-regulated function of EZH2 can result in the wrong inactivation of tumor suppressor genes, which at the end leads to cancer[114]. Different studies have recently displayed that EZH2 is overexpressed and related to aggressiveness, metastasis and poor prognosis of a variety of solid tumors (table 3.2) including prostate[115,116], breast[117,118], bladder[119], colon[120] and skin[121] cancers, glioblastoma multiform (GBM) as well as blood malignancies like lymphoma[122]; consequently it has stood out as an attractive anti-cancer drug target.

Type of cancer	Functions
Prostate cancer	Cellular transformation Proliferation Invasion and metastasis
Breast carcinoma	Cellular transformation Proliferation Invasion and metastasis
Lymphomas	Proliferation
Myeloma	Proliferation Anti-differentiation
Bladder carcinoma	Cellular transformation Proliferation
Colon cancer	Proliferation
Cutaneous melanoma	Proliferation
Hepatocellular carcinoma	Proliferation Invasion and metastasis

Endometrial cancer	Proliferation
Lung cancer	Proliferation Anti-differentiation
Pancreatic cancer	Proliferation Anti-apoptosis
Gastric cancer	Proliferation Invasion and metastasis
Ewing's sarcoma	Proliferation Invasion and metastasis

Table 3.2. EZH2 aberrations and cancer.

EZH2 mainly exerts its activity as the catalytic subunit of the Polycomb Repressive Complex 2 (PRC2), which is a multi-protein cluster, essentially active as chromatin modifier, that is highly conserved across the organisms from plants to flies and humans[123]. Polycomb Group (PcG) proteins include two members: the polycomb repressive complex 1 (PRC1) and 2 (PRC2)[124], whose transcriptional repressive outcome is counteracted by the activity of another big family of chromatin regulating proteins: the Trithorax Group (TrxG) proteins.

PcG and TrxG proteins control the expression of genes involved in cellular early embryo development and differentiation (e.g. Hox transcription factors), through two opposing histone marks: the transcriptional repressive EZH2-dependent methylation of H3K27 and the activating MLL (Mixed –Lineage Leukemia)-dependent methylation of H3K4, respectively[114]. Thus, PcG and TrxG proteins act together to regulate chromatin dynamics and to maintain differential gene expression patterns (cellular memory) throughout the life of a multicellular organism (Tritorax group proteins are not subject of this thesis, for more informations see ref. 114).

PRC2 complex includes five highly cooperative subunits: EZH2, EED (Ectoderm Embryonic Development), SUZ12 (Suppressor of Zeste 12), RbAp48/46 (also called Retino Blastoma Binding Protein 4 or RBBP4 and RBBP7, respectively) and AEBP2 (Figure 3.6), and it silences genes primary involved in stem cell differentiation and embryo development. The exposed surface of the PRC2 complex offers interfaces for the

recruitment of other protein factors that can modulate directly or indirectly the methyltransferase activity or strengthen the epigenetic H3K27me3-related biological effect, even though they are not core components. In the former case human EZH2 can also associate with PHF1 (Plant Homeodomain Finger protein 1) which enhances its trimethyltransferase activity instead of the dimethyltransferase one[125].
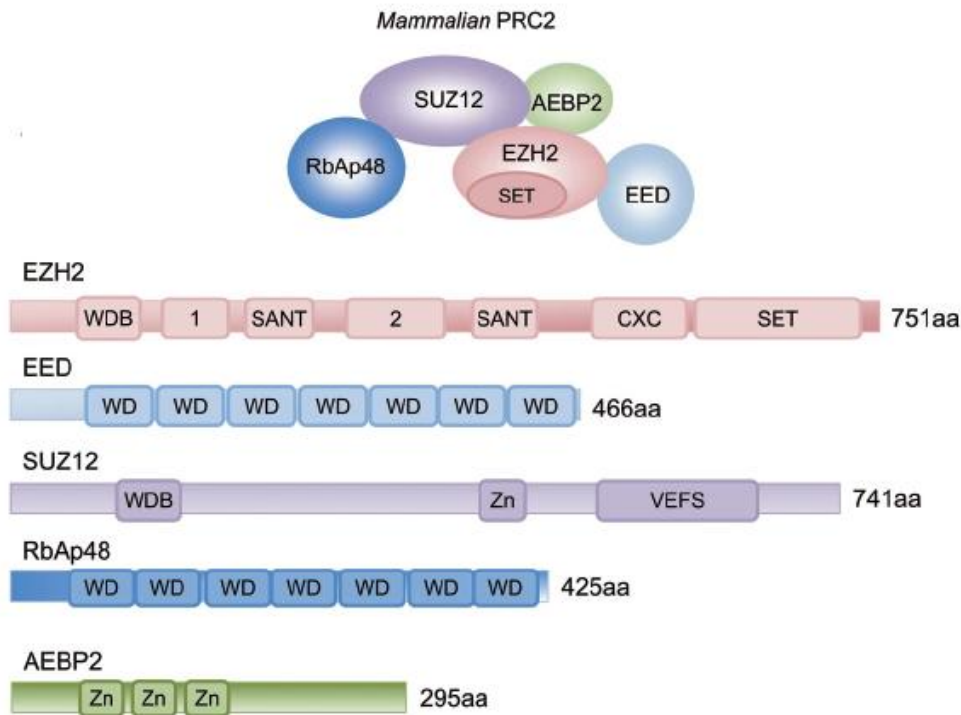
Figure 3.6. Architecture of mammalian PRC2 complex and domain organization of each subunit. Domain "1", binding region for PHF1 in human cells; domain "2", binding region for SUZ12; CXC, cysteine-rich domain; SANT, domain that allows chromatin remodeling protein to interact with histones; SET, catalytic domain of EZH2; VEFS, VRN2-EMF2-FIS2-SUZ12 domain; WD, WD-40 domain; WDB, WD-40 binding domain; Zn, Zn-finger region.

(Image courtesy of Tan, J. e*t al*. Acta Pharmacologica Sinica 2014)

EZH2 lacks a methyltransferase activity on its own but displays a robust turnover when in complex with two non-catalytic subunits of PRC2: namely the WD40-repeat protein EED and the zinc-finger protein SUZ12[126]. Among the PRC2 non-catalytic subunits, EED is the most characterized one since its crystal structure has been determined: it consists of a sequence of WD (Trp-Asp) domains that fold into a seven bladed β-propeller[127]. Three modules have been defined up to now, among them the surface on the bottom of the β-propeller (residues 39-68) is responsible for the interaction with an N-terminal fragment of EZH2, while a pocket on the top of it binds H3K27me3 or other histone marks and

mediates the allosteric activation of EZH2[128]. Concerning SUZ12 it's still unclear how it cooperates to the overall activity of PRC2. However SUZ12 has a highly conserved domain on its C-terminus, namely VRN2-EMF2-FIS2-SUZ12 (VEFS) and it's deletion prevents the SUZ12-EZH2 interplay[129]. Moreover it has been reported that the presence of chromatin activation marks such as H3K4me3, H3K36me2, and H3K36me3 can inhibit PRC2 activity if they are located in *cis* on the same histone peptide which is next to be methylated on the target lysine H3K27, and SU(Z)12 is responsible for mediating this inhibition in conjunction with the E(Z) SET domain[130]. About the two remaining PRC2 components: AEBP2 is a zinc finger protein and is endowed of interfaces to bind all the other PRC2 subunits so it acts as a stabilizing co-factor, while the exact role of RbAp48 hasn't been fully unraveled yet.

Concerning the cellular localization EZH2 is usually found into the nucleus fractions, most probably owing to the fact that it has nuclear localization signals (NLS), however recent studies have shown that in *ex vivo* isolated thymocytes EZH2 fractions are present also in cytoplasm[131]. Next generation sequence analysis have deeply assisted the discovery of mutations of KMTs in cancer and even if in rare cases EZH2 heterozygous mutations have been found in blood malignancies. Initially considered as a disactivating switch, the point mutation of tyrosine 641 (Y641) is presently recognized to result in a gain of function and it has been found in 7% of follicular lymphomas and 22% of germinal center B-cell and diffuse B-cell lymphomas (DLBCLs)[132]. Y641 mutants (Y641F, Y641N, Y641S, Y641H and Y641C) show an increased affinity for the di-methylated form of H3K27, thus increasing the levels of H3K27me3, while they lose affinity for the unmethylated and mono-methylated H3K27, characteristic of the wild type EZH2[133]. Therefore co-expression of heterozygous Y641 mutants with wild-type EZH2 increase the overall levels of H3K27me3 and may functionally correspond to overexpression of EZH2. The same functional outcome has been observed consequently to another point mutation (A677G) in a very small fraction of lymphoma cell lines (2-3%). As for the mutation of Y641, the replacement of alanine with glycine results in an increased affinity for H3K27me2, but differently the wild type-like activity on unmethylated and monomethylated substrates is still present[134], so the A677G replacement leads to a mutant efficiently active on all the three form of H3K27.

One of the astonishing feature of the EZH2 (and of course of PRC2) function and activity as "*writer*" of the histone code is the strong cooperation with the other epigenetic, generally silencing, enzymes. Comprehensive studies have indeed shown that there are physical and functional links between EZH2, the polycomb repressive complex 1 (PRC1), the DNA Methyltransferases (DNMTs) and the Histone Deacetylases (HDACs), strengthening the hypothesis of the existence of a wide-spreading *crosstalk* between different epigenetic factors.

PRC1 complex is a multi-protein cluster composed of different homolog of chromo-domain-containing proteins (CBX2, CBX4, CBX8), polyhomeotic proteins (PHC1, PHC2, PHC3), BMI1 and RING-finger proteins (RING1, RNF2)[135]. According to the currently proposed model transcription factors and their associated molecular machinery point out the loci to be silenced and recruit *in situ* the PRC2 complex to tag these promoters by methylating H3K27. This mark is then recognized and finally bound by the chromodomain-containing proteins (CBXs) within the PRC1 complex, which in turn is responsible of the ubiquitynation of the lysine 119 on histone H2A, strengthening the incipient silencing mark[136]. In addition, evidences arising from *in vitro* assays suggest that PRC1 can cooperate with PRC2-mediated transcription silencing also by blocking the anchoring of transcriptional activating factors[137], and therefore the RNA Polymerase II (RNA Pol II) and then preventing its elongation[138]. However, the details of the molecular partnership between PRC2 and PRC1 are not fully unravel yet, not all the PRC2 genes are then bound by PRC1, and in some cases PRC1 and PRC2 have been found simultaneously bound to DNA, thus the sequential mechanism in which PRC2 tags loci that afterwards will undergo ubiquitination on H2AK119 has to be still elucidated[139].

The close interplay between PRC2 and PRC1 is even more evident if we consider that EZH2 represses the transcription of several microRNAs (miRNAs), including miR181a, miR181b, miR200b, miR200C and miR293, generally involved in the regulation of PRC1 components. Repressing the transcription of this microRNAs, EZH2 in turn induces the de-repression or the upregulation of PRC1 proteins, therefore playing a positive feedback[140].

Concerning the functional synergism between EZH2-mediated lysine methylation and lysine deacetylation, HDAC1 and HDAC2 have been purified in human PRC2

complexes[141], moreover PRC2-mediated transcriptional silencing is blocked by HDAC inhibitor TSA[142]. Taken together these biochemical data suggest that HDACs are not core subunit of PRC2, but can transiently associate to it and have a positive influence on histone lysine methylation. In this view, since a lysine can't be methylated as far as it's acetylated on its side chain, HDACs could directly deacetylate H3K27 to make the ε amino group available for methylation by PRC2 or alternatively HDACs could modify the surrounding histone marks (on H3K9, H3K14, H4K8 for example) to allow the following H3K27 methylation[143] (Figure 3.7).

Although DNA methylation has been thought for a long as an independent genes silencing mechanism, a pioneering study[144] showed that PRC2 subunits (EZH2 and EED) co-immuneprecipitated with human DNMTs (DNMT1, DNMT3A, DNMT3B)[145]. Following studies on stem cells displayed that genes undergoing H3K27 methylation by EZH2 were predisposed to DNA hypermethylation on their CpG islands, as result of triggering inputs during the normal development, arising the hypothesis that EZH2 could prompt some distinct genes for the subsequent long-term transcriptional inactivation by GpC hypermethylation[146]. Further RNAi knockdown analysis in osteosarcoma cells exhibited that EZH2 presence is mandatory for DNMTs binding and the following CpG methylation but that, on the contrary, DNMTs are not necessary for the EZH2 recruitment, proving the idea that this synergism could be exploited also in cancer cells for silencing tumor suppressor genes. However it hasn't been elucidated yet if the DNMTs are recruited directly by EZH2 through a mutual protein-protein interaction or by the methyl H3K27 histone mark. As a whole, all these studies depict a scenario in which EZH2 tags certain genes for later undergoing to CpG hypermethylation, and therefore long-term silencing during the normal cellular development and differentiation, but this cooperation has been found also in cancer cells[147] (Figure 3.7).
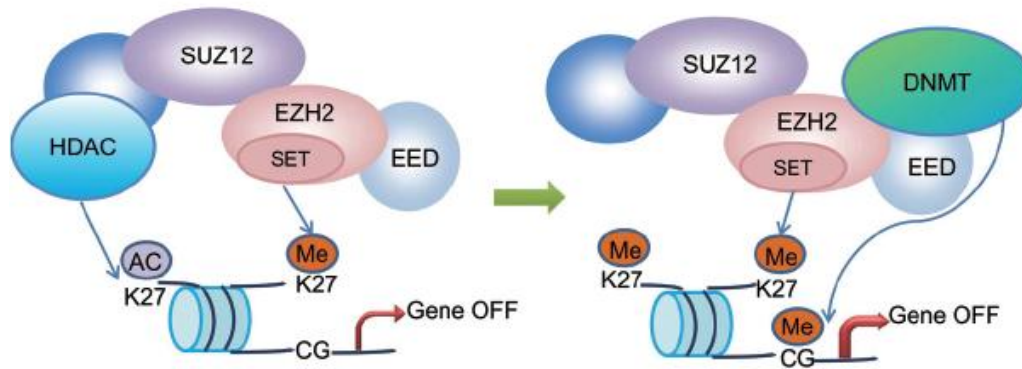
Figure 3.7. A proposed model for the synergism among epigenetic silencing enzymes, including the core subunits of PRC2 complex: SUZ12, EZH2, EED; histone deacetylase (HDAC) and DNA methyltransferase (DNMT). The hypothesis considers that if K27 is acetylated, HDAC may deacetylate it at first, then allowing the target genes to be then silenced through K27 methylation by PRC2 complex. DNMTs can also be recruited after pre-tag by EZH2-mediated methylation, and mediate long-term silencing by hypermethylation of CpG islands. Ac: acetylation; Me: methylation.
(Image courtesy of Tan, J. e*t al*. Acta Pharmacologica Sinica 2014)

Although EZH2, by virtue of the tri-methylation of H3K27, is widely considered a transcriptional repressive histone methyltransferase, recent evidences have raised a new and functionally opposite activity of EZH2. Xu *et al*[148] reported that the oncogenic function of EZH2 in castration-resistant prostate cancer relies on a transcriptional activation rather than on silencing of its target genes and moreover this activation is PRC2 independent. As proof of concept, they showed that in hormone-refractory prostate cancer cells a subset of EZH2-responsive genes didn't bind SUZ12 subunit neither exhibited H3K27me3 histone mark, moreover some of these genes were transcriptionally silenced after EZH2 knockdown and EZH2 methyltransferase activity was determinant for androgen-independent growth.

In the effort to explain this unexpected result Xu *et al* hypothesized that EZH2 may shift it's activity, from a polycomb repressive to a transcriptionally activating outcome, after the PI3K-Akt phosphorylation on its Ser21. The phosphorylated EZH2 then could methylated the Androgen Receptor (AR) or other associated proteins, enabling the activation of its target genes. This finding reveals a new role of EZH2 in the methylation of non-histone proteins and prompts the possible development of inhibitors that selectively target the activating function of EZH2 in hormone refractory prostate cancer cells (Figure 3.8).
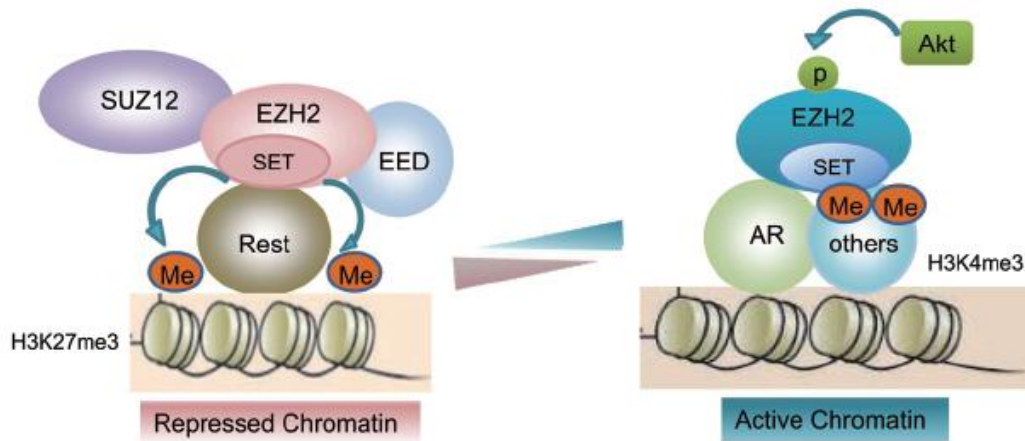
Figure 3.8. A proposed model of the functional switch from a 35olycomb repressor to a transcriptional activator in castration-resistant prostate cancer.

(Image courtesy of Tan, J. E*t al*. Acta Pharmacologica Sinica 2014)

EZH2 establishes thick interplays not only with other epigenetic effectors as previously mentioned, like PRC1, HDACs and DNMTs, but also with different transcriptional factors, enzymatic modulators and signaling effectors. In this view, one clear example is represented by the interrelation between EZH2 and p53. This well established tumor suppressor has been found in correspondence of the EZH2 promoter, where it represses its expression maintaining the genetic stability. One of the implications of this evidence could be that cancer progression associated with loss of p53 can be partially attributable to the increased activity of histone methylation as a consequence of EZH2 de-repression[149].

Furthermore, Myc transcription factor has been proved to influence EZH2 cellular levels by two different mechanisms. It directly binds to the EZH2 promoter, thus increasing the mRNA amount of EZH2, whereas it is simultaneously capable to repress transcription of the host gene encoding miR-26a and miR-26b, which exert a negative control on the EZH2 mRNA. Both these mechanisms have been found to contribute to prostate cell transformation and carcinogenesis[150,151].

E2F, a target of the reti-noblastoma protein (pRB), plays a critical role in regulating cell cycle progression through activating genes that control entry into the S phase and genes associated with DNA replication, in this concern, after phosphorylation of pRB, E2F turns activated and binds to the promoter of EZH2 and EED, positively modulating their expression.[152].

EZH2 expression is also controlled by hypoxia through HIF response elements (HRE) in the EZH2 gene promoter In hypoxic microenvironment, EZH2 expression is increased and thereby promotes proliferation of breast tumor initiating cells[153].

3.2.2 EZH2 aberrations and cancer

Soon after the discovery of EZH2 and its characterization as an histone modifying enzyme, many reports appeared displaying it as deeply involved in cancer cells transformation and maintenance. Generally EZH2 is not expressed in adult tissues, but its aberrations, coming from mutations, overexpression, hyperactivation are correlated with aggressiveness, metastasis, and poor prognosis in most of the above mentioned cancers, among these, altered EZH2 activity has been most completely described in prostate and breast cancer. Apart from some exceptions, as the recently reported co-activator function in castration-resistant prostate cancers, EZH2 oncogenic properties in cancer tissues rely on the silencing of genes that promote differentiation, restrain proliferation and arrest cell cycle progression.

Gene profiling studies ranked EZH2 as the most significant gene up-regulated in metastatic prostate cancer compared to clinically localized prostate cancer[154]. Loss of EZH2 gene inhibits growth of prostate cancer cells while its over-expression led to silencing of a set of more 100 target genes, whose expression is dependent on a fully active SET domain. All these findings suggest that EZH2 methyltransferase activity is essential for its oncogenic function in prostate cancer cells and seems to be related to its lysine chromatin hypermethylation. EZH2 levels could provide a valuable prognostic indicator of patient outcome too and subsequent studies have described the prognostic value of combined sets of prostate markers that include EZH2 overabundance. Another report focused on the interplay between EZH2 and androgen signaling cascade, showed that EZH2 expression is repressed by androgens and this repression requires a functional androgen receptor (AR). Thus a controversial hypothesis on EZH2 involvement in castration-resistant prostate cancer could be that its oncogenic role may implicate the activation of AR-repressed genes as EZH2 is frequently overexpressed in hormone-refractory prostate cancers.

EZH2 expression has been shown to be negatively modulated at the post-transcriptional level by miRNAs. This represent another proof of involvement of EZH2 in prostate cancer since over the years miR-101, miR-26a, and miR-26b have been found significantly decreased in prostate cancer through miRNA profiling studies[155,156,157].

One of the characteristic genetic signature in prostate cancers is the fusion between the androgen-responsive TMPRESS2 promoter and the ERG coding sequence, this fusion gene is able to substantially upregulate ERG expression, which at the end run to cell proliferation and invasion[158]. In this concern, a milestone in supporting EZH2 involvement in prostate cancer is that ERG can directly activate EZH2, which synergistically result in cancer progression through a process of de-differentiation associated with histone methylation[159]. Among the multitude of silenced genes it was demonstrated that EZH2 can activate Ras and NF-κB pathway by epigenetically repressing the expression of homolog-2-interacting protein (DAB2IP), which is a negative modulator of the aforementioned signaling pathways[160], thus turning at the end to promotion of initiation and metastasis of prostatic tumors. Moreover, EZH2 can trigger cancer cell invasiveness and progression to advanced tumor stage by silencing CDH1 gene, which encodes for the epithelial marker E-cadherin, whose loss often prompts epithelial-mesenchymal transition[161]. Likewise, another mechanism by means of EZH2 can stimulate progression in prostate cancer is the downregulation (by trimethylation of H3K27) of MSMB gene, which encodes for PSP94 that is known to promote prostatic tumor cell apoptosis, to inhibit secretion of matrix metalloproteinases (MMPs) and decrease VEGF-mediated angiogenesis[162].

A direct link between EZH2 and the MMPs TIMP2 and TIMP3, which are tissue inhibitors of metalloproteinases has been recently uncovered. This further evidence strengthens the idea that EZH2 can lead to degradation of extracellular matrix (ECM) and subsequently cell invasion in prostate cancer[163].
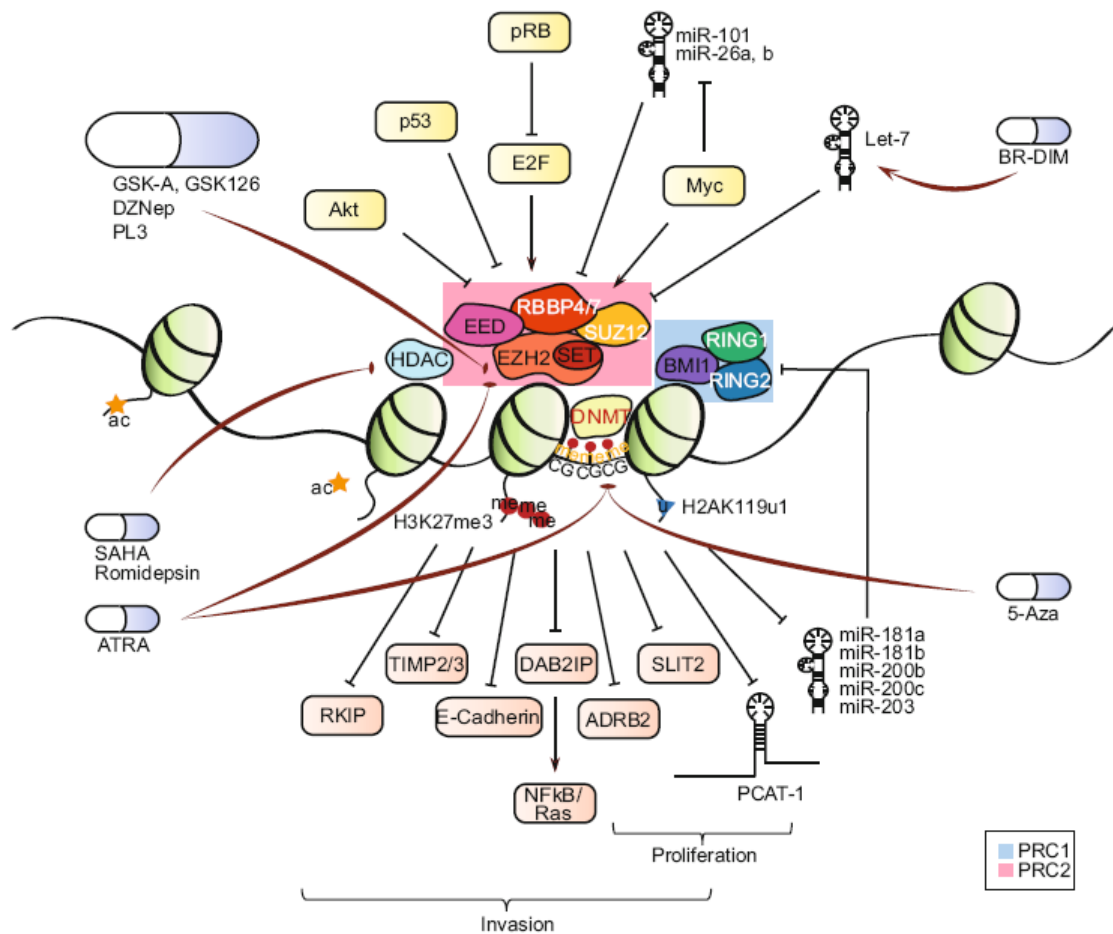
Figure 3.9. EZH2 regulation and function in prostate cancer.

(Image courtesy of Yang, Y.A. e*t al*. Protein Cell 2013)

Aberrantly elevated EZH2 levels have been described to be deeply linked with invasiveness and increased cellular proliferation in breast carcinomas too. Likewise for prostate cancer, it has been proposed that EZH2 could be a promising biomarker for aggressive breast cancers with a poor prognosis and that it can be an independent indicator of clinical outcome.

One of the most common molecular aberration in breast cancer is the mutation of BRCA1, which is responsible for the onset of basal like breast carcinomas that are ER, PR and Her2-neu negative and which intriguingly are characterized also by increased levels of EZH2[164]. Germline Brca1 mutations are also reliable prognostic markers for breast cancer in women, and this is partly due to the BRCA1's role in DNA repair and genomic stability as well as in estrogen receptor modulation[165]. EZH2 overexpression inhibits BRCA1 phosphorylation at Ser1423 thus promoting an increase of Cdc25C, an essential player for G2/M checkpoint control, which leads to the end to cell progression into cell cycle. This

evidences support the hypothesis that elevated EZH2 concentrations in ER-negative breast cancer cell lines confer increased cell proliferation partly through the inhibition of BRCA1 phosphorylation[166]. A member of runt-related (RUNX) family of transcriptional factors: *RUNX3* has been found functionally correlated with EZH2. Inactivation of *RUNX3* expression through DNA hyper-methylation has been reported in various cancers, including those of prostate, lung and pancreas, but intriguingly upon EZH2 levels reduction in MCF-7 breast cancer cell line, RUNX3 expression was recovered. RUNX3 expression also increased upon treatment with the deacetylase inhibitor TSA, therefore it has been suggested that RUNX3 downregulation may be controlled by H3K27me3 through EZH2 and HDAC1[167]. RUNX3 reduction leads to the decrease of the cyclin-dependent kinase inhibitor p21WAF/Cip1 expression, which finally results in the induction of cell proliferation in breast cancer[168].

The Wnt signalling pathway, which regulates the ability of the β-catenin protein to prompt the activation of specific target genes, is nowadays gaining momentum as an important cause of the development of different human cancers[169]. DACT3, a Wnt antagonist interacting with Dishevelled, has been found transcriptionally repressed in colorectal cancer[170], upon H3K27me3 chromatin modification, this lead to the activation of Wnt/ β-catenin signalling, allowing cancer cells to escape from apoptosis[171].

3.3 Targeting Histone Arginine and Lysine Methyltransferases

Over the past decade, knowledge of the proteins involved in the post-translational modification of histones has grown tremendously, and this is due not only to the intense efforts made by cell biologist in unrevealing the tangled epigenetic pathways but also to the development of small molecules able to modulate this molecular targets. These proteins includes several families of related enzymes and chromatin-interacting proteins, and are a rich source of potential therapeutic targets. Despite that, only four drugs have been developed up to now, including DNMT inhibitors 5-azacytidine (Vidaza[R]) and decitabine[172] (20-deoxy-5-azacytidine, Dacogen[R]) and the histone deacetylase (HDAC) inhibitors suberoylanilide hydroxamic acid[173] (SAHA, Zolinza[R]) and the natural product romidepsin[174] (Istodax[R]) (Figure 3.10). 5-azacytidine and decitabine were approved by the

FDA for treatment of haematological malignancies like acute myeloid leukemia and myelodysplastic syndrome, while SAHA and romidepsin are currently second line therapeutic options for the treatment of cutaneous T cell lymphoma (CTCL).
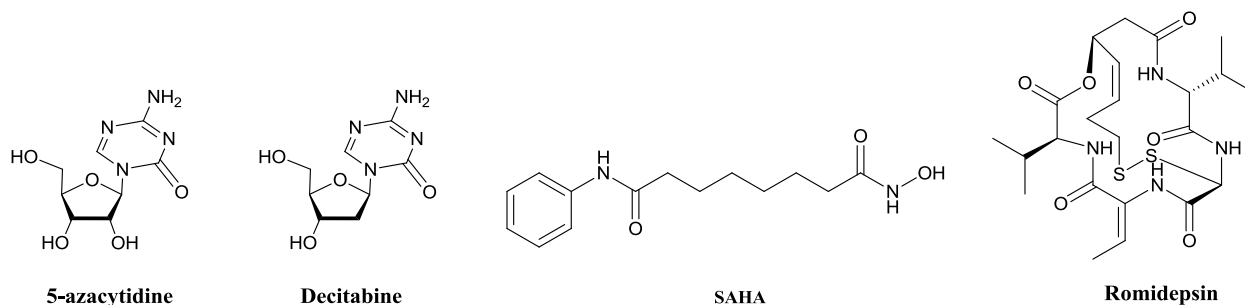
Figure 3.10. Structures of approved drugs addressing epigenetic targets

These DNMT inhibitors are nucleoside structures and are characterized by a low specificity to DNMTs and tumor cells too, on the other hand histone deacetylases have broad substrate specificity, being involved in the modification of different proteins, including many non-histone proteins that are not involved in epigenetic regulation[175,176]. Consequently, the "proof of concept" supporting the theory of epigenetic therapies using DNMT and HDAC inhibitors for specific cancer treatment, is still far away from being accomplished. In contrast to HDACs and DNMTs that generally control gene expression on different cell types, recent evidences pointed out that histone arginine/lysine methyltransferases (PRMTs and HKMTs) and histone lysine demethylases (KDMs) may affect gene expression in specific way non only in normal cells, but in cancerous cells too[177].

Moreover, HMTs and KDMs are frequently affected by genetic alterations in cancer cells including chromosomal translocations, gene mutations and fusion proteins, which recently have been linked to oncogenic transformation by loss of tumor suppressing functions, as well as linked to the developmental plasticity of cancer cells. Taken together, these observations strengthen the hypothesis that targeting aberrant HMTs and KDMs in cancer may achieve a higher degree of specificity in epigenetic therapy and prevention by blocking tumor specific epigenetic alterations or mutations.

The first non-nucleoside specific inhibitors of PRMTs were discovered in 2004 by Bedford and co-workers[178], through a random screening approach of 9000 compounds from ChemBridge, using RNA binding protein, Npl3p, as substrate of the yeast Hmt1p arginine

methyltransferase (Figure 3.11). The hits found were named Arginine Methyltransferase Inhibitors (AMIs) and were able to inhibit the human PRMT1 with potency ranging from 0.19 to 16 μM. Further studies were carried out to determine specificity among the nine active compounds, thus AMIs were tested on a set of PRMTs. In this concern AMI-1 arose as a selective type II PRMT5, but afterwards it showed, even if in less extent, activity over some lysine methyltransferases like Suv39H1, Suv39H2, SET7/9 and DOT1L and some Sirtuins (class III histone deacetylase)[179].
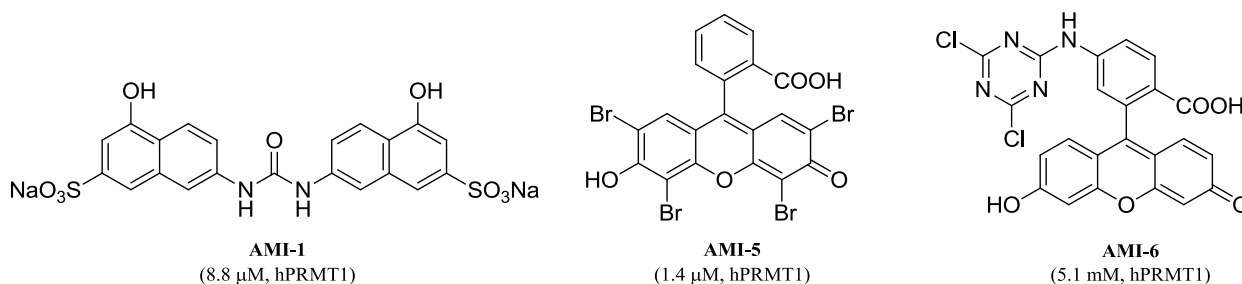
Figure 3.11. Structures of Arginine Methyltransferases Inhibitors (AMIs)

Several groups have used AMIs as leads for PRMTs drug discovery programs and in particular their bromo- and dibromo phenolic moiety have been object of structural simplification approaches which at the end led to the synthesis of a number of analogs exhibiting selectivity for PRMT4 over PRMT1 and SET7/9 at a concentration of 100 μM[180,181] (**1**, Figure 3.12).

Following attempts by Bonham and co-workers to develop a less polar analog of AMI-1 prompt them to synthesize a scaffold bearing structural elements from AMI-1, like aminonaphtol sulfonate, decorated with elements from AMI-6 and AMI-9[182]. The most potent compound obtained was compound **2** (Figure 3.12).
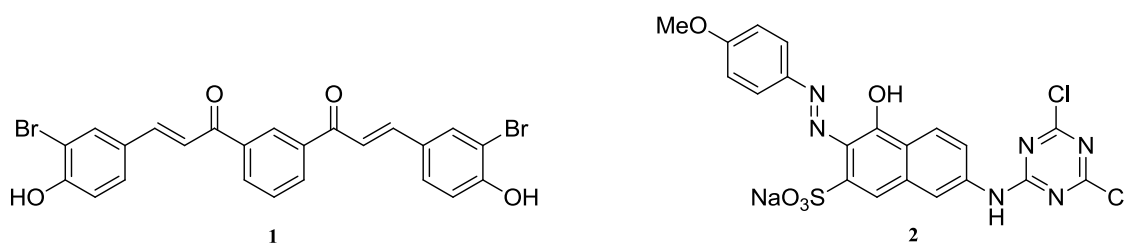
Figure 3.12. Structures of analogues obtained by AMI-5

Further hit discovery programs also made use of target based virtual screening study for PRMTs Spannhoff and co-workers[183,184], in 2007, virtually screened hPRMT1 and fungal

RmtA, a PRMT1 homologue, against the NCI diversity subset (1990 compounds). Compounds that were successfully docked, were then tested *in vitro* against RmtA and recombinant hPRMT1. In this study, seven of the 36 virtual hits were able to inhibit RmtA and hPRMT1 with micromolar potency (IC50 hPRMT1 = 2–90 μM). Two of the hits, allantodapsone and stilbamidine (Figure 3.13), exhibited inhibition of methylation at the PRMT1 target H4R3 in a dose-dependent manner with only a marginal effect on methylation levels of PKMT target H3K4. In addition, kinetic assays showed allantodapsone and stilbamidine did not inhibit RmtA in a SAM-competitive manner but were rather competitive with regard to the histone substrate. On the follow up of this approach, ChemBridge compound collection, containing 328.000 compounds, was used in another virtual screening study and a after a first filter using a pharmacophore search, nine inhibitors of PRMT1 were found (with an IC_{50} rangin from 13 to 37 μM). The three most potent compounds are depicted as follows, together with the Allantodapsone and Stilbamidine.
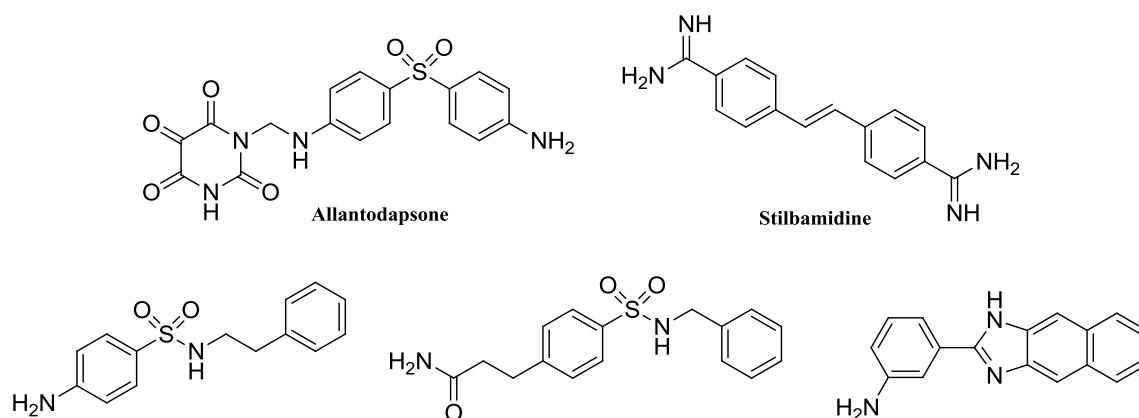
Figure 3.13. Arginine methyltransferase inhibitors obtained by virtual screening approach.

Chaetocin, a fungal mycotoxin (Figure 3.14), was the first small-molecule inhibitor of recombinant *Drosophila* Su(var)3-9 (IC_{50} = 0.6 μM) to be identified in 2005, after a screening of a library of ca. 3,000 compounds using a standard radioactive filter-binding assay.[185] Chaetocin was also found to inhibit H3K9 PKMT SUV39H1 (IC_{50} = 0.8 μM), the human orthologue of Su(var)3-9. Subsequently mechanistic studies unravelled chaetocin mechanism as a SAM-competitive inhibitor, which remained active even after the reduction of disulfide bonds.

The first selective small-molecule inhibitor of G9a and GLP: BIX01294 (Figure 3.14), was identified by a high throughput screening of ca. 125,000 compounds from the Boehringer Ingelheim compounds collection. It showed also weaker potency *in vitro* assay (not below 45 μM) over other H3K9 PKMTs including SUV39H1 and SETDB1, H3K4 PKMT like SET7/9, and arginine methyltransferase PRMT1[186]. In vitro experiments attested that BIX01294 inhibited G9a and GLP with IC_{50} values of 1.9 μM and 0.7 μM, respectively whereas in cellular assays BIX01294 exhibited toxicity at a concentrations of more than 4.1 μM.

As a proof of concept for BIX01294 selectivity, when cells were treated at an inhibitor concentration of 4.1 μM, it reduced H3K9me2 levels of bulk histones, while methylation levels of other lysine residues, including H3K27, H3K36, and H4K20, remained unaffected. Subsequent X-ray crystal structure studies of GLP in complex with BIX01294 (PDB: 3FPD) have revealed that differently from chaetocin, it didn't act as a SAM-competitive inhibitors but rather interact with the histone peptide binding pocket. The same X-ray structure revealed that while BIX01294 did not bind in the SAM-binding site, it also did not fits into the lysine binding channel[187]. Through the same aforementioned approach were also discovered non-selective Lys and Arg methyltransferase inhibitors like BIX01338 (Figure 3.14).
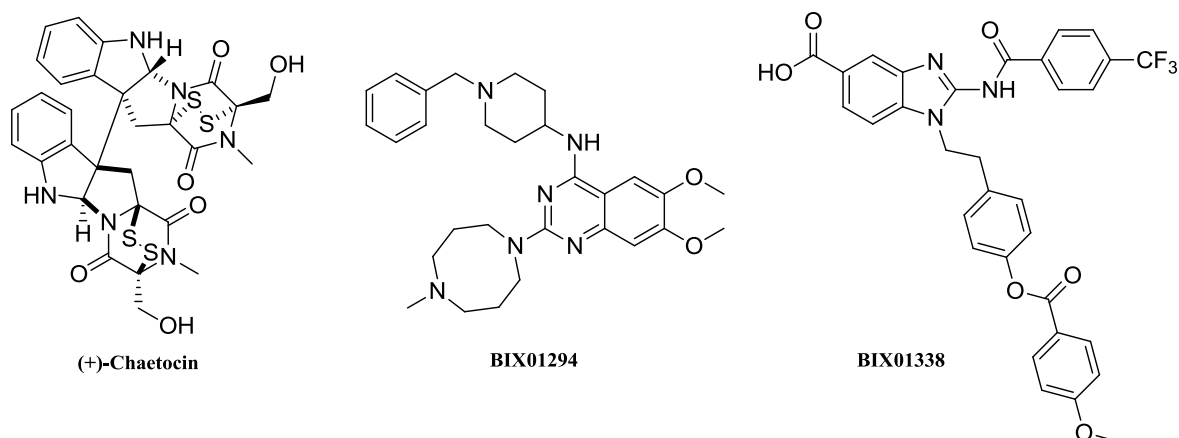
Figure 3.14. Structure of Chaetocin and of first inhibitors developed by Boehringer Ingelheim

Starting from crystal structure of GLP in complex with BIX01294, structure activity relationships studies were carried out, and in this concern the 7-methoxy moiety of the quinazoline scaffold was investigated with the aim to design analogs that would interact

with the lysine channel. Using the G9a ThioGlo assay, these efforts led to the identification of UNC0224 (Figure 3.15), which is a seven times more potent G9a inhibitor (IC_{50}=15 nM) in comparison with BIX01294 (IC_{50}=106 nM), this result was also confirmed by isothermal titration calorimetry too[188]. UNC0224 proved to be 1000 fold selective over other PKMTs, such as SET7/9 and SETD8 and over a broad panel of G-protein coupled receptors, ion channels and transporters, however it exhibited a G9a-like potency against GLP (IC_{50}=20 nM). Nonetheless UNC0224 represents the first small molecule inhibitor with a high resolution (1.7 Å) X-ray co-crystal structure (PDB: 3K5K) in complex with G9a and showing the 7-dimethylamino propoxy side chain occupying the lysine binding channel of G9a.

UNC0321 (Figure 3.15), the most potent G9a inhibitor to date (IC_{50}=6 nM with AlphaScreen; 9 nM, in ThioGlo assay) was developed starting from the evidences that 7-alkoxy side chain did not completely occupy the lysine binding channel. Further SAR studies of the 7-alkoxy side chain of UNC0224 were made to explore the space left in the channel and led to the synthesis of analogs bearing a longer side chain[189].

Differently from UNC0224, UNC0321 showed some selectivity for G9a (IC_{50}=6 nM, with AlphaScreen) over GLP (IC_{50}=23 nM) and exhibited specificity over other PKMTs, like SET7/9 and SETD8, as well as PRMT3 (IC_{50}> 40µM in ThioGlo assay).

To overcome UNC0321 poor cellular activity and improve membrane permeability new series of analog compounds were designed and synthesized. Among them UNC0638 had excellent *in vitro* potency (Morrison *K*i G9a = 3.7 nM; *K*i = 3.0 nM) and was more then 100-fold selective over different epigenetic and non epigenetic targets[190]. As well as its precursors, like UNC0224, the newly synthesized UNC0638 (Figure 3.15) occupied the substrate binding groove and lysine binding channel and not the SAM binding pocket, as the X-ray crystal structure of the G9a-UNC0638-SAH complex (2.56 Å resolution, PDB: 3RJW) confirmed. UNC0638 excellent biochemical properties corresponded to good cellular activity too. Treatment of a variety of cell lines with UNC0638 led to the reduction of global H3K9me2 levels but more importantly it reduced the H3K9me2 mark at the promoter of known G9a-regulated endogenous genes and did not reduce the H3K9me2 mark at the promoter of a non-G9a-regulated gene, proving its selectivity in cellular assays

too and making UNC0368 a valuable tool for further investigating the biological function of G9a its role in health and disease.

Another potent G9a inhibitor, discovered by Chang and co-workers on the follow up of the previous quinazoline scaffolds was E72 (Figure 3.15). It exhibited high activity on G9a and GLP (IC$_{50}$ GLP=100 nM) with binding affinities determined by ITC (K_d GLP=136 nM; K$_d$ G9a=164 nM) and it was also crystallized in GLP in presence of SAH (resolution 2.19 Å, PDB: 3MO5). Resolution of co-crystal structure showed that E72 occupied both the surface of the peptide binding cleft and the lysine binding channel similar to UNC0224 with G9a[191].
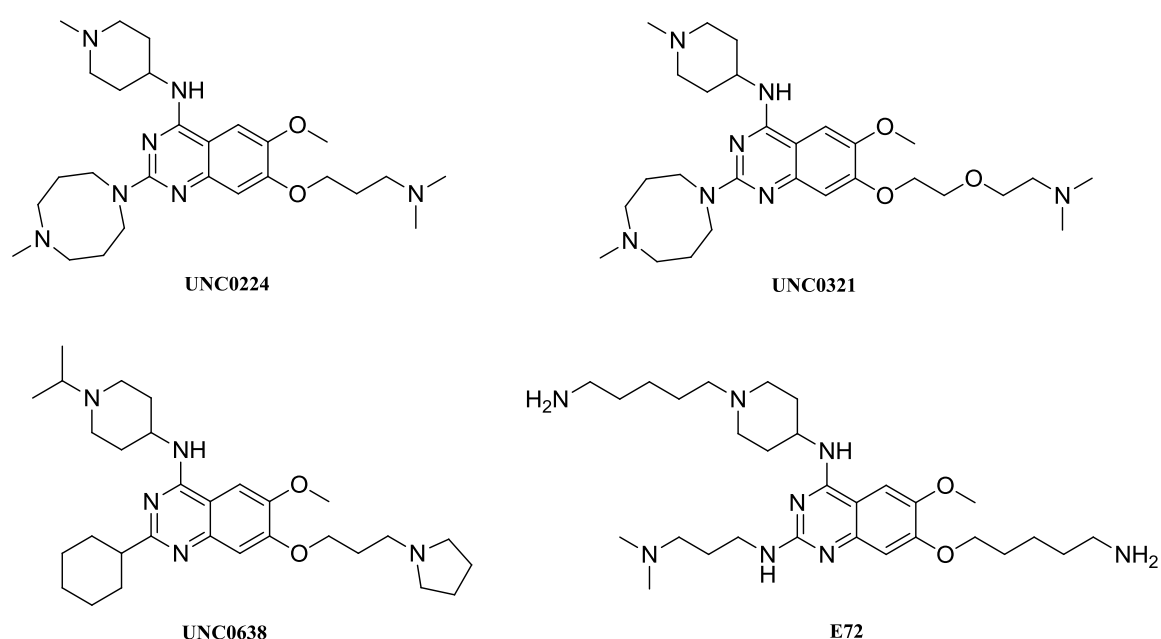
Figure 3.15. Structures of G9a and GLP inhibitors

Even more efforts have been done to target selectively DOT1L methyltransferase and different inhibitors have been found, all of them competing with the enzyme SAM cofactor and sharing a common adenosine scaffold. Different research groups attempted to developed selective and potent inhibitors of DOT1L (for more details see Ref. 71) but currently only one molecule is in phase I clinical trial for patients with MLL-rearranged leukemia: EPZ5676 (actually it's the only HMT inhibitor to be evaluated in a clinic). Modification of the urea-containing inhibitor EPZ004777 (K$_i$=0.3 nM, Figure 3.16) led to the identification of EPZ5676 possessing an increased potency (K$_i$=0.08 nM) and selectivity, over a panel of eight HMTs (only weakly active against PRMT5). The -

CH$_2$CH$_2$CH$_2$- linker and the 4-tert-butylphenyl substituted urea moiety of EPZ4777 were replaced with a *cis*-ethylcyclobutane linker and a 5-tert-butylbenzimidazole ring in order to reduce conformational flexibility and hydrogen bond donors[192].
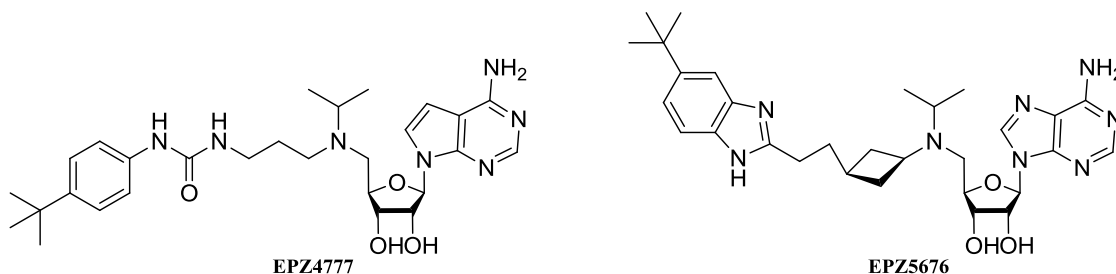
Figure 3.16. Structures of selective DOT1L inhibitors developed by Epizyme.

As far as the EZH2 inhibitors are concerned, till 2012 only a few inhibitors were known but these exhibited low potency and poor selectivity. Among them 3-deazaneplanocin A (DZNep, Figure 3.17), a *S*-adenosylhomocysteine hydrolase inhibitor, stunts EZH2 activity and induces the decrease of H3K27me3 levels. DZNep interferes with *S*-adenosylmethionine and SAH metabolism being an inhibitor of *S*-adenosylhomocysteine (SAH) hydrolase and its mechanism is believed to be related to the increased cellular SAH concentration, an inhibitory byproduct of cellular methyltransferase reactions, which at the end leads to the degradation of the PRC2 complex[193]. DZNep treatment can induce apoptosis in breast and colon cancer cells[194], however the interpretation of induced cellular phenotypes is complicated as DZNep reduces methylation at multiple histone residues targeted by different protein methyltransferases, in addition to EZH2. As a proof of the close epigenetic interaction between EZH2 methyltransferase activity and other histone marks like the aforementioned acetylation and DNA methylation, it has been reported that DZNep is synergistic with histone deacetylase inhibitors and DNA methyltransferase inhibitors in the activation of silenced genes[195].

SAH, the universal product of SAM hydrolysis, can also be used as EZH2 inhibitor (K_i =75μM, IC$_{50}$=0.1–20μM) but because of its own nature it suffers of poor selectivity against the other methyltransferases. As well DZNep, the natural product sinefungin (Figure 3.17) is another nonspecific SAM analog that has similar potency (IC$_{50}$=0.1–20μM)[196].
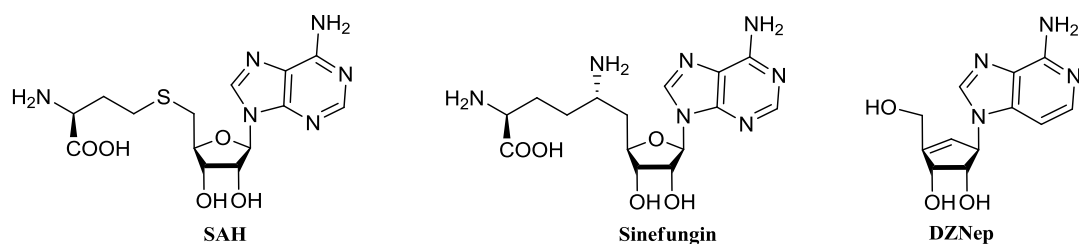
Figure 3.17. First generation of EZH2 inhibitors addressing the SAM binding pocket

Soon after an high-throughput screening program in 2012, different SAM-competitive potent inhibitors, with K_i value in the low nanomolar range, were identified, all of them bearing a 4,6-dialkyl-pyrid-2-one scaffold.

EPZ005687 (Figure 3.18) was the first highly selective SAM-competitive EZH2 inhibitor to be announced. It has a K_i value of 24 nM and is over 500-fold more selective for EZH2 versus 15 other PMTs (Protein Methyltransferases) and 50-fold more selective for EZH2 versus the closely related enzyme EZH1. Treatment of lymphoma cells bearing an EZH2 Tyr641 or Ala677 mutation with EPZ005687 leads to concentration-dependent cell killing, whereas this shows minimal effects on the proliferation of lymphoma cell lines containing wild-type EZH2[197].

EI1, another highly potent inhibitor of EZH2 developed by Novartis (Figure 3.18), shows comparable selectivity with a low K_i value (approximately 13 nmol/L, $IC_{50}=15nM$). EI1 exhibited equal activity against both wild type and the Y641 mutant form of EZH2, and the inhibition of the EZH2 Y641 mutant in B-cell lymphomas leads to decreased proliferation, cell cycle arrest, and apoptosis[198].

Further improvements into the SAR studies led to the most potent inhibitor of EZH2 as yet identified. GSK126 (K_i= 0.5–3nM, Figure 3.18) has a selectivity more of 1000-fold higher over 20 human methyltransferases containing SET or non-SET domains, and it is over 150-fold more selective for EZH2 than for EZH1. GSK126 efficacy has been evaluated on EZH2 mutants in DLBCL cells and more importantly in studies on animals, where it inhibits the growth of EZH2-mutant DLBCL xenografts in mice[199].

UNC1999 (Figure 3.18), an analogue of GSK126, represents the first orally bioavailable inhibitor that has high *in vitro* potency against wild type and mutant EZH2 over a broad range of epigenetic and non-epigenetic targets. UNC1999 potently reduced H3K27me3 levels in cells ($IC_{50}<50nM$) and selectively killed DLBCL cell lines harboring the Y641N

mutation[200]. Since no crystal structure of EZH2 is available at the moment, it is still not clear how structural changes contribute to the high selectivity of GSK126 (over 150-fold) versus UNC1999 (approximately 10-fold) for EZH2/EZH1.

In 2013, Epizyme announced the development of a new compound: EPZ6438 (Figure 3.18), with a superior potency and pharmacokinetic properties relative to their previously described tool compound EPZ005687. EPZ6438 inhibits the activity of human wild-type EZH2 with an inhibition constant (K_i) value of 2.5±0.5 nM, and in a similar extent, all its mutant forms. It exhibits excellent selectivity (more than 4500-fold) over a panel of 14 HMTs and of 35-fold over EZH1. It displayed apoptotic effects and induced differentiation on SMARCB1-deficient rabdoid tumor cells, leading to dose-dependent decreasing of trimethylation levels of lysine 27 on histone H3 and prevention of tumor regrowth after dosing cessation[201].

Although EZH2 inhibitors are not currently approved for treatment of human diseases, on February 2014 successful pre-clinical trial outcome of candidate EPZ6438 on genetically defined Non-Hodgkin lymphoma has been made available, strengthening the assessment of EZH2 as an attractive anti-tumor target.

EPZ005687

EI1

GSK126

UNC1999

EPZ6438
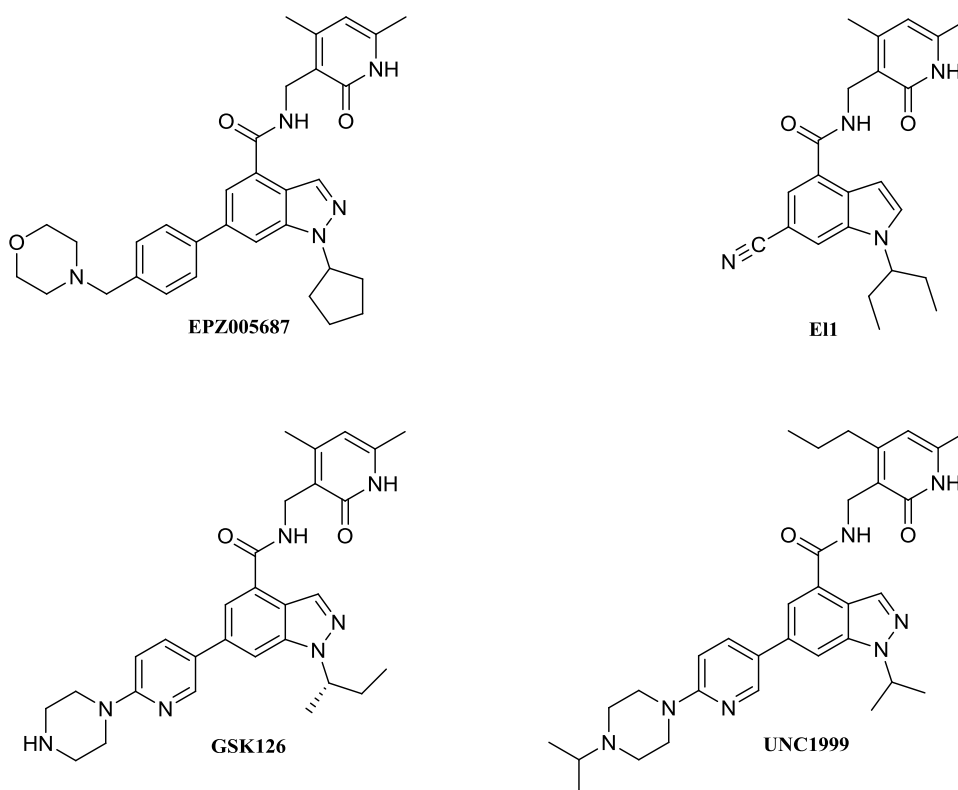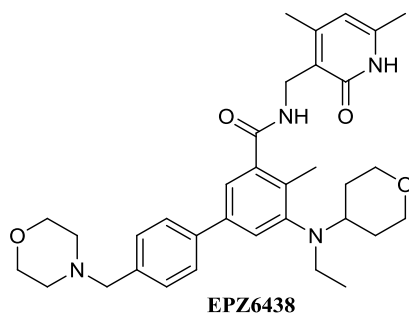
Figure 3.18. Structures of second generation of selective EZH2 inhibitors addressing the SAM binding pocket.

4. DESIGN, SYNTHESIS AND BIOLOGICAL EVALUATION OF NOVEL EZH2 HISTONE METHYLTRANSFERASE INHIBITORS

As previously stated in 2004 Cheng and co-workers first reported some dye-like small molecules as inhibitors of PRMTs and HKMTs[202]. In particular they described AMI-1 (see above in the arginine and lysine methyltransferase inhibitors paragraph) as the first specific PRMT inhibitor and AMI-5 also known as Eosin (Figure 4.1) as a potent but not selective inhibitor of different epigenetic enzymes. As part of previous medicinal chemistry projects, AMI-5 structure was selected as template to design and to develop series of simplified analogues, postulating the presence of two dibromo-hydroxy-phenyl moieties as crucial for PRMT and/or HKMT inhibitory activity[203,204]. In this concern, a large series of compounds bearing bis(monobromo- or bis(dibromohydroxy-phenyl portions separated by variously substituted spacers were synthesized (Figure 4.1) and then tested against two PRMTs (PRMT1 and CARM1, also known as PRMT4) and against SET7 as representative of HKMTs family. Since the structure of the designed compounds reminded of chemical features typical of HAT and SIRT modulators[205,206] such as curcumin and resveratrol (Figure 4.1), some of them were tested against p300 HAT and SIRT1/2 enzymes. From these assays, it resulted that compounds carrying two 3,5-dibromo-4-hydroxyphenyl moieties linked through a penta-1,4-dien-3-one, 2,6-dimethylene(hetero)cycloalkanone, 1,1-(1,3-phenylene)diprop-2-en-1-one, or hepta-1,6-diene-3,5- dione spacer behaved as epigenetic multiple ligands (epi-MLs), inhibiting at the same time all the tested PRMT, HAT, and SIRT enzymes, as well as SET7[205]. Among the 1,4-diphenylpenta-1,4-dien-3-one derivatives, those showing either a 3-bromo-4-hydroxy/3,5-dibromo-4-hydroxy or a bis(3,5-dibromo-4-hydroxy) substitution at the phenyl rings (compounds **1** and **2**) were epi-MLs, while the bis(3-bromo- 4-hydroxy) analog (**3**) showed PRMT1, CARM1, and SET7 inhibition, but was totally inactive against HATs and SIRTs.
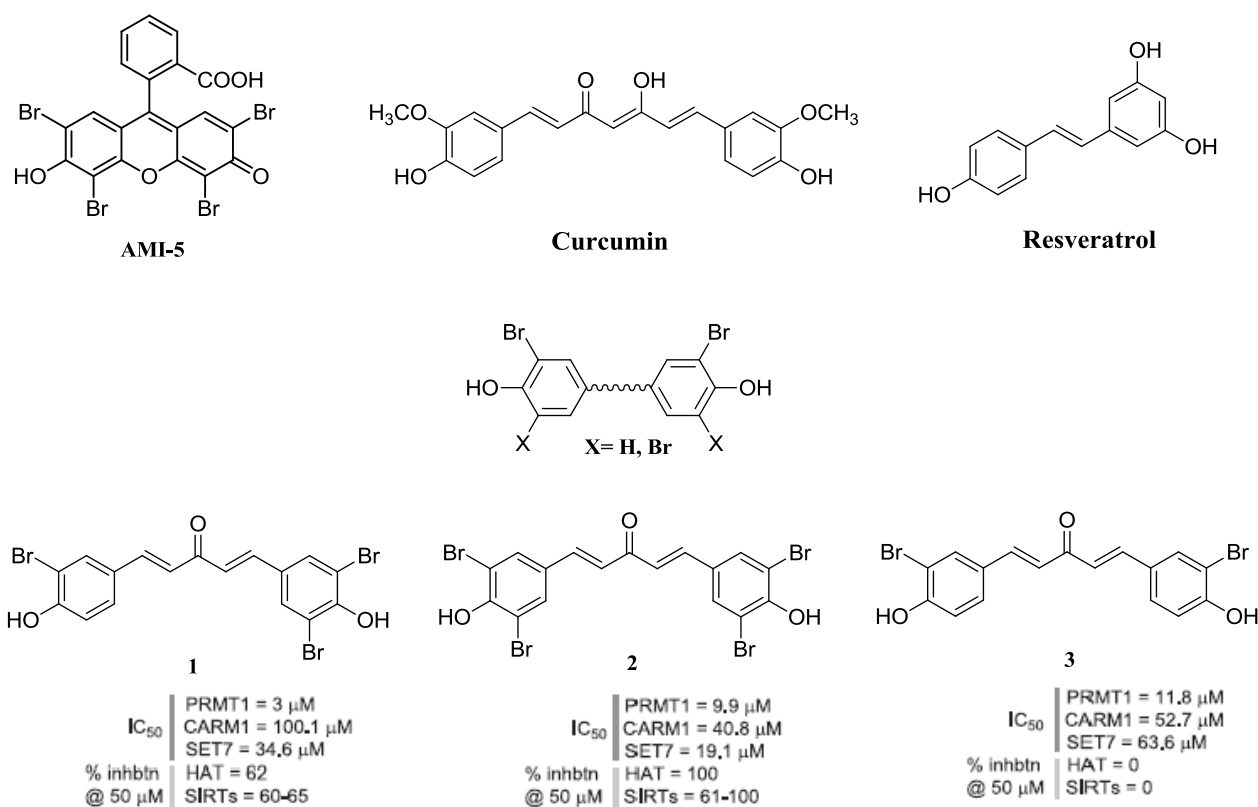
Figure 4.1. AMI-5, curcumin, resveratrol and some simplified AMI-5 analogues.

To further investigate the effect of such compounds against HKMTs, we tested compound **1-3** against PR-SET7, G9a, and SET7/9, three HKMTs different from SET7. In particular, PR-SET7 is a H4K20 lysine methyltransferase highly involved in cell cycle regulation and progression[207], G9a[208] acts on H3K9 and has been found expressed in aggressive lung cancer cells, with its elevated expression related to poor prognosis[209], and SET7/9 (with its epigenetic mark H3K4me1) has been associated to inflammatory diseases and diabetes[210]. As expected, **1-3** confirmed their wide inhibitory spectrum against epigenetic targets, and the results are reported in the following table.

compd	EC_{50}, μM		
	PR-SET7	G9a	SET7/9
1	17.4	44.6	31.9
2	23.8	62.5	55.9
3	4.3	11.0	9.6

Table 4.1. Enzymatic activity of compound 1-3 on PR-SET7, G9a and SET7/9.

Then, with the aim to identify selective HKMT inhibitors among this library of compounds, we noticed that analogs of derivatives **1-3**, bearing methoxy instead of

hydroxyl group on the two phenyl wings of the penta-1,4-dien-3-one scaffold (**4** and **5**, Figure 4.2) as well as simplified products such as the bis(3,5-dibromo-4-hydroxyphenyl)methanone **6** and the 4-(3- bromo- and 3,5-dibromo-4-hydroxyphenyl)but-3-en-2-ones **7** and **8** (Figure 4.2), led to compounds inactive against PRMT1, CARM1 and SET7, or endowed with slight CARM1 inhibiting activity (compound **5**)[211]. Thus, we prepared the 2,6-bis(3-bromo- and 3,5-dibromo-4-methoxybenzylidene)cyclohexanones **9** and **10** (Figure 4.2) as constrained analogs of **4** and **5**, and we tested the derivatives **4**-**10** against PR-SET7, G9a, and SET7/9. In addition, selected bis(bromo or dibromo-methoxyphenyl) compounds **4**, **5**, **9**, and **10** were tested against Enhancer of Zeste Homolog 2 (EZH2), to assess their capability to inhibit its enzymatic activity. Moreover, compounds **4**, **5**, **9**, and **10** were tested in human leukemia U937 cells to determine their effects on some methylation marks, H4K20me1, H3K9me2, H3K4me1, and H3K27me3, related to PR-SET7, G9a, SET7/9, and EZH2 activity, respectively. Such compounds have been tested in the same cellular model to study their outcome on cell cycle, cell death induction and granulocytic differentiation.
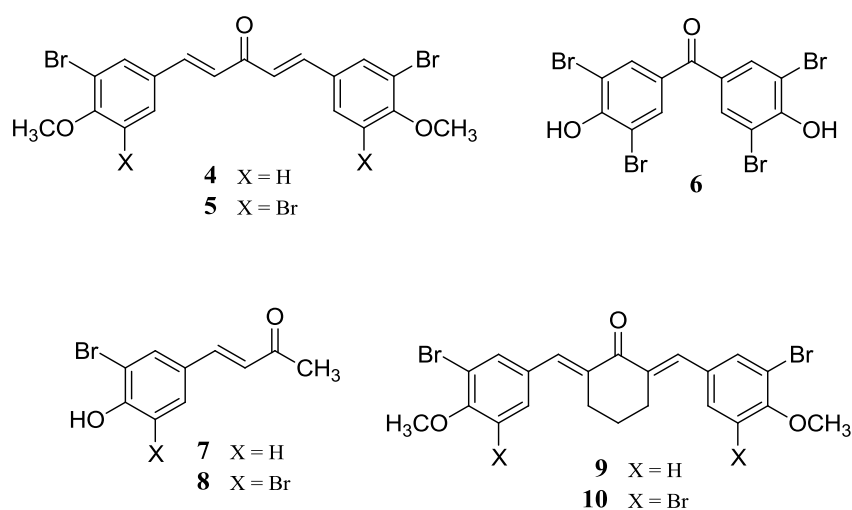
Figure 4.2. Structure of compound **4**-**10**.

The 2,6-bis(3-bromo- and 3,5-dibromo-4-methoxybenzylidene) cyclohexanones **9** and **10** were prepared by condensation of cyclohexanone with 2 equivalents of the properly substituted benzaldehyde in presence of barium hydroxide in methanol at room temperature (Scheme 4.1).
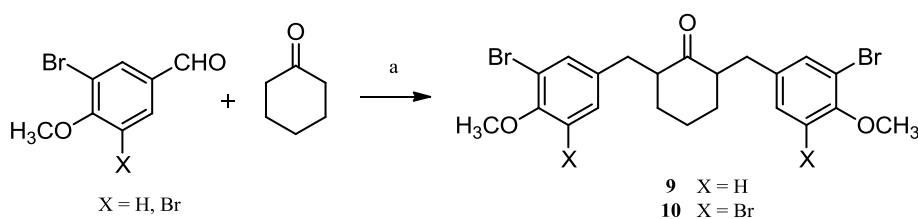
Scheme 4.1. Synthesis of compounds **9** and **10**; reagents and conditions: Ba(OH)$_2$, CH$_3$OH, room temperature, 2 h, 78-82%.

Compounds **4**-**10** (Figure 4.2) were tested against PR-SET7 using nucleosome as a substrate, and against G9a and SET7/9 using in both cases the histone octamer as a substrate. The resulting EC$_{50}$ (effective compound concentration able to inhibit 50% of the enzyme activity) values are reported in Table 4.2. The bis(bromo- and dibromo-methoxyphenyl) derivatives **4**, **5**, **9**, and **10** as well as the bis(3,5-dibromo-4-hydroxyphenyl)methanone **6** were able to selectively inhibit PR-SET7, whereas the 4-phenylbut-3-en-2-ones **7** and **8** were totally ineffective. Against PR-SET7, the bis(3,5-dibromo-4-methoxyphenyl) analogs **5** and **10** displayed the highest potency, while the benzophenone **6** was the less potent. Selected compounds **4**, **5**, **9**, and **10** were then tested against EZH2 (Table 4.2). In this assay, the human 5-component PRC2 (containing EZH2, EED, SUZ12, RBAP48, and AEBP2) was used as the enzyme source, and histone H3 was used as a substrate. Against EZH2, the bis(3-bromo-4- methoxyphenyl) derivatives **4** and, to a lesser extent, **9** were the most effective inhibitors, suggesting that in this case the bis(3,5- dibromo) substitution, respect to the bis(monobromo) substitution, is detrimental for the inhibiting activity.

Compound	IC$_{50}$, (μM)			
	PR-SET7	G9a	SET7/9	EZH2 (IC$_{50}$ or % inhibition)
4	9.0	>250	>250	74.9
5	3.3	>250	>250	8.7% @ 75 μM
6	38.8	>250	>250	-
7	>250	>250	>250	-
8	>250	>250	>250	-
9	10.2	>250	>250	313.8
10	2.6	>250	164.4	6.2% @ 75 μM

Table 4.2. Inhibitory activity of compounds **4**-**10** on PR-SET7, G9a, SET7/9 and EZH2. Activity on EZH2 was determined only for the most interesting compounds. Values are means ± SD determined from at least three experiments.

Western blot analyses were performed with **4**, **5**, **9**, and **10** at 50 μM in human leukemia U937 cells treated for 24 h (Figure 4.3). H3 methylation marks, H3K4me1 H3K9me2 and H3K27me3, and H4K20me1 have been evaluated using specific antibodies. Concerning H4K20me1 compound **5** and, to a lesser extent, **9** and **10** displayed a signal reduction, in agreement with the PR-SET7 inhibitory data. Differently, H3K9me2 and H3K4me1 expression levels appear unmodified after treatment with **4**, **5**, **9**, and **10**, according to their lack of G9a and SET7/9 inhibitory activity. On the other hand, H3K27me3 strongly decreased after treatment with **4** and **9**, and was less evident with **5** and **10**, in accordance with their different degree of EZH2 inhibition.

Figure 4.3. Western blot analyses for compounds **4**, **5**, **9**, and **10** in U937 cells: levels of H3K4me1, H3K9me2, H4K20me1, and H3K27me3 methylation. Ponceau Red (PR) staining of histones or total histone H4 were used for equal loading.

Compounds **4**, **5**, **9**, and **10** were tested at 25 and 50 μM in human leukemia U937 cells for 30 h, to determine their effect on cell cycle, cell death (pre-G1 peak), and granulocytic differentiation (Figure 4.4). In the tested conditions, only derivatives **4** (at 25 μM) and **5** (at 25 and 50 μM) affected cell cycle, inducing a slight increase of the cells at the G1 phase. At 50 mM it was not possible to analyze the cell cycle effect of **4** due to the extensive cell death caused. As regards cell death induction (pre-G1 peak), at 50 μM compound **4** displayed a massive effect (near 100%, we considered a cut-off of 90%), and **5** induced 41% of cell death. Granulocytic differentiation was evaluated by determining the number of CD11c positive cells with subtraction of the propidium iodide (PI) positive cells (% CD11c+/PI- cells). In such assay, compounds **4** and **10** at 50 μM showed high differentiation effects, with 28 and 20% of CD11c positive cells.
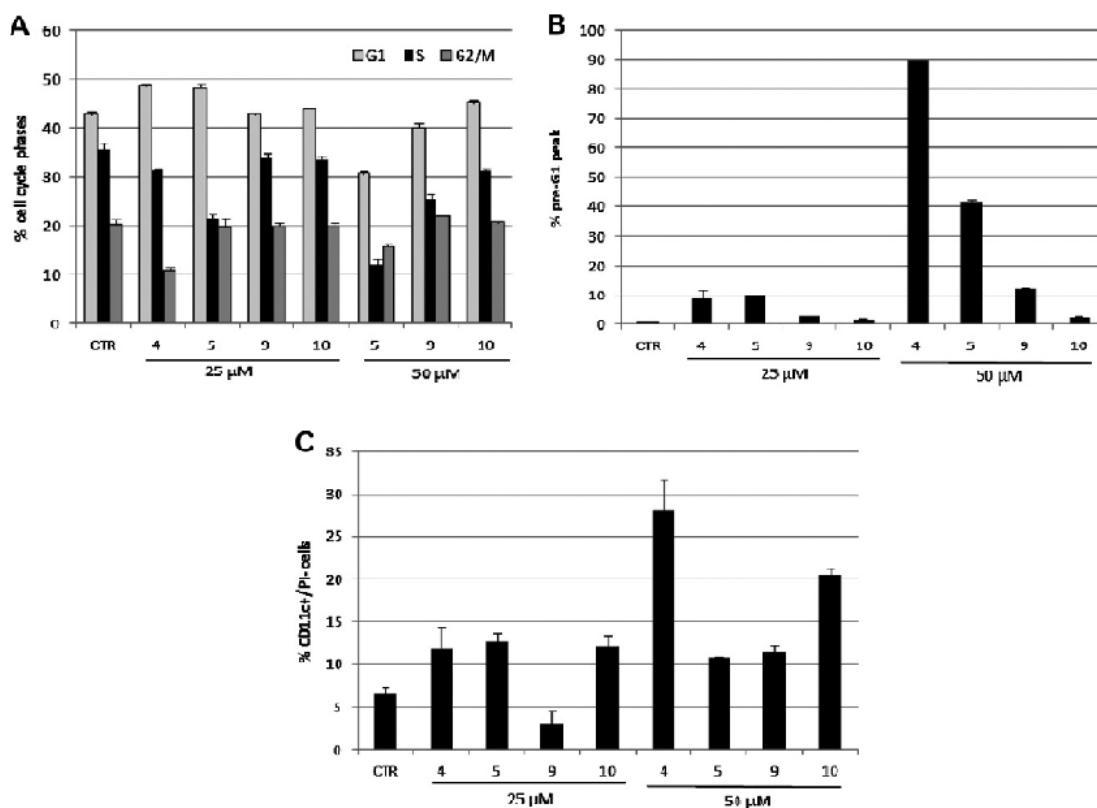
Figure 4.4. Effects of treatment of U937 cells with **4**, **5**, **9**, and **10** for 30 h at the indicated concentrations: A) Cell cycle effect; B) Cell death induction (pre-G1 peak); C) Granulocytic differentiation (CD11c method).

After these preliminary studies and with aim to shed light on to the effect of the solely bromine atom, we prepared other derivatives, removing the 4-methoxy substitution and progressively introducing a bromine substitution in ortho, meta and para of the two phenyl rings, separated by a penta-1,4-dien-3-one as spacer. We also explored the effect given by the central linker, maintaining the 3 bromo substitution as fixed and inserting different etero-aliphatic cyclic spacers. The above mentioned compounds were prepared by condensating etero-aliphatic ketones with 2 equivalents of the properly substituted benzaldehyde in presence of barium hydroxide in methanol at room temperature, and for the piperid-4-onic compounds, by performing the alkylation reaction with benzyl cloride in presence of K_2CO_3 in acetonitrile at room temperature or 60 °C (Scheme 4.2).
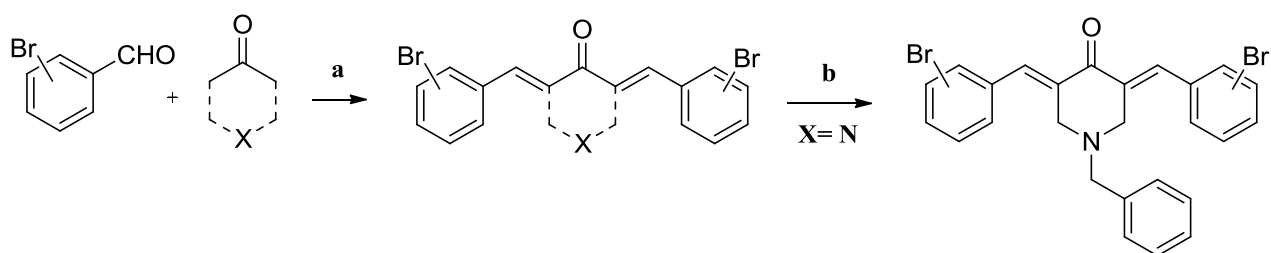
Scheme 4.2. Synthesis of bis-monobromine compounds; reagents and conditions: a) Ba(OH)$_2$, CH$_3$OH, R.T.; b) benzyl chloride, K$_2$CO$_3$, acetonitrile, R.T. or 60 °C

EZH2 assays were carried out using histone H3 as substrate and afforded results showing this general trend for the phenyl substitution position: ortho>meta>para (Table 4.3). Among the tested cyclic linkers, the *N*-benzyl moiety afforded the best enzymatic activity (**MC2884**: IC$_{50}$ = 46.4 μM) and was selected to confirm bromine substitution trend. Again, the bis-orthobromine analogue (**MC2908**) arose as the most effective derivative (IC$_{50}$ = 30.6 μM), even compared to the bis(3,5-dibromo) compound (**MC2910**) (Table 4.3).

Structure	Compound	X/Br position	IC$_{50}$, (μM) or % inhibition
	MC2911	CH$_2$	16% (75 μM)
	MC2912	O	36% (75 μM)
	MC2913	S	13% (75 μM)
	MC2914	N-CH$_3$	62.6
	MC2887	2	7.94
	MC1945	3	14.2
	MC2886	4	44.8
	MC3084	3,5	28% (75 μM)
	MC2908	2	30.6
	MC2884	3	46.4
	MC2909	4	66.9
	MC2910	3,5	11% (75 μM)

Table 4.3. Inhibitory activity on EZH2 of bis-monobromo series compounds. Values are means ± SD determined from at least three experiments.

To evaluate the activity *in vivo*, and specifically the effect on cell cycle and cell death (pre-G1 peak) cellular assays on U937 cells (human leukemia) were carried out at 25 µM for an incubation time of 30 h, using SAHA a well known HDAC inhibitor as positive reference (Figure 4.5).

In the tested conditions, *N*-benzyl derivatives exhibited effects on cell cycle distribution, in particular compound **MC2908**, namely the bis-orthobromine *N*-benzyl piperidone analogue, induced a strong arrest in all the cell cycle stages. Within the same series also the bis-meta (**MC2884**) and bis-para (**MC2910**) substituted derivative showed cell cycle activity, being able to lead to G1/S and G2 arrest, respectively. Among the other analogues, compound **MC2914** elicited an arrest in G1 and G2, with no cell detected in phase S. Likewise, N-benzyl piperidone compounds proved to exert pro-apoptotic effects, with particular regard to **MC2908**, which exhibited an extremely robust pre-G1 accumulation (more than 90% of the cells) in respect to the positive reference SAHA (Figure 4.5); this effect was so intense to require in the future a new measurement but at a lower concentration.
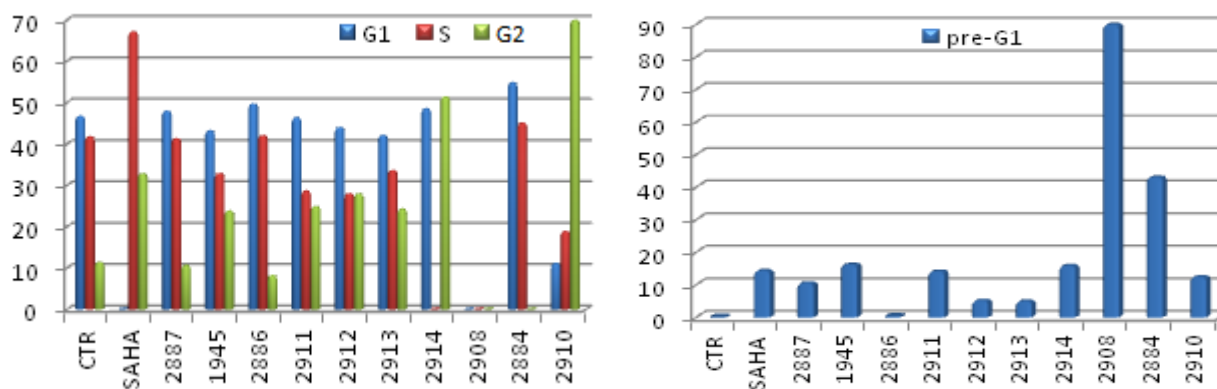
Figure 4.5. Celle cycle effect and pro-apoptotic induction in U937 leukemia cells.

To further investigate the potential of our bis-monobromo derivatives *in vivo*, we selected most active compounds: **MC2887**, **MC1945** and **MC2908**, to be tested on two different cell lines of colon cancer stem cells (colon CSC CRO and 1.1) and glioblastoma cancer stem cells (GBM CSC 30P and 30PT). These two cell lines strongly resemble the phenotype of cancer cells responsible for the recurrence of cancer in patients, and are useful models to predict the activity on highly undifferentiated cancer cells that are characteristic of the most advanced stages in tumors. Compounds **MC2887** and **MC2908**

showed comparable CC_{50} activity in the single digit or submicromolar range in each cell line of cancer stem cells and similarly to the *in vitro* and *in vivo* assay results showed above, they exhibited higher activity in respect to the bis-metabromine derivative **MC1945**, further confirming our initial phenyl rings substitution trend. Cellular activities were measured in triplicate and are reported as CC_{50} in Table 4.4 and 4.5.

compd	colon CSC CRO		colon CSC 1.1	
	CC_{50}, µM	slope	CC_{50}, µM	slope
MC2887	0.37	1.7	0.98	2
MC1945	5.25	2	11.4	3.9
MC2908	0.80	4.6	1.0	3.8

Table 4.4. Cellular activity of compounds MC2887, MC1945 and MC2908 on colon cancer stem cells.

compd	GBM CSC 30P		GBM CSC 30PT	
	CC_{50}, µM	slope	CC_{50}, µM	slope
MC2887	1.8	3.25	1.2	3
MC1945	27	5.4	26	2.5
MC2908	0.9	3	2.5	1.6

Table 4.5. Cellular activity of compounds MC2887, MC1945 and MC2908 on glioblastoma cancer stem cells.

After subsequent studies on 3,5-bis(3-bromine-4-hydroxybenzylidene)piperid-4-one analogues, originally developed as CARM1 and PRMT5 selective inhibitors, another

compound (**MC2298)**, bearing a *N*-(2-oxo-phenylethyl) substitution, ascended into prominence as EZH2 inhibiting hit compound (Figure 4.6).

According to our previous results and knowledge on phenyl "wings" substitutions patterns, and in the perspective of increasing enzymatic activity on EZH2, we decided to remove the 4-hydroxy substituent and to shift the bromine atom in ortho and meta of the phenyl rings. Furthermore, since we hypothesized that the enhance in activity could be due by the insertion of the benzoyl carbonyl group we planned to explore this effect by increasing in turn its distance from the phenyl substituent and the nitrogen of the piperidonic scaffold. Moreover we also designed some derivatives lacking the carbonyl group, thus bearing only a ω-phenyl aliphatic chain moiety (Figure 4.6).
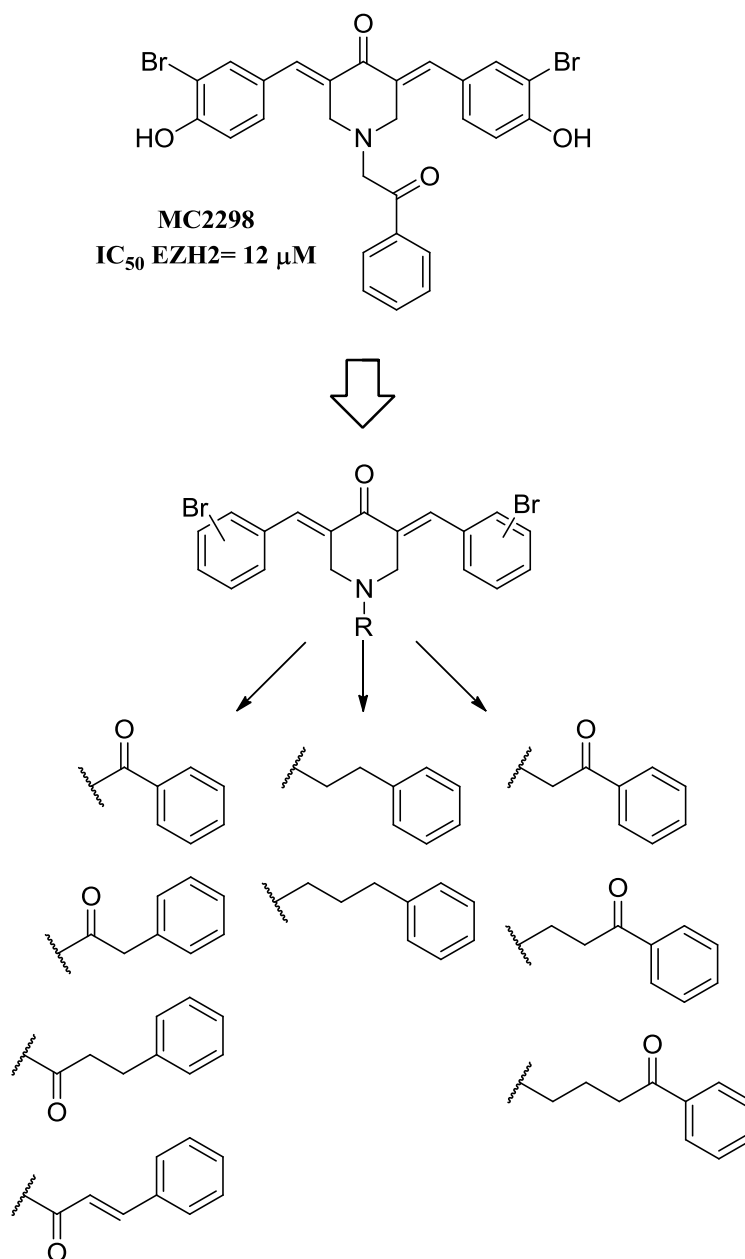
Figure 4.6. Structure of MC2298 and MC2298-like derivatives.

Likewise to the previously described compounds, the central nucleus was prepared by condensing the piperid-4-one with 2 equivalents of the properly substituted benzaldehyde in presence of barium hydroxide and methanol. Subsequent *N*-alkylation with corresponding chloride was performed with K_2CO_3 in acetonitrile at room temperature or heating to 60°C, whereas the *N*-acyl series was obtained by treating the common intermediate with respective acylclorides in presence of triethylamine and DCM at 0°C. Finally the 4-phenyl-butan-4-one derivative was achieved by reductive amination of the common piperidone with the proper aldehyde (Scheme 4.3).
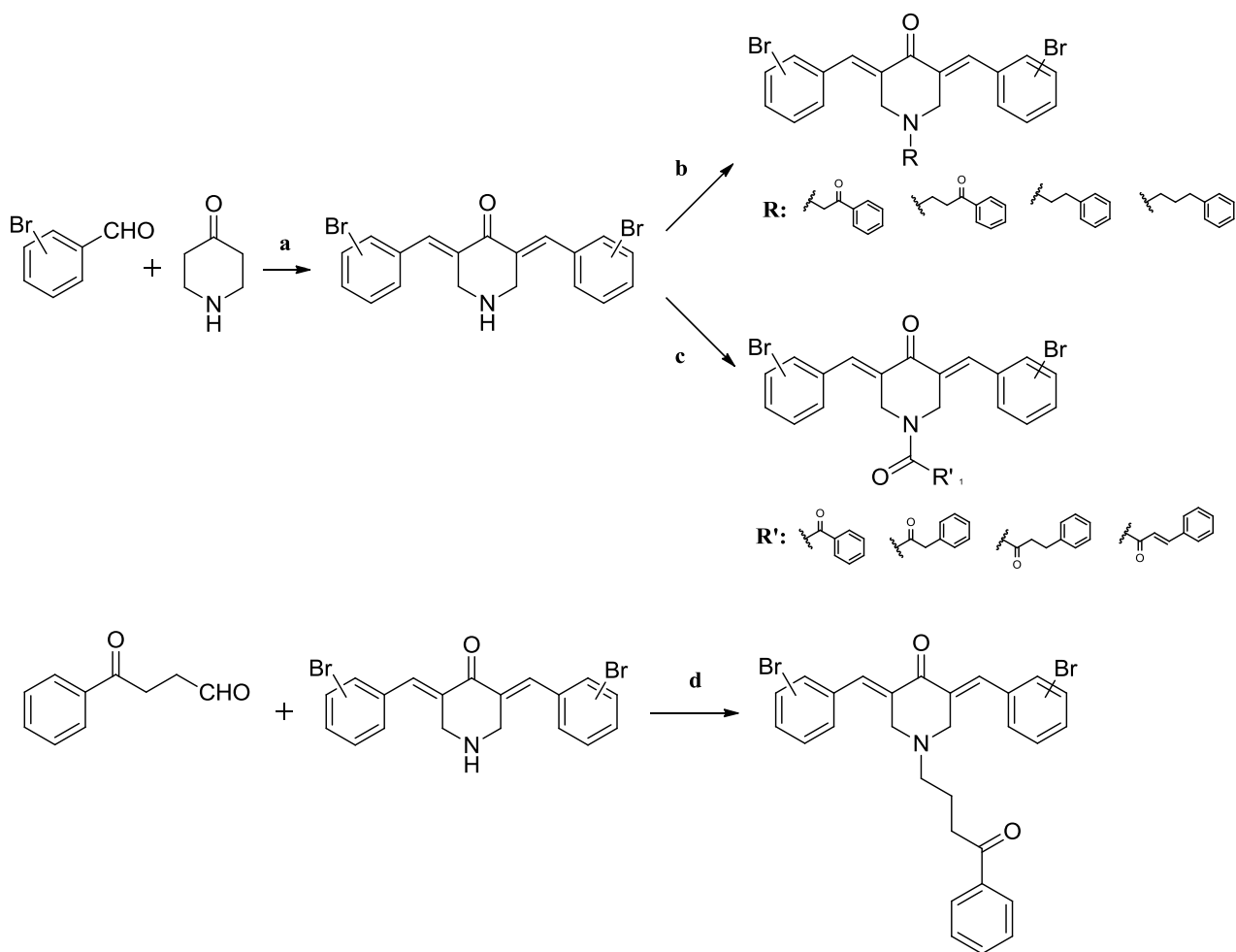
Scheme 4.3. Synthesis of MC2298-like compounds; reagents and conditions: a) $Ba(OH)_2$, CH_3OH, R.T.; b) $PhCO(CH_2)_nCl/Ph(CH_2)_nCl$, K_2CO_3, CH_3CN, R.T. or 60°C; c) Et_3N, RCOCl, DCM, 0°C; d) $(AcO)_3BHNa$, DCM, R.T.

Compound	Structure	M.P. (°C)	Solvent of crystallization	Yield (%)
MC3127		124-126	Cyclohexane/Benzene	76
MC3146		135-137	Cyclohexane/Benzene	78

Compound	Structure	M.P. (°C)	Solvent of crystallization	Yield (%)
MC3128		126-128	Cyclohexane/Benzene	67
MC3183		139-141	Cyclohexane/Benzene	70
MC3141		95-97	Cyclohexane	69
MC3187		113-115	Cyclohexane	67
MC3182		98-100	Cyclohexane	60
MC3206		106-108	Cyclohexane	63
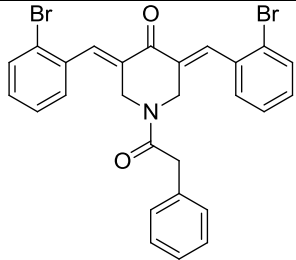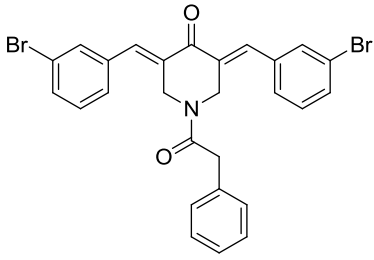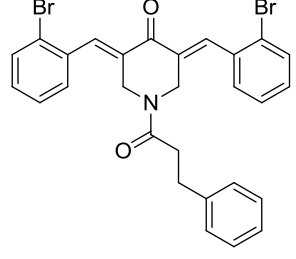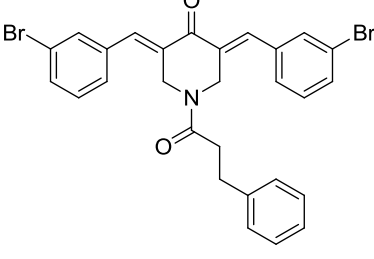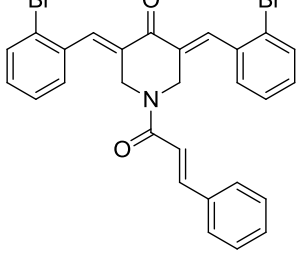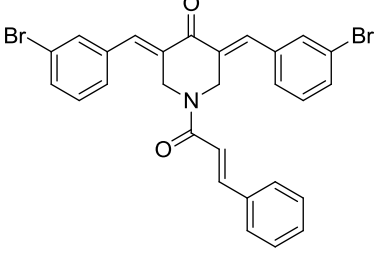
Compound	Structure	M.P. (°C)	Solvent of crystallization	Yield (%)
MC3201		109-111	Cyclohexane	78
MC3207		121-123	Cyclohexane/Benzene	75
MC3208		95-97	Cyclohexane	69
MC3199		100-102	Cyclohexane	71
MC3243		84-86	Cyclohexane	74
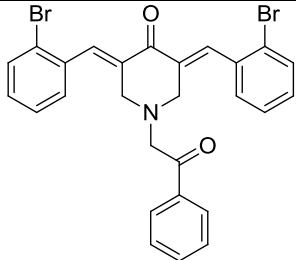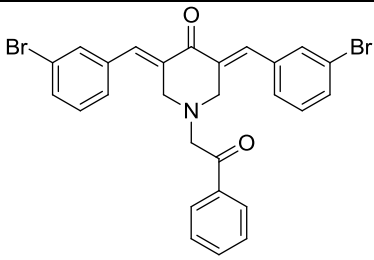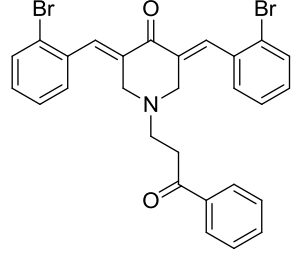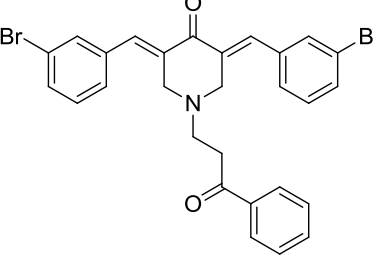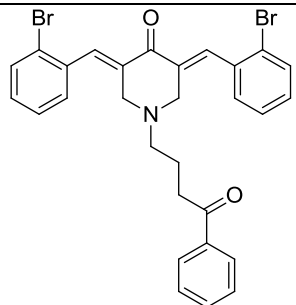
Compound	Structure	M.P. (°C)	Solvent of crystallization	Yield (%)
MC3240		93-95	Cyclohexane	70
MC3268		105-107	Cyclohexane	65
MC3269		120-123	Cyclohexane/Benzene	63
MC3271		93-95	Cyclohexane	67
MC3272		121-123	Cyclohexane/Benzene	75
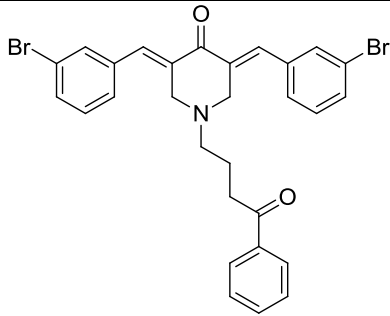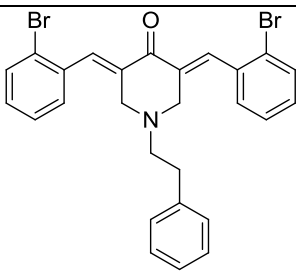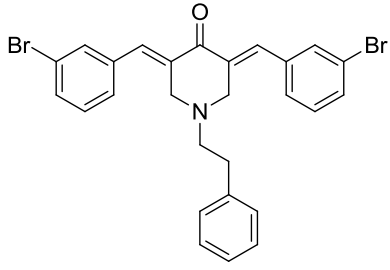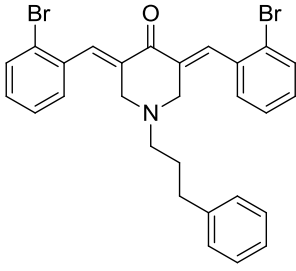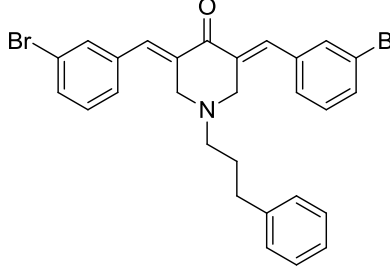
Table 4.6. Physico-chemical data of MC2298-like compounds.

Compounds were initially tested *in vitro* on EZH2 in single dose duplicate mode at a concentration of 100 μM to preliminary evaluate their activity. Assay reactions were carried out at 1 μM of SAM and results, expressed as percentage of inhibition, are reported in table 4.7.

Compound	EZH2 % inhibition
MC3127	28.69
MC3146	2.15
MC3128	34.90
MC3183	38.63
MC3141	15.79
MC3187	28.02
MC3182	N.I.
MC3206	32.62
MC3201	28.15
MC3207	23.31
MC3208	37.61
MC3199	N.I.
MC3243	17.99
MC3240	36.81
MC3268	22.37
MC3269	20.30
MC3271	15.15
MC3272	22.14

Table 4.7. Enzymatic activity expressed as percentage of inhibition on EZH2. N.I: No Inhibition

In vivo activity for described compounds was assessed on U937 cells. Evaluation on cell cycle, pro-apoptotic effect (pre-G1 arrest) and cytodifferetiating effect were obtained by treating leukemia cells for 30 hours at a dose of 25 μM of our compounds and using SAHA and MS-275 (also known as SNDX-275), two well known HDACs inhibitors, as positive references (25 μM). Cellular assessment results are displayed only for compounds showing most interesting compounds (Figure 4.7). As shown, compounds **MC3127**, **MC3128**, **MC3141** and **MC3187** and **MC3206**, namely compounds in which the

piperidone scaffold and phenyl ring are connected by an *N*-acyl bond, exhibited a strong G1 arrest comparable with MS275 reference, with no cell detected in S phase, except for the analogue **MC3127** which however showed a reduced number of cells in this phase in comparison with the control. Likewise, these compounds also induced a robust accumulation in the G2 phase (around 40%), again **MC3127** was the less effective in this sense. Compounds **MC3199**, **MC3201**, **MC3207** and **MC3240**, derivatives obtained by N-alkylation of piperidone and showing the carbonyl group flanking the phenyl ring, led to cell cycle alterations, decreasing the number of cell in G1 phase and inducing a remarkable arrest in G2 phase (around 40%)(Figure 4.7, A).

Accordingly with our previously and aforementioned results, bis-orthobromine substitution of phenyl rings afforded higher activity in respect to corresponding bis-metasubstituted compounds, as can be readily appreciated comparing the cell cycle profile of **MC3128** and **MC3127** with **MC3146** and **MC3183**, respectively bis-ortho and bis-meta derivatives of *N*-benzoyl and *N*-phenylacetyl analogues. Instead, out of line with the general trend bis-ortho *N*-cinnamoyl analogue **MC3183** showed less cellular activity in respect to the corresponding bis-meta compound **MC3206** (Figure 4.7 A).

Concerning the pro-apoptotic induction, all the MC2298-like compounds displayed higher activity in comparison to the control. Moreover compounds **MC3199**, **MC3201**, **MC3207** and **MC3240**, the same inducing cell cycle alteration in G1 and G2 phase, exhibited an outstanding pro-apoptotic activity (around 30-40%), which is comparable with the FDA approved drug SAHA (Figure 4.7, B).
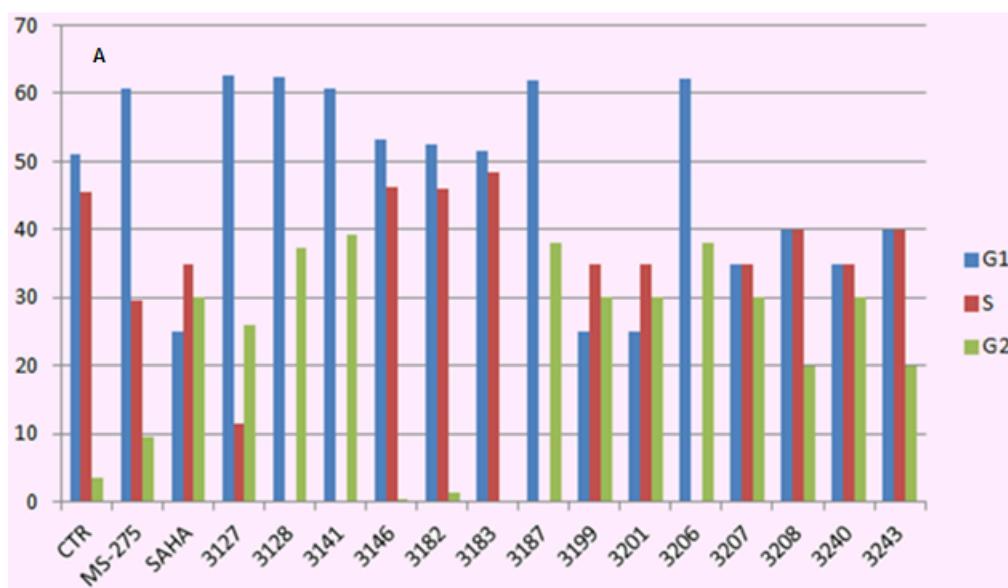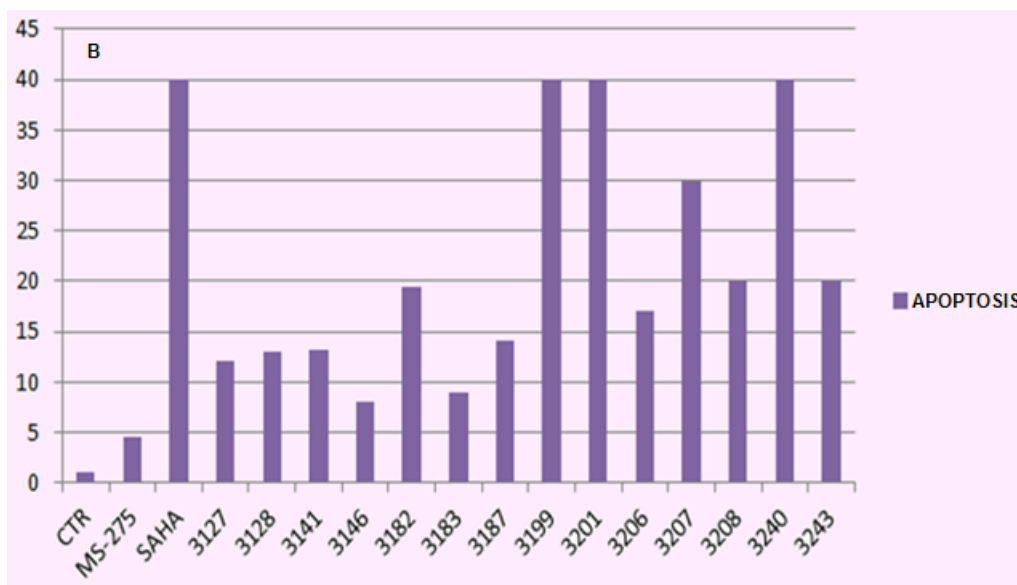
Figure 4.7. MC2298-like compounds cellular assay results. A) Cell cycle effects on U937 leukemia cells. B) Pro-apoptotic induction on U937 cells.

To confirm the activity of our compounds western blot analyses were performed on U937 leukemia cells (Figure 4.8) using histone H4 and Ponceau Red as reference and SAHA and MS275 as negative control. Compounds were tested at 10 µM and after an exposure time of 15 minutes. For experimental procedure regarding the assay and the histone extraction see the experimental part section.

Figure 4.8. Western blot analysis results.

Experimental section

Chemistry. Melting points were determined on a Buchi 530 melting point apparatus. ^{1}H-NMR and ^{13}C-NMR spectra were recorded at 400 MHz using a Bruker AC 400 spectrometer; chemical shifts are reported in δ (ppm) units relative to the internal reference tetramethylsilane (Me$_4$Si). Mass spectra were recorded on a API-TOF Mariner by Perspective Biosystem (Stratford, Texas, USA), samples were injected by an Harvard pump using a flow rate of 5−10 μL/min, infused in the Electrospray system. All compounds were routinely checked by TLC and 1H NMR. TLC was performed on aluminum-backed silica gel plates (Merck DC, Alufolien Kieselgel 60 F254) with spots visualized by UV light or using a KMnO$_4$ alkaline solution. All solvents were reagent grade and, when necessary, were purified and dried by standard methods. Concentration of solutions after reactions and extractions involved the use of a rotary evaporator operating at reduced pressure of ~ 20 Torr. Organic solutions were dried over anhydrous sodium sulfate. Elemental analysis has been used to determine purity of the described compounds, that is >95%. Analytical results are within 0.40% of the theoretical values. All chemicals were purchased from Sigma Aldrich s.r.l., Milan (Italy) or from TCI Europe N.V., Zwijndrecht (Belgium), and were of the highest purity. As a rule, samples prepared for physical and biological studies were dried in high vacuum over P$_2$O$_5$ for 20h at temperatures ranging from 25 to 40 °C, depending on the sample melting point.

Syntheses of compounds **4**-**8** was carried out as reported in literature and their chemical and physical data can be found at Ref. 211.

General Procedure for the synthesis of the 2,6-bis(3-bromo and 3,5-dibromo-4-methoxybenzylidene)cyclohexanones (9-10).

Example: synthesis of 2,6-bis(3-bromo-4-methoxybenzylidene) cyclohexanone (9).
Cyclohexanone (1.15 mmol, 0.12 mL) was added to a suspension of barium hydroxide octahydrate (4.6 mmol, 1.45 g) in methanol (20 mL), and the mixture was stirred for 5 min. Then a solution of 3- bromo-4-methoxybenzaldehyde (2.3 mmol, 0.5 g) in methanol (10 mL) was added, and the resultant mixture was stirred for 2 h at room temperature. The precipitate was filtered, washed with water, dried and recrystallized by acetonitrile to afford the pure product. Melting point: 170-172 °C; yield: 82%; ^{1}H-NMR (DMSO-d_6) δ_H/ppm: 1.72-1.75 (m, 2H, cyclohexanone protons), 2.86-2.89 (m, 4H, cyclohexanone

protons), 3.90 (s, 6H, OCH_3), 7.19-7.21(d, 2H, benzene protons), 7.55-7.59 (m, 4H, benzene protons and PhCH=CCO), 7.78 (s, 2H, benzene protons); ^{13}C-NMR (DMSO-d_6) δ_C/ppm 25.1, 26.1 (2C), 55.1 (2C), 112.1 (2C), 112.2 (2C), 128.4 (2C), 129.2 (2C), 130.9 (2C), 132.2 (2C), 137.1 (2C), 156.2 (2C), 190.4; MS (EI): m/z [M+H]$^+$: 491.98.

2,6-bis(3,5-dibromo-4-methoxybenzylidene)cyclohexanone (10). ^{1}H-NMR (DMSO-d_6) δ_H/ppm: 1.73-1.76 (m, 2H, cyclohexanone protons), 2.84-2.87 (m, 4H, cyclohexanone protons), 3.84 (s, 6H, OCH_3), 7.51 (s, 2H, PhCH=CCO), 7.83 (s, 4H, benzene protons); ^{13}C-NMR (DMSO-d_6) δ_C/ppm:δ 25.1, 26.1 (2C), 60.8 (2C), 118.3 (4C), 129.9 (4C), 131.9 (2C), 132.2 (2C), 137.1 (2C), 154.2 (2C), 190.4; Recrystallized by: acetonitrile; melting point: 204-206 °C; yield: 78%; MS (EI): m/z [M+H]$^+$: 649.80.

General Procedure for the synthesis of 1,5-bis(2/3-bromobenzylidene)penta-1,4-dien-3-ones, 2,6- bis(2/3-bromobenzylidene)-cyclohexanones, 3,5 bis(2/3-bromobenzylidene)-pyranones, -thiopyranones, N-methyl and N-benzylpiperidones.
Example: synthesis of (3E,5E)-1-benzyl-3,5-bis(3-bromobenzylidene)piperidin-4-one (MC 2884). 1-benzylpiperidin-4-one (1.06 mmol, 0.2 mL) was added to a suspension of barium hydroxide octahydrate (4.24 mmol, 1.34 g) in methanol (10 mL), and the mixture was stirred for 5 min. Then a solution of 3- bromo-benzaldehyde (2.12 mmol, 0.39 g) in methanol (10 mL) was added, and the resultant mixture was stirred at room temperature. After 2 hours water was added and the resulting suspension was filtered, the precipitate was washed with water (3 x 10 mL), dried and recrystallized by acetonitrile to afford the pure product. m.p.: 238-240 °C; yield: 78%; ^{1}H-NMR (DMSO-d_6) δ_H/ppm: 3.71 (s, 2H, PhCH_2), 3.81 (s, 4H, N(CH_2)$_2$, 7.19 (s, 5H, benzene protons), 7.37-7.45 (m, 4H, benzene protons), 7.60-7.65 (m, 6H, benzene protons and PhCH=CCO); ^{13}C-NMR (DMSO-d_6) δ_C/ppm: 53.4 (2C), 64.4, 123.0 (2C), 127.2, 127.5 (2C), 128.4 (2C), 128.8 (2C), 129.6 (2C), 130.8 (2C), 132.6, 132.7 (2C), 136.1 (2C), 140.6 (2C), 145.9 (2C), 186.0; MS (EI): m/z [M+H]$^+$: 523.46.

(3E,5E)-2,6-bis(3-bromobenzylidene)cyclohexan-4-one (MC 2911). ^{1}H-NMR (DMSO-d_6) δ_H/ppm: 1,73 (m, 2H, cyclohexanone ring), 2.88 (m, 4H, cyclohexanone ring), 7.41-7.44 (m, 2H, PhCH=CCO), 7.54-7.61 (m, 6H, benzene protons), 7.73 (s, 2H, benzene

protons); ^{13}C-NMR (DMSO-d_6) δ_C/ppm: 22.7, 25.3 (2C), 115.1 (2C), 126.9 (2C), 128.0 (2C), 130.8 (2C), 131.5 (2C), 135.2 (2C), 138.8 (2C), 185.4; recrystallized by benzene/acetonitrile; for m.p. see literature[212]; yield 69%; MS (EI): m/z [M+H]$^+$: 429.87.

(3E,5E)-3,5-bis(3-bromobenzylidene)dihydro-2H-pyran-4(3H)-one (MC 2912). ^{1}H-NMR (DMSO-d_6) δ_H/ppm: 4.91 (s, 4H, O(CH_2)$_2$, 7.43-7.45 (m, 4H, benzene protons), 7.65-7.69 (m, 6H, benzene protons and PhCH=CCO); ^{13}C-NMR (DMSO-d_6) δ_C/ppm: 67.3 (2C), 123.0 (2C), 127.5 (2C), 129.6 (2C), 130.8 (2C), 132.7 (2C), 136.1 (2C), 143.8 (2C), 146.1 (2C), 186.0; recrystallized by benzene/acetonitrile; m.p. 170-172 °C: yield: 83%; MS (EI): m/z [M+H]$^+$: 433.93.

(3E,5E)-3,5-bis(3-bromobenzylidene)dihydro-2H-thiopyran-4(3H)-one (MC 2913). ^{1}H-NMR (DMSO-d_6) δ_H/ppm: 3.97 (s, 4H, O(CH_2)$_2$, 7.41-7.45 (t, 2H, benzene protons), 7.53-7.57 (m, 4H, benzene protons), 7.61-7.63 (d, 2H, benzene protons), 7.73 (s, 2H, PhCH=CCO); ^{13}C-NMR (DMSO-d_6) δ_C/ppm: 30.2 (2C), 123.0 (2C), 127.5 (2C), 129.6 (2C), 130.8 (2C), 132.7 (2C), 136.1 (2C), 139.0 (2C), 146.9 (2C), 186.0; recrystallized by benzene, m.p.; 148-150 °C; yield: 80%; MS (EI): m/z [M+H]$^+$: 449.91.

(3E,5E)-3,5-bis(3-bromobenzylidene)-1-methylpiperidin-4-one (MC 2914). ^{1}H-NMR (DMSO-d_6) δ_H/ppm: 2.39 (s, 3H, CH_3), 3.73 (s, 4H, N(CH_2)$_2$, 7.42-7.46 (t, 2H, benzene protons), 7.50-7.52 (d, 2H, benzene protons),7.57 (s, 2H, benzene protons),7.62-7.64 (d, 2H, benzene protons), 7.71 (s, 2H, PhCH=CCO); ^{13}C-NMR (DMSO-d_6) δ_C/ppm: 45.0, 56.0 (2C), 123.0 (2C), 127.5 (2C), 129.6 (2C), 130.8 (2C), 132.7 (2C), 136.1 (2C), 140.6 (2C), 145.9 (2C), 186.0; recrystallized by cyclohexane/benzene; m.p.: 130-132 °C; yield: 74%; MS (EI): m/z [M+H]$^+$: 446.97.

(1E,4E)-1,5-bis(2-bromophenyl)penta-1,4-dien-3-one (MC 2887). ^{1}H-NMR (DMSO-d_6) δ_H/ppm: 7.34-7.42 (4H, m, benzene protons and PhCH=CHCO), 7.49-7.52 (t, 2H, benzene protons), 7.75-7.77 (d, 2H, benzene protons), 7.95-8.00 (m, 4H, benzene protons and PhCH=CHCO); ^{13}C-NMR (DMSO-d_6) δ_C/ppm: 120.3 (2C), 122.9 (2C), 125.1 (2C), 127.9

(2C), 128.7 (2C), 133.0 (2C), 138.1 (2C), 147.1 (2C), 183.3; for m.p. see literature[213], yield: 71%; MS (EI): m/z [M+H]$^+$: 389.56.

(1E,4E)-1,5-bis(3-bromophenyl)penta-1,4-dien-3-one (MC 1945). ^{1}H-NMR (DMSO-d_6) δ_H/ppm: 7.38-7.44 (m, 4H, benzene protons and PhCH=C*H*CO), 7.63-7.65 (d, 2H, benzene protons), 7.75-7.79 (m, 4H, benzene protons and PhC*H*=CHCO), 8.04 (s, 2H, benzene protons); ^{13}C-NMR (DMSO-d_6) δ_C/ppm:123.0 (2C), 123.3 (2C), 127.5 (2C), 129.6 (2C), 130.8 (2C), 133.1 (2C), 137.4 (2C), 142.2 (2C), 188.6; recrystallized by methanol; m.p.: 118-120 °C; yield: 97%; MS (EI): m/z [M+H]$^+$: 391.91.

(1E,4E)-1,5-bis(4-bromophenyl)penta-1,4-dien-3-one (MC 2886). ^{1}H-NMR (DMSO-d_6) δ_H/ppm: 7.36-7.40 (d, 2H, PhC*H*=CHCO), 7.69-7.98 (m, 10H, benzene protons and PhCH=C*H*CO); ^{13}C-NMR (DMSO-d_6) δ_C/ppm: 119.8 (2C), 123.1 (2C), 125.8 (4C), 133.7 (4C), 135.0 (2C), 140.3 (2C), 183.6; for m.p. see literature[214]; yield: 81%; MS (EI): m/z [M+H]$^+$: 389.43.

(1E,4E)-1,5-bis(3,5-dibromophenyl)penta-1,4-dien-3-one (MC 3084). ^{1}H-NMR (DMSO-d_6) δ_H/ppm: 7.43-7.47 (d, 2H, PhCH=C*H*CO), 7.72-7.76 (d, 2H, PhC*H*=CHCO), 7.92 (s, 2H, benzene protons), 8.06 (s, 4H, benzene protons); ^{13}C-NMR (DMSO-d_6) δ_C/ppm: 123.3 (6C), 128.9 (4C), 133.9 (2C), 142.2 (2C), 144.1 (2C), 188.6; recrystallized by acetonitrile; m.p.: 230-232 °C; yield: 70%; m/z [M+H]$^+$: 549.74

(3E,5E)-1-benzyl-3,5-bis(2-bromobenzylidene)piperidin-4-one (**MC 2908**). ^{1}H-NMR (DMSO-d_6) δ_H/ppm: 3.60 (s, 2H, PhC*H$_2$*), 3.71 (s, 4H, N(C*H$_2$*)$_2$), 7.16 (s, 5H, benzene protons), 7.30-7.42 (m, 7H, benzene protons), 7.73-7.75 (m, 4H, benzene protons and PhC*H*=CCO); ^{13}C-NMR (DMSO-d_6) δ_C/ppm: 53.4 (2C), 64.4, 125.2 (2C), 127.0 (2C), 127.2, 127.5 (2C), 127.6 (2C), 128.4 (2C), 128.8 (2C), 132.6 (3C), 134.3 (2C), 140.6 (2C), 145.9 (2C), 186.0; recrystallized by benzene; m.p.: 144-146 °C; yield: 82%; MS (EI): m/z [M+H]$^+$: 522.70.

(3E,5E)-1-benzyl-3,5-bis(4-bromobenzylidene)piperidin-4-one (MC 2909). ^{1}H-NMR (DMSO-d_6) δ_H/ppm: 3.71 (s, 2H, PhCH_2), 3.80 (s, 4H, N(CH_2)$_2$), 7.20-7.25 (m, 5H, benzene protons), 7.39 (m, 4H, benzene protons), 7.58-7.64 (m, 6H, benzene protons and PhCH=CCO); ^{13}C-NMR (DMSO-d_6) δ_C/ppm: 53.0 (2C), 57.8, 124.0 (2C), 125.3, 126.8 (2C), 128.3 (2C), 130.7 (4C), 133.0 (4C), 134.9, 136.3 (2C), 138.9 (2C), 141.7 (2C), 187.4; m.p.: 178-180 °C; yield: 73%; MS (EI): m/z [M+H]$^+$: 523.78.

(3E,5E)-1-benzyl-3,5-bis(3,5-dibromobenzylidene)piperidin-4-one (MC 2910). ^{1}H-NMR (DMSO-d_6) δ_H/ppm: 3.71 (s, 2H, PhCH_2), 3.79 (s, 4H, N(CH_2)$_2$), 7.22 (s, 4H, benzene protons), 7.56 (s, 2H, benzene protons), 7.87 (s, 2H, PhCH=CCO); ^{13}C-NMR (DMSO-d_6) δ_C/ppm: 53.4 (2C), 64.4, 123.3 (4C), 127.2, 128.4 (2C), 128.8 (2C), 128.9 (4C), 132.6, 133.9 (2C), 139.6 (2C), 140.6 (2C), 145.9 (2C), 186.0; recrystallized by benzene/acetonitrile; m.p.: 178-180 °C; yield: 73%; MS (EI): m/z [M+H]$^+$: 680.82.

General procedure for the synthesis of *N*-acyl 3,5-bis(2/3-bromobenzylidene)piperidin-4-onic compounds. Example: synthesis of (3E,5E)-3,5-bis(3-bromobenzylidene)-1-(3-phenylpropanoyl) piperidin-4-one (MC3187).

To a stirring solution of (3E,5E)-3,5-bis(3-bromobenzylidene)piperidin-4-one (0.45 mmol, 195 mg) and Et$_3$N (0.76 mmol, 0.11 mL) in dry dichloromethane (5 mL), hydrocynnamicacyl chloride (0.67 mmol, 0.1 mL) was slowly added at 0 °C. The resulting mixture is then allowed to stir at room temperature. After 1 hour the reaction was quenched with water (50 mL) and extracted with dichloromethane (3 x 30 mL). The collected organic layers were washed with HCl 2N (3 x 30 mL) and then with a saturated solution of NaCl (30 mL). The organic phase was dried with anhydrous Na$_2$SO$_4$, filtered and evaporated under vacuum to afford a crude that was then purified on silica gel (AcOEt/n-hexane 1:3) to afford the desired product (170 mg, 67%). ^{1}H-NMR (DMSO-d_6) δ_H/ppm: 2.45-2.49 (t, 2H, -COCH_2), 2.83-2.87 (t, 2H, PhCH_2), 4.57 (s, 2H, -NCH_2), 4.90 (s, 2H, -NCH_2), 6.98-7.00 (d, 2H, benzene protons), 7.18-7.63 (m, 9H, benzene protons), 7.77 (s, 2H, benzene protons); ^{13}C-NMR (DMSO-d_6) δ_C/ppm: 31.4, 33.6, 47.4 (2C), 123.0 (2C), 125.9, 127.5 (2C), 127.7 (2C), 128.6 (2C), 129.6 (2C), 130.8 (2C), 132.7 (2C), 136.1 (2C), 140.6 (2C), 141.3, 145.9 (2C), 172.3, 186.0; MS (EI): m/z [M+H]$^+$: 565.24.

General procedure for the synthesis of *N*-alkyl 3,5-bis(2/3-bromobenzylidene)piperidin-4-onic compounds. Example: synthesis of (3E,5E)-3,5-bis(3-bromobenzylidene)-1-(4-oxo-4-phenylbutyl)piperidin-4-one (MC 3243). To a stirring solution of (3E,5E)-3,5-bis(3-bromobenzyliden)piperidin-4-one (0.46 mmol, 0.2 g) and 4-oxo-4-phenylbutanal (0.46 mmol, 0.075 g) in dry dichlorometane (10 mL), sodium triacetoxy borohydride (0.55 mmol, 0.117 g) was added portionwise and the resulting suspension is stirred at room temperature. After two hours the reaction was quenched with H_2O (30 mL) and extracted with dichloromethane (4 x 20 mL). The collected organic phases were then washed with a saturated solution of NaCl (30 mL) and then dried with anhydrous Na_2SO_4, filtered and evaporated under vacuum to afford a crude that was purified on silica gel (AcOEt/n-hexane 1:3) to obtain the desired compound (197 mg, 74%). ^{1}H-NMR (DMSO-d_6) δ_H/ppm: 1.90-1.94 (m, 2H, -NCH₂C*H*₂CH₂CO-), 2.65-2.68 (t, 2H, -NC*H*₂CH₂CH₂CO-), 2.97-3.01 (t, 2H, -NCH₂CH₂C*H*₂CO-), 3.80 (s, 4H, piperidonic protons), 7.32-7.33 (m, 4H, benzene protons), 7.40-7.44 (t, 2H, benzene protons), 7.52-7.54 (m, 5H, benzene protons), 7.72 (s, 2H, PhC*H*=CCO), 7.89-7.91 (d, 2H, benzene protons); ^{13}C-NMR (DMSO-d_6) δ_C/ppm: 22.2, 36.4, 53.8 (2C), 56.9, 123.0 (2C), 127.5 (2C), 128.6 (2C), 128.8 (2C), 129.6 (2C), 130.8 (2C), 132.7 (2C), 133.1, 136.1 (2C), 136.7, 140.6 (2C), 145.9 (2C), 186.0, 200.1; MS (EI): *m/z* [M+H]$^+$: 578.87.

General procedure for the synthesis of N-alkylphenyl piperidonic compounds. Example: **synthesis of (3E,5E)-3,5-bis(2-bromobenzyliden)-1-(3-phenylpropyl) piperidin-4-one (MC 3271).** To a suspension of anhydrous K_2CO_3 (0.69 mmol, 0.954 g) in acetonitrile (10 mL), the (3E,5E)-3,5-bis(2-bromobenzyliden)piperidin-4-one (0.46 mmol, 0.2 g) and the 3-bromo-1-phenylpropane (1.38 mmol, 0.21 mL) were added and the resulting suspension was stirred at 60 °C. After 2 hours the solvent was evaporated, water (50 mL) was added and the aqueous solution was extracted with dichloromethane (3 x30 mL). The collected organic phases were washed with a saturated solution of NaCl (30 mL) and then dried with anhydrous Na_2SO_4, filtered and evaporated under vacuum to afford a crude that was purified on silica gel (AcOEt/n-hexane 1:3) to obtain the desired compound (170 mg, 67%). ^{1}H-NMR (DMSO-d_6) δ_H/ppm: 1.65-1.71 (m, 2H, -NCH₂C*H*₂CH₂Ph), 2.47-

2.51 (t, 2H, -NCH$_2$CH$_2$C*H*$_2$Ph), 2.54-2.58 (t, 2H, -NC*H*$_2$CH$_2$CH$_2$Ph), 3.68 (s, 4H, piperidonic protons), 7.05-7.38 (m, 11H, benzene protons), 7.67-7.69 (d, 2H, benzene protons), 7.96 (s, 2H, PhC*H*=CCO); ^{13}C-NMR (DMSO-d_6) δ_C/ppm:27.5, 31.0, 53.8 (2C), 57.0, 125.2 (2C), 126.0, 127.0 (2C), 127.5 (2C), 127.6 (2C), 128.1 (2C), 128.8 (2C), 132.6 (2C), 134.3 (2C), 140.6 (2C), 142.0, 145.9 (2C), 186.0; MS (EI): *m/z* [M+H]$^+$: 551.41.

Biochemical assay procedures for compound 1-10

2.2.1. PR-SET7, G9a, and SET7/9 inhibitory assays Assays were performed essentially as described previously for PR-SET7[215], G9a[208], and SET7/9[216]. Briefly, the samples were incubated at 30 °C for 10-60 min in a reaction buffer containing 50 mM TriseHCl (pH 8.5), 5 mM MgCl$_2$, 4 mM DTT, and 1 mM Sadenosyl- L-[methyl-3H]methionine (Amersham Pharmacia Biotech). Two micrograms of octamer, oligonucleosomes, or mononucleosome were used as substrates. The total volume of the reaction mixture was adjusted to 25 mL. The reaction was stopped by addition of SDS sample buffer and then fractionated on 15% SDSPAGE. Separated histones were then transferred onto an Immobilon-P membrane (Millipore) and visualized by CBB staining. The membrane was sprayed with EN3HANCE (NEN), and exposed to Kodak XAR film overnight.

EZH2 inhibitory assay

Reagent. Reaction buffer; 50 mM TriseHCl (pH 8.0), 50 mM NaCl, 1 mM EDTA, 1 mM DTT, 1 mM PMSF, 1% DMSO.

Reaction conditions. EZH2: Complex of human EZH2 (Gen- Q1 Bank Accession No. NM_004456), (amino acids 2-end) with N-terminal His tag, MW = 86 kDa, human EED (NM_003797) (a-a 2-end) with N-terminal Flag tag, MW = 51 kDa, human SUZ12 (NM_015355) (a-a 2-end) with N-terminal His tag, MW = 87 kDa, Human AEBP2 (NM_153207) (a-a 2-end) with N-terminal His tag, MW = 53 kDa, and human RbAp48 (NM_005610) (a-a 2-end) with N-terminal His tag, MW = 48 kDa, co-expressed in baculovirus expression system. Substrate: 5 mM Histone H3. Methyl donor: 1 mM S-adenosyl-L-[methyl-3H]methionine. Enzyme: 100 nM EZH2 complex. Reaction Procedure: prepare indicated substrate in freshly prepared reaction buffer; deliver EZH2 into the substrate solution and mix gently; deliver compounds in DMSO into the EZH2 reaction mixture by using Acoustic Technology (Echo 550, LabCyte Inc. Sunnyvale, CA)

in nanoliter range, incubate for 15 min; deliver 3H-SAM into the reaction mixture to initiate the reaction; incubate for 1 h at 30 °C; deliver reaction mixture to filter-paper for detection.

Cellular assays

Compounds. All compounds were dissolved in DMSO (Sigma-Aldrich) and used at 25 mM or 50 mM.

Cell lines. U937 (human leukemic monocyte lymphoma cell line-ATCC) were grown in RPMI 1640 medium (Euroclone) supplemented with 10% heat-inactivated FBS (Euroclone), 1% glutamin (Lonza), 1% penicillin/streptomycin (Euroclone) and 0.1% gentamycin (Lonza), at 37 °C in air and 5% CO_2.

Cell cycle analysis. 2.5×10^5 U937 cells were collected by centrifugation after 30 h stimulation with compounds at 25 μM and 50 μM. The cells were resuspended in 500 μL of hypotonic buffer (0.1% NP-40, 0.1% sodium citrate, 50 μg/mL PI, RNAse A) and incubated in the dark for 30 min. The analysis was performed by FACS-Calibur (Becton Dickinson) using the Cell Quest Pro software (Becton Dickinson) and ModFit LT version 3 software (Verity). The experiment was performed in triplicate.

Granulocytic differentiation analysis. 2.5×10^5 U937 cells were collected by centrifugation after 30 h stimulation with compounds at 25 μM and 50 μM. The cells were washed with PBS and incubated in the dark at 4 °C for 30 min with 10 μL of PE-conjugated anti-CD11c surface antigen antibody or with 10 μL of PE-conjugated IgG, in order to define the background signal. At the end of the incubation the samples were washed again and resuspended in 500 μL of PBS containing 0.25 μg/mL PI. The analysis was performed by FACS-Calibur (Becton Dickinson) using the Cell Quest Pro software (Becton Dickinson). The experiment was performed in triplicate and PI positive cells were excluded from the analysis.

Histone extraction. After stimulation with compounds, the cells were collected by centrifugation and washed two times with PBS. Then the samples were resuspended in Triton extraction buffer (PBS containing 0.5% Triton X 100 (v/v), 2mMPMSF, 0.02%

(w/v) NaN_3), and the lysis was performed for 10 min at 4 °C. Next, the samples were centrifugated at 2000 rpm for 10 min at 4 °C, and the pellets were washed in TEB (half the volume). After a new centrifugation under the same conditions, the samples were resuspended in 0.2 N HCl and the acid histone extraction was carried out overnight at 4 °C. The supernatant was recovered by centrifugation and the protein content was ensured by BCA^{TM} Protein Assay (Pierce).

Western blot. 5 mg of histonic extracts were loaded on 15% polyacrylamide gel. The histone H3 methylation was assessed with anti-dimethyl-K9-histone H3 antibody (Abcam), with anti-monomethyl K20 histone H4 (Diagenode), with anti-monomethyl K4 histone H3 (Diagenode), and with anti-trimethyl-K27-histone H3 antibody (Diagenode). To check for equal loading, Ponceau Red (Sigma) staining and the anti-histone H4 antibody (Abcam) were used.

5. HISTONE LYSINE DEMETHYLASES

Differently from other histone post-translational modifications, like acetylation and phosphorylation whose epigenetic "writers" and "erasers" were almost simultaneously identified, till 2003 a plenty of histone lysine methyltransferases were known, but no histone lysine demethylases weren't identified yet. Therefore histone lysine dimethylation was strongly believed irreversible, also because of the high thermodynamic stability of the C-N bond. Regeneration of un-methylated proteins seemed to be possible only after a complete cellular protein new synthesis.

This wide-spread idea completely changed in 2004 soon after the discovery of the first histone lysine demethylases, namely the Lysine Specific Demethylase 1 or *LSD1*. Afterwards, other histone lysine demethylases (HKDMs or KDMs) had been identified and classified into two classes based on a enzymatic mechanistic criteria. The former includes the lysine-specific demethylase 1 (LSD1, also known as KDM1A) and LSD2 (also known as KDM1B), which are flavin-dependent amine oxidase domain-containing enzymes, whereas the latter comprises the recently discovered Jumonji domain-containing protein (JMJD) histone demethylases, which are Fe(II) and α-ketoglutarate-dependent enzymes. Hence, lysine-specific demethylases (KDMs) work in coordination with histone lysine methyltransferases to maintain global histone methylation patterns.

Figure 5.1. Phylogenetic tree of histone Lysine Demethylases (KDMs).

(Image courtesy of Arrowsmith C.H. *et al*. Nature review/Drug discovery 2012)
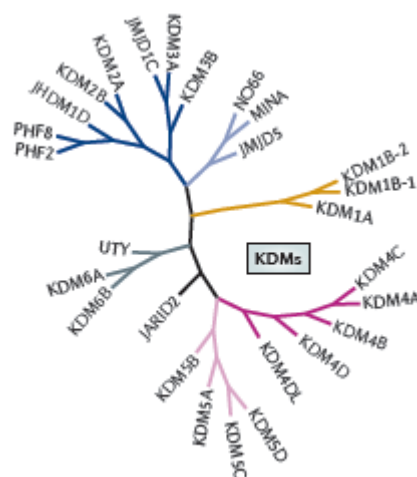
As various evidences underlined HKDMs have been found correlated with different disease states and are thus emerging as attractive targets for new drugs development.

Name (alternative name)	Substrate	Effect on transcription	Disease
KDM1A (LSD1)	H3K4me1/2; H3K9me1/2	Repression Activation	Overexpressed in neuroblastoma, retinoblastoma, prostate, breast, lung, pancreatic and bladder cancers; regulates transcription in herpes simplex and varicella zoster viruses
KDM1B (LSD2)	H3K4me1/2	Activation/not clear	Not Known
KDM2A (FBXL11)	H3K36me1/2	Repression	Non known
KDM2B (FBXL10)	H3K4me3; H3K36me1/2	Repression	Required for initiation and maintenance of acute myeloid leukemia
KDM3A (JMJD1A)	H3K9me1/2	Activation	Regulates metabolic gene expression and obesity resistance; enhances tumor cell growth
KDM3B (JMJD1B)	H3K9me1/2	Activation	Suppresses MUTZ-1 cell growth
KDM3C (JMJD1C)	H3K9me1/2	Activation	Expressed in diffuse-type gastric cancer

KDM4A (JMJD2A)	H3K9me2/3; H3K36me2/3	Activation Repression	Overexpressed in prostate cancer; involved in bladder cancer initiation and progression; regulates Kaposi's sarcoma-associated herpesvirus replication; promotes cardic hypertrophy
KDM4B (JMJD2B)	H3K9me2/3; H3K36me2/3	Activation Repression	Overexpressed in prostate cancer, breast cancer and desmoplastic medulloblastoma; enhances breast cancer cell growth
KDM4C (JMJD2C)	H3K9me2/3; H3K36me2/3	Activation Repression	Overexpressed/amplified in prostate cancer, esophageal squamous cell carcinoma, desmoplastic medulloblastoma, metastatic lung sarcomatoid carcinoma, breast cancer, primary mediastinal B cell lymphoma, and Hodgkin lymphoma; increases expression of Mdm2 oncogene
KDM4D (JMJD2D)	H3K9me1/2/3; HH3K36me2/3	Unknown Repression	Not known

KDM5A (JARID1A)	H3K4me2/3	Repression	Induces acute myeloid leukemia; overexpressed in gastric cancer and prevents senescence of malignant cells; involved in drug-tolerant state in cancer
KDM5B (JARID1B)	H3K4me2/3	Repression	Overexpressed in breast, testis, and prostate cancer; involved in cancer cell growth
KDM5C (JARID1C)	H3K4me2/3	Repression	Mutated in X-linked mental retardation; involved in neuronal survival and dendritic development; mutated in renal carcinoma
KDM5D (JARID1D)	H3K4me2/3	Repression	Not known
KDM6A (UTX)	H3K27me2/3	Activation	Mutated in cancer
KDM6B (JMJD3)	H3K27me2/3	Activation	Involved in inflammatory signaling cascades; acts as a tumor suppressor; overexpressed in Hodgkin's lymphoma
KDM7A (KIAA1718)	H3K9me2; H3K27me2	Activation	Not known

KDM7B (KIAA1111)	H3K9me1/2; H3K27me2; H4K20me1; H3K36me2	Activation Repression	Mutated in X-linked mental retardation
KDM8 (JMJD5)	H3K36me2	Activation	Overexpressed in cancer; enhances cancer cell growth
NO66 (MAPJD)	H3K4me1/2/3; H3K36me2/3	Repression	Overexpressed in non-small-cell lung cancer; enhances cancer cell growth
Mina53 (NO52)	H3K9me3	Activation	Overexpressed in lymphoma, renal cell carcinoma, neuroblastoma, gastric carcinoma, lung cancer, and hepatocellular carcinoma
PHF2 (KIAA0062)	H3K9me1/2	Activation	Not known

Table 5.1. The Lysine Demethylase Family.

5.1 Lysine Specific Demethylase 1 and 2 (LSD1 and LSD2)

LSD1 was first characterized as a member of CtBP complex by Shi *et al*. in 2004[217] and catalyzes the removal of methyl groups from mono- and dimethylated forms of histone H3 lysine 4 (H3K4me1/2) through flavin adenine dinucleotide (FAD)-dependent oxidation, but not from trimethylated substrates[218]. Subsequently studies by Metzger and co-workers revealed that LSD1 is also able to demethylate mono- and dimethylated lysine 9 of histone H3 in prostate cell lines, when co-localized with the androgen receptor (AR)[219].

LSD2, is the last encompassed member to the flavin-dependent lysine demethylase family, it was identified in 2009[220], and thus far little is known about it. It has been found that H3K4 demethylation by LSD2 seems to cooperate with the DNA methylation during oogenesis[221] and activates transcription[222], moreover it mediates NF-κB demethylation thus affecting the regulatory circuit that controls the expression of pro-inflammatory genes in dendritic cells[223].

Being a monoamine oxidase (MAO) enzyme, LSD1 catalyzes the specific demethylation of mono- or dimethylated histone H3 lysine 4 (H3K4) and H3 lysine 9 (H3K9) via a redox reaction. The X-ray crystal structure resolution together with mechanistic studies helped to unravel the catalytic mechanism by means of LSD1 demethylates lysine substrates, and in particular to understand the reasons lying at the basis of LSD1 inability to act on trimethylated lysines. The initial step of the catalysis, the two single electron oxidation of the ε amino group and the concurrent reduction of the FAD, requires a free lone pair on the nitrogen to occur, and only mono- and dimethyl-lysines accomplish this condition. Then the so obtained iminium intermediate can react with a water molecule, turning into an unstable hemiaminal intermediate, which spontaneously decomposes into formaldehyde and the demethylated lysine. The reduced FADH2 is reoxidized by oxygen in a subsequent step to form FAD and hydrogen peroxide[224, 225, 226] (Figure 5.2).
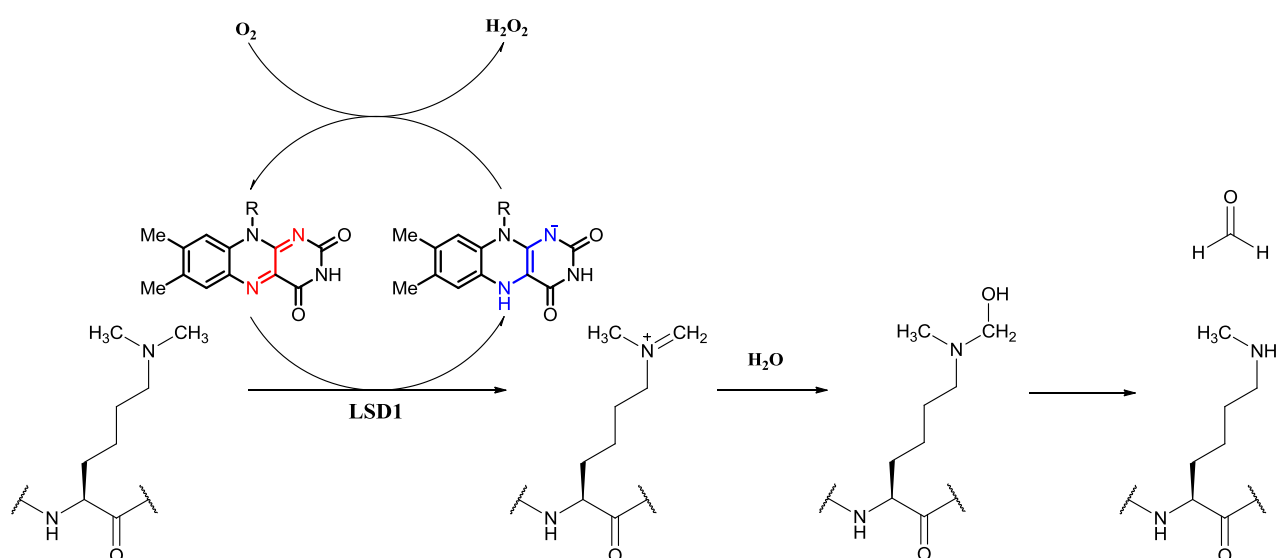
Figure 5.2. Demethylation reaction mechanism catalyzed by LSD1

LSD1 crystal structure was solved for the first time by Cheng and *et al* in 2006[227]. The structure of LSD1 contains three domains, two of them, the SWIRM (residues 172-270) and AOL (residues 271-417 and 523-833) domains strongly interact each other through extensive contacts resulting in a overall globular structure. The SWIRM domain consists of α-helices and it is the last characterized structural module, while the AOL domain folds into a compact structure which shares several structural topologies with other flavin-dependent oxidases, especially Mono Amino Oxidase (MAO) enzymes. The third structural domain of LSD1 is represented by an aminoacidic insertion (residues 418-522) that adopts a tower-like conformation (that's why Tower domain) protruding 75 Å away from the AOL and SWIRM modules[228] (Figure 5.3).
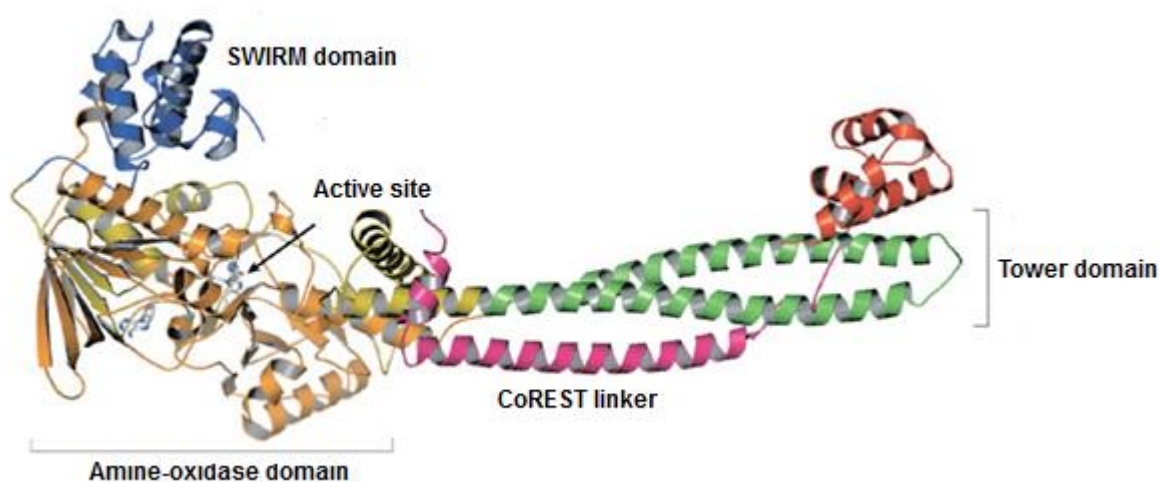
Figure 5.3. Representation of LSD1 structure.

The SWIRM domain of LSD1 is characterized by a long helix, SWα4 surrounded by five other helices (SWα1-6), moreover it has an additional two-stranded β-sheet formed between the SWα4-SWα5 loop and the C terminus of the SWIRM domain. The β-sheet motif helps the SWIRM in anchoring into AOL domain by forcing the SWα6–SWα2 loop to protrude out and to be harbored into an hydrophobic pocket of the AOL domain.

A three amino-acids long sequence (F264-G265-I266) between SWα6 and SWα2 seems to play an important role in the interaction between AOL and SWIRM domains, involving both hydrophobic and hydrogen bonding interactions. These hydrophobic contacts are also reinforced by extensive hydrogen-bonding interactions between the backbone of this motif and the side chains of R295 and Q348.

The AOL domain of LSD1 is functionally subdivided into two well defined subdomains, the FAD binding subdomain and substrate binding subdomain. The former has three aminoacidic fragments (res. 271-356, 559-657, and 770-833) and adopts a mixed α-β structure; whereas the ladder includes three sequences (res. 357-417, 523-558, and 658-769) and is characterized by a six-stranded mixed β-sheet flanked by six α-helices. The space left by the two sub-modules defines a wide-open cavity where catalysis takes place. The cavity protrude into the protein for 23 Å and in its bottom there is the binding site for the flavin rings of the FAD cofactor. The cavity delineates four small "chambers" with distinct chemical properties that could be used for the specific binding of side chains in their native state but also after undergoing post-translational modifications[229]. The first pocket exposes the isoalloxazine ring of the FAD cofactor and forms the catalytic chamber of LSD1. The residues that create this hydrophobic chamber and lie close to the isoalloxazine ring are Val317, Gly330, Ala331, Met332, Val333, Phe538, Leu659, Asn660, Lys661, Trp695, Ser749, Ser760 and Tyr761. The remaining three pockets of the active site cavity are probably required for the binding of histone tail residues directly adjacent to the substrate lysine. Compared with other flavin-dependent oxidases, as PAOs (polyamine oxidases) whose catalytic center is placed in a narrow U-shaped tunnel, LSD1 contains a large catalytic cavity between the FAD- and substrate-binding subdomains and this reflects the different nature of substrates of the two enzymes; indeed the substrates of LSD1 are methylated histone peptides while the substrates of PAOs are smaller linear polyamine like spermidine[230]. Another structural characteristic important for the substrate recognition is that the two diagonally interacting helices, Sα1 and Sα3, form a highly acidic surface at the entrance of the catalytic cavity thus serving as an additional substrate discrimination factor for the basic histone H3 tail.

The tower domain is formed by two long α-helices, TαA and TαB, which pack each other forming a left-handed superhelix. Being organized as a coiled-coil secondary structure, the tower domain is composed of a repetitive pattern of seven residues (abcdefg)n, in which the position a and d are generally occupied with hydrophobic amino acids (Figure 5.4). The tower domain acts as hub for the interaction with other protein, especially molecular adaptors like CoREST, owing to that LSD1 is able to express its demethylating activity on nucleosomal substrates and to be protected from proteosomal degradation. The tower

domain by itself is sufficient for a stable interaction with CoREST, infact a deletion mutant of LSD1 (LSD1ΔTower), in which the tower domain was replaced by a pentaglycine loop, proved not to be able in reducing the methylation level at K4 on histone H3. These evidences indicate that the SWIRM and AOL domains of LSD1 do not significantly contribute to the interaction with CoREST and that the tower domain represents the binding site for it as well as for other molecular partners.
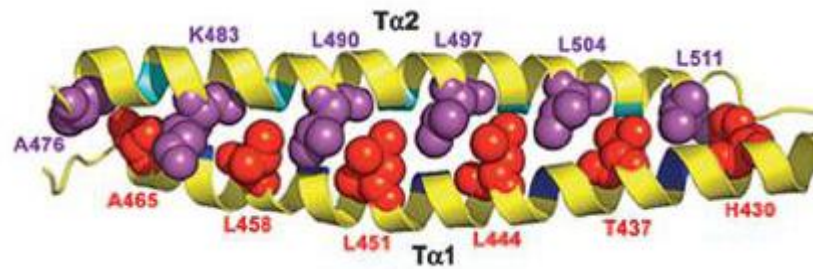
Figure 5.4. Ribbon diagram of the coiled coil of the tower domain. The amino acids at the *d* positions of the heptad repeat of the two helices are in space-filling representation and colored in red (Tα1) and purple (Tα2), respectively.

(Image courtesy of Cheng Y. *et* al. Proc.Natl.Acad.Sci. 2006)

Despite initially recognized as active only on histonic substrates, further studies have illustrated that LSD1 can demethylates also lysines on a l arge portfolio of non-histonic targets, including: p53[231], DNA methyltransferase 1 (DNMT1)[232], transcription factors like for E2F1[233] and STAT3[234], the myosin phosphatase MYPT120[235] and other proteins, finally modulating their cellular activities.

Hence, playing essential roles in regulating gene expression and transcription LSD1 can affect different cellular functions such as cellular development and differentiation, self-renewal and pluripotency capacity, that once aberrantly modulated may lead or promote cancer onset and progression. Moreover, what reinforces the idea that LSD1 could be an attractive target for cancer therapy is that it is found overexpressed in various cancer cells and tissues, among these: neuroblastoma[236], retinoblastoma[237], prostate[238,239], breast[240,241], lung[242], pancreatic[243] and bladder cancers[189].

It has been also found that it regulates viral gene transcription in herpes simplex viruses (HSV) and varicella zoster viruses (VZV)[244]. To exploit the host cell transcriptional machinery, HSV and VZV require an increase in methylation of H3K4 and decrease in

methylation of H3K9, and in doing so viruses recruit host cell factor 1 (HCF-1) and an HKMT. LSD1 has been found to interact with HCF-1 and to demethylate H3K9 in virus infected cells, moreover its inhibition leads to the arrest of viral gene transcription, therefore suggesting that LSD1 inhibitors may be used as anti-HSV and anti-VZV agents[245].

The role of LSD1 in regulating gene expression and transcription is still not straightforward since it has been found in different transcriptional complexes acting as a co-repressor or a co-activator, depending on its molecular partner and its target. According to this, LSD1 can act as a transcriptional co-repressor within the CoREST-HDAC1/2 and in NuRD (Nucleosome Remodelling and Deacetylase) complexes[246], where it catalyzes the demethylation of mono- and dimethyl forms of lysine 4 on histone H3 (H3K4me2/me1), which are two transcriptional activating histone marks. In hematopoiesis, the LSD1-CoREST-HDAC complex interplays with growth factor independent 1 transcription repressor (Gfi-1) repressing Gfi-1 target genes[247]. LSD1-CoREST-HDAC plays also an important role in silencing mature B-cell genes through the interaction with the transcriptional repressor B lymphocyte-induced maturation protein-1 (Blimp-1)[248]. Another molecular evidence suggesting the likely impact of LSD1 in cancer as a transcriptional co-repressor arises considering the role of CoREST/HDACs/LSD1 complex in the recruitment of the oncoprotein ZNF217, which in turn downregulates the tumor suppressor gene p15^{INK4B}.[249]

LSD1 is also a transcriptional co-activator when recruited by nuclear androgen[250] (AR) and estrogen[251] (ER) receptors, shifting it's substrate specificity from H3K4me2/me1 to H3K9me2/me1, these last two being transcriptional silencing histone marks. Responsible of this shifting seems to be the protein kinase C, which once localized on AR target promoters, phosphorylates the threonine 6 of histone H3 (H3T6), blocking the H3K4 demethylating activity by LSD1, which in turn becomes responsive for H3K9me2/me1[252] (Figure 5.5). Such a role seems to be corroborated by a cooperation of LSD1 with JMJD2C, a jumoji domain-containing demethylase specific for H3K9me3, into a specific demethylase complex on AR target genes, which was found to co-localize with the androgen receptor in both normal prostate tissue and in prostate carcinoma. Coherently with this view, LSD1 knock-down resulted in decreased activation of AR-responsive

promoters. Moreover genome-wide analysis of LSD1 promoter occupancy on MCF7 cells, previously treated with estrogen hormones, has indicated that LSD1 occupies nearly 20 % of the whole tested promoters and 84 % of these promoters were associated with RNA polymerase II and additionally with activation markers such as dimethyl-H3K4 and acetyl-H3K9 suggesting that LSD1 was deeply involved in gene activation[253].
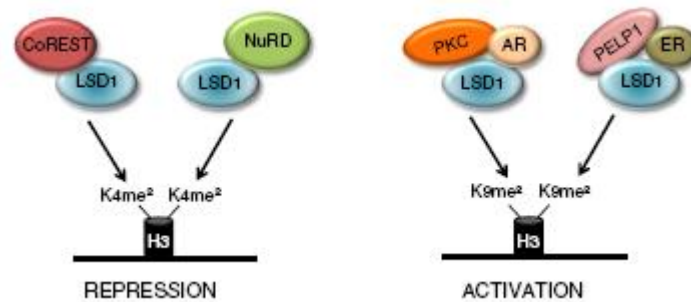
Figure 5.5. LSD1 complexes regulating gene expression.
(Image courtesy of Amente S. e*t al*. Biochimica et Biophysica Acta 2013)[254]

An intriguing hypothesis that has been proposed recently is that ER and Myc interplay with LSD1 since, releasing H_2O_2, it might prompt DNA oxidation and therefore the recruitment of base excision repair enzymes, like 8-oxoguanine-DNA glycosylase (OGG1), thus favoring chromatin looping for transcriptional activation or repression[255]. It has been reported that this mechanism could be exploited also to trigger Myc-induced transcription[256]. More recently, LSD1 was found to be part of protein complexes responsible for transcription elongation: the ELL complex, containing the P-TEFb transcriptional elongation factor, and the MLL super-complex, containing both transcriptional activators and repressors[257].

As stated above, LSD1 can demethylate also non histonic proteins, thus affecting global or specific gene expression patterns not only by direct activity on chromatin dynamics, but also through dimethylation of transcriptional factors/modulators. LSD1-mediated demethylation of K370me2 on tumor suppressor p53 protein, blocks the interaction of p53 with its co-activator 53BP1 (p53 binding protein 1). This modification represses the transcriptional activation of p53 responsive genes and switches off the DNA damage response pathway and the subsequent apoptosis induction[258, 259]. Another way by means of LSD1 can inhibit DNA damage-induced cell death is through the modulation of the E2F transcription factors stability: demethylation of the activating transcription factor E2F1 on

lysine 185 prevents other E2F post-translational modifications that mark E2F degradation, thus favoring E2F1 accumulation and un-responsive cell cycle progression even in presence of a DNA damage[260].

LSD1 also demethylates the myosin phosphatase MYPT1, a phosphatase involved in retinoblastoma (Rb) dephosphorylation. Rb is a tumor suppressor protein, its major function is to impede cell cycle progression from phase G1 to S by binding E2F transcription factors, and thus interfering with the function of the active dimers of E2F-DP proteins that finally lead the cell into the phase S[261]. Rb proteins are active when hypophosphorylated and indeed during cell cycle progression CDKs (Cyclin Dependent Kinases) phosphorylate, thus inactivating, retinoblastoma proteins. LSD1-mediated MYPT1 demethylation enhances its ubiquitination and cellular instability, consequently, MYPT1 degradation enhances Rb phosphorylation and inactivation.

Among the LSD1 substrates there is also DNMT1, which have an important role in the development and differentiation in embryonic stem cells (ESC), through the maintaining of the whole DNA methylation states in silenced genes. As proof of concept evidences have displayed that LSD1 knock out in mouse embryonic stem (ES) cells leads to a decrease in DNMT1 protein levels and to a concomitant loss of DNA methylation[262], moreover combination treatment of DNMT and LSD1 inhibitors against colon cancer xenograft mice, afforded a remarkably inhibition of the growth of the tumor.[263]

LSD1 impact on gene expression and transcription affects a multitude of cellular activities, notably the early development and pluripotency of embryo stem cells. Genetic studies in multiple model systems such as mouse, *C. elegans* and *Drosophila* have displayed that alteration in the LSD1activity may lead to defects in many meiotic steps. In mice, loss of LSD1 causes embryonic lethality at approximately day 6. Other reports indicate that LSD1 is required for cellular differentiation in adipogenesis[264], skeletal-muscle apparatus[265] and remarkably in the epithelial to mesenchymal transition (EMT), which is a changing in the cell phenotype characterized by the loss of epithelial characteristics and a gaining of mesenchymal properties. One of the distinctive feature of EMT is the reduction of H3K9me2 levels and the increasing of H3K4me3 and H3K36me3 levels, that are histone marks dependent by LSD1; moreover loss of LSD1 function affects EMT-driven cell migration and chemoresistance[266]. Another prove supporting LSD1 role in the EMT, arise

if we consider that in human cancer EMT is largely due to Snail mediated transcriptional repression of epithelial genes and it has been shown that LSD1 functionally interacts with Snail and it is recruited on E-caderine promoters, where it prompts silencing by demethylation of H3K4me2 mark[267]. Sequence similarity comparisons between SNAIL and the histone H3 protein suggested that SNAIL could bind to LSD1 in the same cleft of the histone H3. Accordingly, Baron *et al*. found that a 20-amino-acid peptide corresponding to SNAIL1 N-terminal residues effectively inhibits LSD1-CoREST and as a prove of the concept they determined the crystal structure of the ternary complex LSD1-CoREST/SNAIL1 peptide at 3.0 Å resolution[268] (Figure 5.6). Alignment of the N-terminal sequences of the SNAG domain of SNAIL1 (that is quite conserved among SNAIL/Scratch protein families) and H3 reveals that the residues that are key for binding to LSD1 are conserved among almost all SNAIL1-related proteins. This observation could suggest that other transcription factors of the SNAIL/Scratch family are could interplay with LSD1 following the same molecular mechanism.
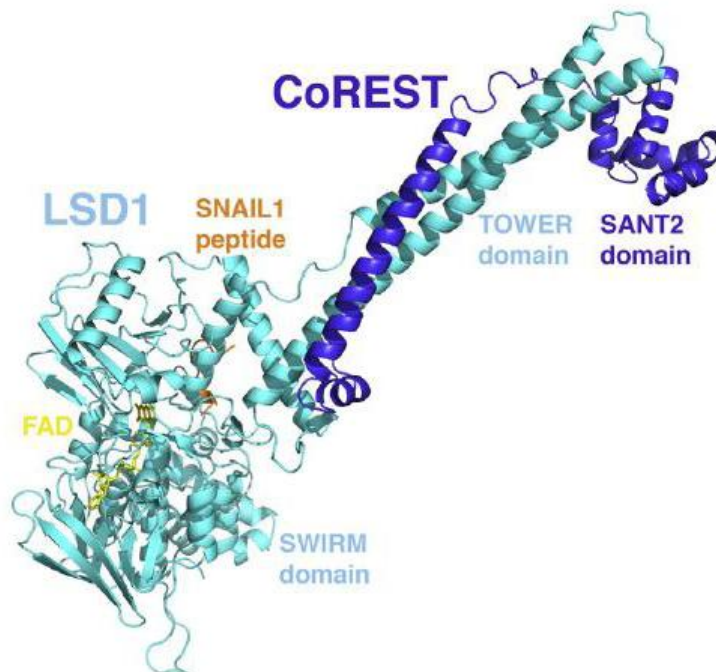
Figure 5.6. Ribbon representation of LSD1 (cyan), CoREST (blue) and SNAIL (orange). FAD cofactor is represented in yellow sticks.

(Image courtesy of Baron R. *et al*. Structure 2011)

Pluripotency and self-renewal capacities are characteristics recognizable in embryonic stem cells as well as in cancer cells, therefore unraveling the mechanisms lying behind the

"stemness" might be useful to understand the de-differentiation process resulting in cancer. Even if this hypothesis is intriguing, presently most of the evidences seem to support the fact that the signaling pathways involved in the regulation of stem and cancer cells belong to functionally separable modules. Despite that, LSD1 has been reported to control gene expression during embryonic stem cell (ESC) differentiation, like, as stated above, in controlling the activity of DNMT1, a so the overall DNA methylation status, by regulating the methylation state on DNMT1 K1096[204]. Moreover LSD1 occupies the enhancer and core promoters of actively transcribed genes in embryonic stem cells and that the enzyme is required during differentiation in these cells, for enhancer silencing specific genes through the involvement of NuRD complex[269].

5.2 LSD1 aberrations and cancer

As previously stated LSD1 is involved in many types of cancers. In particular it has been found strongly upregulated in a poor treated subset of breast cancer: estrogen receptor (ER) negative cancer. Downregulation of LSD1 obtained through the treatment with tranylcypromine, a MAO inhibitor, led to ER-negative breast cancer cells growth inhibition, coherently LSD1 silencing by siRNA treatment increased the expression of tumor suppressor p21^{WAF1} and the downregulation of oncogenes such as CCNA2 and ERBB2[270]. LSD1 is also involved in neuroblastoma, where its upregulation is correlated with poor clinical prognosis and cellular indifferentiation[271]. Another brain cancer in which LSD1 seem to play a pivotal role is medulloblastoma, a highly malignant primary tumor generally affecting children and easily developing metastasis, with a dramatic and poor prognosis and for the survivors cognitive and neurological disabilities after aggressive treatments. In medulloblastoma LSD1 overexpression has been widely recognized and its knockdown induced apoptosis and suppressed proliferation, but also impaired migratory

capacity. Treating medulloblastoma cells with the specific KDM1A inhibitor, NCL-1, significantly inhibited growth in vitro.[272]

Recent studies in both mouse and human models of human MLL-AF9 leukemia, indicates LSD1 as an essential regulator of leukemia stem cells (LSC)[273]. The extent of LSD1

knockdown significantly correlated with loss of the LSC potential of acute myeloid leukemia (AML) cells through fainting of differentiation and apoptosis, moreover cells without active LSD1 are unable to form colonies and are not capable of inducing leukemia when transfected into mice[274]. An hypothesis could be that LSD1 might regulate a subset of genes that activate the oncogenic program associated with MLL-AF9 leukemia, in this concern chromatin immunoprecipitation and next generation sequencing, (ChIP-Seq), confirmed that H3K4me2 increase is the only detectable change at MLL-AF9 promoters following LSD1 silencing.

T-cell acute lymphoblastic leukemia (T-ALL) originates from the malignant transformation of T-cell progenitors. Mutations in Notch1 leading to aberrant and constitutively active Notch1 signaling, contribute to this oncogenic transformation and are hallmarks of this disease. It has been recently found that LSD1 takes part into the Notch-containing complex; and it has been found that together with the PFH8 demethylase it is involved in the epigenetic modification of Notch1 target genes. It is known that the DNA-binding factor CSL binds and represses Notch responsive genes in the absence of Notch itself, whereas the presence of Notch converts CSL in a transcriptional activator. LSD1 interacts with CSL and determines gene repression by removing the H3K4me2 marks at the promoters of Notch target genes (in the absence of Notch), while in its presence the enzyme acts preferentially on H3K9me2 leading to activation of target genes[275].

Recently, high intracellular levels of LSD1 have been also found in pancreatic cancer cells too. LSD1 knock-down pancreatic cells exhibited low proliferative rate and, more importantly, a decrease in glucose uptake and lactate production[REF 190, Yi Qin, whehwy zuh CANCER LETTER 2014].

Pancreatic cancer is characterized by numerous and severe hypoxic regions generally correlated with tumor aggressiveness and poor prognosis, compared with well-oxygenated tumors. An hypoxic environment in pancreatic cancer cells not only favors their resistance to chemotherapy but leads to a glycolysis-based metabolism transformation to ensure the cell its energetic and biosynthetic demands[276]. The knowledge on the molecular basis for glycolytic phenotype in cancer, has been recently deepen owing to advances in the understanding of the hypoxia-inducible factor (HIF1α) cellular role[277].

LSD1 positively correlates with glycolysis process in pancreatic cancer likely owing to an increased HIF1α protein stability as a result of the interaction between LSD1 and HDAC2, which was reported (together with other members HDACs like HDAC1 and HDAC4) to enhance HIF1α protein stability under hypoxia conditions in an deaceylation dependent manner. Another evidence showed that a decreased LSD1 expression resulted in transcription down-regulation of HIF1a target genes, which are rate-limiting glycolytic enzymes.

Given the wide-spread influence of LSD1 on gene transcription, targeting LSD1 in pancreatic cancer cells could be beneficial for two reasons: the expressional gene profile could be altered thus dampening the uncontrolled proliferation and metastasis of pancreatic cancer cells. On the other hand, intervention of LSD1 may interrupt the glycolysis process, the most fundamental and vital step that sustains pancreatic cancer malignancies supporting its energetic metabolism.

5.3 Targeting Lysine Specific Demethylase 1

LSD1 shares a sequence similarity of 17.6% with monoamino oxidases (MAOs) A and B, and PAO (polyamine oxidases)[278,279] therefore soon after its discovery, well-known MAO and PAOs inhibitors were tested on LSD1 to evaluate their activity.

Among the MAOs inhibitors, pargiline (**1**, Figure 5.7), a propargyl-amine-based compound, was the first to be tested and weakly showed to block dimethylation of H3K9 (active at 1 mM) and to arrest androgen receptor-dependent gene transcription[280]. Phenelzine (**3**, Figure 5.7), another anti-MAO drug bearing a hydrazine moiety, was initially recognized as ineffective LSD1 inhibitor, and only when its activity was re-investigated it exhibited an improved potency (K_i=17.6 μM) but with a poor selectivity[281]. Finally also tranylcypromine (*trans*-2-phenyl-cyclopropyl-1-amine or *trans*-PCPA or tPCPA, **2**, Figure 5.7) was tested and it inactivated LSD1 with a K_i value ranging from 477 to 22 μM (depending on the type of assay)[282]. Despite the poor activity trans-TCPA turned to be useful for the future development of LSD1 inhibitors. A Schmidt and McCafferty study based on kinetics and mass spectrometry analysis demonstrated that the trans-TCPA

inhibited LSD1 via an irreversible reaction between the cyclopropyl ring and the N(5) of FAD.
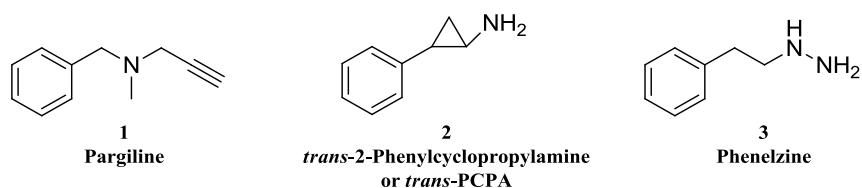
Figure 5.7. MAO inhibitors active on LSD1.

Starting from X-ray crystal structure analysis of LSD1 in complex with tPCPA, three different covalent adducts have been identified (Figure 5.8). Yu and co-workers showed that the structure of tPCPA-FAD complex in LSD1 is a five-membered ring adduct[283], later Yokohama and co-workers stated that an N(5) adduct intermediate (A) could also participate to the tPCPA-FAD construct[284]. Finally, structural analyses of LSD1 complexed with enantiomeric pure PCPAs and its derivatives showed that (1R,2S)-tPCPA reacts with FAD yielding N(5) adducts, whereas (1S,2R)-tPCPA leads to an another unexpected N(5) adduct (B)[285].
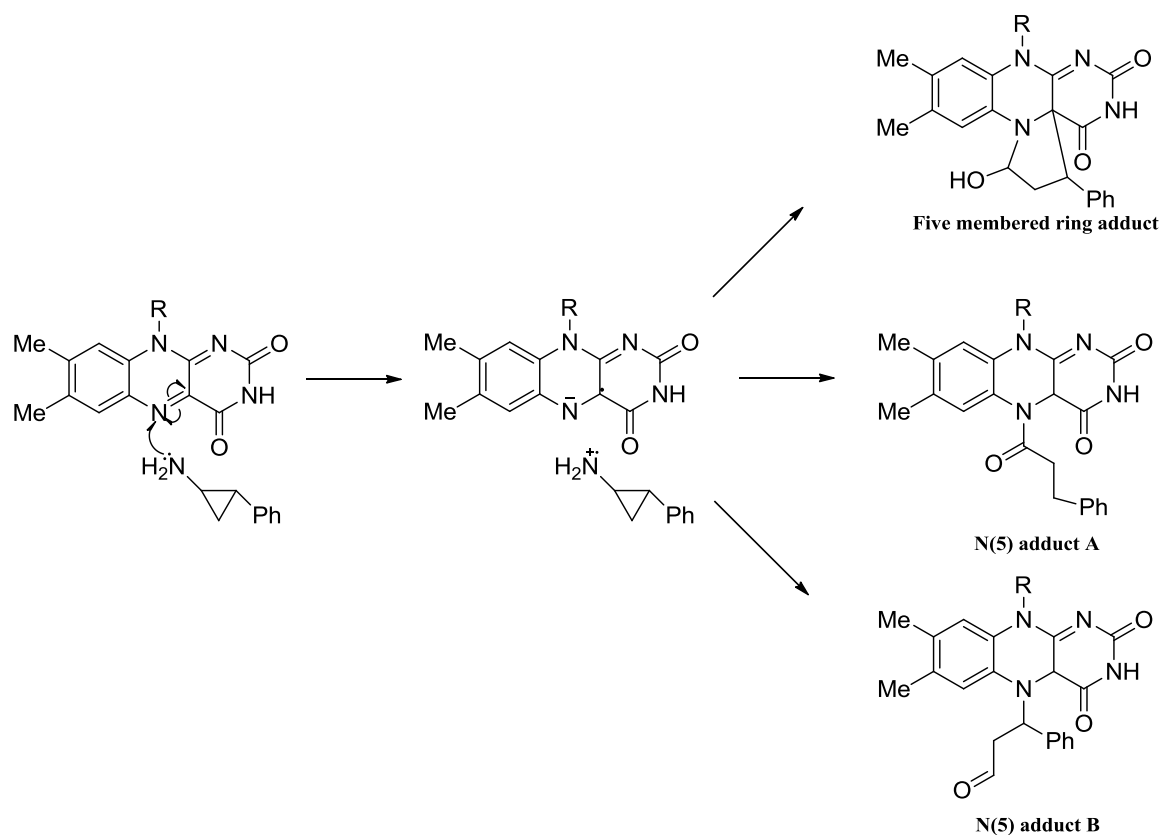
Figure 5.8. LSD1 covalent adducts with tPCPA.

Although MAO-inhibitors didn't exhibit an excellent activity over LSD1, they were however able to induce an increase of global H3K4 methylation state at low micromolar concentration and a growth inhibition of neuroblastoma cell and bladder cancer cells[286]. These inhibitors were thus used as hit compounds for further development, and this is true especially for tPCPA (**2**). Different groups efficiently synthesized several PCPA derivatives, inserting some substitutions on its phenyl ring, and examined their inhibitory activity toward LSD1, MAO A, and MAO B, among these, compounds **4** (Figure 5.9; IC_{50} LSD1=188 µM; IC_{50} MAO A=87 µM, IC_{50} MAO B=21 µM)[287] and **5** (Figure 5.9; IC_{50} LSD1=3.7 µM) displayed higher potency and selectivity for LSD1 than **2**. In addition, compound **5** (1R,2S)-4-bromo-PCPA exhibited a good inhibition of cellular growth on human prostate LNCaP cells[288]. An increased selectivity was achieved by the introduction of a branched substituent at the 4 position of the benzene ring, thus exploiting the wider space left available by the FAD cofactor into the cavity of the AO domain of LSD1 in respect to MAOs. In this view other tPCPA analogs (**6-7**, Figure 5.9) were designed as lysine-PCPA hybrid compounds and proved to be the first cell-active LSD1-selective inhibitors with a selectivity of 400-11000 times greater than that of tPCPA (**6**: IC_{50} LSD1=5.7 µM; IC_{50} MAO A=230 µM, IC_{50} MAO B=740 µM; **7**: IC_{50} LSD1=3.1 µM; IC_{50} MAO A=250 µM, IC_{50} MAO B=1700 µM)[289]. Almost at the same time Mai and co-workers reported compound **8** (Figure 5.9) as a selective inhibitor of LSD1 and MAO A over LSD2 and MAO B (IC_{50} LSD1=1.3 µM; IC_{50} LSD2=38 µM; IC_{50} MAO A=1.2 µM, IC_{50} MAO B>133 µM), which displayed synergistic effects with retinoic acid, an antileukemia drug, thus causing cell growth inhibition in acute promyelocytic leukemia cells[290]. Recently, completely new derivatives of tPCPA have been designed and synthesized. N-alkylated PCPA analogues such as **9** and **10** (Figure 5.9) have been reported to inhibit LSD1 with high potency and selectivity over MAO A and MAO B (**9**, IC_{50} LSD1=5.0 nM; IC_{50} MAO A=16 µM, IC_{50} MAO B=7.4 µM; **10**, IC_{50} LSD1=9.0 nM; IC_{50} MAO A=15 µM, IC_{50} MAO B>40 µM), even if detailed data haven't been disclosed yet[291].
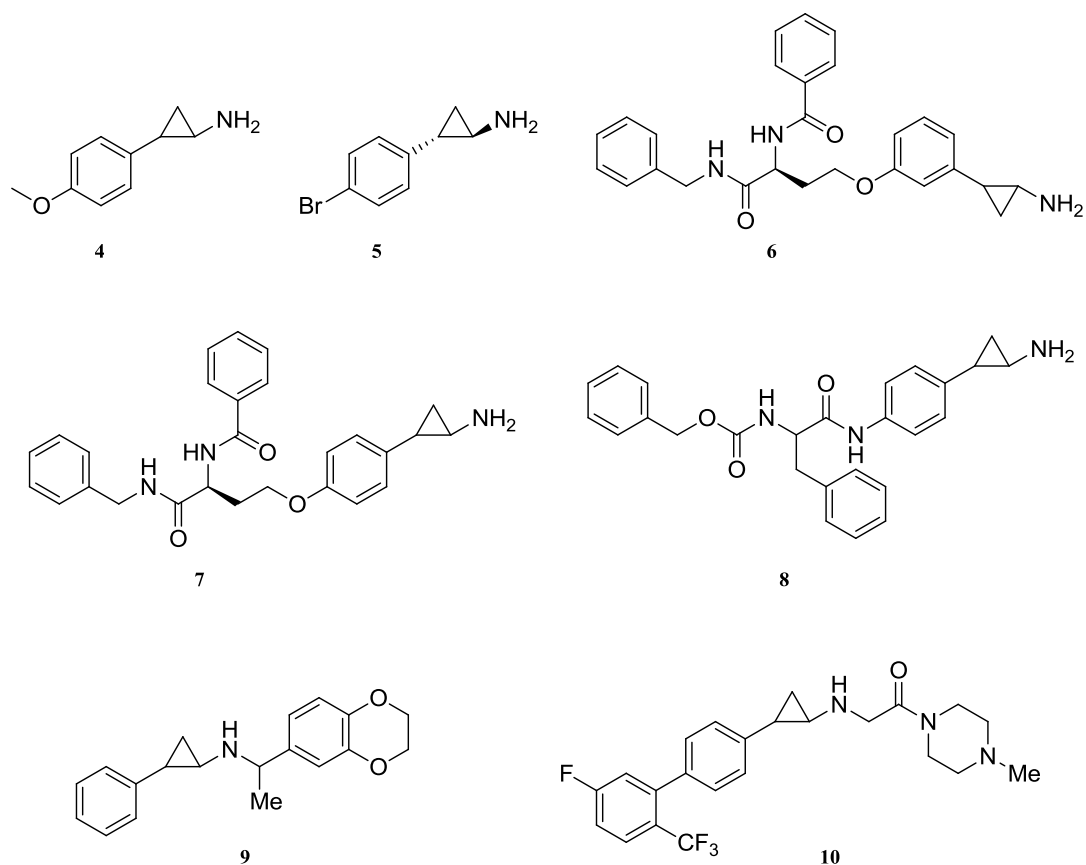
Figure 5.9. Further LSD1 inhibitors developed by tPCPA.

According to the notion that LSD1 can demethylate either mono- and dimethylated form of Lys 4 on histone H3 as well as H3-tail peptides affording at least 15 flanking aminoacids; the H3-peptide scaffold has been functionalized with different warheads, arising from the knowledge of MAO inhibitors development. Among these derivatives the propargyl-Lys-derivatized peptide (**11**) and the hydrazine-Lys-4 H3-21 peptide (**12**) were designed as a mechanism based inhibitors able to covalently target the FAD cofactor and they exhibited an IC_{50} of 0.77 0.00435 µM, respectively[292,293].
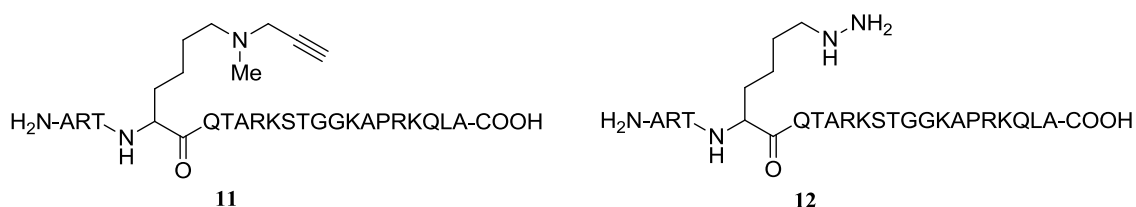
Figure 5.10. Peptide inhibitors of LSD1.

5.4 Jumonji C domain-containing demethylases (JMJDs)

The second family of histone lysine demethylases is characterized by the presence of the catalytic Jumonji C (JmjC) domain. The first JmjC domain protein was characterized in a gene profiling for factors involved in neural tube development, these studies showed abnormal groove formation on the neural plate and a defect in neural tube closure, this abnormality lead to the formation of an additional groove at the future midbrain–hindbrain boundary which crossed the normal neural groove, resulting in a ''cross''-shaped cut on the neural plate, for this reason Takeuchi et al. called this mutation jumonji (Jmj), which in Japanese means cruciform[294]. The JmjC domain has been found in 31 proteins within the human proteome and nearly 20 of these have exhibited to demethylate specific lysines on histones (Table 7.1). In contrast with LSD1/2 which require FAD as cofactor to catalyze demethylation reaction, JmjC domain-containing demethylases (or JMJDs) are Fe^{2+} ion and 2-oxoglutarate (2OG) dependent oxigenases, which act with a different catalytic mechanism and for the same reason are able to demehtylate also trimethylated forms of lysines.

The JMJDs belong to the superfamily of oxygenases, which catalyse the introduction of oxygen atoms directly from molecular dioxygen into their products. The first 2OG-dependent oxygenases to be identified were the collagen hydroxylases and since this pioneering study the number of proteins belonging to this family increased and emerged as a widely distributed family[295]. 2OG oxygenases catalyse a wide range of oxidative reactions, possibly the larger of any other enzyme family, ranging from 'simple' hydroxylations and demethylations (via methyl group hydroxylation) to ring closures and epimerisations[296]. Structurally the JMJDs demethylases belong to the broader "cupin" superfamily of oxygenases, which are characterized by a distorted double-stranded β-helix (DSBH) fold, also known as a 'jelly-roll' or 'cupin' fold.

Albeit considerable unexplained points remain in the mechanistic knowledge of JMJDs, including a lack of detailed displaying of the conformational changes that occur during catalysis, biochemical studies have shed light onto the sequence of chemical events occurring during JMJDs catalyzed demethylation. The proposed mechanism of action is commonly assumed to be similar to that of other Fe^{2+} containing and α-ketoglutarate-dependent hydroxylases and it is reported in Figure 5.11.[297]
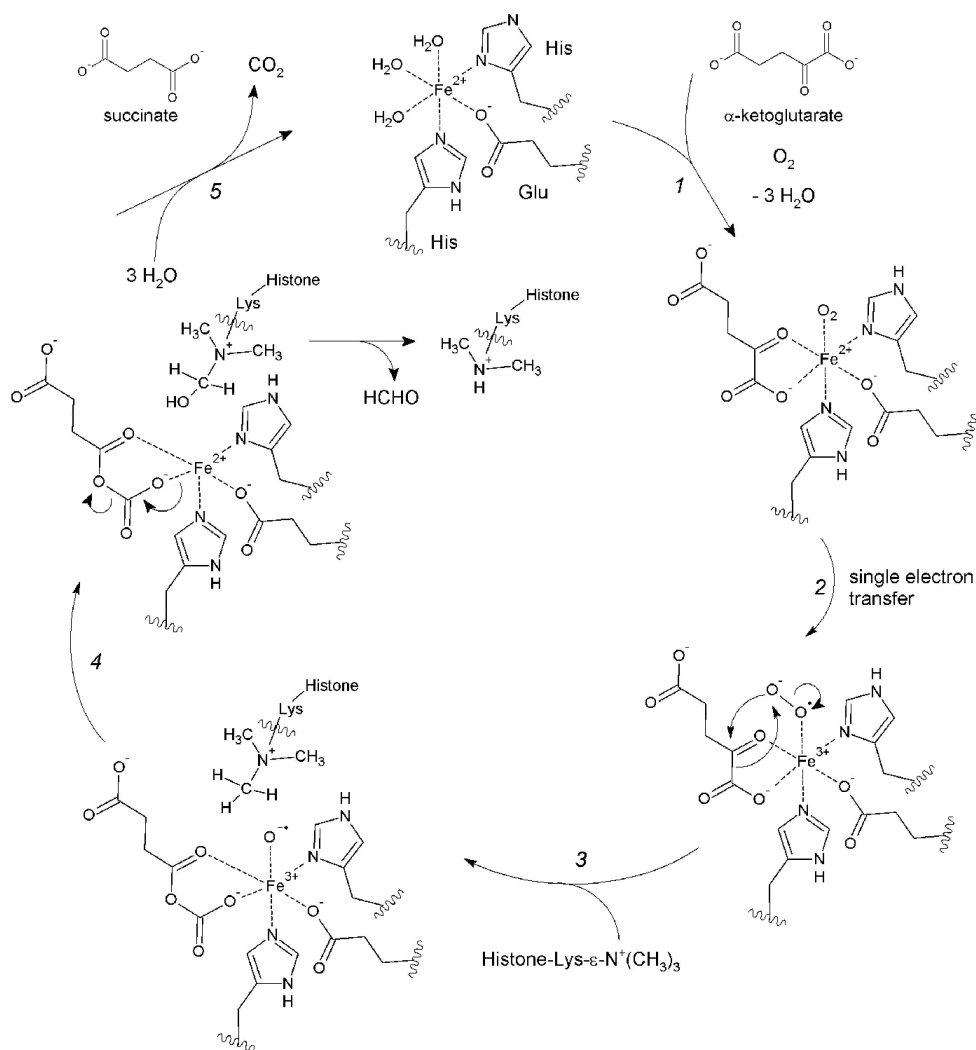
Figure 5.11. Catalytic mechanism of JmjC demethylases.

The catalytically active Fe^{2+} ion is coordinated by two histidine residues, a glutamate residue and three molecules of water. Initially, the co-substrate α-ketoglutarate as well as molecular oxygen are coordinated onto the iron center, displacing the water ligands (step 1). Then, a single electron transfer occurs from the iron(II) ion onto the coordinated oxygen affording a reactive peroxide radical anion species (step 2). This can, in turn, attack the α-ketoglutarate ligand yelding a mixed anhydride bound to the remaining iron(III)-hydroxyl radical anion (step 3). The so formed reactive hydroxyl radical is able to attack the stable C-H bond of the incipient lysine methyl group on the substrate thus forming an hydroxymethyl lysine via a first proton transfer and then a subsequent addition of the hydroxyl group onto the methyl carbon atom (step 4) releasing the central Fe^{2+} ion in the same electronic state of the beginning of the catalytic cycle. Upon dissociation of the

bound mixed anhydride from the central iron, α-ketoglutarate decomposes into carbon dioxide and succinate as byproducts (step 5). Binding of three molecules of water regenerates the original catalytic species. As explained, the Fe^{2+} ion catalytic center together with the ligands, can affect the trimethylat lysine, as well as the other froms, since the overall mechanism, as far as is known so far, does not require the initial formation of an intermediate iminium cation, explaining why JMJDs are able to demethylate methyl lysines in all their forms.

Comprehensive crystallographic analyses of 2OG oxygenases afforded insights into the iron and cosubstrate binding sites and what emerged is that the active sites contain a very highly, but likely not universally, conserved $HXD/E…X_{n…}H$ iron binding motif comprising one aspartyl/glutamyl and two histidyl residues[298]. This three residues forms one half of a Fe^{2+} binding site, with an octahedral binding geometry. 2OG (together with O_2) completes the octahedral complex and it coordinates the metal in a bidentate manner via its 1-carboxylate and 2-oxo groups, displacing two ligating water molecules , as seen above in Figure 5.11. The observed coordination position of the 2-oxo group is almost invariant in the available crystal structures, and is always positioned trans to the metal coordinating carboxylate of D/E. In contrast, the position of the 2OG 1-carboxylate varies between being flanking to the prime substrate binding site (trans to the N-terminal histidyl of the $HXD/E. . .X_n. . .H$ motif) or being in the available coordination position more on the interior of the protein[299]. The different coordination modes of 2OG within JMJDs is an important aspect of their structural characterization and it can be considered in the design of inhibitors that chelate in the active site.

As far as the substrate binding mode is concerned the target lysine residue is bound in a wide cleft formed primarily by the side chains of hydrophobic residues, which position the ε-amino methyl group next to the active site Fe^{2+}. Variations in the size of the active site region binding the ε amino methyl group are proposed, in part, to confer methylation state selectivity; the degree of selectivity varies with the particular enzyme or subfamily. The crystal structure of the catalytic core of JMJD2A (Figure 5.12) shows that, although the JmjC domain contains the sites of interaction for the two cofactors, Fe(II) and α-ketoglutarate, additional domains are needed for catalytic activity[300].
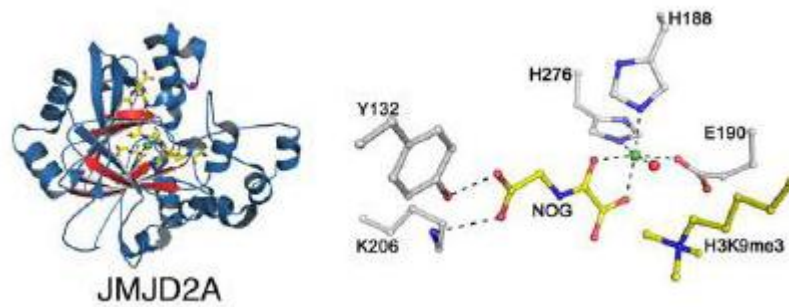
Figure 5.12. Catalytic domain of the histone demethylase JMJD2A in complex with a fragment of H3K9me3.

In the JMJD2 family, two regions within the N terminus and a region immediately upstream of the JmjC domain complete the catalytic centre. In contrast to LSD1, the structure of the JmjC demethylase JMJD2A shows that the binding pocket specifically recognizes and fits trimethylated Lys residues. H3K36me3 and H3K9me3, which are substrates for JMJD2A, bind JMJD2A equally but in a different conformation, the former (H3K9me3) fold into a open conformation while the latter (H3K36me3) exhibits a tightly bent U-shaped conformation. JMJD2A in complex with different H3 peptides is a straightforward example showingthat it is the sequence of the H3 peptide nearby the Lys residues that is determinant for substrate specificity. In the case of H3K9me3 two nearby Gly residues seem to be important for acquiring the required conformation, whereas two Gly residues and a Pro residue afford binding specificity for H3K36me3[301]. In this concern Lys residues on other substrate that lack these adjacent amino acids in their primary structure cannot access the catalytic centre.

Depending on the homology of the JmjC domain and the presence of other domains, these histone lysine demethylases can be divided into seven subfamilies[302].

FBXL11 (F-box and leucine-rich repeat protein 11) has been the first JmjC domain-containing protein to be exhibit histone lysine demethylase activity. FBXL11 and FBLX10 have been demonstrated to catalyze H3K36me2/me1 demethylation[303]. In addition, mammalian FBXL10 has been suggested to act as an H3K4me3 demethylase, even if this activity is not yet fully elucidated[304]. FBXL10 besides having the catalytic JmjC domain, contain an F-box, a signature domain for a component of SCF (SKP1–cullin-1–F-box) E3 ligases) and a CXXC DNA-binding domain. Interestingly a recent study displayed that

FBXL10 regulates the expression of Polycomb target genes suggesting that FBXL10 might contribute to tumorigenesis through the regulation of these genes[305].

Studies have pointed out that FBXL10 could act either as a tumour suppressor being able to cause lymphoma in BLM (Bloom syndrome RecQ protein-like-3 DNA helicase)-deficient mice after induced mutagenesis[306] or as a proto-oncogene since expression data from human cancers show over-expression of FBXL10 in lymphomas and adenocarcinomas, though the same studies revealed reduced expression of FBLX10 and FBXL11 in prostate cancer and in the most aggressive of the primary brain tumours, the glioblastoma multiform[307].

JMJD1A subfamily encompasses histone demethylases specific for H3K9me2/me1 and it includes other two homologues in human cells: JMJD1B and JMJD1C[308].

JMJD1A has a characteristic LXXLL motif that is involved in nuclear receptor interactions. The expression of JMJD1A has been implicated in demethylation of H3K9me2 of androgen receptor (AR) target genes. Moreover studies on knockout mice revealed a pivotal role for JMJD1 in germ cell development and metabolism[309,310]. Indeed, JMJD1A is highly and dynamically expressed during spermatogenesis, and male mice with defected JMJD1A are infertile, with small testes and a severe reduction in sperm count. JMJD1A knockout mice also exhibit an increased adult onset of obesity phenotype and likely as a result of the transcriptional control of metabolic genes in muscle and adipose tissues.

Another effect of JMJD1A is that during hypoxia it stimulates the expression of HIF target genes in colon cancer, like adrenomedullin (ADM), which facilitates the growth of colon carcinoma cells[311,312].

JMJD2 subfamily demethylases, containing four members JMJD2A, JMJD2B, JMJD2C and JMJD2D, are selective for the tri- and di-methylated form of different lysines on histone H3. JMJD2D can demethylate H3K9me2 and H3K9me3 but not H3K36me2 and H3K36me which is turn targeted by.JMJD2A[313]. Sequence alignment of JMJD2A and JMJD2D shows that a variable Ser/Ala position in the binding pocket is responsible for this different selectivity, and by generating Ser288Ala and Ala291Ser mutations in JMJD2A and JMJD2D, respectively, it is possible to switch the substrate specificity of the

two enzymes[314]. Strong genetic data have linked the loss of H3K9 trimethylation to the development of cancer in various mouse models, therefore being JMJD2 family, a subset of demethylases for H3K9me3 and H3K9me2, it is plausible that overexpression of these proteins would result in similar effects. Furthermore several studies have shown that JMJD2C is required for growth in an array of different cancer cell lines, including squamous cell carcinoma[315], prostate carcinoma[316], breast carcinoma[317] and diffuse large B cell lymphoma[318]. Introduction of JMJD2C gene in normal breast MCF10A cells could increase the capacity to generate mammospheres, a phenotype of cancer stem cells, suggesting that GASC1 acts as a transforming gene. The involvement of JMJD2C in tumorigenesis has been supported further by a recent study demonstrating the positive functional synergism between JMJD2C and AR in prostate carcinoma, especially in the transcriptional activation of AR responsive genes and proliferation of prostate cancer cells. Although LSD1 and JMJD1A only demethylate H3K9me2/1, JMJD2C is especially capable of efficiently demethylating H3K9me3, inducing a robust cooperative stimulation of AR transcriptional activity. Thus, specific modulation of JMJD2C activity alone, or in combination with LSD1, may be a promising therapeutic strategy (it will be clearly reported later) to control AR activity in tissues whereas it has a key physiological role.

The members of the JARID1 subfamily (JARID1A-D) are able to demethylase tri- and dimethylated H3K4. JARID1A has a role in the regulation of circadian clock length that is an indirect result of its inhibition of histone deacetylase HDAC1, moreover JARID1A forms a complex with CLOCK and BMAL1, transcription factors that are key in the regulation of animal circadian rhythms. In mammalian cells, deletion of JARID1A causes a reduction in the activation of circadian genes and a shortening of the circadian rhythm[319]. These changes in gene expression are accompanied by reduced histone H3K9 acetylation which can be obtained again by catalytic inactivation of JARID1A. Moreover JARID1A has been shown to be a key effector of retinoblastoma protein (pRB) mediated cell cycle withdrawal and differentiation by interacting with the tumor suppressor pRB[320].
Recently it has been found that JARID1A is overexpressed in gastric cancer and that its inhibition leads to cellular senescence of gastric and cervical cancer cells by derepressing cyclin dependent kinase inhibitors like p27, p21 and p16[321]. Enhanced JARID1A

expression was found to contribute to drug tolerance in a non-small cell lung carcinoma (NSCLC) cell-system , and this was related to its H3K4 demethylating activity[322].

Another component of JARID family, JARID1B, targets H3K4me2 and H3K4me3 and it is mainly associated with transcription start sites (TSSs) and coding regions in embryonic stem (ES) cells[323]. Depletion of JARID1B leads to a failure in the initiation program for the ectodermal differentiation *in vitro*, thus, the most likely function of JARID1B is to maintain H3K4me3 at low levels at its target genes, thereby fine-tuning transcription levels and ensuring the proper execution of differentiation programmes. More importantly JARID1B is overexpressed in various different cancers, including breast[324], prostate[325] and bladder carcinoma[326]. Differently from the others member of JARID subfamily, JARID1C is implicated in X-linked mental retardation and epilepsy[327].

UTX (ubiquitously transcribed tetratricopeptide repeat, X chromosome) and JMJD3 are histone demethylases able to specifically remove di- and trimethyl marks from H3K27 and, thereby counteracting PcG-mediated histone modification by EZH2[328]. Despite its activity, JMJD3 depletion only affects the expression of relatively few genes and does not result in an overall increase of H3K27me3, JMJD3 might instead serve as a safeguard against further H3K27 methylation, thereby ensuring the activation of target genes in response to LPS treatment. Indeed JMJD3 activity has been correlated to the response of macrophages to lipopolysaccharides and to the activation and maintenance of the so called "alternatively activated" status of macrophages, which is considered functionally associated with to the response to parasites, tissue remodelling and angiogenesis[329,330]. UTX is associated with MLL3/4 complexes and was the first reported mutated histone demethylase gene associated with cancer[331]. Somatic mutations of UTX in several human cancers (with highest prevalence in multiple myeloma) clearly suggested UTX role as a tumor suppressor gene[332].

Finally PHF2/PHF8 subfamily includes PHF2, PHF8 and KIAA1718; which are characterized by a plant homeo domain (PHD)-type zinc finger motif in addition to a JmjC domain[333]. PHF8 acts on H3K9me1 and H3K9me2, whereas its close relative KIAA1718 catalyses demethylation reaction of both mono- and dimethylated H3K9 and H3K27[334]. The different substrate specificity has been justified with a different distances between the

JmjC and PHD finger domains in the two enzymes. Indeed, they associate with H3K4me3 through their PHD domain, but while PHF8 has a shorter and more flexible linker which assumes a bent conformation and allowing to the JmjC domain to interact with demethylate H3K9me1 and H3K9me2. For KIAA1718, the linker is longer and more rigid, resulting in an relaxed conformation that renders it inactive towards H3K9me1 and H3K9me2 in the presence of nearby H3K4me3, and leads to selectivity towards H3K27me1 and H3K27me2 *in vitro*[335].

KIAA1718 plays an important role in neural differentiation too, studies on mouse embryonic stem cells(ESC) revealed that KIAA1718 mediated neural promoting effect is related to FGF4 induced transcription. How KIAA1718 is recruited to the promoter region of FGF4 gene remains however unclear, it has been hypothesized that KIAA1718 could recruit a protein complex that contains DNA- or histone-binding activities[336].

PHF8 also binds to H3K4me3-positive genes but not necessarily to regions that carry its target histone modifications. The loss of PHF8 most often affects the expression of genes to which it binds, but the expression of 95% of PHF8 target genes remains unchanged. Furthermore, the depletion of PHF8 does not lead to detectable changes in H3K9me2 levels and only produces minor changes in H3K9me1 and H4K20me1 levels associated with target genes[337].

5.5 Targeting Jumonji C domain-containing demethylases

Taking advantages from the notions available on the JMJD demethylases catalytic mechanism and three-dimensional crystal structures, several JMJD inhibitors have been identified and analysed in recent years. Initially it was discovered that high concentrations of succinate (>10 mM, **1**) inhibits JMJD demethylases in a yeast model[338] most probably by shifting toward the reactants the equilibrium in the reaction:

enzyme α-ketoglutarate + methylated lysine $\Leftrightarrow$ enzyme succinate + demethylated lysine.

In addition, it was found that Ni(II) ion replaces Fe(II) in the KDM3A catalytic site causing inhibition in the micro molar range (IC_{50} = 25 μM), results supporting the inhibition of JMJD3A were also found in cellular evaluations on BEAS-2B cells[339].

However most interesting inhibitors emerged considering structural analogues of the α-

ketoglutarate co-factor, which exhibited competitive inhibition. Among them we can mention α-hydroxyglutarate (**2**, Figure 5.13), which is able to bind in the micro molar range (24-106 μM) the JMJDs KDM2A (or FBXL11), KDM4A (or JMJD2A) and KDM4C (or JMJD2C)[340], *N*-Oxalylglycine (NOG, **3**, Figure 5.13) and its prodrug dimethyloxalyglycine (DMOG, **4**, Figure 5.13), that can inhibit JMJD proteins *in vitro* and *in vivo* respectively[341], supporting indications that DMOG could be hydrolyzed in NOG in the intracellular environment. In particular, NOG and DMOG are thought to inhibit JMJDs by chelating the Fe (II) ion of the active site in a bidentate manner, moreover co-crystal structure of NOG in KDM4A showed that it can also form an hydrogen bond with Tyr132[342]. Thanks to this evidence, new and more potent inhibitors have been designed and synthesized. Unlike α-hydroxyglutarate (**2**) and *N*-oxalylglycine (**3**), which act on several Fe(II)/α-ketoglutarate dependent enzymes such as prolyl hydroxylases domain-containing proteins (PHDs) and factor-inhibiting hypoxia-inducible factor (FIH), the D-tyrosine derivative of NOG (**5**) showed some degrees of selectivity preferring KDM4A (JMJD2A) over PHD2, owing to its tyrosinyl side chain which has been hyphotesized to interact with a set of hydrophobic amino acids residues in a subpocket of KDM4A active site[343].

The promiscuous 2,4-pyridinedicarboxylic acid (PCA, **6**, Figure 5.13) beside binding to a wide range of Fe(II)/α-ketoglutarate oxygenases was also reported to be a potent ($IC_{50}=$ 0.7-4.7 μM) inhibitor of JMJD2A and JMJD2E with a similar binding mode of NOG and NOG derivatives, that is it binds to Ni(II) (replacing Fe^{2+} ion) in a bidentate manner through its nitrogen atom and 2-carboxylate oxygen. Further insights into crystal structure showed that 4-carboxylate oxygen of **6** also forms hydrogen bonds with NH of Lys241 and OH of Tyr177 and that the pyridine ring forms hydrophobic interactions with Tyr177, Phe185, and Trp208[344]. Analysis of the three-dimensional structures solved for the complex KDM4A-PCA allows to identify position (C-3) of the heteroaromatic ring of PCA as a suitable site to improve KDM4 selectivity. Steric-hindered groups will not fit inside the active cavity of PHD2 while they will accommodate well inside KDM4 active site. This notion leads to the aniline analogue of PCA (**7**, JMJD2E IC_{50} = 2.5 μM, PHD2 IC_{50} > 400 μM) which retains the potent activity on KDM4A (JMJD2A) while losing the ability to bind PHD2[345].
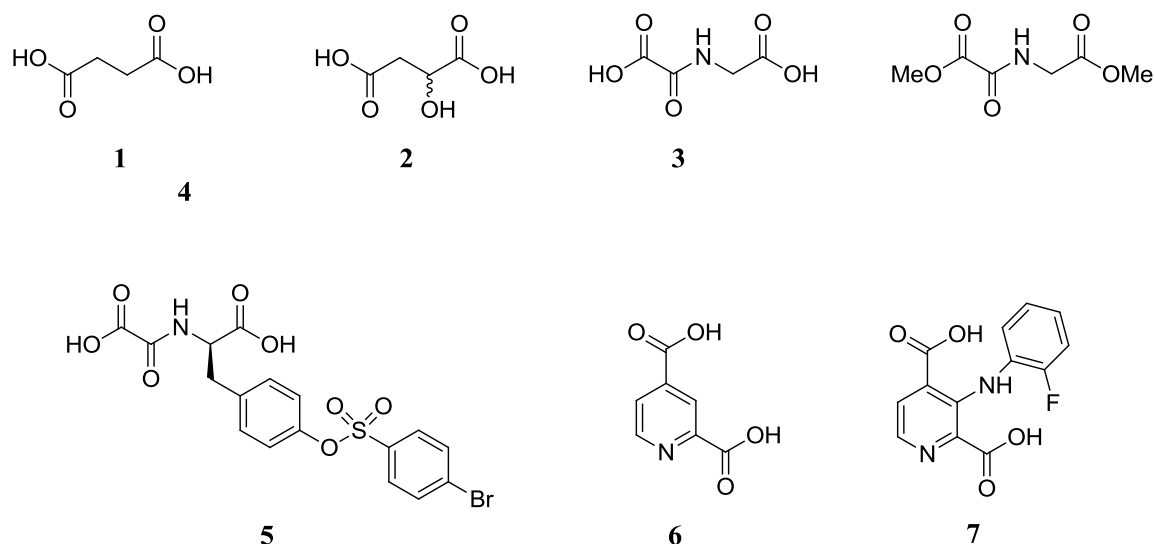
Figure 5.13. JMJDs inhibitors.

Subsequent efforts in high-throughput screening led to another PCA-related compound (**8**, JMJD2A IC$_{50}$ =1.7 µM, JMJD2E IC$_{50}$ = 2.4 µM, FIH IC$_{50}$ = 21 µM, PHD2 IC$_{50}$ = 14 µM) which shares the same chelating ability of PCA using the quinoline nitrogen and the 8-hydroxyl group to bind the Ni(II) in the active site and the C-5-carboxylate function to interact with Lys206 and Tyr132 (Figure 5.14). Interestingly, compound **8** also showed dose-dependent JMJD2A-inhibitory activity *in vivo* at concentrations ranging from 100 to 300 µM that is around 40-fold more higher than that exhibited by DMOG[346].

As well as 8-hydroxyl quinoline, bypiridine scaffold has been recently associated to KDM4E inhibitory activity too. Compound **9** (Figure 5.14) binds KDM4A and KDM4E (KDM4E IC$_{50}$ = 0.18 µM) to the active site metal using the two pyridines nitrogen and is able to interact with Lys206 and Tyr132 through its carboxylate moiety whereas the amide group establishes two hydrogen bonds via water molecules with the phenolic oxygen atom of Tyr177 and the backbone of Glu169[347].

The three-dimensional structure of KDM4C predicted by homology modeling techniques has also been used to gain insights into the active site and design compound **10** (Figure 5.14, NCDM-32). It has a 500-fold greater activity towards KDM4C also known as JMJD2C (KDM4C IC50 = 1.0 µM, KDM4A IC$_{50}$ = 3.0 µM) and 9100-fold greater KDMC4/PHD selectivity than the lead compound NOG (PHD1 IC$_{50}$ > 100 µM, PHD2 IC$_{50}$ > 100 µM), proving that structure prediction could be helpful in gaining information on the structure activity relationships between compounds and enzymes[348].

Recently a novel hydroxamate compound **11** has been found to preferentially inhibit the subfamily of Jumonji demethylases in respect to other Fe(II)/α-ketoglutarate oxygenases (JMJD2A IC_{50} = 4.3 μM, JMJD2C IC_{50} = 3.4 μM, JMJD2E IC_{50} = 5.9 μM, PHD1 IC_{50} = 54 μM, PHD2 IC_{50} = 83 μM, FIH IC_{50} = 22 μM). More important methylstat the prodrug of **11** electively inhibited JMJD demethylases in cells and showed growth inhibition of esophageal carcinoma KYSE150 cells[349], in which KDM4C is highly expressed.

Finally disulfiram analogues (Figure 5.14) have been found to inhibit JMJD2A (**12**, JMJD2A IC_{50} = 3.3 μM), they seems to act by removing Zn^{2+} ion from the Zn-binding site of JMJD2A, thus opening the way to Zn removal as an approach to achieve JMJD2 selectivity over JMJDs that lack Zn-binding site[350].
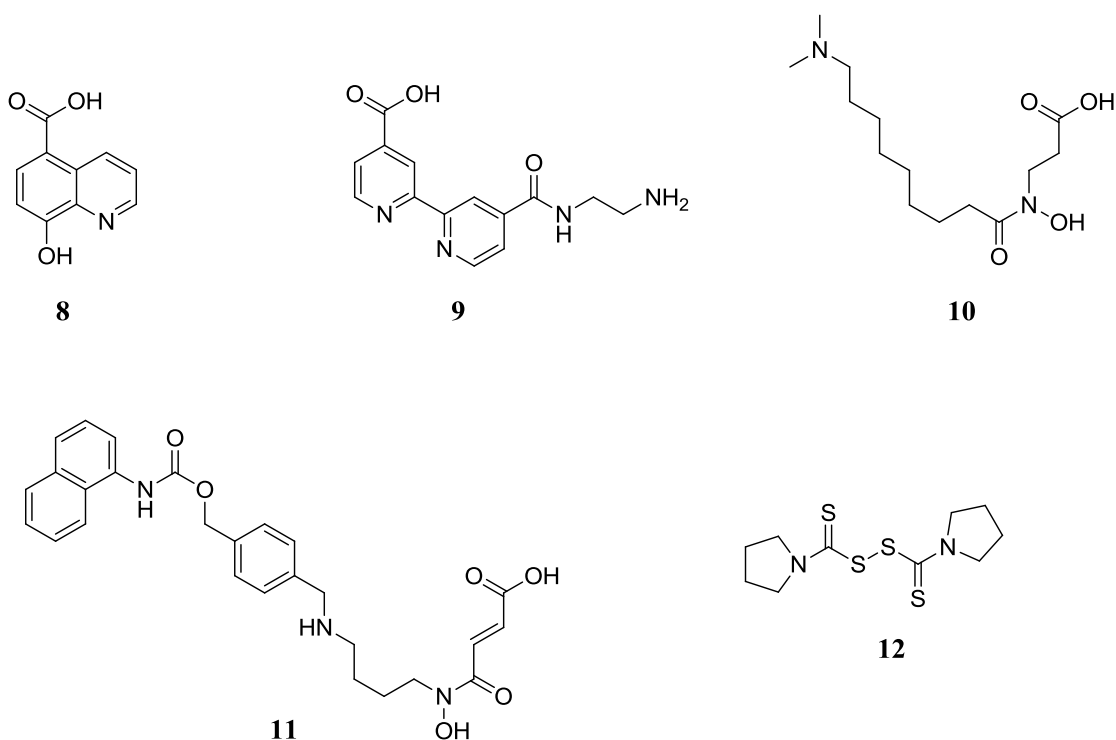
Figure 5.14. JMJDs inhibitors.

6. PAN-HISTONE DEMETHYLASE INHIBITORS SIMULTANEOUSLY TARGETING JUMONJI C AND LYSINE SPECIFIC DEMETHYLASES DISPLAY HIGH ANTICANCER ACTIVITIES

As displayed in the text above, histone lysine demethylases play an important role in gene expression and transcription regulation, together with the histone mark writers, readers and erasers they establish a tangled and cross-talking molecular "dialect" (histone code) which acts as a bookmark to gain a controlled and precise access to the genetic information in according to the cellular needs. The epigenetic mechanism affects a plenty of cellular functions, especially the cell cycle progression control, and when it is aberrant, may lead to the onset and progression of different cancers. In one of the recent studies appeared in literature, focusing on the effects of KDM4A/C (JMJ2C/E) inhibitors on human prostate cancers, it was showed that these inhibitors were found not to inhibit prostate (LNCaP and PC3) and colon (HCT116) cancer cell growth in isolation, but displayed anti-proliferative effects in combination with NCL-2[351], an LSD1 inhibitor, suggesting a potential for synergy in LSD and JmjC KDM inhibition. In multifactorial diseases such as cancer, central nervous system disorders, diabetes, or immunoinflammatory diseases, which involve multiple altered cellular pathways and signals, the use of single-target drugs (the "one drug, one target" concept) can result in unsatisfactory treatment outcomes[352,353,354]. Combination therapies employing two or more drugs, can be more efficient in controlling such complex disease systems and less prone to resistance[355,356]. An alternative strategy to combination therapy is to develop a single chemical entity that is able to modulate multiple targets simultaneously (designed multiple ligands, DMLs)[357,358,359]. The overall goal of the DML approach is to enhance the efficacy and/or improve the safety of therapy respect to drug combination. Additional advantages of DMLs are the reduction of pill burden for patients, due to the administration of a single compound, a lower risk of drug-drug interactions, and improvement in medication adherence. As follow up of previous works[360,361,362], they are describe here pan-demethylase inhibitors **1-6** (Figure 6.1) that simultaneously inhibit both LSD1 and JmjC KDMs. Compounds **1-6** were designed by coupling tranylcypromine (**7**), a known LSD1 inhibitor[363], and 4-carboxy-4'-carbomethoxy-2,2'-bipyridine **8**[364] or 5-carboxy-8-hydroxyquinoline (**9**, 5-carboxy-8HQ)[365], two 2OG competitive templates developed for JmjC inhibition (Figure 6.1). The

molecular weight of these pan-demethylase inhibitors is acceptable because they result from combination of low molecular weight molecules.
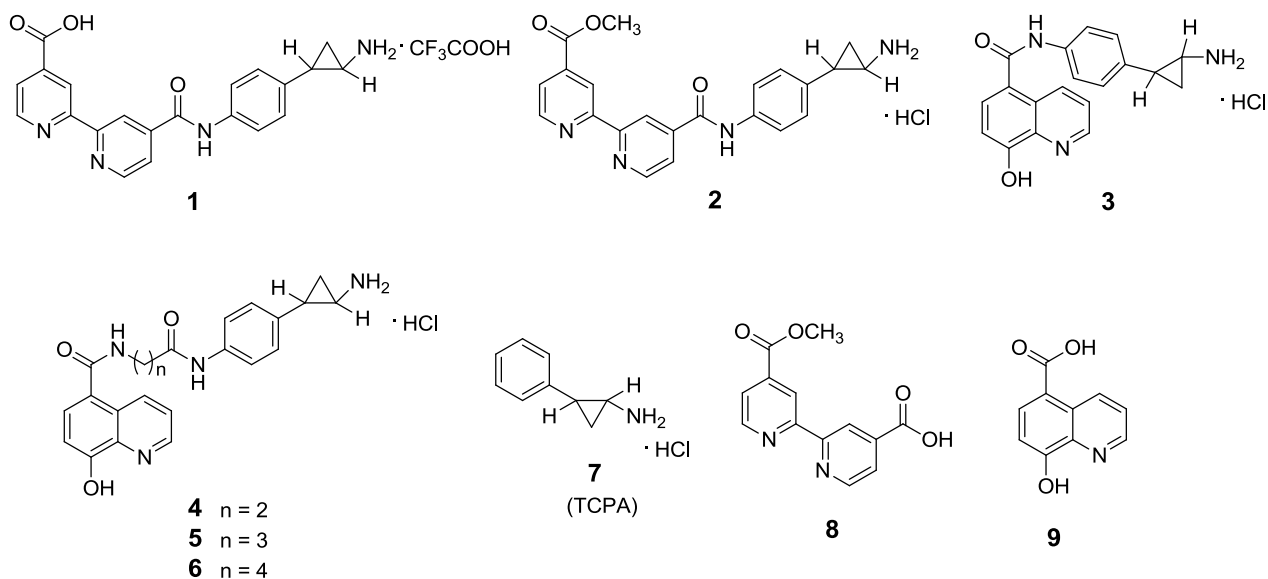
Figure 6.1. Pan-demethylase and their single target precursors structures.

The compounds were selected based on known inhibition results and crystallographic analyses of both the LSDs and JmjC KDMs. Based on manual docking studies (Figure 6.2), we proposed that conjugation of tranylcypromine to the carboxylate group of either 4-carboxy-4'-carbomethoxy-2,2'-bipyridine **8** or 5-carboxy-8-hydroxyquinoline **9** (to form compounds **1, 2** and **3-6** respectively), would give compounds that are capable of binding to both the LSD and KDM4 active sites (details will be presented later in the experimental part). Based on the LSD1 structure (PDB 2XAJ)[257], the bipyridyl (for **1**) and hydroxyquinoline (for **3**) rings are predicted to protrude into the LSD1 substrate binding pocket, with the tranylcypromine moiety conjugating to FAD, as occurs during inhibition by tranylcypromine **7** alone (Figure 6.2-A). Analysis of the active site of KDM4A (PDB 3PDQ)[366] leads to the proposal that both compounds **1** and **3** can chelate the protein-bound iron via their bipyridyl and hydroxyquinoline groups respectively, as observed for a known bipyridyl inhibitor[367] and 5-carboxy-8HQ **9**. Moreover, the primary amines of **1** and **3** may be involved in hydrogen bonding and/or electrostatic interactions with KDM4A (Figure 6.2-B).
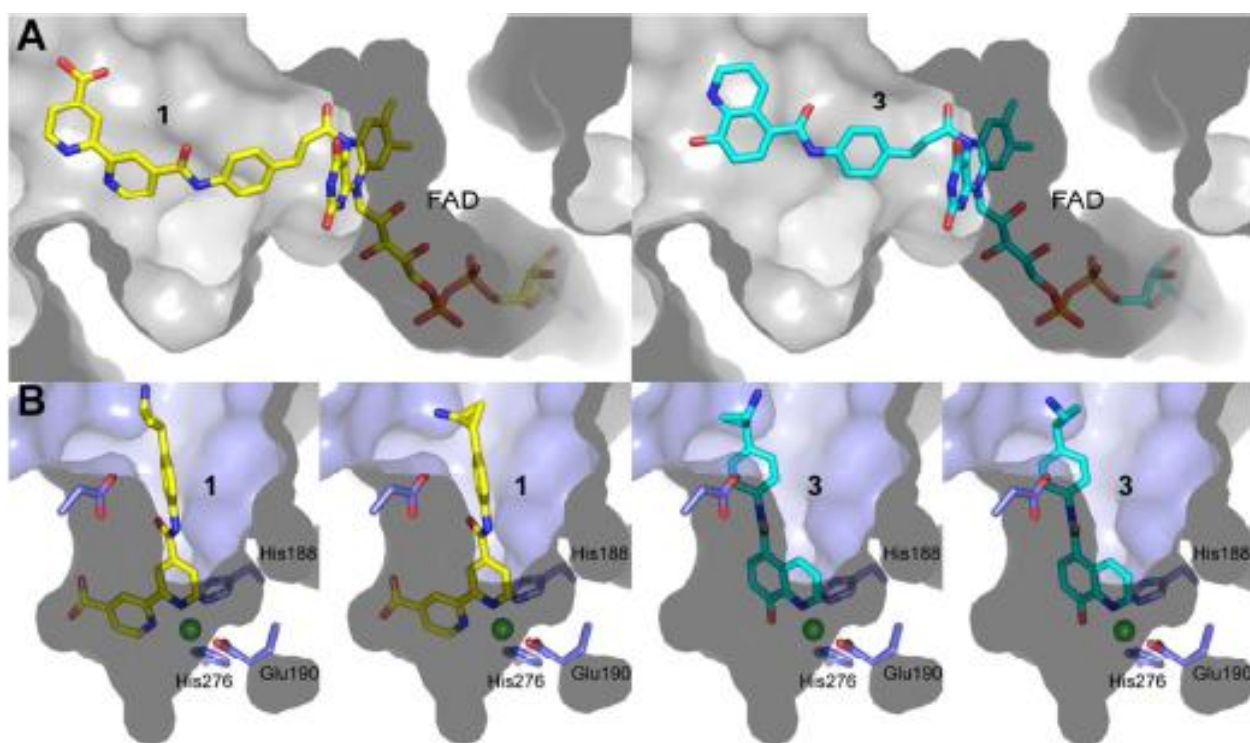
Figure 6.2. Manual docking of compounds **1** (yellow) and **3** (blue) in LSD1 (A) and KDM4A (B) active sites. In LSD1 (A), **1** and **3** are proposed to react with active site bound FAD, opening the cyclopropyl ring. The bipyridyl (in the case of **1**), and the 8-hydroxyquinolyl (in the case of **3**) groups protrude toward the histone substrate-binding pocket. In KDM4A (B), **1** and **3** are proposed to chelate to the active site bound Fe(II) via the bipyridyl and 8-hydroxyquinolyl groups respectively. The tranylcypromine moiety in both compounds likely protrudes towards the histone substrate binding pocket, potentially forming hydrogen bonding and/or electrostatic interactions via the primary amine. Models of both enantiomers of **1** and **3** bound to KDM4A are shown.

Compounds **1** and **2** (route A) were prepared by coupling 4-carboxy-4'-carbomethoxy-2,2'-bipyridine **8** with *trans-N*-Boc-2-(4-aminophenyl)cyclopropylamine **10** using HOBt/EDCI to give amide **11**; ester hydrolysis to give **12** followed by *N*-Boc deprotection with CF$_3$CO$_2$H gave initial target **1** (Scheme 6.1), all hybrid compounds were prepared as *trans* racemates). Alternatively, **11** was directly hydrolyzed in 4N HCl to give ester **2**. To prepare 8-hydroxyquinoline compounds **3**-**6** (route B), 5- carboxy-8HQ **9** as its *O*-MOM-protected derivative (**13**) was condensed with **10**, and intermediate **14** was treated with 4N HCl to provide **3**. Reaction of **13** with the requisite methyl-ω-aminoalkanoate hydrochlorides[368] gave methyl esters **15**-**17**, which after alkaline hydrolysis were condensed with **10** to give the intermediates **18**-**20**. Subsequent acid de-protection of **18**-**20** afforded final compounds **4**-**6**. Alternatively, intermediates **15**-**17** were MOM group de-

protected to give the 8HQ methyl esters **21**-**23**, which were hydrolyzed to give acids **24**-**26**.

a

b
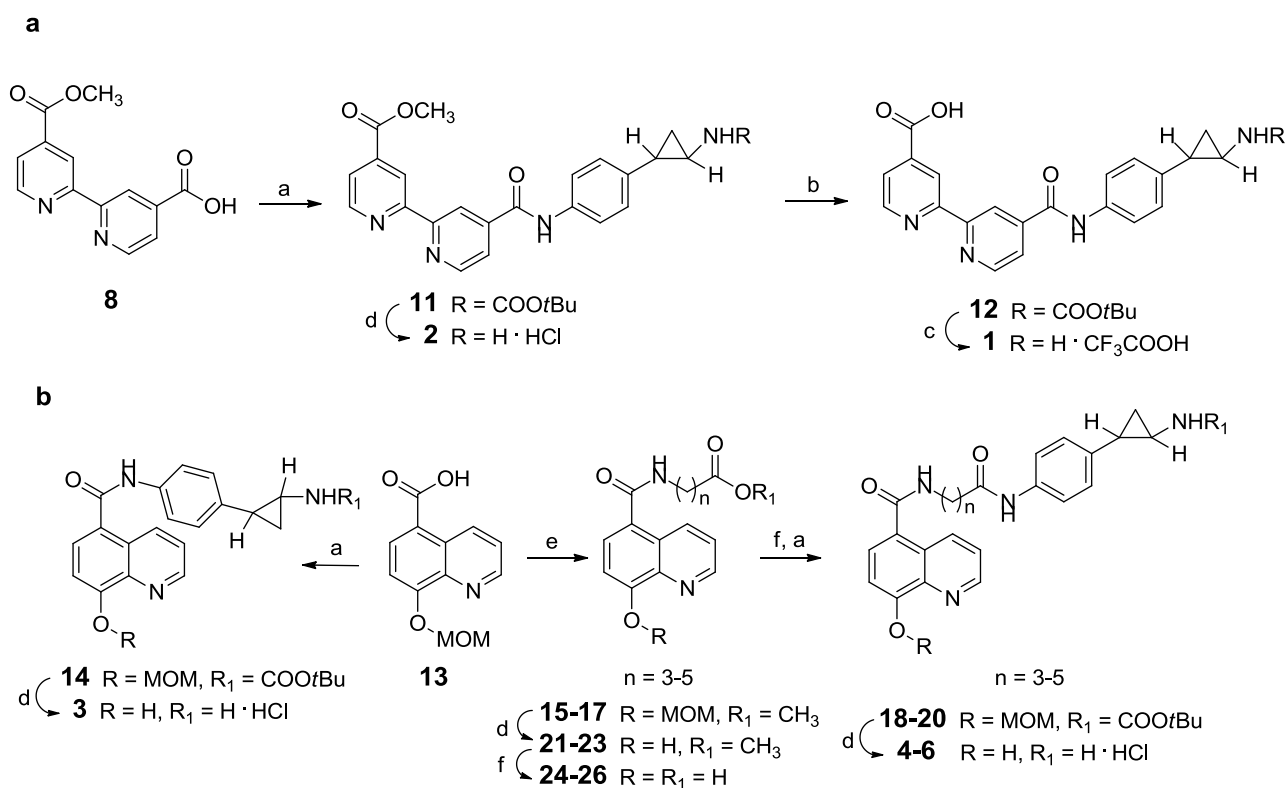
Scheme 6.1. (a) racemic *trans-N*-Boc-2-(4-aminophenyl)cyclopropylamine **10**, HOBt, EDCI, Et$_3$N, DMF, RT; (b) 0.2N NaOH, MeOH, RT; (c) CF$_3$COOH, 0 °C to RT; (d) 4N HCl in 1,4-dioxane, THF/MeOH, RT; (e) methyl ω–aminoalkanoate hydrochloride, HOBT, EDCI, Et3N, DCM, RT; (f) 2N LiOH, THF, RT.

Compounds **1**-**6** were tested against LSD1 and a subfamily representative panel of JmjC KDMs including KDM4. In the LSD1 inhibition assays, the tested compounds all showed single-digit (**1**, **5**, **6**) or submicromolar (**2**-**4**) IC$_{50}$ values, with similar or increased potencies respect to the reference **7** (Table 6.1). Compounds **1**-**3** were also tested against MAO-A and MAO-B to assess their selectivity towards LSD1: at the tested conditions, **1** and **3** were definitively more effective in inhibiting LSD1 than MAOs, while **2** was less potent against MAO-B but showed similar inhibitory potency against MAO-A respect to LSD1, analogously to what observed with other tranylcypromine based compounds. Inhibition of the JmjC KDMs by the hybrid compounds **1**-**6** (Table 6.1) and 8HQ esters (**21**-**23**) and acids (**24**-**26**) was then investigated, using **8** and **9** as references and is reported in Table 6.2. Interestingly, both 8HQ (compounds **3**-**6**) and bipyridine (compound **1**) hybrid inhibitors showed similar potencies against JmjC KDMs as the reference

compounds **8** and **9**, demonstrating that the conjugation of tranylcypromine does not adversely affect activity. Compound **1** displayed low- or sub-micromolar activity against all the tested JmjCs, thus being the most potent of the series. Importantly, when tested against the hypoxia inducible factor hydroxylases FIH and PHD2, the former of which is closely related to the JmjC KDMs, **1** showed no/weak inhibition, revealing high KDM-selectivity. Consistent with previous SAR for the bipyridine derivatives, the free acid is required for high potency against JmjC KDMs as the ester "pro-drug" form (**2**) weakens the potency. Single digit (9 out of 10) values were obtained for **2**-**6** against KDM4, the KDM subfamily that has been shown to work synergistically with LSD1[351](Table 6.1).

cpd	IC$_{50}$, μM								
	LSD1 *(KDM1)*	MAO A	MAO B	FBXL11 *(KDM2/7)*	JMJD1A *(KDM3)*	JMJD2C *(KDM4)*	JMJD2E *(KDM4)*	JARID1C *(KDM5)*	JMJD3 *(KDM6)*
1	2.2	35.4	47.0	0.22	0.14	0.07	0.42	0.19	2.7
2	0.5	<1	43.3	12.2	37.3	2.7	15.6	8.6	75.5
3	0.3	8.9	81.0	7.8	30.8	1.2	3.9	26.2	27.1
4	0.8	-	-	12.0	12.5	4.5	5.5	35.7	17.9
5	1.6	-	-	8.2	9.7	3.1	3.5	20.7	14.0
6	1.0	-	-	11.5	9.1	2.5	5.1	36.7	15.7
7	2.1	4.5	2.5	>100	>100	>100	>100	>100	>100
8	>100	-	-	4.8	1.1	3.5	5.0	0.03	11.2
9	N.D.	-	-	15	0.17	0.6	0.3	25	0.14

Table 6.1. Inhibition of LSD1, MAOs, JmjC and other 2OG-dependent Enzymes by Pan-demethylase Inhibitors **1**-**6**.*a* The KDM Subfamily of Each Demethylase Enzyme is Reported among Brackets. Single Family-specific Target Inhibitors **7**-**9** were used as references.
*a*Inhibition assays were performed in duplicate. The errors in determinations of IC$_{50}$s are within ±10% of their values. *b*ND, Not Detectable. Compound **9** interferes with the peroxidase used in the coupled enzymatic assay and the inhibition could not be reliably measured.

cpd	IC$_{50}$, µM					
	FBXL11	JMJD1A	JMJD2C	JMJD2E	JARID1C	JMJD3
21	57	39	4.5	5.1	38	23
22	35.6	12.2	8.0	10.1	85.6	13.1
23	26	22	5.4	9.7	39	13
24	>100	31	4.7	5.8	37	41
25	32.5	9.0	9.1	9.5	75	13.7
26	32	37	4.8	10	57	14
9	15	0.17	0.6	0.3	25	0.14

Table 6.2. Inhibitory activities of methyl 2-(8-hydroxyquinoline-5-carboxamido)alkanoates **21**-**23** and 2-(8-hydroxyquinoline-5-carboxamido)alkanoic acids **24**-**26** against JmjC enzymes.

We then investigated whether the pandemethylase inhibitors **1**, **2** and **3** affect selected global histone methylation states in HeLa cells, using immunofluorescence based methods (Figure 6.3). Compounds **7** for LSD1, and **8a** (a pro-drug form of **8**[369], Figure 6.1) and **9** for JmjC enzymes, were used as references. The hybrid inhibitors **2** and **3** caused substantial, dose-dependent increases of methyl marks at lower concentrations than **9** whereas **7** caused essentially no changes in the overall methylation levels (including H3K4 methylations), in agreement with previous studies[370,371]. The lack of effects on H3K4me3 may reflect the weaker inhibition of H3K4 demethylases (JARID/KDM5) over H3K9me3 KDMs (KDM4), coupled to the simultaneous effect of inhibiting the H3K4me2 selective demethylase LSD1 (Table 6.1) or more complex effects due to inhibition of multiple targets. The 2,2'-bipyridine derivative **2** caused a H3K9me2/3-specific dosedependent hypermethylation effect, whereas **8a** and **7** alone had no effect. This observation suggests that the "hybridization" of the bipyridyl and tranylcypromine motif has a synergistic effect, with respect to inhibition of LSD1 and KDM4/3 families. There was a general decrease in the immunofluorescence signal at higher doses where toxicity was observed (Figure 6.4-I).
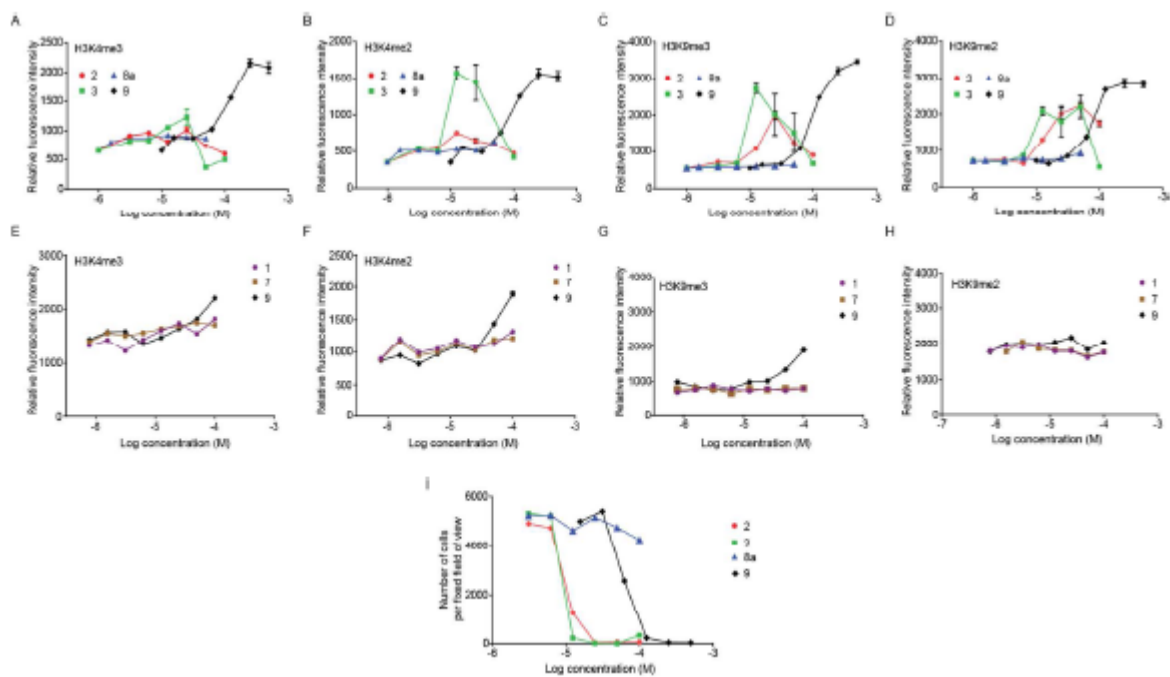
Figure 6.4. Detection of changes in the global histone methylation levels in HeLa cells after treatment with **1**, **2**, **3**, **7**, **8a** and **9** over 72 h using an immunofluorescence-based assay (A-H). Cytotoxicity of compounds **2**, **3** and **8a** at high doses is shown as number of cells per fixed field of view (I).

Compounds **1**-**6** (50 µM) were tested in human prostate LNCaP and colon HCT116 cancer cells to investigate their effects on cell cycle (after 30 h), apoptosis (after 30 h) and differentiation (after 48 h), using **7**-**9** as references. In LNCaP cells, **2**, **3** and **6** caused a strong G1 phase arrest (≥ 90%) with a substantial fraction of the cells in pre-G1 stage consistent with apoptosis induction, especially for **2** and **3** (Figure 6.5-A). In HCT116 cells, the pan-inhibitors **3** and **5** and the JmjC selective inhibitor **9** displayed cell cycle alteration when compared to controls; however, as with the LNCaP cells, only compounds **2** and **3** induced the pre-G1 phase accumulation (Figure 6.5-B). Dose-response curves for apoptosis in LNCaP and HCT116 cells were detected after treatment of cells for 48 h with **2** and **3** at doses from 10 to 100 µM (Figure 6.5-C).
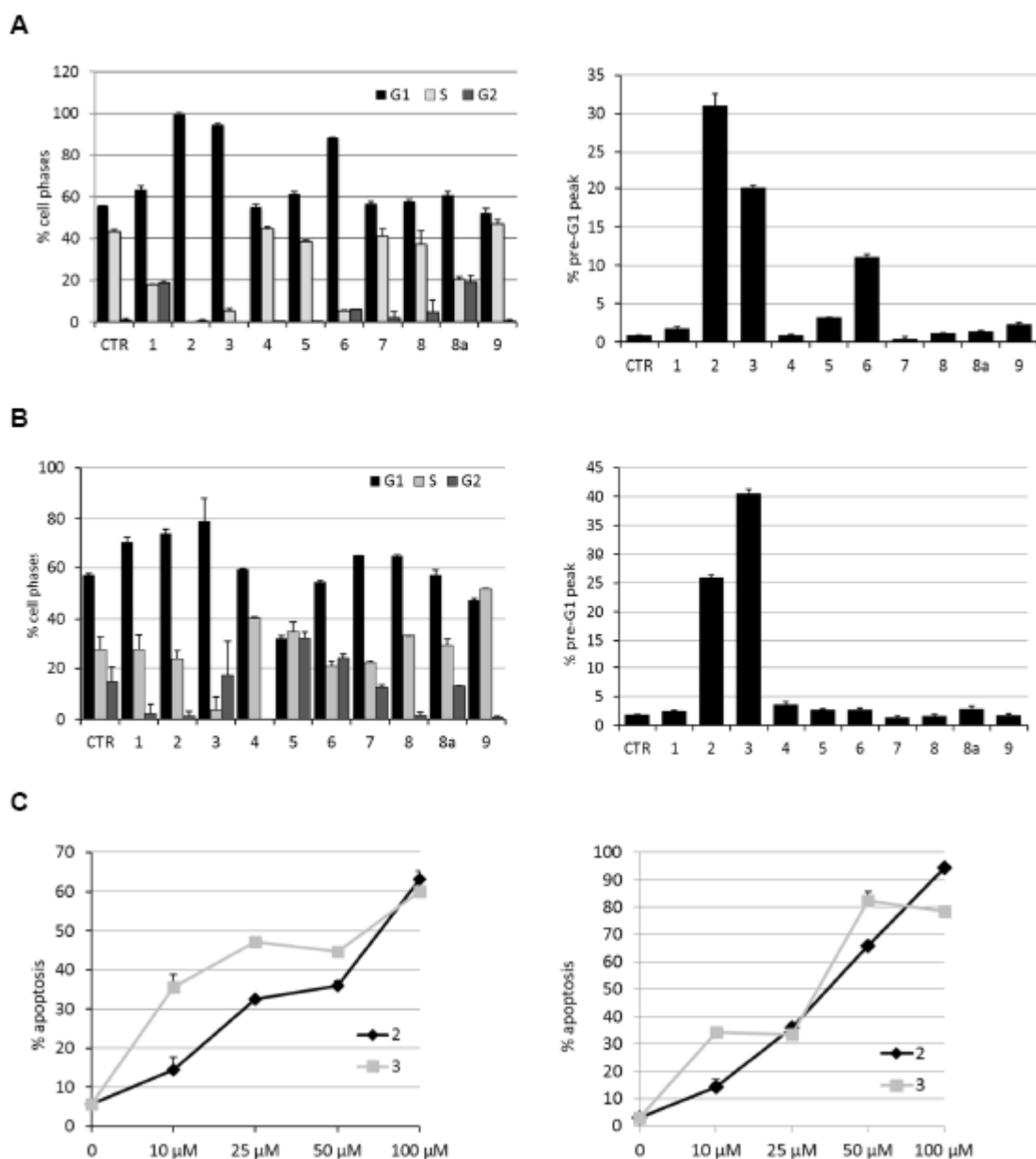
Figure 6.5. Effects of pan-demethylase inhibitors **1-6** in LNCaP and in HCT116 cells. Cell cycle effect (left) and percentage of cells at pre-G1 peak (right) of **1-9** (50 μM, 30 h) in LNCaP (A) and HCT116 (B) cells. (C) dose-response curves with **2** and **3** for apoptosis (48h) in LNCaP (left) and HCT116 (right) cells.

When compared in independent experiments to a combination of the single-family target Inhibitors **7** and **8**, **2** and **3** showed much more efficacy in inducing apoptosis both in LNCaP and HCT116 cells (at 50 μM for 24 h; Figure 6.5). To assess their differential toxicity, compounds **2** and **3** were also tested (50 μM, 24 h) in mesenchymal progenitor (MePR) cells[372]: in this non-cancer cell line **2** increased the pre-G1 peak percentage from 8.4 to 12.8% respect to the control, while with **3** the same value was under the control value (4.2%), suggesting a cancer cell-selective apoptotic induction for the two pan-KDM

114

inhibitors (Figure 6.6). Despite differences in number of cells in pre-G1 phase among Figure 6.5 and 6.6, compounds **2** and **3** induced cell death in cancer specific manner. These differences, however, could be due to cell populations (i.e. the value of percentage of pre-G1 for the untreated HCT116 cells was around 2% in Figure 6.5 and around 8% in Figure 6.6). Also times of induction (30 h in Figure 6.5 and 24 h in Figure 6.6) could justify the differences among percentages in data.
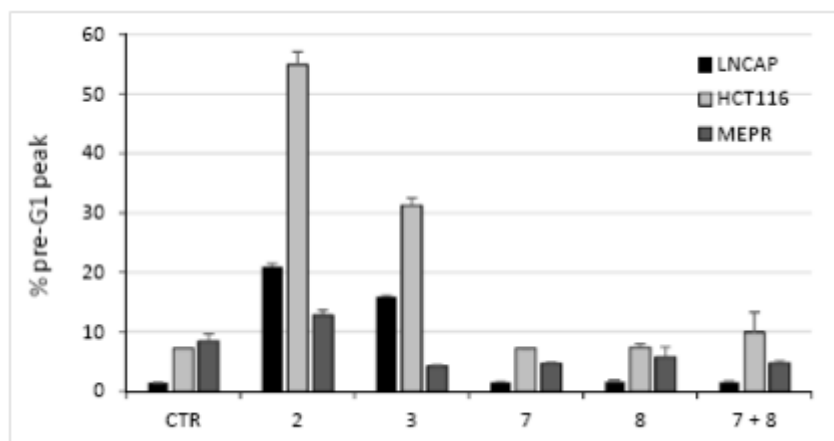
Figure 6.6. Comparison of effects on pre-G1 peak accumulation for **2**, **3**, **7**, **8** and combination of **7** plus **8** (50 μM, 24 h) in LNCaP, HCT116, and MePR cells.

Effects on cell proliferation and migration were detected by treating LNCaP and HCT116 cells with 50 μM **2** and **3** up to 72 h, using the HDAC inhibitor SAHA as a positive control. In LNCaP cells, **2** showed similar growth arrest as SAHA, while **3** was less effective (Figure 6.7-A, left) (In the experimental section will be presented the whole 72 h-assay). Nevertheless, differently from SAHA, neither **2** or **3** was able to stop migration in this cell line (Figure 6.7-A, right). In HCT116 cells, strong antiproliferative effects for **2** and **3** were detected even after 6 h (Figure 6.7-B, left), while the corresponding SAHA effect appeared only at 72 h (Figure 6.9, Experimental section). In this cell line, **2** and SAHA strongly hampered migration, while **3** had no effect (Figure 6.7-B, right).
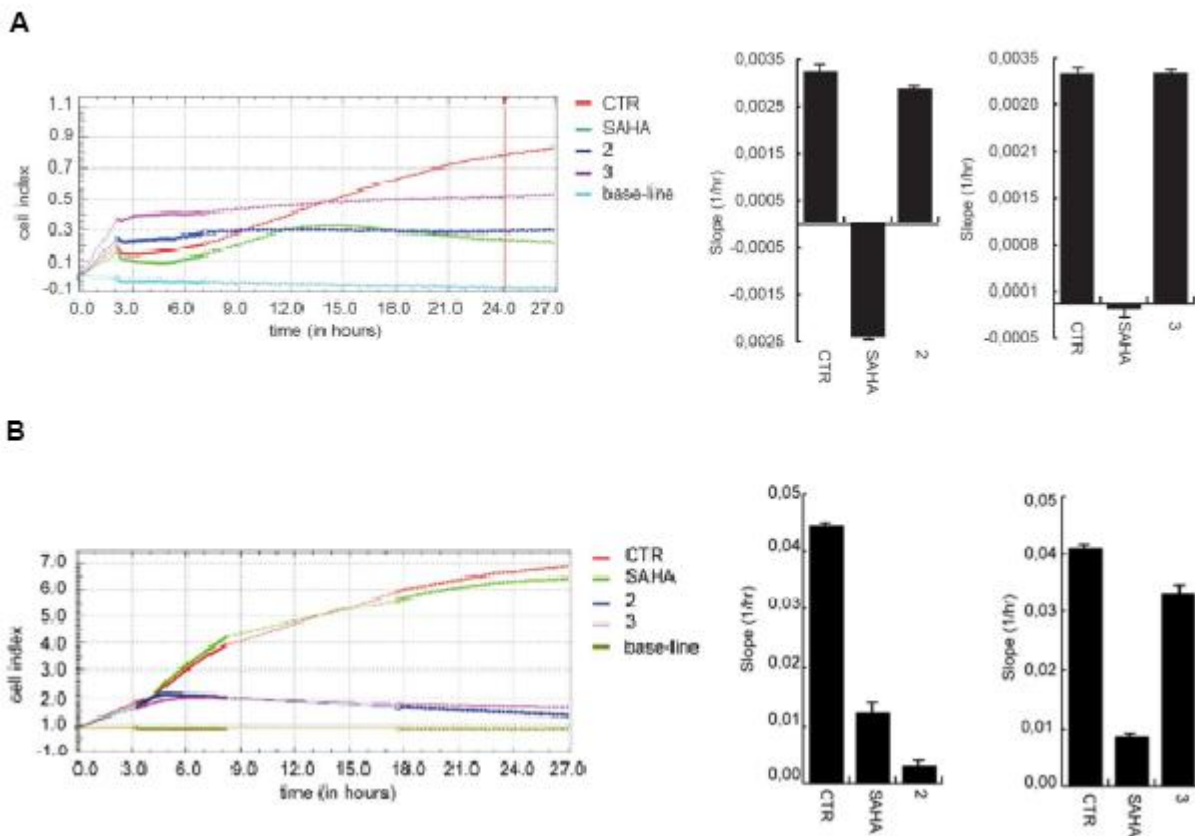
Figure 6.7. Proliferation curves and cell migration relative to LNCaP (A) and HCT116 (B) cell lines after 24h. The HDAC inhibitor SAHA was used as a reference drug. Left: proliferation curves after 24h. Control (untreated cells) in red, cells treated with SAHA (5 μM) in green, cells treated with **2** (50 μM) in blue, cells treated with **3** (50 μM) in violet, in sky-blue (LNCaP, A) or yellow-green (HCT116, B) the base lines. Right: cell migration after 24 h. Histograms have been represented by slope relative to the control (untreated cells), cells treated SAHA (5 μM), cells treated with **2** (50 μM) and cells treated with **3** (50 μM). Data show the mean value from three parallel experiments with error bars showing the standard deviations on top of each column.

Western blot analysis using mark-specific antibodies supported the proposal that the effects of **2** and **3** in LNCaP and HCT116 cells are due to both LSD1 and JmjC inhibition. Figure 6.8 shows increased H3K4me2/3 and H3K9me3 methylation after treatment with 50 μM **2** and **3.**
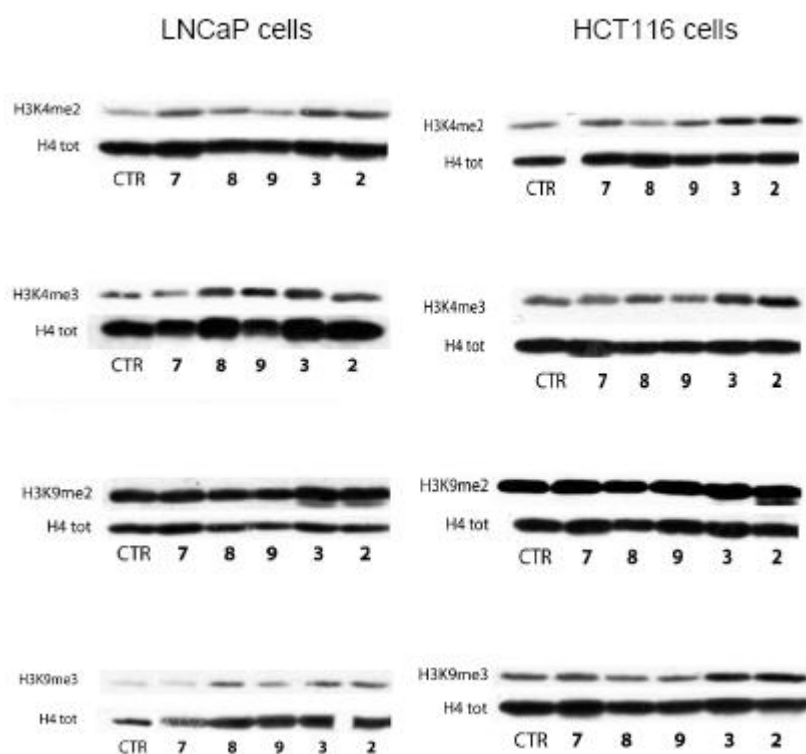
Figure 6.8. Western blot analyses of H3K4me2/3 and H3K9me2/3 methylation after treatment of LNCaP (left) and HCT116 (right) cells with **2**, **3** and the references **7-9**.

In conclusion, we have shown that "pan-KDM" inhibitors can be obtained by coupling the chemical features of tranylcypromine, a known LSD1 inhibitor, with the 2,2'-bipyridine or 5-carboxy-8HQ scaffolds, two 2OG competitive moieties developed for JmjC inhibition. Such compounds are able to inhibit LSD1 as well as JmjC enzymes while have little or no effect against other tested 2OG enzymes lacking KDM activity. It is also interesting that the tranylcypromine-moieties act as covalently binding inhibitors, whereas the JmjC inhibitor scaffolds bind reversibly (note the excellent safety record of covalent clinical candidates and marketed agents that has been recently described)[373]. The application of such LSD/JmjC hybrid inhibitors to cells enables simultaneous increases in levels of H3K4me2/3 and H3K9me2/3 as well as high growth arrest and apoptosis (**2** and **3**) in LNCaP prostate and HCT116 colon cancer cells, whereas the related family-specific single-target inhibitors **7-9** as well as a combination of **7** plus **8** were inactive. When tested in MePR non-cancer cells to assess their differential toxicity, **2** and **3** showed very low (**2**) or no (**3**) ability to increase the pre-G1 accumulation. It should be noted that since a single KDM may target multiple substrates, different biological effects depending on the context could manifest. To the best of our knowledge, these are the first pan-KDM inhibitors to be described. More generally, the results demonstrate that hybrid molecules inhibiting

117

different classes of histone modifying enzymes have substantial potential as functional probes or histone methylation, and we suggest that combining other types of inhibitors targeting histone modifying enzymes may be productive with respect to regulating the expression of specific (sets of) genes. Our pan-demethylase inhibitors may also be useful for medicinal chemistry efforts relating to cancer, in line with what happens with SAHA, which likely owes its anticancer activity to its pan-HDAC inhibitor profile[374].

Experimental section

Chemistry. Melting points were determined on a Buchi 530 melting point apparatus. ^{1}H-NMR and ^{13}C-NMR spectra were recorded at 400 MHz using a Bruker AC 400 spectrometer; chemical shifts are reported in δ (ppm) units relative to the internal reference tetramethylsilane (Me$_4$Si). Mass spectra were recorded on a API-TOF Mariner by Perspective Biosystem (Stratford, Texas, USA), samples were injected by an Harvard pump using a flow rate of 5−10 μL/min, infused in the Electrospray system. All compounds were routinely checked by TLC and 1H NMR. TLC was performed on aluminum-backed silica gel plates (Merck DC, Alufolien Kieselgel 60 F254) with spots visualized by UV light or using a KMnO$_4$ alkaline solution. All solvents were reagent grade and, when necessary, were purified and dried by standard methods. Concentration of solutions after reactions and extractions involved the use of a rotary evaporator operating at reduced pressure of ~ 20 Torr. Organic solutions were dried over anhydrous sodium sulfate. Elemental analysis has been used to determine purity of the described compounds, that is >95%. Analytical results are within 0.40% of the theoretical values. All chemicals were purchased from Sigma Aldrich s.r.l., Milan (Italy) or from TCI Europe N.V., Zwijndrecht (Belgium), and were of the highest purity. As a rule, samples prepared for physical and biological studies were dried in high vacuum over P$_2$O$_5$ for 20h at temperatures ranging from 25 to 40 °C, depending on the sample melting point.

trans-**Methyl 4'-((4-(2-((*tert*-Butoxycarbonyl)amino)cyclopropyl)phenyl)carbamoyl)-[2,2'-bipyridine]-4-carboxylate (11).** The reagents HOBT (62 mg, 0.39 mmol, 1.2 eq), EDCI (75 mg, 0.39 mmol, 1.2 eq) and Et$_3$N (0.15 mL, 1.11 mmol, 3.4 eq) were added in sequence to a mixture of compound **8** (101 mg, 0.39 mmol, 1.2 eq) and *trans-tert*-butyl 2-(4- aminophenyl)cyclopropylcarbamate **10** (81 mg, 0.33 mmol, 1.0 eq) in dry DMF (2.1

mL), and the resulting solution was stirred at room temperature overnight. The reaction was quenched with brine (5 mL) and concentrated under reduced pressure, and the aqueous phase was extracted with AcOEt (4 × 30 mL). The combined organic phases were washed with NaHCO$_3$ saturated solution (2 × 7 mL) and brine (5 mL). The organic phases were collected, dried over anhydrous Na$_2$SO$_4$, filtered and concentrated *in vacuo* to give a crude product that was purified by column chromatography on silica gel (eluent: CHCl$_3$/MeOH 100/1) to give compound **11** (127 mg, 80%) as an off-white solid. Mp: 196-199 °C (EtOH). ^{1}H-NMR (DMSO-d_6) δ$_H$/ppm: 1.10 (m, 2H, -CH_2- cyclopropane ring), 1.43 (s, 9H, NHCO$_2$C(CH_3)$_3$), 1.91 (m, 1H, -CH- cyclopropane ring), 2.62 (m, 1H, -CH-cyclopropane ring), 3.98 (s, 3H, CO$_2$CH_3), 7.12 (d, 2H, benzene ring), 7.24 (bs, 1H, CHNHCO$_2$tBu), 7.70 (d, 2H, benzene ring), 7.97 (m, 2H, bipyridine rings), 8.89 (s, 2H, bipyridine rings), 8.93 (m, 1H, bipyridine ring), 8.98 (m, 1H, bipyridine ring), 10.64 (bs, 1H, ArNHCO). ^{13}C-NMR (DMSO-d_6) δ/ppm: 15.6, 22.4, 29.3, 31.3, 49.7, 81.2, 117.8, 118.2, 121.1, 121.8, 122.6, 126.5, 132.4, 137.6, 142.8, 149.2, 150.0, 154.8, 155.3, 156.0, 159.2, 166.7, 168.8. MS, m/z: 489 [M+H]$^+$.

General Procedure for the Synthesis of *trans*-Methyl 4'-((4-(2-Aminocyclopropyl)phenyl)carbamoyl)-[2,2'-bipyridine]-4-carboxylate hydrochloride (2), *trans*-N-(4-(2-Aminocyclopropyl)phenyl)-8-hydroxyquinoline-5-carboxamide hydrochloride (3) and *trans*-N-(ω-((4-(2-Aminocyclopropyl)phenyl)amino)-ω-oxoalkyl)-8-hydroxyquinoline-5-carboxamide hydrochlorides (4-6). Example: *trans*-N-(4-((4-(2-Aminocyclopropyl)phenyl)amino)-4-oxobutyl)-8-hydroxyquinoline-5-carboxamide hydrochloride (4). Compound **18** (100 mg, 0.18 mmol, 1.0 eq) was dissolved in a mixture of dry THF/MeOH (1.4 mL/1.4 mL) and the solution stirred at 0 °C, then 4N HCl in 1,4-dioxane (3.65 mL, 14.58 mmol, 80 eq) was added dropwise and the mixture was allowed to warm at room temperature. After 3 hours, the suspension was cooled at 0 °C, and 4N HCl in 1,4-dioxane (1.82 mL, 7.29 mmol, 40 eq) was added dropwise again. After 8 hours, when conversion was complete, the suspension was filtered and washed with dry THF and then with dry Et$_2$O to afford compound **4** (68 mg, 85%) as a yellow hygroscopic solid. Mp: >250 °C (THF/MeOH). ^{1}H-NMR (DMSO-d_6) δ$_H$/ppm: 1.15 (m, 1H, -CHH- cyclopropane ring), 1.35 (m, 1H, -CHH- cyclopropane ring), 1.90 (m, 2H, CH$_2$CH_2CH$_2$), 2.28 (m, 1H, -CH- cyclopropane ring), 2.42 (m, 2H, CH$_2$C$H2$CO), 2.74 (m,

1H, -CH- cyclopropane ring), 7.06 (d, 2H, benzene ring), 7.30 (d, 1H, quinoline ring), 7.52 (d, 2H, benzene ring), 7.87 (m, 2H, quinoline ring), 8.47 (bs, 3H, CHNH_2 .HCl), 8.65 (bs, 1H, CONHCH2), 9.02 (d, 1H, quinoline ring), 9.24 (d, 1H, quinoline ring), 10.01 (s, 1H, ArNHCO), 11.40 (bs, 1H, quinoline OH). ^{13}C-NMR (DMSO-d_6) δ_C/ppm: 14.9, 22.8, 26.2, 28.5, 34.1, 40.1, 112.4, 119.7, 124.5, 126.7, 128.2, 128.5, 130.5, 131.1, 133.6, 135.3, 138.9, 150.3, 157.7, 162.1, 180.6. MS (relative to free amine), m/z: 405 [M+H]$^+$.

***trans*-Methyl 4'-((4-(2-Aminocyclopropyl)phenyl)carbamoyl)-[2,2'-bipyridine]-4-carboxylate hydrochloride (2).** Mp: >250 °C (THF/MeOH). Yield: 61%. ^{1}H-NMR (DMSO-d_6) δ_H/ppm: 1.22 (m, 1H, -CHH- cyclopropane ring), 1.39 (m, 1H, -CHH- cyclopropane ring), 2.34 (m, 1H, -CH cyclopropane ring), 2.81 (m, 1H, -CH- cyclopropane ring), 3.97 (s, 3H, CO$_2$CH_3), 7.19 (d, 2H, benzene ring), 7.76 (d, 2H, benzene ring), 7.99 (m, 2H, bipyridine rings), 8.43 (bs, 3H, CHNH_2 .HCl), 8.89 (s, 2H, bipyridine rings), 8.94 (d, 1H, bipyridine ring), 8.98 (d, 1H, bipyridine ring), 10.71 (bs, 1H, ArNHCO). ^{13}C-NMR (DMSO-d_6) δ_C/ppm: 14.5, 22.4, 28.3, 52.0, 117.6, 118.1, 120.8, 122.1, 123.0, 125.8, 133.4, 137.5, 144.1, 149.9, 150.5, 155.2, 156.8, 158.2, 165.3, 166.4. MS (relative to free amine), m/z: 389 [M+H]$^+$.

***trans*-N-(4-(2-Aminocyclopropyl)phenyl)-8-hydroxyquinoline-5-carboxamide hydrochloride (3).** Mp: >250 °C (THF/MeOH). Yield: 71%. ^{1}H-NMR (DMSO-d_6) δ_H/ppm: 1.23 (m, 1H, -CHHcyclopropane ring), 1.38 (m, 1H, -CHH- cyclopropane ring), 2.32 (m, 1H, -CH- cyclopropane ring), 2.80 (m, 1H, -CH- cyclopropane ring), 7.17 (d, 2H, benzene ring), 7.28 (d, 1H, quinoline ring), 7.72 (d, 2H, benzene ring), 7.79 (m, 1H, quinoline ring), 7.94 (d, 1H, quinoline ring), 8.38 (bs, 3H, CHNH_2 .HCl), 9.00 (m, 2H, quinoline ring), 10.47 (s, 1H, ArNHCO). ^{13}C-NMR (DMSO-d_6) δ_C/ppm: 14.8, 22.6, 28.2, 113.8, 121.7, 125.7, 126.8, 128.0, 129.1, 130.2, 130.9, 134.1, 135.8, 137.9, 152.1, 159.3, 165.1. MS (relative to free amine), m/z: 320 [M+H]$^+$.

***trans*-N-(5-((4-(2-Aminocyclopropyl)phenyl)amino)-5-oxopentyl)-8-hydroxyquinoline-5- carboxamide hydrochloride (5).** Mp: >250 °C (THF/MeOH). Yield: 65%. ^{1}H-NMR (DMSO-d_6) δ_H/ppm: 1.17 (m, 1H, -CHH- cyclopropane ring), 1.33 (m, 1H, -CHH- cyclopropane ring), 1.64 (m, 4H, CH$_2$CH_2CH_2CH$_2$), 2.26 (m, 1H, -CH- cyclopropane ring), 2.36 (t, 2H, CH$_2$CH_2CO), 2.75 (m, 1H, -CH cyclopropane ring), 7.07 (d, 2H,

benzene ring), 7.21 (d, 1H, quinoline ring), 7.53 (d, 2H, benzene ring), 7.78 (m, 2H, quinoline ring), 8.35 (bs, 3H, CHNH_2 .HCl), 8.57 (bs, 1H, CONHCH$_2$), 8.97 (d, 1H, quinoline ring), 9.06 (d, 1H, quinoline ring), 9.92 (s, 1H, ArNHCO), 11.10 (bs, 1H, quinoline OH). ^{13}C-NMR (DMSO-d_6) δ_C/ppm: 14.5, 22.3, 23.1, 28.0, 29.4, 38.3, 39.0, 114.4, 121.9, 125.4, 126.6, 127.9, 128.8, 130.5, 131.1, 134.7, 135.4, 138.9, 151.7, 159.3, 162.4, 179.7. MS (relative to free amine), m/z: 419 [M+H]$^+$.

trans-_N_-(6-((4-(2-Aminocyclopropyl)phenyl)amino)-6-oxohexyl)-8-hydroxyquinoline-5- carboxamide hydrochloride (6). Mp: >250 °C (THF/MeOH). Yield: 89%. ^{1}H-NMR (DMSO-d_6) δ_H/ppm: 1.18 (m, 1H, -CHH- cyclopropane ring), 1.38 (m, 3H, -CHH- cyclopropane ring and –CH$_2$- aliphatic chain), 1.61 (m, 4H, aliphatic chain), 2.32 (m, 3H, -CH- cyclopropane ring and CH$_2$CH_2CO), 2.75 (m, 1H, -CH- cyclopropane ring), 3.33 (t, 2H, NHCH_2CH$_2$), 7.06 (d, 2H, benzene ring), 7.33 (d, 1H, quinoline ring), 7.52 (d, 2H, benzene ring), 7.85 (d, 1H, quinoline ring), 7.89 (m, 1H, quinoline ring), 8.43 (bs, 3H, CHNH_2 .HCl), 8.62 (bs, 1H, CONHCH$_2$), 9.03 (d, 1H, quinoline ring), 9.24 (d, 1H, quinoline ring), 9.92 (s, 1H, ArNHCO). ^{13}C-NMR (DMSO-d_6) δ_C/ppm: 14.3, 22.2, 25.2, 25.7, 28.1, 29.5, 38.4, 39.5, 114.3, 121.5, 125.8, 126.9, 127.7, 128.7, 130.4, 131.3, 134.5, 135.3, 138.8, 151.7, 159.5, 162.7, 179.8. MS (relative to free amine), m/z: 433 [M+H]$^+$.

4'-((4-(2-((_tert_-Butoxycarbonyl)amino)cyclopropyl)phenyl)carbamoyl)-[2,2'-bipyridine]-4- carboxylic acid (12). Compound **11** (111 mg, 0.227 mmol, 1.0 eq) was suspended in 4 mL of MeOH and cooled in an ice bath, then NaOH (27.3 mg, 0.682 mmol, 3.0 eq) in water (0.7 mL) was added dropwise and the mixture was allowed to stir at room temperature. After 9 hours the organic solvent was removed _in vacuo_ and the aqueous phase, cooled at 0 °C, was acidified to pH 2 with a solution of 0.5N KHSO4. The obtained suspension was filtered to afford the desired compound **12** (96 mg, 89%) as a yellow solid. Mp: >250 °C (EtOH). ^{1}H-NMR (DMSO-d_6) δ_H/ppm: 1.11 (m, 2H, -CH_2- cyclopropane ring), 1.39 (s, 9H, NHCO$_2$C(CH_3)$_3$), 1.90 (m, 1H, -CH- cyclopropane ring), 2.62 (m, 1H, -CH cyclopropane ring), 7.12 (d, 2H, benzene ring), 7.24 (bs, 1H, CHNHCO$_2$tBu), 7.70 (d, 2H, benzene ring), 7.95 (m, 2H, bipyridine rings), 8.88 (s, 2H, bipyridine rings), 8.94 (m, 2H, bipyridine ring), 10.64 (bs, 1H, ArNHCO), 13.89 (bs, 1H, COOH). ^{13}C-NMR (DMSO-d_6) δ_C/ppm: 14.1, 21.9, 27.8, 32.7, 80.3, 117.6, 118.2, 118.4, 120.1, 121.5, 124.4,

125.3, 134.0, 137.4, 144.9, 149.1, 149.9, 154.9, 155.4, 155.9, 159.5, 164.8, 170.1. MS, m/z: 475 [M+H]$^{+}$.

trans-4'-((4-(2-Aminocyclopropyl)phenyl)carbamoyl)-[2,2'-bipyridine]-4-carboxylic acid trifluoroacetate (1). Trifluoroacetic acid (1.04 mL, 13.54 mmol, 230 eq) was added to **12** (28.2 mg, 0.059 mmol, 1.0 eq) placed in an ice bath, and the mixture was allowed to stir at room temperature. After 5 hours the solvent was removed at low temperature under reduced pressure, then the solid was stirred as suspension in dry Et$_2$O for 1 hour and filtered to provide the desired compound **1** (26 mg, 90%) as a dark red solid. Mp: >250 °C (THF/MeOH). ^{1}H-NMR (DMSO-d_6) δ_H/ppm: 1.23 (m, 1H, - C*H*H- cyclopropane ring), 1.33 (m, 1H, -C*H*H- cyclopropane ring), 2.28 (m, 1H, -C*H*- cyclopropane ring), 2.84 (m, 1H, -C*H*- cyclopropane ring), 7.20 (d, 2H, benzene ring), 7.74 (d, 2H, benzene ring), 7.96 (m, 2H, bipyridine rings), 8.26 (bs, 3H, N*H*$_2$ .CF$_3$COO*H*), 8.88 (s, 2H, bipyridine rings), 8.94 (m, 2H, bipyridine ring), 10.69 (bs, 1H, ArN*H*CO). ^{13}C-NMR (DMSO-d_6) δ_C/ppm: 14.9, 22.6, 28.2, 117.3, 117.9, 118.7, 120.7, 121.2, 124.1, 125.5, 134.5, 138.7, 144.9, 149.2, 149.8, 155.2, 156.1, 159.8, 162.2, 164.9, 170.4. MS (relative to free amine), m/z: 375 [M+H]$^{+}$.

8-(Methoxymethoxy)quinoline-5-carboxylic acid (13). 8-Hydroxyquinoline-5-carboxylic acid (2.41 g, 12.8 mmol, 1 eq) was added portion wise to a stirring suspension of 60% NaH (1.28 g, 31.9 mmol, 2.5 eq) in dry THF (30 mL) at 0 °C, and the resulting mixture was stirred under inert atmosphere (N$_2$) for 30 min. Then MOM-Br (2.5 mL, 30.6 mmol, 2.4 eq) dissolved in dry THF (20 mL) was added dropwise, and the suspension was allowed to warm to room temperature under inert atmosphere (N$_2$). After 4 hours, a solution of LiOH (1.22 g, 51.0 mmol, 4.0 eq) in water (25.5 mL) was added at 0 °C, and the resulting mixture was stirred at room temperature overnight. The reaction mixture was acidified with glacial acetic acid to pH 4 and then extracted with DCM (5 × 90 mL); the organic phases were collected, dried over anhydrous Na2SO4, filtered and the solvent removed under reduced pressure to give compound **13** (2.92 g, 98%) as a white solid. Mp: 157-159 °C (CH$_3$CN/MeOH). ^{1}H-NMR (CD$_3$OD) δ_H/ppm: 2.09 (s, 3H, CH$_2$OC*H*$_3$), 4.08 (s, 2H, OC*H*$_2$OCH$_3$), 5.97 (d, 1H, quinoline ring), 6.18 (m, 1H, quinoline ring), 6.83 (d, 1H, quinoline ring), 7.39 (d, 1H, quinoline ring), 8.06 (d, 1H, quinoline ring). ^{13}C-NMR

(CD$_3$OD) δ_C/ppm: 55.1, 95.3, 104.5, 119.0, 122.7, 126.5, 131.3, 133.1, 140.0, 148.1, 159.7, 167.5. MS, m/z: 234 [M+H]$^+$.

trans-tert-Butyl(2-(4-(8-(Methoxymethoxy)quinoline-5-carboxamido)phenyl)cyclo-propyl) carbamate (14). Compound **14** was prepared following the same procedure used for **11**, starting from **13** and **10**. Mp: 188-191 °C (CH$_3$CN). Yield: 67%. ^{1}H-NMR (CDCl$_3$) δ_H/ppm: 1.19 (m, 2H, -CH_2- cyclopropane ring), 1.49 (s, 9H, NHCO$_2$C(CH_3)$_3$), 2.07 (m, 1H, -CH- cyclopropane ring), 2.74 (m, 1H, -CH- cyclopropane ring), 3.61 (s, 3H, CH$_2$OCH_3), 5.58 (s, 2H, OCH_2OCH$_3$), 7.21 (d, 2H, benzene ring), 7.44 (d, 1H, quinoline ring), 7.56 (m, 3H, quinoline ring and benzene ring), 7.67 (s, 1H, CONHAr), 7.80 (d, 1H, quinoline ring), 8.93 (d, 1H, quinoline ring), 9.04 (d, 1H, quinoline ring). ^{13}C NMR (CDCl$_3$) δ_C/ppm: 15.2, 23.3, 29.0, 32.8, 55.4, 80.5, 95.1, 107.8, 121.8, 125.3, 126.0, 127.7, 128.3, 130.0, 131.4, 133.8, 136.5, 138.1, 151.5, 156.4, 161.2, 164.4. MS, m/z: 464 [M+H]$^+$.

General Procedure for the Synthesis of 8-(Methoxymethoxy)quinoline-5-carboxyamidoalkyl Methyl Esters (15-17). Example: Methyl 4-({[8-(Methoxymethoxy)quinolin-5- yl]carbonyl}amino)butanoate (15). The reagents HOBT (382 mg, 2.40 mmol, 1.2 eq), EDCI (460 mg, 2.40 mmol, 1.2 eq) and Et$_3$N (1.12 mL, 8 mmol, 4.0 eq) were added in sequence to a mixture of **13** (560 mg, 2.40 mmol, 1.2 eq) and methyl 4-aminobutanoate hydrochloride (306 mg, 2 mmol, 1 eq) in dry DCM (12 mL), and the solution was stirred at room temperature. After overnight stirring, the reaction mixture was diluted with DCM (90 mL) and the organic phase washed with Na$_2$CO$_3$ (2 × 50 mL) and brine (2 × 50 mL), dried over anhydrous Na$_2$SO$_4$, filtered and concentrated *in vacuo* to give a residue that was purified by column chromatography on silica gel (eluent: DCM/MeOH 35/1). The collected fractions were evaporated and the resulting crude was finally recrystallized from benzene/cyclohexane to afford compound **15** (550 mg, 83%) as a white solid. ^{1}H-NMR (CDCl$_3$) δ_H/ppm: 2.04 (m, 2H, NCH$_2$CH_2CH$_2$), 2.52 (t, 2H, CH$_2$CH_2CO$_2$Me), 3.61 (m, 5H, NHCH_2CH$_2$ and CO$_2$CH_3), 3.70 (s, 3H, OCH$_2$OCH_3), 5.56 (s, 2H, OCH_2OCH$_3$), 6.32 (bs, 1H, CONHCH$_2$), 7.39 (d, 1H, quinoline ring), 7.53 (m, 1H, quinoline ring), 7.66 (d, 1H, quinoline ring), 8.91 (d, 1H, quinoline ring), 9.01 (d, 1H, quinoline ring). ^{13}C-NMR (CDCl$_3$) δ_C/ppm: 22.8, 29.5, 40.3, 50.7, 55.4, 92.7, 107.8, 126.3,

129.7, 130.1, 131.3, 131.9, 137.5, 151.3, 163.4, 165.0, 176.1. m.p.: 115-117 °C (benzene/cyclohexane). MS, m/z: 333 [M+H]$^+$.

Methyl 5-({[8-(Methoxymethoxy)quinolin-5-yl]carbonyl}amino)pentanoate (16). ^{1}H-NMR (CDCl$_3$) δ_H/ppm: 1.77 (m, 4H, CH$_2$CH$_2$CH$_2$CH$_2$), 2.44 (t, 2H, CH$_2$CH$_2$CO$_2$Me), 3.53 (m, 2H, NHCH$_2$CH$_2$), 3.60 (s, 3H, CO$_2$CH$_3$), 3.71 (s, 3H, OCH$_2$OCH$_3$), 5.56 (s, 2H, OCH$_2$OCH$_3$), 6.16 (bs, 1H, CONHCH$_2$), 7.39 (d, 1H, quinoline ring), 7.53 (m, 1H, quinoline ring), 7.67 (d, 1H, quinoline ring), 8.89 (d, 1H, quinoline ring), 9.00 (d, 1H, quinoline ring). ^{13}C-NMR (CDCl$_3$) δ_C/ppm: 22.3, 30.1, 32.4, 39.7, 52.6, 56.6, 92.7, 111.2, 128.1, 128.7, 130.2, 132.1, 133.7, 137.9, 155.3, 163.4, 164.1, 176.7. m.p.: 96-98 °C (benzene/cyclohexane). Yield: 52%. MS, m/z: 347 [M+H]$^+$.

Methyl 6-({[8-(Methoxymethoxy)quinolin-5-yl]carbonyl}amino)hexanoate (17). ^{1}H-NMR (CDCl$_3$) δ_H/ppm: 1.50 (m, 2H, aliphatic chain), 1.72 (m, 4H, aliphatic chain), 2.38 (t, 2H, CH$_2$CH$_2$CO$_2$Me), 3.55 (m, 2H, NHCH$_2$CH$_2$), 3.60 (s, 3H, CH$_2$OCH$_3$), 3.69 (s, 3H, CO$_2$CH3), 5.56 (s, 2H, OCH$_2$OCH$_3$), 6.06 (bs, 1H, CONHCH$_2$), 7.39 (d, 1H, quinoline ring), 7.53 (m, 1H, quinoline ring), 7.65 (d, 1H, quinoline ring), 8.87 (d, 1H, quinoline ring), 9.01 (d, 1H, quinoline ring). ^{13}C-NMR (CDCl$_3$) δ_C/ppm: 24.3, 25.2, 30.1, 32.9, 41.6, 51.7, 57.6, 93.2, 109.8, 123.2, 128.9, 129.6, 131.2, 132.3, 135.2, 153.8, 161.1, 162.8, 175.8. m.p.: 121-123 °C (benzene/cyclohexane). Yield: 66%. MS, m/z: 361 [M+H]$^+$.

General Procedure for the Synthesis of *trans-tert*-Butyl (2-(4-(ω-(8-(Methoxymethoxy)quinoline-5-carboxamido)alkylamido)phenyl)cyclopropyl) carbamate (18-20). Example: *trans-tert*-Butyl(2-(4-(6-(8-(Methoxymethoxy)quinoline-5-carboxamido)hexanamido)phenyl) cyclopropyl)carbamate (20). LiOH (102 mg, 4.26 mmol, 4.0 eq.) dissolved in water (3 mL) was added to a stirred solution of **17** (360 mg, 1.07 mmol, 1.0 eq.) in THF (4 mL) placed on an ice bath, and the resulting mixture was stirred at room temperature overnight. The reaction was acidified with glacial acetic acid to pH 4-5, then diluted with DCM (50 mL) and extracted; the aqueous phase was further extracted with DCM (9 × 50 mL). The organic phases were collected, dried over anhydrous Na$_2$SO$_4$, filtered and concentrated *in vacuo* to afford the 5-({[8-(methoxymethoxy)quinolin-5-yl]carbonyl}amino)hexanoic acid (300 mg, 85%) as a white solid that was used in the next step without further purification. HOBT (92 mg, 0.58 mmol,

1.1 eq.), EDCI (110 mg, 0.58 mmol, 1.1 eq.) and Et$_3$N (0.24 mL, 1.70 mmol, 3.2 eq.) were added in sequence to a mixture of 5-({[8-(methoxymethoxy)quinolin-5-yl]carbonyl}amino)hexanoic acid (190 mg, 0.58 mmol, 1.1 eq.) and *trans-tert*-butyl 2-(4-aminophenyl)cyclopropylcarbamate **10** (132 mg, 0.53 mmol, 1.0 eq.) in dry DMF (4.2 mL) and the resulting solution was stirred at room temperature. After 18 hours the solvent was evaporated under reduced pressure and the residue partitioned between AcOEt (100 mL) and brine (20 mL). The organic phase was further washed with NaHCO$_3$ saturated solution (2 × 40 mL) and the aqueous phases back-extracted with AcOEt (40 mL). The organic phases were collected, dried over anhydrous Na$_2$SO$_4$, filtered and concentrated *in vacuo* to give a crude product that was purified by column chromatography on silica gel (eluent: CHCl$_3$/MeOH 30/1) to give compound **20** (226 mg, 74%) as a yellow foam. ^{1}H-NMR (CDCl$_3$) δ$_H$/ppm: 1.15 (m, 2H, -C*H$_2$*- cyclopropane ring), 1.47 (s, 9H, NCO$_2$C(C*H$_3$*)$_3$), 1.53 (m, 2H, aliphatic chain), 1.72 (m, 2H, aliphatic chain), 1.81 (m, 2H, aliphatic chain), 2.02 (m, 1H, -C*H*- cyclopropane ring), 2.40 (t, 2H, CH$_2$C*H$_2$*CO), 2.68 (m, 1H, -C*H*- cyclopropane ring), 3.57 (m, 5H, NHC*H$_2$*CH$_2$ and CH$_2$OC*H$_3$*), 4.88 (bs, 1H, CHN*H*CO$_2$tBu), 5.55 (s, 2H, OC*H$_2$*OCH$_3$), 6.28 (bs, 1H, CON*H*CH$_2$), 7.07 (d, 2H, benzene ring), 7.35 (m, 2H, quinoline ring and ArN*H*CO), 7.40 (d, 2H, benzene ring), 7.50 (m, 1H, quinoline ring), 7.65 (d, 1H, quinoline ring), 8.87 (d, 1H, quinoline ring), 9.00 (d, 1H, quinoline ring). ^{13}C-NMR (CDCl$_3$) δ$_C$/ppm: 16.3, 21.7, 24.6, 26.7, 29.1, 29.7, 32.5, 37.6, 39.3, 53.8, 79.1, 89.4, 107.5, 124.6, 127.3, 127.8, 128.2, 129.3, 132,5, 133.6, 135.0, 139.2, 140.6, 151.0, 153.3, 159.8, 162.7, 182.9. m.p.: 69-72 °C (cyclohexane). MS, m/z: 577 [M+H]$^+$.

***trans-tert*-Butyl-(2-(4-(4-(8-(Methoxymethoxy)quinoline-5-carboxamido)butanamido) phenyl) cyclopropyl)carbamate (18).** ^{1}H-NMR (CDCl$_3$) δ$_H$/ppm: 1.14 (m, 2H, -C*H$_2$*- cyclopropane ring), 1.47 (s, 9H, NCO$_2$C(C*H$_3$*)$_3$), 2.02 (m, 1H, -C*H*- cyclopropane ring), 2.09 (m, 2H, CH$_2$C*H$_2$*CH$_2$), 2.53 (t, 2H, CH$_2$C*H$_2$*CONH), 2.69 (m, 1H, -C*H*- cyclopropane ring), 3.59 (s, 3H, CH$_2$OC*H$_3$*), 3.66 (m, 2H, NHC*H$_2$*CH$_2$), 4.89 (bs, 1H, CHN*H*CO$_2$tBu), 5.54 (s, 2H, OC*H$_2$*OCH$_3$), 6.65 (bs, 1H, CON*H*CH$_2$), 7.08 (d, 2H, benzene ring), 7.32 (d, 1H, quinoline ring), 7.50 (m, 3H, benzene ring and quinoline ring), 7.65 (d, 1H, quinoline ring), 8.46 (bs, 1H, ArN*H*CO), 8.89 (d, 1H, quinoline ring), 9.00 (d, 1H, quinoline ring). ^{13}C-NMR (CDCl$_3$) δ$_C$/ppm: 16.0, 22.1, 26.8, 27.5, 32.3, 35.8, 39.0, 53.5, 80.2, 95.5, 107.4,

119.6, 126.6, 126.9, 128.3, 129.3, 131.5, 133.9, 135.1, 137.7, 141.8, 148.8, 155.9, 159.5, 165.6, 184.4. m.p.: 184-186 °C (benzene/cyclohexane). Yield: 88%. MS, m/z: 549 [M+H]$^+$.

***trans-tert*-Butyl-(2-(4-(5-(8-(Methoxymethoxy)quinoline-5-carboxamido)penta namido)phenyl) cyclopropyl)carbamate (19).** ^{1}H-NMR (CDCl$_3$) δ_H/ppm: 1.15 (m, 2H, -C*H$_2$*- cyclopropane ring), 1.47 (s, 9H, NHCO$_2$C(C*H$_3$*)$_3$), 1.78 (m, 2H, aliphatic chain) 1.87 (m, 2H, aliphatic chain), 2.02 (m, 1H, -C*H*- cyclopropane ring), 2.09 (m, 2H, CH$_2$C*H$_2$*CH$_2$), 2.49 (t, 2H, CH$_2$C*H$_2$*CO), 2.68 (m, 1H, -C*H*- cyclopropane ring), 3.58 (m, 5H, NHC*H$_2$*CH$_2$ and CH$_2$OC*H$_3$*), 4.87 (bs, 1H, N*H*CO$_2$tBu), 5.56 (s, 2H, OC*H$_2$*OCH$_3$), 6.41 (bs, 1H, CON*H*CH$_2$), 7.07 (d, 2H, benzene ring), 7.38 (d, 1H, quinoline ring), 7.45 (m, 3H, benzene ring and quinoline ring), 7.64 (bs, 1H, ArN*H*CO), 7.68 (d, 1H, quinoline ring), 8.85 (d, 1H, quinoline ring), 9.00 (d, 1H, quinoline ring). ^{13}C-NMR (CDCl$_3$) δ_C/ppm: 15.8, 21.7, 21.9, 27.8, 29.1, 29.8, 37.7, 39.4, 53.0, 80.1, 93.8, 106.9, 123.4, 126.6, 127.0, 127.5, 128.4, 130.0, 131.8, 136.1, 137.7, 138.1, 149.7, 156.5, 161.2, 164.4, 182.2. m.p.: 111-114 °C (cyclohexane). Yield: 74%. MS, m/z: 563 [M+H]$^+$.

General Procedure for the Synthesis of ω-(8-Hydroxyquinoline-5-carboxamido)alkyl Methyl Esters (21-23). Example: Methyl 5-(8-Hydroxyquinoline-5-carboxamido)pentanoate (22). Compound **16** (150 mg, 0.43 mmol, 1.0 eq.) was dissolved in a mixture of dry THF/MeOH (2 mL/2 mL) and the solution was stirred at 0 °C, then 4N HCl in 1,4-dioxane (6.5 mL, 25.98 mmol, 60 eq.) was added dropwise, and the mixture was allowed to warm to room temperature. After 6 hours, when conversion was complete, the suspension was filtered and washed with dry Et$_2$O to give compound **22** (125 mg, 95%) as a yellow solid. ^{1}H-NMR (DMSO-d_6) δ_H/ppm: 1.60 (m, 4H, CH$_2$C*H$_2$*C*H$_2$*CH$_2$), 2.38 (t, 2H, CH$_2$C*H$_2$*CO$_2$Me), 3.32 (m, 2H, NHC*H$_2$*CH$_2$), 3.60 (s, 3H, CO$_2$C*H$_3$*), 7.44 (d,1H, quinoline ring), 7.92 (d, 1H, quinoline ring), 8.00 (m, 1H, quinoline ring), 8.70 (bs, 1H, CON*H*CH$_2$), 9.08 (d, 1H, quinoline ring), 9.39 (m, 1H, quinoline ring), 12.17 (bs, 1H, ArO*H*). ^{13}C-NMR (DMSO-d_6) δ_C/ppm: 22.9, 29.7, 32.8, 40.1, 50.8, 111.6, 126.5, 128.5, 131.6, 132.0, 134.9, 140.2, 153.0, 161.2, 163.8, 175.9. m.p.: 175-177 °C (CH$_3$CN). MS, m/z: 303 [M+H]$^+$.

Methyl 6-(8-Hydroxyquinoline-5-carboxamido)hexanoate (23). ^{1}H-NMR (DMSO-d_6) δ_H/ppm: 1.37 (m, 2H, aliphatic chain), 1.59 (m, 4H, aliphatic chain), 2.33 (t, 2H, CH$_2$C*H*$_2$CO$_2$Me), 3.30 (m, 2H, NHC*H*$_2$CH$_2$), 7.28 (d, 1H, quinoline ring), 7.82 (d, 1H, quinoline ring), 7.87 (m, 1H, quinoline ring), 8.57 (bs, 1H, CON*H*CH$_2$), 9.02 (d, 1H, quinoline ring), 9.18 (d, 1H, quinoline ring), 11.35 (bs, 1H, ArO*H*). ^{13}C-NMR (DMSO-d_6) δ_C/ppm: 24.5, 26.4, 30.0, 32.7, 40.4, 51.5, 109.5, 122.6, 130.4, 130.8, 133.0, 133.7, 134.0, 152.5, 160.8, 163.0, 174.1. m.p.: 164-166 °C (CH$_3$CN). Yield: 97%. **MS,** m/z: 317 [M+H]$^+$.

Methyl 4-(8-Hydroxyquinoline-5-carboxamido)butanoate (21). ^{1}H-NMR (DMSO-d_6) δ_H/ppm: 1.84 (m, 2H, CH$_2$C*H*$_2$CH$_2$), 2.42 (t, 2H, CH$_2$C*H*$_2$CO$_2$Me), 3.61 (s, 3H, CO$_2$C*H*$_3$), 7.09 (d, 1H, quinoline ring), 7.62 (m, 1H, quinoline ring), 7.69 (d, 1H, quinoline ring), 8.43 (bs, 1H, CON*H*CH$_2$), 8.87 (m, 2H, quinoline ring), 10.21 (bs, 1H, ArO*H*). ^{13}C-NMR (DMSO-d_6) δ_C/ppm: 23.6, 30.0, 39.7, 50.2, 107.7, 126.8, 129.8, 130.0, 133.1, 133.8, 136.8, 151.2, 162.7, 164.9, 176.0. m.p.: 185-186 °C (CH$_3$CN). Yield: 77%. **MS,** m/z: 289 [M+H]$^+$.

General Procedure for the Synthesis of ω-(8-Hydroxyquinoline-5-carboxamido)alkanoic acids (24-26). Example: 5-(8-Hydroxyquinoline-5-carboxamido)pentanoic acid (25). A solution of LiOH (47 mg, 1.11 mmol, 3.0 eq.) in water (0.6 mL) was added to a stirred solution of compound **22** (112 mg, 0.37 mmol, 1.0 eq.) in THF (1.3 mL) placed on an ice bath, and the resulting mixture was stirred at room temperature overnight. The solvent was removed, NaHCO$_3$ saturated solution (10 mL) was added and the aqueous phase was washed with AcOEt (3 × 10 mL). The aqueous solution was acidified with glacial acetic acid to pH 4, then extracted with AcOEt (5 × 20 mL). The organic phases were collected, dried over anhydrous Na$_2$SO$_4$, filtered and concentrated *in vacuo* to afford compound **25** (102 mg, 96%) as an off yellow solid. ^{1}H-NMR (DMSO-d_6) δ_H/ppm: 1.58 (m, 4H, aliphatic chain), 2.30 (t, 2H, CH$_2$C*H*$_2$CO$_2$H), 7.08 (d, 1H, quinoline ring), 7.62 (m, 1H, quinoline ring), 7.68 (d, 1H, quinoline ring), 8.41 (bs, 1H, CON*H*CH$_2$), 8.84 (d, 1H, quinoline ring), 8.88 (d, 1H, quinoline ring), 10.17 (bs, 1H, ArO*H*), 11.98 (bs, 1H, CH$_2$CO$_2$*H*). ^{13}C-NMR (DMSO-d_6) δ_C/ppm: 22.6, 29.8, 33.3, 39.9, 111.1, 126.3, 128.4,

128.7, 131.8, 132.7, 136.0, 151.0, 160.1, 162.9, 177.9. m.p.: 207-209 °C (EtOH). MS, m/z: 289 [M+H]$^+$.

5-(8-Hydroxyquinoline-5-carboxamido)hexanoic acid (26). ^{1}H-NMR (DMSO-d_6) δ_H/ppm: 1.38 (m, 2H, aliphatic chain), 1.57 (m, 4H, aliphatic chain), 2.23 (t, 2H, CH$_2$C*H*$_2$CO$_2$H), 7.08 (d, 1H, quinoline ring), 7.62 (m, 1H, quinoline ring), 7.69 (d, 1H, quinoline ring), 8.41 (bs, 1H, CON*H*CH$_2$), 8.83 (d, 1H, quinoline ring), 8.88 (d, 1H, quinoline ring), 10.16 (bs, 1H, ArO*H*), 12.00 (bs, 1H, CH$_2$CO$_2$*H*). ^{13}C-NMR (DMSO-d_6) δ_C/ppm: 24.3, 27.2, 29.0, 34.5, 40.1, 110.4, 125.8, 128.8, 129.1, 131.9, 132.5, 133.9, 153.4, 158.5, 162.3, 175.5. m.p.: 187-189 °C (CH$_3$CN). Yield: 66%. MS, m/z: 303 [M+H]$^+$.

5-(8-Hydroxyquinoline-5-carboxamido)butanoic acid (24). ^{1}H-NMR (DMSO-d_6) δ_H/ppm: 1.79 (m, 2H, CH$_2$C*H*$_2$CH$_2$), 2.32 (m, 2H, CH$_2$C*H*$_2$CO$_2$H), 7.08 (d, 1H, quinoline ring), 7.62 (m, 1H, quinoline ring), 7.69 (d, 1H, quinoline ring), 8.44 (bs, 1H, CON*H*CH$_2$), 8.84 (d, 1H, quinoline ring), 8.89 (d, 1H, quinoline ring), 10.20 (bs, 1H, ArO*H*), 12.05 (bs, 1H, CH$_2$CO$_2$*H*). ^{13}C-NMR (DMSO-d_6) δ_C/ppm: 23.2, 33.2, 39.5, 110.8, 126.0, 128.5, 128.7, 131.9, 132.2, 135.5, 151.0, 159.7, 162.9, 178.8. m.p.: 217-218 °C (EtOH). Yield: 86%. MS, m/z: 275 [M+H]$^+$.

The chemical and physical data of the intermediate **11**-**26** and final compounds **1**-**6** are reported in Table 6.3 and Table 6.4, respectively.

Cpd	mp, °C	recrystall. Solvent	Yield %
11	196-199	A	80
12	>250	A	89
13	157-159	B	75
14	188-191	C	67
15	115-117	D	83
16	96-98	D	52
17	121-123	D	66
18	184-186	D	88
19	111-114	E	74
20	69-72	E	74
21	185-186	C	77
22	175-177	C	95
23	164-166	C	97
24	217-218	A	86
25	207-209	A	96
26	187-189	C	66

A: ethanol; B: acetonitrile/cyclohexane; C: acetonitrile; D: benzene/cyclohexane; E: cyclohexane

Table 6.3. Chemical and physical data of intermediates **11-26**.

Cpd	mp, °C	recrystall. Solvent	Yield %
1	>250	A	90
2	>250	A	61
3	>250	A	71
4	>250	A	85
5	>250	A	65
6	>250	A	89

A: tetrahydrofuran/methanol

Table 6.4. Chemical and physical data of intermediates **1-6**.

The elemental analyses of compounds **1-6** and **11-26** are reported in Table 6.5.

compd	MW	calculated, %			found, %		
		C	H	N	C	H	N
1	488.42	56.56	3.92	11.47	56.13	3.80	11.79
2	424.88	62.19	4.98	13.19	62.34	5.09	12.95
3	355.82	64.13	5.10	11.81	63.89	4.98	12.07

4	440.92	62.65	5.71	12.71	62.98	5.86	12.43
5	454.95	63.36	5.98	12.31	63.06	6.11	12.12
6	468.98	64.03	6.23	11.95	64.32	6.30	11.72
11	488.54	66.38	5.78	11.47	66.11	5.84	11.67
12	474.51	65.81	5.52	11.81	65.64	5.50	12.02
13	233.22	61.80	4.75	6.01	62.08	4.89	5.77
14	463.53	67.37	6.31	9.07	67.54	6.42	8.88
15	332.35	61.44	6.07	8.43	61.21	5.93	8.62
16	346.38	62.42	6.40	8.09	62.58	6.49	7.87
17	360.40	63.32	6.71	7.77	63.11	6.64	7.98
18	548.63	65.68	6.61	10.21	65.33	6.52	10.45
19	562.66	66.17	6.81	9.96	65.94	6.74	10.16
20	576.68	66.65	6.99	9.72	66.44	7.09	9.88
21	288.30	62.49	5.59	9.72	62.69	5.64	9.43
22	302.33	63.56	6.00	9.27	63.79	6.13	8.89
23	316.35	64.54	6.37	8.86	64.19	6.31	9.09
24	274.27	61.31	5.14	10.21	61.17	5.01	10.44
25	288.30	62.49	5.59	9.72	62.57	5.64	9.49
26	302.33	63.56	6.00	9.27	63.19	5.92	9.59

Table 6.5. Elemental Analyses of Compounds **1-6**, **11-26**.

LSD1 assay. His-tagged recombinant form of human LSD1 comprising residues 171-836 was copurified with a glutathione transferase-tagged CoREST protein (residues 308-440) as described. The potency of the inhibitors was evaluated by measuring their IC_{50} using a coupled enzymatic assay monitoring hydrogen peroxide formation. A peptide corresponding to the *N*-terminal 21 amino acids of H3 monomethylated on Lysine 4 was used as substrate at the fixed concentration of 29 μM (five-fold the Km). The reaction mixture contained 50 mM Hepes pH 7.5, 0.1 mM 4-aminoantipyrine, 1 mM 3,5- dichloro-2-hydroxybenzenesulfonic acid, 2.8 μM horseradish peroxidase, 1 μM LSD1/CoREST. The enzyme was incubated for five minutes at room temperature before measuring the enzymatic activity.

MAO-A and MAO-B assays. Recombinant human MAO-A and -B were expressed in *P. pastoris* and purified as described. IC_{50} values were measured with the peroxidase-coupled assay using benzylamine (MAO-B) and kynuramine (MAO-A) as substrates, at the fixed concentration of 333 μM (1.5 fold the Km). The protein (16.7 nM) was titrated with increasing concentrations of inhibitor (5-minute incubation at room temperature). The reaction mixture contained 50 mM Hepes pH 7.5, 0.025% (w/v) reduced Triton-X100, 0.1 mM Amplex Red, 2.8 μM horseradish peroxidase, 16 nM enzyme.

JmjC inhibitory assays. *Materials.* Anti-histone H3 (dimethyl K9) (Abcam, cat. No.: ab1220), antihistone H3 (trimethyl K9) (Abcam, cat. No.: ab8988), anti-histone H3 (dimethyl K4) (Abcam, cat. No.: ab32356), anti-histone H3 (trimethyl K4) (Diagenode, cat. No.: pAb-003-010) goat anti-mouse Alexafluor 488 (Invitrogen, cat. No.: A21121) or goat anti-rabbit Alexafluor 488 (Invitrogen, cat. No.:A11034).

2OG oxygenase enzyme assay. All recombinant 2OG oxygenase enzymes were produced as described[375]. The IC_{50} values of inhibitors against JmjC containing KDMs were determined using AlphaScreen as described[375]. RapidFire mass spectrometry based assay methods used for PHD2 and FIH will be reported elsewhere.

Cell culturing. HeLa cells were maintained in OptiMEM media supplemented with 0.5% foetal calf serum and 1% penicillin-streptomycin. Cells (1500 cells per well) were seeded into 96-well optical grade plate (Becton Dickinson) and left overnight to adhere. Test compounds were diluted in culture medium at a concentration of 100 μM, further serially diluted at a ratio of 1:2 (1% DMSO final), and incubated on the adhered HeLa cells. Media containing inhibitors was replaced every 24 h for 3 day period.

Immunostaining. Cells were rinsed with phosphate buffered saline (PBS) and fixed in 4% paraformaldehyde (20 min) and permeabilised with 0.5% TritonX-100 (10 min), followed by another PBS rinse. The cells were blocked (30 min) with 3% foetal calf serum diluted in PBS and further incubated overnight in primary antibody (1:500) diluted in blocking solution. Cells were rinsed three times with PBS, followed by incubation with the secondary antibody for 1 hour. After PBS rinses (×3), cells were stained with DAPI.

Image acquisition and analysis. The Pathway (Beckton Dickinson), an automated high-content imaging platform, was used to image the immunostained cells in the 96-well plate configuration. For each well, the system acquired a 3-by-3 tile-scanned image for Alexafluor 488 and DAPI. During analysis, the Pathway's software used the DAPI staining to identify nuclei as regions-of-interests (ROI). For each nucleus, the software extracted the average intensity of the histone staining, followed by the average intensity of all the nuclei in that particular well. The number of remaining cells and average nuclear size of each well was also calculated from the DAPI image. These three parameters from each well were then plotted against the corresponding concentration to obtain a dose response curve, which was plotted in GraphPad Prism 5.

LNCaP prostate cancer, HCT116 colon cancer and MePR mesenchimal progenitor cell assays.

Cell lines. HCT116 (human colorectal carcinoma cell line-ATCC) were grown at 37 °C in air and 5% CO_2 in DMEM medium (Euroclone) and LNCaP (human prostate cancer cell line-ATCC) and MePR (Mesenchimal PRogenitor non cancer-cell line) were grown at 37 °C in air and 5% CO_2 in RPMI medium (Euroclone). Both media were supplemented with 10% heat-inactivated FBS (Euroclone), 1% glutamine (Lonza), 1% penicillin/streptomycin (Euroclone) and 0.1% gentamycin (Lonza).

Cell cycle analysis. 2.5×105 cells (HCT116, LNCaP and MePR) were collected by centrifugation after stimulation at several times with reference or testing compounds at 50 µM. The cells were resuspended in 500 XL of hypotonic buffer (0.1% NP-40, 0.1% sodium citrate, 50 Xg/mL PI, RNAse A) and incubated in the dark for 30 min. The analysis was performed by FACS-Calibur (Becton Dickinson) using the Cell Quest Pro software (Becton Dickinson) and ModFit LT version 3 software (Verity). Pre- G1 picks were analyzed as indicative of sub-G1 apoptotic population. The experiments were performed in triplicate and shown data represent independent media values.

Dose-dependent apoptosis evaluation. 2.5×105 HCT116 and LNCaP cells were treated with increasing doses (10, 25, 50, 100 µM) of **2** and **3**. Cell cycle distribution of 10,000 cells was analyzed with a FACS-Calibur flow cytometer (Becton Dickinson, Franklin Lakes, NJ) by ModFit version 3 Technology (Verity). Pre-G1 picks were analyzed as indicative of sub-G1 apoptotic population. All the experiments were performed at least 3 times and values were expressed in mean • ± SD.

Histone Extraction. After stimulation with compounds, cells (HCT116 and LNCaP) were collected by centrifugation and washed two times with PBS. Then the samples were resuspended in Triton extraction buffer (PBS containing 0.5% Triton X 100 (v/v), 2 mM PMSF, 0.02% (w/v) NaN_3), and the lysis was performed for 10 min at 4 °C. Next, samples were centrifugated at 2000 rpm for 10 min at 4 °C, and the pellets were washed in TEB (half the volume). After a new centrifugation under the same conditions, the samples were re-suspended in 0.2 N HCl and the acidic histone extraction was carried out overnight at 4 °C. The supernatant was recovered by centrifugation and the protein content was quantified with BCA™ Protein Assay (Pierce).

Western blot analysis. Histone extracts (10 μg) were denatured and boiled in buffer (0.25 M Tris-HCl pH 6.8, 8% SDS, 40% glycerol, 5% 2-mercaptoethanol, bromophenol blue 0.05%) for 3 min before electrophoresis. Proteins were subjected to SDS–PAGE (15% polyacrylamide gels) in Tris-glycine- SDS (25 μM Tris, 192 μM glycine, 0.1% SDS). After electrophoresis, proteins were transferred to nitrocellulose membranes (Biorad Mini-protean gel and Transblot Turbo, Transfer System Biorad). The membranes were stained with Ponceau red, before to start with blocking (5% non-fat dry milk in TBS 1x/Tween 0.1%), and then incubated with the primary antibodies overnight at 4 °C. The employed antibodies were H3K4me2 and H3K4me3, H3K9me2 and H3K9me 3 (Abcam); total H4 (Cell Signalling) was used to normalize for equal loading of histone extracts.

Determining cell proliferation with the xCELLigence system. Tumour cell proliferation was monitored with the xCELLigence system (Roche, Mannheim, Germany). LNCaP and HCT116 cells were suspended in DMEM and RPMI media respectively and added into a 96 well microtiter plate that is specifically designed to measure cellular impedance (E-Plate, Roche, Mannheim, Germany). The measured impedance, which is dependent on the level of confluence, was expressed as an arbitrary unit called Cell Index. The Cell Index at each time point is defined as $(Rn-Rb)/(15X)$, where Rn is the cell electrode impedance of the well when it contains cells and Rb is the background impedance of the well with the media alone. xCELLigence monitors cellular events in real time measuring electrical impedance across interdigitated micro-electrode integrated on the bottom of tissue culture E-Plates. The impedance measurement provides quantitative information about the biological status of the cells, including cell number, viability, and morphology. For experiments, both LNCaP and HCT116 cell lines, were starved in DMEM/10% FBS and RPMI/10% FBS respectively, overnight before being seeded on an E-Plate 96. Two hours after seeding, scalar cell concentrations were added in triplicate. Dynamic CI values were monitored in 30-minute intervals from the time of plating until the end of the experiment. CI values were calculated and plotted on the graph. Standard deviation of tetraplicates of wells for the two types cells with different treatments were analysed with the RTCA Software.
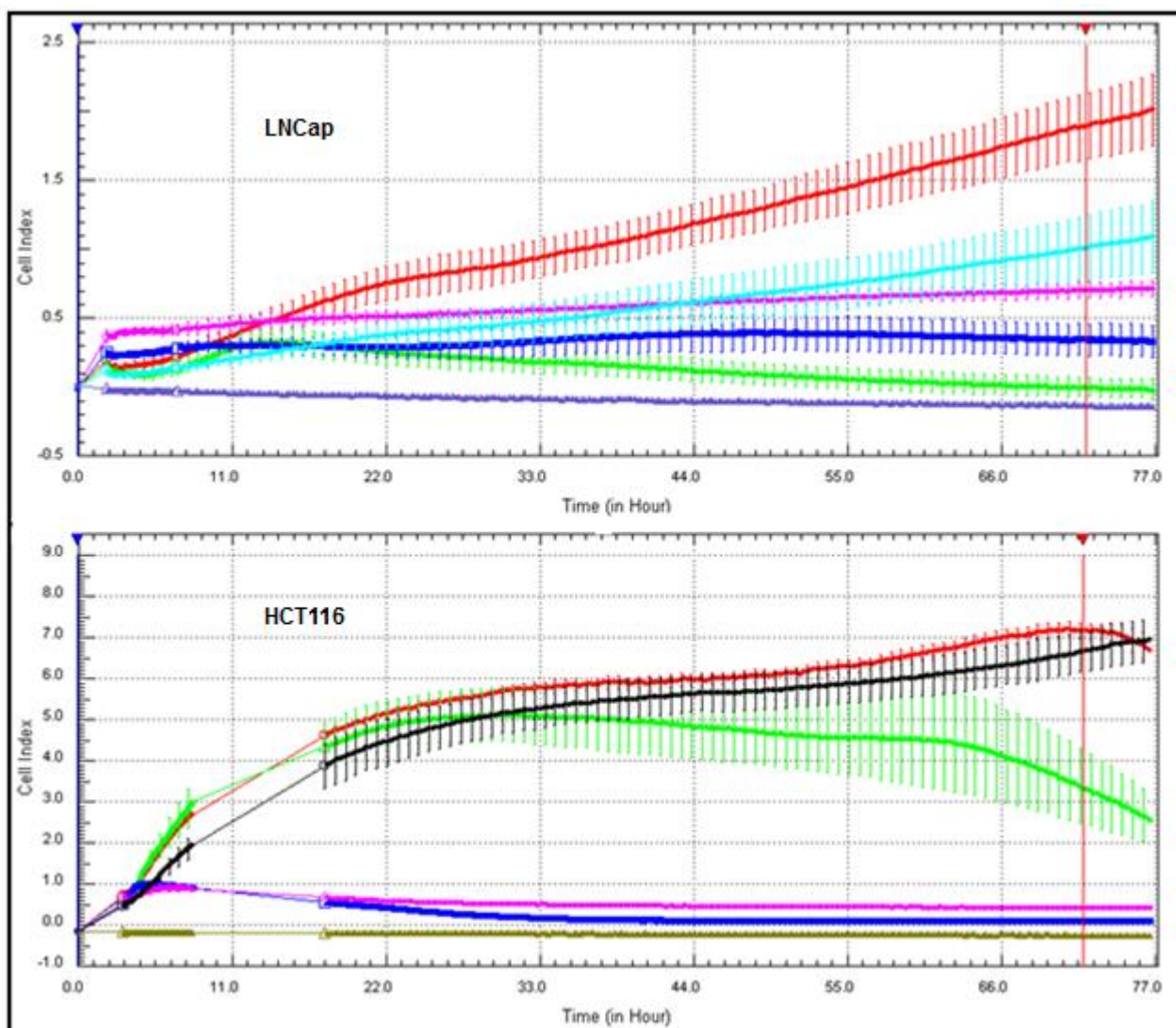
Figure 6.9. Proliferation curve relative to LNCaP and HCT116 cell lines after 72 h. In red is described the control (untreated cells), in green cells treated with the HDAC inhibitor SAHA used at a final concentration of 5 μM, in blue cells treated with the compound **2**, used at a final concentration of 50 μM, in violet cells treated with the compound **3**, used at a final concentration of 50 μM and in sky-blue the base line.

Cell migration assay. The kinetic information about cell migration by dynamically recording the whole cell migration process in real time without labelling cells, has been performed with the Roche xCELLigence Real-Time Cell Analyzer (RTCA) DP instrument. The RTCA DP instrument uses the CIM (cellular invasion/migration)-Plate 16 featuring microelectronic sensors integrated into the underside of the microporous polyethylene terephthalate (PET) membrane of a Boyden-like chamber. In this way cells migrate from the upper chamber through the membrane into the bottom chamber in response to the chemoattractant (we used foetal bovine serum) so contacting and adhering

134

to the electronic sensors on the underside of the membrane, resulting in an increase of the impedance. The impedance increase is proportional to increasing numbers of migrated cells on the underside of the membrane. Moreover cell-index values reflecting impedance changes are recorded by RTCA DP instrument. The CIM-Plate has been assembled by placing the top chamber into the bottom chamber and snapping the two together. Serum-free medium has been placed in the top chamber to hydrate and pre-incubate the membrane for 1 h in the CO_2 incubator at 37 °C before obtaining a background measurement. LNCaP and HCT116 cells were resuspended at the indicated concentration in serum-free medium. Once the CIM-Plate has equilibrated, it has been placed in the RTCA DP station and the background cell index values have been measured. The CIM-Plate was then removed from the RTCA DP station and then cells have been added to the top chamber at the desired concentration. The CIMPlate was placed in the RTCA DP station and migration has been monitored every 2 minutes for several hours. Cells have been analysed in absence or presence of 10% FBS in the bottom chamber. Cell migration was detected by automated real time monitoring and the low and high seeding densities were quantitatively monitored and reflected by the cell index values.

7. REFERENCES

[1] Ho, L.; Crabtree, G.R. Chromatin remodelling during develompent. *Nature* 2010, *463*(7280), 474–484.

[2] Allis, C.D.; Muir, T.W. Spreading Chromatin into chemical biology. *ChemeBioChem* 2011, *12*, 264-279.

[3] Katz, J.E.; Dlakic, M.; and Clarke, S. Automated identification of putative methyltransferases from genomic open reading frames. *Mol. Cell. Proteomics* 2003, *2*, 525–540.

[4] Martin, C.; Zhang, Y. The diverse functions of histone lysine methylation. *Nat. Rev. Mol. Cell. Biol.* 2005, *6*, 838-849

[5] Bedford, M.T.; Clarke, S. G. Protein arginine methylation in mammals: who, what, and why. *Mol. Cell* 2009, *33*, 1–13.

[6] Tripsianes, K. *et al.* Structural basis for dimethylarginine recognition by the Tudor domains of human SMN and SPF30 proteins. *Nature Struct. Mol. Biol.* 2011, *18*, 1414–1420.

[7] Luscombe, N.M.; Laskowski, R.A.; and Thornton, J.M. Amino acidbase interactions: a three-dimensional analysis of protein-DNA interactions at an atomic level. *Nucleic Acids Res.* 2001, *29*, 2860-2874.

[8] Calnan, B.J.; Tidor, B.; Biancalana, S.; Hudson, D.; Frankel, A.D. Arginine-mediated RNA recognition: the arginine fork. *Science* 1991, *252*, 1167–1171.

[9] Mitchell, J.B.; Thornton, J.M.; Singh, J.; Price, S.L. Towards an understanding of the arginine-aspartate interaction. *J. Mol. Biol.* 1992, *226*, 251–262.

[10] (a) Gary, J.D.; and Clarke, S. RNA and protein interactions modulated by protein arginine methylation. *Prog. Nucleic Acid Res. Mol. Biol.* 1998, *61*, 65–131.

[11] Yang, Y.; Bedford, M.T. Protein arginine methyltransferases and cancer. *Nature reviews*, 2013, *13*, 37-50.

[12] Scorilas, A.; Black, M.H.; Talieri, M.; and Diamandis Genomic organization, physical mapping, and expression analysis of the human protein arginine methyltransferase 1 gene. *Biochem. Biophys. Res. Commun.* 2000, *278*, 349–359.

[13] Taneda, T.; Miyata, S.; Kousaka, A.; Inoue, K.; Koyama, Y.; Mori, Y.; Tohyama, M. Specific regional distribution of protein arginine methyltransferase 8 (PRMT8) in the mouse brain. *Brain Res.* 2007, 1155, 1–9

[14] Lee, J.; Sayegh, J.; Daniel, J.; Clarke, S.; Bedford, M.T. PRMT8, a new membrane-bound tissue-specific member of the protein arginine methyltransferase family. *J. Biol. Chem.* 2005, *280*, 32890–32896.

[15] Pawlak, M.R.; Scherer, C.A.; Chen, J.; Roshon, M.J.; and Ruley, H.E. Arginine N-methyltransferase 1 is required for early postim-plantation mouse development, but cells deficient in the enzyme are viable. *Mol. Cell. Biol.* 2000, *20*, 4859–4869.

[16] Yadav, N.; Lee, J.; Kim, J.; Shen, J.; Hu, M.C.; Aldaz, C.M.; Bedford, M.T. Specific protein methylation defects and gene expression perturbations in coactivator-associated arginine methyltransferase 1-deficient mice. *Proc. Natl. Acad. Sci.* 2003, *100*, 6464–6468.

[17] Najbauer, J.; Johnson, B.A.; Young, A.L.; Aswad, D.W. Peptides with sequences similar to glycine, arginine-rich motifs in proteins interacting with RNA are efficiently recognized by methyl- transferase(s) modifying arginine in numerous proteins. *J. Biol. Chem.*, 1993, *268*, 10501–10509.

[18] Cheng, D.; Cote, J.; Shaaban, S.; Bedford, M.T. The arginine methyltransferase CARM1 regulates the coupling of transcription and mRNA processing. *Mol. Cell.*, 2007, *25*, 71–83.

[19] Lee, J.; Bedford, M. T. PABP1 identified as an arginine methyltransferase substrate using high-density protein arrays. *EMBO Rep.*, 2002, *3*, 268–273.

[20] Branscombe, T. L. *et al.* Prmt5 (janus kinase-binding protein 1) catalyzes the formation of symmetric dimethylarginine residues in proteins. *J. Biol. Chem.*, 2001, *276*, 32971–32976.

[21] Jansson, M.; Durant, S.T.; Cho, E.C. *et al*. Arginine methylation regulates the p53 response. *Nat Cell Biol*, 2008, *10*, 1431-1439.

[22] Chuikov, S.; Kurash, J.K.; Wilson, J.R. *et al*. Regulation of p53 activity through lysine methylation. *Nature*, 2004, *432*, 353-360.

[23] Huang, J.; Berger, S.L.; The emerging field of dynamic lysine methylation of non-histone proteins. *Curr Opin Genet Dev*, 2008, *18*, 152-158.

[24] Katz, J.E.; Dlakic, M.; and Clarke, S. Automated identification of putative methyltransferases from genomic open reading frames. *Mol. Cell. Proteomics*, 2003, *2*, 525–540.

[25] Cheng, X.; Collins, R.E.; Zhang, X. Structural and sequence motifs of protein (histone) methylation enzymes. *Annu. Rev. Biophys. Biomol. Struct.*, 2005, *34*, 267–294.

[26] Zhang, X.; Zhou, L.; Cheng, X. Crystal structure of the conserved core of protein arginine methyltransferase PRMT3. *EMBO J.*, 2000, *19*, 3509–3519.

[27] Zhang, X.; Cheng, X. Structure of the predominant protein arginine methyltransferase PRMT1 and analysis of its binding to substrate peptides, *Structure*, 2003, *11*, 509–520.

[28] Troffer-Charlier, N.; Cura, V.; Hassenboehler, P.; Moras, D.; Cavarelli, J. Functional insights from structures of coactivator-associated arginine methyltransferase 1 domains. *EMBO J.*, 2007, *26*, 4391–4401.

[29] Weiss, V.H.; McBride, A.E.; Soriano, M.A.; Filman, D.J.; Silver, P.A.; Hogle, J.M. The structure and oligomerization of the yeast arginine methyltransferase, Hmt1. *Nat. Struct. Biol.*, 2000, *7*, 1165–1171.

[30] Wu, H.; Min, J.; Lunin, V.V. *et al*. Structural biology of human H3K9 methyltransferases. *PLoS One*, 2010, *5*, 8570.

[31] Yue, W.W.; Hassler, M.; Roe, S.M.; Thompson-Vale, V.; Pearl, L.H. Insights into histone code syntax from structural and biochemical studies of CARM1 methyltransferase. *EMBO J.*, 2007, *26*, 4402–4412.

[32] Frankel, A.; Yadav, N.; Lee, J.; Branscombe, T.L.; Clarke, S.; Bedford, M.T. The novel human protein arginine N-methyltransferase PRMT6 is a nuclear enzyme displaying unique substrate specificity, *J. Biol. Chem.* , 2002, 277, 3537–3543.

[33] Osborne, T.C.; Obianyo,O.; Zhang, X.; Cheng, X.; Thompson, P.R. Protein arginine methyltransferase 1: positively harged residues in substrate peptides distal to the site of methylation are important for substrate binding and catalysis. *Biochemistry*, 2007, 46, 13370–13381.

[34] Chen, C.; Nott, T. J.; Jin, J.; Pawson, T. Deciphering arginine methylation: Tudor tells the tale. *Nature Rev. Mol. Cell Biol.* 2011, *12*, 629–642.

[35] Liu, K. *et al.* Crystal structure of TDRD3 and methyl-arginine binding characterization of TDRD3, SMN and SPF30. *PLoS ONE* 2012, *7*, e30375.

[36] Tang, J. *et al.* PRMT1 is the predominant type I protein arginine methyltransferase in mammalian cells. *J. Biol. Chem.* 2000, *275*, 7723–7730.

[37] Strahl, B. D. *et al.* Methylation of histone H4 at arginine 3 occurs *in vivo* and is mediated by the nuclear receptor coactivator PRMT1. *Curr. Biol.* 2001, *11*, 996–1000.

[38] Wang, H. *et al.* Methylation of histone H4 at arginine 3 facilitating transcriptional activation by nuclear hormone receptor. *Science* 2001, *293*, 853–857.

[39] Seligson, D. B. *et al.* Global histone modification patterns predict risk of prostate cancer recurrence. *Nature* 2005, *435*, 1262–1266.

[40] Yang, Y. *et al.* TDRD3 is an effector molecule for arginine-methylated histone marks. *Mol. Cell* 2010, *40*, 1016–1023.

[41] Cheung, N.; Chan, L.C.; Thompson, A.; Cleary, M.L.; So, C.W. Protein arginine-methyltransferase-dependent oncogenesis. *Nat. Cell Biol.* 2007, *9*, 1208–1215.

[42] Goulet, I.; Gauvin, G.; Boisvenue, S.; Cote, J. Alternative splicing yields protein arginine methyltransferase 1 isoforms with distinct activity, substrate specificity, and subcellular localization. *J. Biol. Chem.* 2007, *282*, 33009–33021.

[43] Boisvert, F. M.; Rhie, A.; Richard, S.; Doherty, A. J. The GAR motif of 53BP1 is arginine methylated by PRMT1 and is necessary for 53BP1 DNA binding activity. *Cell Cycle* 2005, *4*, 1834–1841.

[44] Mitchell, T. R.,; Glenfield, K.; Jeyanthan, K.; Zhu, X. D. Arginine methylation regulates telomere length and stability. *Mol. Cell. Biol.* 2009, *29*, 4918–4934.

[45] Le Romancer, M. *et al.* Regulation of estrogen rapid signaling through arginine methylation by PRMT1. *Mol. Cell* 2008, *31*, 212–221.

[46] Le Romancer, M.; Treilleux, I.; Bouchekioua-Bouzaghou, K.; Sentis, S.; Corbo, L. Methylation, a key step for nongenomic estrogen signaling in breast tumors. *Steroids* 2010, 75, 560–564.

[47] Chevillard-Briet, M.; Trouche, D.; Vandel, L. Control of CBP co-activating activity by arginine methylation. *EMBO J.* 2002, *21*, 5457–5466.

[48] Xu, W. *et al.* A transcriptional switch mediated by cofactor methylation. *Science* 2001, *294*, 2507–2511

[49] Lee, Y. H.; Bedford, M. T.; Stallcup, M. R. Regulated recruitment of tumor suppressor BRCA1 to the p21 gene by coactivator methylation. *Genes Dev.* 2011, *25*, 176–188.

[50] Hong, H. *et al.* Aberrant expression of CARM1, a transcriptional coactivator of androgen receptor, in the development of prostate carcinoma and androgen-independent status. *Cancer* 2004, *101*, 83–89.

[51] Majumder, S.; Liu, Y.; Ford, O. H.; Mohler, J. L.; Whang, Y. E. Involvement of arginine methyltransferase CARM1 in androgen receptor function and prostate cancer cell viability. *Prostate* 2006, *66*, 1292–1301.

[52] El Messaoudi, S. *et al.* Coactivator-associated arginine methyltransferase 1 (CARM1) is a positive regulator of the Cyclin E1 gene. *Proc. Natl Acad. Sci. USA* 2006*, 103*, 13351–13356.

[53] Lahusen, T.; Henke, R. T.; Kagan, B. L.; Wellstein, A.; Riegel, A. T. The role and regulation of the nuclear receptor co-activator AIB1 in breast cancer. *Breast Cancer Res. Treat.* 2009, *116*, 225–237.

[54] Frietze, S.; Lupien, M.; Silver, P. A.; Brown, M. CARM1 regulates estrogen-stimulated breast cancer growth through up-regulation of E2F1. *Cancer Res.* 2008, *68*, 301–306.

[55] Kim, Y. R. *et al.* Differential CARM1 expression in prostate and colorectal cancers. *BMC Cancer* 2010, *10*, 197-204.

[56] Fabbrizio, E. *et al.* Negative regulation of transcription by the type II arginine methyltransferase PRMT5. *EMBO Rep.* 2002, *3*, 641–645.

[57] Pal, S.; Vishwanath, S. N.; Erdjument-Bromage, H.; Tempst, P. & Sif, S. Human SWI/SNF-associated PRMT5 methylates histone H3 arginine 8 and negatively regulates expression of ST7 and NM23 tumor suppressor genes. *Mol. Cell. Biol.* 2004, *24*, 9630–9645.

[58] Pal, S. *et al.* Low levels of miR-92b/96 induce PRMT5 translation and H3R8/H4R3 methylation in mantle cell lymphoma. *EMBO J.* 2007, *26*, 3558–3569.

[59] Pal, S.; Yun, R.; Datta, A.; Lacomis, L.; Erdjument-Bromage, H.; Kumar, J.; Tempst, P.; Sif, S. mSin3A/histone deacetylase 2- and PRMT5-containing Brg1 complex is involved in transcriptional repression of the Myc target gene cad. *Mol. Cell. Biol.* 2003, *23*, 7475–7487.

[60] Ancelin, K.; Lange, U.C.; Hajkova, P.; Schneider, R.; Bannister, A.J.; Kouzarides, T.; Surani, M.A. Blimp1 associates with Prmt5 and directs histone arginine methylation in mouse germ cells. *Nat. Cell Biol.* 2006, *8*, 623–630.

[61] Hou, Z. *et al.* The LIM protein AJUBA recruits protein arginine methyltransferase 5 to mediate SNAIL-dependent transcriptional repression. *Mol. Cell. Biol.* 2008, *28*, 3198–3207.

[62] Cho, E. C. *et al.* Arginine methylation controls growth regulation by E2F-1. *EMBO J.* 2012, *31*, 1785–1797.

[63] Hou, Z. *et al.* The LIM protein AJUBA recruits protein arginine methyltransferase 5 to mediate SNAIL-dependent transcriptional repression. *Mol. Cell. Biol.* 2008, *28*, 3198–3207.

[64] Powers, M. A.; Fay, M. M.; Factor, R. E.; Welm, A. L.; Ullman, K. S. Protein arginine methyltransferase 5 accelerates tumor growth by arginine methylation of the tumor suppressor programmed cell death 4. *Cancer Res.* 2011, *71*, 5579–5587

[65] Hsu, J. M. *et al.* Crosstalk between Arg 1175 methylation and Tyr 1173 phosphorylation negatively modulates EGFR-mediated ERK activation. *Nature Cell Biol.* 2011, *13*, 174–181.

[66] Guo, Z. *et al.* Methylation of FEN1 suppresses nearby phosphorylation and facilitates PCNA binding. *Nature Chem. Biol.*, 2010, *6*, 766–773.

[67] Sakamaki, J. *et al.* Arginine methylation of BCL-2 antagonist of cell death (BAD) counteracts its phosphorylation and inactivation by Akt. *Proc. Natl Acad. Sci*, 2011, *108*, 6085–6090.

[68] Feng, Q. *et al.* Biochemical control of CARM1 enzymatic activity by phosphorylation. *J. Biol. Chem.*, 2009, *284*, 36167–36174.

[69] Higashimoto, K.; Kuhn, P.; Desai, D.; Cheng, X.; Xu, W. Phosphorylation-mediated inactivation of coactivator-associated arginine methyltransferase 1. *Proc. Natl Acad. Sci.*, 2007, *104*, 12318–12323.

[70] Bedford, M.T.; Yang, Y. Protein arginine methyltransferases and cancer. *Nature Rev./Cancer* 2013, *13*, 37-50.

[71] Liu, F. *et al.* JAK2V617F-mediated phosphorylation of PRMT5 downregulates its methyltransferase activity and promotes myeloproliferation. *Cancer Cell*, 2011, *19*, 283–294.

[72] Yue, W. W.; Hassler, M.; Roe, S. M.; Thompson-Vale, V.; Pearl, L. H. Insights into histone code syntax from structural and biochemical studies of CARM1 methyltransferase. *EMBO J.*, 2007, *26*, 4402–4412.

[73] An, W.; Kim, J.; Roeder, R. G. Ordered cooperative functions of PRMT1, p300, and CARM1 in transcriptional activation by p53. *Cell*, 2004, *117*, 735–748.

[74] Feng, Y. *et al.* Histone H4 acetylation differentially modulates arginine methylation by an in Cis mechanism. *J. Biol. Chem.*, 2011, *286*, 20323–20334.

[75] Friesen, W. J. *et al.* A novel WD repeat protein component of the methylosome binds Sm proteins. *J. Biol. Chem.* 2002, *277*, 8243–8247.

[76] Aggarwal, P. *et al.* Nuclear cyclin D1/CDK4 kinase regulates CUL4 expression and triggers neoplastic growth via activation of the PRMT5 methyltransferase. *Cancer Cell* 2010, *18*, 329–340.

[77] Pal, S.; Vishwanath, S. N.; Erdjument-Bromage, H.; Tempst, P.; Sif, S. Human SWI/SNF-associated PRMT5 methylates histone H3 arginine 8 and negatively regulates expression of ST7 and NM23 tumor suppressor genes. *Mol. Cell. Biol.* 2004, *24*, 9630–9645.

[78] Lacroix, M. *et al.* The histone-binding protein COPR5 is required for nuclear functions of the protein arginine methyltransferase PRMT5. *EMBO Rep.* 2008, *9*, 452–458.

[79] Lei, N. Z. *et al.* A feedback regulatory loop between methyltransferase PRMT1 and orphan receptor TR3. *Nucleic Acids Res.* 2009, *37*, 832–848.

[80] Robin-Lespinasse, Y. *et al.* hCAF1, a new regulator of PRMT1-dependent arginine methylation. *J. Cell Sci.* 2007, *120*, 638–647.

[81] Pak, M. L. *et al.* A protein arginine N-methyltransferase 1 (PRMT1) and 2 heteromeric interaction increases PRMT1 enzymatic activity. *Biochemistry 2001, 50*, 8226–8240.

[82] Wang, L.; Pal, S.; Sif, S. Protein arginine methyltransferase 5 suppresses the transcription of the RB family of tumor suppressors in leukemia and lymphoma cells. *Mol. Cell. Biol.* 2008, *28*, 6262–6277.

[83] Mallappa, C. *et al.* The expression of myogenic microRNAs indirectly requires protein arginine methyltransferase (Prmt)5 but directly requires Prmt4. *Nucleic Acids Res.* 2011, *39*, 1243–1255.

[84] Min, J.; Feng, Q.; Li, Z.; Zhang Y.; Xu R.M. Structure of the catalytic domain of human DOT1L, a non-SET domain nucleosomal histone methyltransferase. *Cell* 2003, *112*, 711-723.

[85] Anglin, J.L.; Song, Y. A Medicinal Chemistry Perspective for Targeting Histone H3 Lysine-79 Methyltransferase DOT1L. *J. Med. Chem.* 2013, *56*, 8972−8983.

[86] Frye, S.V.; Heightman ,T.; Jin, J. Targeting methyl lysine. *Annu. Rep. Med. Chem.* 2010, *45*, 329-343.

[87] Xiao, B.; Jing C.; Wilson J.R. *et al.* Structure and catalytic mechanism of the human histone methyltransferases SET7/9. *Nature* 2003, *421*, 652-656.

[88] Dillon, S.C.; Zhang, X.; Trievel, R.C.; Cheng, X. The SET-domain protein superfamily: protein lysine methyltransferases. *Genome Biol.* 2005, 6, 227-235.

[89] Min, J.; Zhang, X.; Cheng, X.; Grewal, S.I.; Xu, R.M. Structure of the SET domain histone lysine methyltransferase Clr4. *Nat Struct Biol* 2002, *9*, 828–832.

[90] Schapira, M. Structural chemistry of human SET domain protein methyltransferases. *Curr.Chem.Gen.* 2011, *5*, 85-94.

[91] Wu, H.; Min, J.; Lunin, V.V.; Antoshenko, T.; Dombrovski, L. *et al.* Structural biology of human H3K9 methyltransferases. *PLoS One* 2010, *5*, e8570.

[92] Collins, R.E.; Tachibana, M.; Tamaru, H.; Smith, K.M.; Jia, D. *et al.* *In vitro* and *in vivo* analysis of a Phe/Tyr switch controlling product specificity of histone lysine methyltransferases. *J. Biol. Chem.* 2005, *280*, 5563-5570.

[93] Rathert, P.; Dhayalan, A.; Murakami, M. *et al.* Protein lysine methyltransferases G9a acts on non-histone targets. *Nat. Chem. Biol.* 2008, *4*, 344-346.

[94] Van Duyne, R.; Easley, R.; Wu, W.L. *et al.* Lysine methylation of HIV-1 Tat regulates transcriptional activity of the viral LTR. *Retrovirology* 2008, *5*, 40.

[95] Pagans, S.; Kauder, S.E.; Kaehleke, K. *et al.* The cellular lysine methyltransferases SET7/9-KMT7 binds HIV-1 TAR RNA, monomethylates the viral transactivator Tat and enhances HIV transcription. *Cell. Host. Microbe* 2010, *7*, 234-244.

[96] Okada, Y.; Jiang, Q.; Lemieux, M.; Jeannotte, L.; Su, L.; Zhang, Y. Leukaemic transformation by CALM-AF10 involves upregulation of Hoxa5 by hDOT1L. *Nat Cell Biol.* 2006, *8*, 1017-1024.

[97] Shi, X.B.; Kachirskaia, L.; Yamaguchi, H. *et al.* Modulation of p53 function by SET8-mediated methylation at lysine 382. *Mol Cell* 2007, *27*, 636-646.

[98] Chuikov, S.; Kurash, J.K.; Wilson, J.R. *et al.* Regulation of p53 activity through lysine methylation. *Nature* 2004, *432*, 353-360.

[99] Huang, J.; Dorsey, J.; Chuikov, S. *et al.* G9a and Glp methylate lysine 373 in the tumor suppressor p53. *J Biol Chem* 2010, *285*, 9636-9641.

[100] Mosammaparast, N.; Shi, Y. Reversal of histone methylation: biochemical and molecular mechanisms of histone demethylases. *Annu. Rev. Bioche.* 2010, *79*, 155-179

[101] Arrowssmith, C.H.; Bountra, C.; Fish, P.V.; Lee, K.; Schapira, M. Epigenetic protein families: a new frontier for drug discovery. *Nature Review/Drug Discovery* 2012, *11*, 384-400.

[102] Krivtsov, A.V.; Armstrong, S.A. MLL translocations, histone modifications and leukaemia stem-cell development. *Nat. Rev. Cancer* 2007, *7*, 823–833.

[103] Ayton, P.M.; Cleary, M.L. Transformation of myeloid progenitors by MLL oncoproteins is dependent on Hoxa7 and Hoxa9. *Genes Dev.* 2003, *17*, 2298–2307.

[104] Li, Z., Luo, R. T., Mi, S., Sun, M., Chen, P., Bao, J., Thirman, M. J. Consistent deregulation of gene expression between human and murine MLL rearrangement leukemias. *Cancer Res* 2009, *69*, 1109-1116.

[105] Okada, Y.; Feng, Q.; Lin, Y.; Jiang, Q.; Li, Y. *et* al. hDOT1L links histone methylation to leukemogenesis. *Cell* 2005, *121*, 167–178.

[106] Park, J.H.; Roeder, R.G. GAS41 is required for repression of the p53 tumor suppressor pathway during normal cellular proliferation. *Mol. Cell. Biol.* 2006, *26*, 4006-4016.

[107] Chen, X.; El Gazzar, M.; Yoza, B. K.; McCall, C. E. The NF-κB factor RelB and histone H3 lysine methyltransferase G9a directly interact to generate epigenetic silencing in endotoxin tolerance. *J. Biol. Chem.* 2009, *284*, 27857–27865.

[108] Siebel, A.L.; Fernandez, A. Z.; El-Osta, A. Glycemic memory associated epigenetic changes. *Biochem. Pharmacol.* 2010, *80*, 1853–1859.

[109] Meissner, A. Epigenetic modifications in pluripotent and differentiated cells. *Nature Biotech.* 2010, *28*, 1079–1088.

[110] Shi, Y. *et al.* A combined chemical and genetic approach for the generation of induced pluripotent stem cells. *Cell Stem Cell* 2008, *2*, 525–528.

[111] Orlando, V. Polycomb, epigenomes, and control of cell identity. *Cell* 2003, *112*, 599-606.

[112] Agger, K. *et al.* UTX and JMJD3 are histone H3K27 demethylases involved in HOX gene regulation and development. *Nature* 2007, *449*, 731–734.

[113] Konda, Y.; Epigenetic cross-talk between DNA methylation and histone modifications in human cancers. *Yonsei Med. J.* 2009, *50*, 455–463.

[114] Mills, A.A. Throwing the cancer switch: reciprocal roles of polycomb and trithorax proteins. Nature Review/Cancer 2010, 10, 669-682.

[115] Varambally, S.; Dhanasekaran, S.M.; Zhou, M.;Barrette, T.R. *et al.* The polycomb group protein EZH2 is involved in progression of prostate cancer. *Nature* 2002, *419*, 624–629.

[116] Saramaki, O.R.; Tammela, T.L.; Martikainen, P.M. *et al*. The gene for polycomb group protein enhancer of zeste homolog 2 (EZH2) is amplified in late-stage prostate cancer. *Genes ChromosomesCancer* 2006, *45*, 639–645.

[117] Collett, K.; Eide, G.E.; Arnes, J.; Stefansson, I.M. *et al*. Expression of enhancer of zeste homologue 2 is significantly associated with increased tumor cell proliferation and is a marker of aggressive breast cancer. *Clin. Cancer Res.* 2006, *12*, 1168–1174.

[118] Kleer, C.G.; Cao, Q.; Varambally, S.; Shen, R. *et al*. EZH2 is a marker of aggressive breast cancer and promotes neoplastic transformation of breast epithelial cells. *Proc.Natl. Acad. Sci.U.S.A.* 2003, *100*, 11606–11611.

[119] Weikert, S.; Christoph, F.; Kollermann, J.; Muller, M. *et al*. Expression levels of the EZH2 polycomb transcriptional repressor correlate with aggressiveness and invasive potential of bladder carcinomas. *Int. J. Mol. Med.* 2005, *16*, 349–353.

[120] Mimori, K.; Ogawa, K.; Okamoto, M. *et al*. Clinical significante of enhancer of zeste homolog 2 expression in colorectal cancer cases. *Eur. J. Surg. Oncol.* 2005, *31*, 376–380.

[121] McHugh, J.B.; Fullen, D.R.; Ma, L.; Kleer, C.G.; Su, L.D. Expression of polycomb group protein EZH2 in nevi and melanoma. *J. Cutan. Pathol*. 2007, *34*, 597–600.

[122] Van Kemenade, F.J.; Raaphorst, F.M.; Blokzijl, T. *et al*. Coexpression of BMI-1 and EZH2 polycomb-group proteins is associated with cycling cells and degree of malignancy in B-cell non-Hodgkin lymphoma. *Blood* 2001, *97*, 3896–3901.

[123] O'Meara, M.M.; Simon, J.A.; Inner workings and regulatory inputs that control Polycomb repressive complex 2. *Chromosoma* 2012, *121*, 221–234.

[124] Levine, S.S.; King, I.F.G.; Kingston, R.E. Division of labor in Polycomb group repression. *Trends Biochem. Sci.* 2004, *29*, 478-485.

[125] Sarma, K.; Margueron, R.; Ivanov, A.; Pirrotta, V.; Reinberg, D. EZH2 requires PHF1 to efficiently catalyze H3 lysine 27 trimethylation *in vivo*. *Mol. Cell. Biol*. 2008, *28*, 2718-2731.

[126] Cao, R.; Zhang, Y. SUZ 12 is requie for both the histone methyltransferase activity and the silencing function of the EED-EZH2 complex. *Mol. Cell.* 2004, *15*, 57-67.

[127] Han, Z.; Xing, X.; Hu, M.; Zhang, Y.; Liu, P.; Chai, J. Structural basis of EZH2 recognition by EED. *Structure* 2007, *15*, 1306–1315.

[128] Margueron. R.; Justin, N.; Ohno, K.; Sharpe, M.L.; Son, J.; Drury, W.J. *et al*. Role of the polycomb protein EED in the propagation of repressive histone marks. *Nature* 2009, *461*, 762–767.

[129] Yamamoto, K.; Sonoda, M.; Inokuchi, J.; Shirasawa, S.; Sasazuki, T. Polycomb group suppressor of zeste 12 links heterochromatin protein 1alpha and enhancer of zeste 2. *J Biol Chem* 2004, *279*, 401–406.

[130] Schmitges, F.W.; Prusty, A.B. *et al*. Histone methylation by PRC2 is inhibited by active chromatin marks. *Mol Cell* 2011, *42*, 330–341.

[131] Xiao, Y. Enhancer of Zeste homolog 2: a potential target for tumor therapy. *Int. J. Biochem. & Cell Biol.* 2011, *43*, 474-477.

[132] Morin, R.D.; Johnson, N.A.; Severson, T.M.; Mungall, A.J. *et al*. Somatic mutations altering EZH2 (Tyr641) in follicular and diffuse large B-cell lymphomas of germinal-center origin. *Nat Genet* 2010, *42*, 181–185.

[133] Yap, D.B.; Chu, J.; Berg, T.; Schapira, M.; Cheng, S.W. *et al*. Somatic mutations at EZH2 Y641 act dominantly through a mechanism of selectively altered PRC2 catalytic activity, to increase H3K27 trimethylation. *Blood* 2011, *117*, 2451–2459.

[134] Tan, J.; Yan, Y.; Wang, X.; Jiang, Y.; Xu, H.E. EZH2: biology, disease and structure-based drug discovery. *Acta Pharmacologica Sinica* 2014, *35*, 161-174.

[135] Levine, S.S. *et al*. The coreo f the polycomb repressive complex is compositionally and functionally conserved in flies and humans. *Mol. Cell. Biol.* 2002, *22*, 6070-6078.

[136] Wang, H. *et al*. Role of histone H2A ubiquitination in Polycomb silencing. *Nature* 2004, *431*, 873-878.

[137] Lund, A.H.; Van Lohuizen, M. Polycomb complexes and silencing mechanisms. *Curr.Opin.Cell. Biol.* 2004, *16*, 239–246.

[138] Dellino, G.I. *et al*. Polycomb silencing blocks transcription initiation. *Mol. Cell.* 2004, *13*, 887-893.

[139] Ku, M. *et al*. Genomewide analysis of PRC1 and PRC2 occupancy identifies two classes of bivalent domains. *PLoS Genet.* 2008, *4*, e1000242.

[140] Cao, Q.; Mani, R.S.; Ateeq, B.; Dhanasekaran, S.M.; Asangani, I.A.; Prensner, J.R.; Kim, J.H.; Brenner, J.C.; Jing, X.; Cao, X. *et al.* Coordinated regulation of polycomb group complexes through microRNAs in cancer. *Cancer Cell* 2011, *20*, 187–199.

[141] Sparman, A.; Van Lohuizen, M. Polycombsilencers control cell fate, development and cancer. *Nature Rev. Cancer* 2006, *6*, 846-856.

[142] Varambally, S.; Dhanasekaran, S.M.; Zhou, M. *et al*. The polycomb group protein EZH2 is involved in progression of prostate cancer. *Nature* 2002, *419*, 624-629.

[143] Simon, J.A.; Lange, C.A. ROles of the EZH2 histone methyltransferase in cancer epigenetics. *Mut. Res.* 2008. *647*, 21-29.

[144] Vire, E.; Brenner, C.; Deplus, R.; Blanchon L. *et al*. The Polycomb protein group EZH2 directly controls DNA methylation. *Nature* 2006, *439*, 871-874.

[145] Sauvageau, M.; Sauvageau, G. Polycomb group proteins: multi-faceted regulators of somatic stem cells and cancer. *Cell Stem Cell* 2010, *7*, 299–313.

[146] Schlesinger, Y.; Straussman, R.;Keshert, I. *et al*. Polycomb-mediated methylation on Lys 27 of histone H3 pre-marks genes for *de novo* methylation in cancer. *Nat. Genet.* 2007, *39*, 232-236.

[147] Ohm, J.E.; McGarvey, K.M.; Yu, X.; Cheng, L. *et al*. A stem cell-like chromatin pattern may predispose tumor suppressor genes to DNA hypermethylation and heritable silencing. *Nat. Genet.* 2007, *39*, 237-242.

[148] Xu, K.; Wu, Z.J.; Groner, A.C.; He, H.H.; Cai, C. *et al*. EZH2 oncogenic activity in castration-resistant prostate cancer cells is Polycomb-independent. *Science* 2012, *338*, 1465–1469.

[149] Tang, X.; Milyavsky, M.; Shats, I.; Erez, N.; Goldfinger, N.; Rotter, V. Activated p53 suppresses the histone methyltransferase EZH2 gene. *Oncogene* 2004, *23*, 5759–5769.

150 Koh, C.M.; Iwata, T.; Zheng, Q.; Bethel, C.; Yegnasubramanian, S.; De Marzo, A.M. Myc enforces overexpression of EZH2 in early prostatic neoplasia via transcriptional and post-transcriptional mechanisms. *Oncotarget* 2011, *2*, 669–683.

151 Chang, T.C.; Yu, D.; Lee, Y.S.; Wentzel, E.A.; Arking, D.E.; West, K.M.; Dang, C.V.; Thomas-Tikhonenko, A.; Mendell, J.T. Widespread microRNA repression by Myc contributes to tumorigenesis. *Nature Genet* 2008, *40*, 43–50.

152 Ren, B.; Cam, H.; Takahashi, Y. *et al*. E2F integrates cell cycle pro-gression with DNA repair, replication, and G(2)/M check-points. *Genes Dev*. 2002; *16*, 245-56.

153 Chang ,C.J.; Yang, J.Y.; Xia, W. *et al*. EZH2 promotes expansion of breast tumor initiating cells through activation of RAF1-β-catenin signaling. *Cancer Cell*. 2011, *19*, 86-100.

154 Varambally, S.; Dhanasekaran, S.M.; Zhou, M. *et al*. The polycomb group protein EZH2 is involved in progression of prostate cancer. *Nature* 2002, *419*, 624–629.

155 Lu, J.; Getz. G.; Miska, E.A.; Alvarez-Saavedra, E.; Lamb, J.; Peck, D.; Sweet-Cordero, A.; Ebert, B.L.; Mak, R.H.; Ferrando, A.A. et al. MicroRNA expression profiles classify human cancers. *Nature* 2005, *435*, 834–838.

156 Porkka, K.P.; Pfeiffer, M.J.; Waltering, K.K.; Vessella, R.L.; Tammela, T.L.; Visakorpi, T.. MicroRNA expression profiling in prostate cancer. *Cancer Res* 2007, *67*, 6130–6135.

157 Ozen, M.; Creighton, C.J.; Ozdemir, M.; Ittmann, M. Widespread deregulation of microRNA expression in human prostate cancer. *Oncogene* 2008, *27*, 1788–1793.

158 Kumar-Sinha, C.; Tomlins, S.A.; Chinnaiyan, A.M. Recurrent gene fusions in prostate cancer. *Nature reviews/Cancer* 2008, *8*, 497–511.

159 Yu, J.; Yu, J.; Mani, R.S.; *et al*. An integrated network of androgen receptor, polycomb, and TMPRSS2-ERG gene fusions in prostate cancer progression. *Cancer Cell* 2010, *17*, 443-454.

160 Min, J.; Zaslavsky, A.; Fedele, G. *et al*. An oncogene-tumor suppressor cascade drives metastatic prostate cancer by coordinately activating Ras and nuclear factor-kappa B. *Nature Med* 2010, *16*, 286–294.

161 Cao, Q.; Yu, J.; Dhanasekaran, S.M.; Kim, J.H.; Mani, R.S.; Tomlins, S.A.; Mehra, R.; Laxman, B.; Cao, X.; Yu, J. *et al*. Repression of E-cadherin by the polycomb group protein EZH2 in cancer. *Oncogene* 2008, *27*, 7274–7284.

162 Beke, L.; Nuytten, M.; Van Eynde, A.; Beullens, M.; Bollen, M. The gene encoding the prostatic tumor suppressor PSP94 is a target for repression by the Polycomb group protein EZH2. *Oncogene* 2007, *26*, 4590–4595.

163 Shin, Y.J.; Kim, J.H. The role of EZH2 in the regulation of the activity of matrix metalloproteinases in prostate cancer cells. *PloS One* 2012, *7*, e30393.

164 Puppe, J.; Drost, R.; Liu, X. *et al*. BRCA1-deficient mammary tu-mor cells are dependent on EZH2 expression and sensitive to Polycomb Repressive Complex 2-inhibitor 3-deazaneplanocin A. *Breast Cancer Res*. 2009, *11*, R63.

165 Phillips, K.A. Immunophenotypic and pathologic differences between BRCA1 and BRCA2 hereditary breast cancers. *J Clin Oncol*. 2000, *18*, 107S-12S.

166 Gonzalez, M.E.; Li, X.; Toy, K. *et al*. Downregulation of EZH2 decreases growth of estrogen receptor-negative invasive breast carcinoma and requires BRCA1. *Oncogene*. 2009, *28*, 843-53.

167 Fujii, S.; Ito, K.; Ito, Y. *et al*. Enhancer of zeste homologue 2 (EZH2) down-regulates RUNX3 by increasing histone H3 methylation. *J Biol Chem*. 2008, *283,* 17324-32.

168 Chi, X.Z.; Yang, J.O.; Lee, K.Y. *et al*. RUNX3 suppresses gastric epithelial cell growth by inducing p21WAF1/Cip1 expression in cooperation with transforming growth factor ß-activated SMAD. *Mol Cell Biol*. 2005, *25*, 8097-107.

169 Barker, N.; Clevers, H. Mining the Wnt pathway for cancer therapeutics. *Nat. Rev. Drug Discov*. 2006, *5*, 997-1014.

170 Jiang, X.; Tan, J.; Li, J. *et al*. DACT3 is an epigenetic regulator of Wnt/β catenin signaling in colorectal cancer and is a therapeutic target of histone modifications. *Cancer Cell* 2008, *13*, 529-541.

171 Ying, T.; Tao, Q. Epigenetic disruption of the Wnt/ beta- catenin signaling pathway in human cancers. *Epigenetic* 2009, *4*, 307-312.

172 Kantarjian, H.; Issa, J.P. *et al*. Decitabine improves patient outcomes in myelodysplastic syndromes: results of a phase III randomized study. *Cancer* 2006, *106*, 1794-1803.

173 Mann, B.S.; Johnson, J.R. *et al*. FDA approval summary: vorinostat for treatment of ; primary cutaneous T-cell lymphoma. *Oncologist* 2007, *12*, 1247–1252.

174 VanderMolen, K.M.; McCulloch, W. *et al*. Romidepsin (Istodax, NSC 630176, FR901228, FK228, depsipeptide): a natural product recently approved for cutaneous T-cell lymphoma. *J Antibiot*. 2011, *64*, 525–531.

[175] Stresemann, C.; Lyko, F. Modes of action of the DNA methyltransferase inhibitors azacytidine and decitabine. *Int J Cancer* 2008, *123*, 8–13.

[176] Choudhary, C.; Kumar, C. *et al*. Lysine acetylation targets protein complexes and co-regulates major cellular functions. *Science* 2009, *325*, 834–840.

[177] Kubicek, S.; Gilbert, J.C. *et al*. Chromatin targeting small molecules cause class-specific transcriptional changes in pancreatic endocrine cells. *Proc Natl Acad Sci U S A*. 2012, *109*, 5364–5369.

[178] Cheng, D.H.; Yadav, N. *et al*. Small molecule regulators of protein arginine methyltransferases. *J Biol Chem* 2004, *279*, 23892-9.

[179] Trapp, J.; Meier, R. *et al*. Structure-activity studies on suramin analogues as inhibitors of NAD(+)-dependent histone deacetylases (sirtuins). *ChemMedChem* 2007, *2*, 1419-1431.

[180] Ragno, R.; Simeoni, S.; Castellano, S. *et al*. Small molecule inhibitors of histone arginine methyltransferases: Homology modeling, molecular docking, binding mode analysis, and biological evaluations. *J Med Chem* 2007, *50*, 1241-1253.

[181] Mai, A.; Cheng, D.; Bedford, M.T. *et al*. Epigenetic multiple ligands: mixed histone/protein methyltransferase, acetyltransferase, and class III deacetylase (sirtuin) inhibitors. *J Med Chem* 2008, *51*, 2279-2290.

[182] Bonham, K.; Hemmers, S.; Lim, Y.H. *et al*. Effects of a novel arginine methyltransferase inhibitor on T-helper cell cytokine production. *FEBS J* 2010, *277*, 2096-2108.

[183] Spannhoff, A.; Heinke, R. *et al*. Target-based approach to inhibitors of histone arginine methyltransferases. *J Med Chem* 2007, *50*, 2319-2325.

[184] Heinke, R.; Spannhoff, A. *et al*. Virtual screening and biological characterization of novel histone arginine methyltransferase PRMT1 inhibitors. *ChemMedChem* 2009, *4*, 69-77.

[185] Greiner, D.; Bonaldi, T. *et al*. Identification of a specific inhibitor of the histone methyltransferase SU(VAR)3-9. *Nat Chem Biol* 2005, *1*, 143-145.

[186] Kubicek, S.; O'Sullivan, R.J. *et al*. Reversal of H3K9me2 by a small-molecule inhibitor for the G9a histone methyltransferase. *Mol Cell* 2007, *25*, 473-481.

[187] Chang, Y.; Zhang, X. *et al*. Structural basis for G9a-like protein lysine methyltransferase inhibition by BIX-01294. *Nat Struct Mol Biol* 2009, *16*, 312-317.

[188] Liu, F.; Chen, X. *et al*. Discovery of a 2,4-diamino- 7-aminoalkoxyquinazoline as a potent and selective inhibitor of histone lysine methyltransferase G9a. *J Med Chem* 2009, *52*, 7950- 7953.

[189] Liu, F.; Chen, X. *et al*. Protein lysine methyltransferase G9a inhibitors: Design, synthesis, and structure activity relationships of 2,4-diamino-7-aminoalkoxy-quinazolines. *J Med Chem* 2010, *53*, 5844-5857.

[190] Vedadi, M.; Barsyte-Lovejoy, D. *et al*. A chemical probe selectively inhibits G9a and GLP methyltransferase activity in cells. *Nat Chem Biol* 2011, *7*, 566-574.

[191] Chang, Y.; Ganesh, T. *et al*. Adding a lysine mimic in the design of potent inhibitors of histone lysine methyltransferases. *J Mol Biol* 2010, *400*, 1-7.

[192] Daigle, S. R.; Olhava, E. J. *et al*. Selective killing of mixed lineage leukemia cells by a potent small-molecule DOT1L inhibitor. *Cancer Cell* 2011, *20*, 53−65.

[193] Miranda, T.B. *et al*. DZNep is a global histone methylation inhibitor that reactivates developmental genes not silenced by DNA methylation. *Mol. Cancer Ther.* 2009, *8*, 1579–1588.

[194] Tan, J.; Yang, X.J.; Zhuang, L. *et al*. Pharmacologic disruption of polycomb-repressive complex 2-mediated gene repression selectively induces apoptosis in cancer cells. *Genes Dev* 2007, *21*, 1050–1063.

[195] Sun, F.; Chan, E. *et al*. Combinatorial pharmacologic approaches target EZH2-mediated gene repression in breast cancer cells. *Mol Cancer Ther* 2009, *8*, 3191–3202.

[196] Couture, J.F.; Hauk, G. *et al*. Catalytic roles for carbon-oxygen hydrogen bonding in SET domain lysine methyltransferases. *J Biol Chem* 2006, *281*, 19280–7.

[197] Knutson, S.K.; Wigle, T.J.; Warholic, N.M. *et al*. A selective inhibitor of EZH2 blocks H3K27 methylation and kills mutant lymphoma cells. *Nat Chem Biol* 2012, *8*, 890–896.

[198] Qi, W.; Chan, H.; *et al*. Selective inhibition of Ezh2 by a small molecule inhibitor blocks tumor cells proliferation. *Proc Natl Acad Sci* U S A 2012, *109*, 21360–21365.

[199] McCabe, M.T.; Ott, H.M. *et al*. EZH2 inhibition as a therapeutic strategy for lymphoma with EZH2-activating mutations. *Nature* 2012, *492*, 108–112.

[200] Konze, K.D.; Ma, A. *et al*. An orally bioavailable chemical probe of the lysine methyltransferases EZH2 and EZH1. *ACS Chem Biol* 2013, *8*, 1324–34.

[201] Knutson, S.K.; Warholic, N.M.; Wigle, T.J. *et al*. Durable tumor regression in genetically altered malignant rhabdoid tumors by inhibition of methyltransferase EZH2. *Proc. Nat. Acad. Sci. USA* 2013, *110*, 7922-7927.

[202] Cheng, D.; Yadav, N.; King, R.W.; Swanson, M.S.; Weinstein, E.J.; Bedford, M.T. Small molecule regulators of protein arginine methyltransferases. *J. Biol. Chem*. 2004, *279*, 23892-23899.

[203] Ragno, R.; Simeoni, S.; Castellano, S.; Vicidomini, C.;Mai, A.; Caroli, A.;Tramontano, A. *et al*. Small molecule inhibitors of histone arginine methyltransferases: homology modeling, molecular docking, binding mode analysis, and biological evaluations. *J. Med. Chem*. 2007, *50,* 1241-1253.

[204] Castellano, S.; Milite, C.; Ragno, R. *et al*. Design, synthesis and biological evaluation of carboxy analogues of arginine methyltransferase inhibitor 1 (AMI-1). *ChemMedChem* 2010, *5,* 398e414.

[205] Mai, A.; Cheng, D.; Bedford, M.T.; Valente, S. *et al*. Epigenetic multiple ligands: mixed histone/protein methyltransferase, acetyltransferase, and class III deacetylase (sirtuin) inhibitors. *J. Med. Chem*. 2008, *51*, 2279-2290.

[206] Cheng, D.; Valente, S.; Castellano, S.; Sbardella, G. *et al*. Novel 3,5-bis(bromohydroxybenzylidene)piperidin-4-ones as coactivator-associated arginine methyltransferase 1 inhibitors: enzyme selectivity and cellular activity. *J. Med. Chem*. 2011, *54*, 4928-4932.

[207] Wu, S.; Rice, J.C. A new regulator of the cell cycle: the PR-Set7 histone methyltransferase. *Cell Cycle* 2011, *10*, 68-72.

[208] Patnaik, D.; Chin, H.G.; Esteve, P.O. *et al*. Substrate specificity and kinetic mechanism of mammalian G9a histone H3 methyltransferase. *J. Biol. Chem*. 2004, *279*, 53248-53258.

[209] Chen, M.W.; Hua, K.T.; Kao, H.J. *et al*. H3K9 histone methyltransferase G9a promotes lung cancer invasion and metastasis by silencing the cell adhesion molecule Ep-CAM. *Cancer Res*. 2010, *70*, 7830-7840.

[210] Li, Y.; Reddy, M.A.; Miao, F.; Shanmugam, N. *et al*. Role of the histone H3 lysine 4 methyltransferase, SET7/9, in the regulation of NF-kappaB-dependent inflammatory genes. Relevance to diabetes and inflammation. J. *Biol. Chem.* 2008, *283,* 26771-26781.

[211] Mai, A.; Valente, S.; Cheng, D.; Perrone, A. *et al*. Synthesis and biological validation of novel synthetic histone/protein methyltransferase inhibitors. *ChemMedChem* 2007, *2*, 987-991.

[212] Wan, Y.; Chen, X.M.; Pang, L.L.; Ma, R. *et al*. Synthesis and Fluorescence Properties of α ,α '-Bis(substituted-benzylidene)cycloalkanones Catalyzed by 1-Methyl-3-[2-(sulfooxy)ethyl]-1H-imidazol-3-ium Chloride. *Synthetic Communications* 2010, *40*, 2320-2328.

[213] Xiao, J.; Tan, Y.; Pan, Y.; Liang, G.; Qu, C. *et al*. A new cyclooxygenase-2 inhibitor, (1E,4E)-1,5-bis(2-bromophenyl)penta-1,4-dien-3-one (GL63) suppresses cyclooxygenase-2 gene expression in human lung epithelial cancer cells: coupled mRNA stabilization and posttranscriptional inhibition. *Biological & Pharmaceutical Bulletin* 2010, *33*, 1170-1175.

[214] Grimshaw, J.; Trocha-Grimshaw, J. Electrochemical reactions. XVII. Selective dehalogenation of styrylpyrazoline and styrylpyrazole derivatives**.** Journal of the Chemical Society, Perkin Transactions 1: Organic and Bio-Organic Chemistry (1972-1999) (1974), (12), 1383-8.

[215] Nishioka, K.; Rice, J.C.; Sarma, K.; Erdjument-Bromage, H. *et al*. PRSet7 is anucleosome-specificmethyltransferase thatmodifies lysine20 of histone H4 and is associated with silent chromatin. *Mol. Cell* 2002, *9,* 1201-1213.

[216] Nishioka, K.; Chuikov, S.; Sarma, K. Erdjument-Bromage, H.; Allis, C.D. *et al*. Set9, a novel histone H3 methyltransferase that facilitates transcription by precluding histone tail modifications required for heterochromatin Formation. *Genes Dev*. 2002, *16,* 479-489.

[217] Shi, Y.; Sawada, J. *et al*. Coordinated histone modifications mediated by a CtBP co-repressor complex. *Nature* 2003, *422*, 735–738.

[218] Forneris, F.; Binda, C. *et al*. Histone dimethylation catalysed by LSD1 is a flavin-dependent oxidative process. *FEBS Lett*. 2005, *579*, 2203–2207.

[219] Metzger, E.; Wissmann, M. *et al*. LSD1 demethylates repressive histone marks to promote androgen receptor-dependent transcription. *Nature* 2005, *437*, 436-439.

[220] Karytinos, A.; Forneris, F. *et al*. A novel mammalian flavin-dependent histone demethylase. *J. Biol. Chem*. 2009, *284*, 17775–17782.

[221] Ciccone, D. N.; Su, H. *et al*. KDM1B is a histone H3K4 demethylase required to establish maternal genomic imprints. *Nature* 2009, *461*, 415–418.

[222] Fang, R.; Barbera, A. J. *et al*. Human LSD2/KDM1b/AOF1 regulates gene transcription by modulating intragenic H3K4me2 methylation. *Mol. Cell* 2010, *39*, 222–233.

[223] van Essen, D.; Zhu, Y.; Saccani, S. A feed-forward circuit controlling inducible NF-κBtarget gene activation by promoter histone demethylation. *Mol. Cell*. 2010, *39*, 750-760.

[224] Forneris, F.; Binda, C.; Vanoni, M.A.; Mattevi, A.; Battaglioli, E. Histone demethylation catalysed by LSD1 is a flavin-dependent oxidative process. *FEBS Lett*. 2005, *579*, 2203–2207.

[225] Forneris, F.; Binda, C.; Vanoni, M.A.; Battaglioli, E.; Mattevi, A. Human histone demethylase LSD1 reads the histone code. *J. Biol. Chem*. 2005, *280,* 41360–41365.

[226] Chen, Y.; Yang, Y. *et al*. Crystal structure of human histone lysine-specific demethylase 1 (LSD1). *Proc. Natl. Acad. Sci. U. S. A.* 2006, *103*, 13956–13961.

[227] Chen, Y.; Yang, Y.; Wang, F.; Wan, K. *et al*. Crystal structure of human histone lysine-specific demethylase 1 (LSD1). *Proc. Natl. Acad. Sci.* 2006,*103*,13956-13961.

[228] Binda, C.; Angelini, R.; Federico, R. *et al*. Structural bases for inhibitor binding and catalysis in polyamine oxidase. *Biochemistry* 2001, *40*, 2766-2776.

[229] Shi, Y.; Lan, F.; Matson, C. *et al*. Histone demethylation mediated by the nuclear amine oxidase homolog LSD1. *Cell* 2004, *119*, 941-953.

[230] Binda, C.; Coda, A.; Angelini, R.,; Federico, R.; Ascenzi, P., Mattevi, A. A 30 Å long U-shaped catalytic tunnel in the crystal structure of polyamine oxidase. *Structure* 1999, *7*, 265-276.

[231] Huang, J.; Sengupta, R. *et al*. p53 is regulated by the lysine demethylase LSD1. *Nature* 2007, *449*, 105–108.

[232] Wang, J.; Hevi, S. *et al*. The lysine demethylase LSD1 (KDM1) is required for maintenance of global DNA methylation. *Nat. Genet*. 2009, *41*, 125–129.

[233] Kontaki, H.; Talianidis, I. Lysine methylation regulates E2F1- induced cell death. *Mol. Cell* 2010, *39*, 152–160.

[234] Yang, J.; Huang, J. *et al*. Reversible methylation of promoter bound STAT3 by histone-modifying enzymes. *Proc. Natl. Acad. Sci. U.S.A*. 2010, *107*, 21499–21504.

[235] Cho, H. S.; Suzuki, T. *et al*. Demethylation of RB regulator MYPT1 by histone demethylase LSD1 promotes cell cycle progression in cancer cells. *Cancer Res*. 2011, *71*, 655–660.

[236] Schulte, J. H.; Lim, S. *et al*. Lysine-specific demethylase 1 is strongly expressed in poorly differentiated neuroblastoma: implications for therapy. *Cancer Res*. 2009, *69*, 2065–2071.

[237] Yokoyama, A.; Takezawa, S. *et al*. Transrepressive function of TLX requires the histone demethylase LSD1. *Mol. Cell. Biol*. 2008, *28*, 3995–4003.

[238] Metzger, E.; Wissmann, M. *et al*. LSD1 demethylates repressive histone marks to promote androgen-receptor-dependent transcription. *Nature* 2005, *437*, 436–439.

[239] Wissmann, M.; Yin, N. *et al*. Cooperative demethylation by JMJD2C and LSD1 promotes androgen receptor-dependent gene expression. *Nat. Cell Biol*. 2007, *9*, 347–353.

[240] Lim, S.; Janzer, A. *et al*. Lysine-specific demethylase 1 (LSD1) is highly expressed in ER-negative breast cancers and a biomarker predicting aggressive biology. *Carcinogenesis* 2010, *31*, 512–520.

[241] Wang, Y.; Zhang, H. *et al*. LSD1 is a subunit of the NuRD complex and targets the metastasis programs in breast cancer. *Cell* 2009, *138*, 660–672.

[242] Hayami, S.; Kelly, J. D. *et al*. Overexpression of LSD1 contributes to human carcinogenesis through chromatin regulation in various cancers. *Int. J. Cancer*. 2011, *128*, 574–586.

[243] Qin, Y.; Zhu, W.; Xu, W. *et al*. LSD1 sustains pancreatic cancer growth via maintaining HIF1α-dependent glycolytic process. Cancer Lett. 2014, doi: 10.1016/j.canlet.2014.02.013

[244] Liang, Y.; Vogel, J. L.; *et al*. Inhibition of the histone demethylase LSD1 blocks α-herpesvirus lytic replication and reactivation from latency. *Nat. Med*. 2009, *15*, 1312–1317.

[245] Narayanan, A.; Ruyechan, W. T.; Kristie, T. M. The coactivator host cell factor-1 mediates Set1 and MLL1 H3K4 trimethylation at herpesvirus immediate early promoters for initiation of infection. *Proc. Natl. Acad. Sci. U.S.A*. 2007, *104*, 10835–10840.

[246] Shi, Y.; Sawada, J.; Sui, G. *et al.* Coordinated histone modifications mediated by a CtBP co-repressor complex. *Nature* 2003, *422*, 735–738.

[247] Saleque, S.; Kim, J.; Rooke, H. M. Orkin, S. H. Epigenetic regulation of hematopoietic differentiation by Gfi-1 and Gfi-1b is mediated by the cofactors CoREST and LSD1. *Mol Cell* 2007, *27*, 562-572.

[248] Su, S. T.; Ying, H. Y.; Chiu, Y. K. *et al*. Involvement of histone demethylase LSD1 in Blimp-1-mediated gene repression during plasma cell differentiation. *Mol Cell Biol* 2009, *29*, 1421-1431.

[249] Thillainadesan, G.; Isovic, M.; *et al*. Genome analysis identifies the p15INK4B tumor suppressor as a direct tarhet of the ZNF217/CoREST complex. *Mol. Cell. Biol.* 2008, *28*, 6066-6077.

[250] Metzger, E.; Wissmann, M.; Yin, N. *et al*. LSD1 demethylates repressive histone marks to promote androgen-receptor-dependent transcription. *Nature* 2005, *437*, 436–439.

[251] Perillo, B.; Ombra, M.N.; Bertoni, A. *et al*. DNA oxidation as triggered by H3K9me2 demethylation drives estrogen-induced gene expression. *Science* 2008, *319*, 202–206.

[252] Wissmann, M.; Yin, N. *et* al. Cooperative dimethylation by JMJD2C and LSD1 promotes androgen receptor-dependent gene expression. *Nat. Cell Biol.* 2007, *9*, 347–353.

[253] Garcia-Bassets, I.; Kwon, Y. S. *et al*. Histone methylation-dependent mechanisms impose ligand dependency for gene activation by nuclear receptors. *Cell* 2007, *128*, 505-518.

[254] Amente, S.; Lania, L.; Majello, B. The histone LSD1 demethylase in stemness and cancer transcription programs. *Biochimica et Biophysica Acta* 2013, *1829*, 981-986.

[255] Amente, S.; Lania, L.; Avvedimento, E.V.; Majello, B. DNA oxidation drives Myc mediated transcription. *Cell Cycle* 2010, *9*, 3002–3004.

[256] Amente, S.; Bertoni, A. *et al*. LSD1-mediated demethlation of histone H3 lysine 4 triggers Myc-induced transcription. *Oncogene* 2010, *29*, 3691-3702.

[257] Nakamura, T.; Mori, T. *et al*. ALL-1 is a histone methyltransferase that assembles a supercomplex of proteins involved in transcriptional regulation. *Mol. Cell* 2002, *10*, 1119–1128.

[258] Huang, J.; Sengupta, R. *et al*. p53 is regulated by the lysine demethylase LSD1. *Nature* 2007, *449*, 105–108.

[259] Scoumanne, A.; Chen, X. The lysine-specific demethylase 1 is required for cell proliferation in both p53-dependent and -independent manners. *J. Biol. Chem.* 2007, *282*, 15471–15475.

[260] Kontaki, H.; Talianidis, I. Cross-talk between post-translationalmodifications regulate life or death decisions by E2F1. *Cell Cycle* 2010, *9*, 3836–3837.

[261] Cho, H.S.; Suzuki, T. *et al*. Demethylation of RB regulator MYPT1 by histone demethylase LSD1 promotes cell cycle progression in cancer cells. *Cancer Res.* 2011, *71*, 655–660.

[262] Wang, J.; Hevi, S.; Kurash, J.K. *at* al. The lysine demethylase LSD1 (KDM1) is required for maintenance of global DNA methylation. *Nat. Genet.* 2009, *41*, 125–129.

[263] Huang, Y.; Stewart, T.M. *et al*. Novel oligoamine analogues inhibit lysine-specific demethylase 1 and induce reexpression of epigenetically silenced genes. *Clin. Cancer Res.*2009, *15*, 7217-7228

[264] Musri, M.M.; Carmona, C.; Hanzu, F.A. *et al*. Histone demethylase LSD1 regulates adipogenesis. *J. Biol. Chem.* 2010, *285*, 30034–30041.

[265] Choi, J.; Jang, H. *et al*. Histone demethylase LSD1 is required to induce skeletal muscle differentiation by regulating myogenic factors. *Biochem. Biophys. Res. Commun.* 2010, *401*, 327–332.

[266] McDonald, O.G.; Wu, H.; Timp, W. *et al*. Genome-scale epigenetic reprogramming during epithelial-to-mesenchymal transition. *Nat. Struct. Mol. Biol.* 2011, *18*, 867–874.

[267] Lin, T.; Ponn, A.; Hu, X. *et al*. Requirement of the histone demethylase LSD1 in Snail1-mediated transcriptional repression during epithelial–mesenchymal transition. *Oncogene* 2010, *29,* 896–4904.

[268] Baron, R.; Binda, C.; Tortorici, M.; McCammon, J. A.; Mattevi, A. Molecular mimicry and ligand recognition in binding and catalysis by the histone demethylase LSD1-CoREST complex. *Structure* 2011, *19*, 212-220.

[269] Whyte, W.A.; Bilodeau, S.; Orlando, D.A. *et al*. Enhancer decommissioning by LSD1 during embryonic stem cell differentiation. *Nature* 2012, *482*, 221–225.

[270] Lim, S.; Janzer, A.; Becker, A. *et al*. Lysine specific demethylase 1 (LSD) is highly expressed in ER-negative breast cancers and a biomarker predicting aggressive biology. *Carcinogenesis* 2011, *31*, 512-520.

[271] Schulte, J.H.; Lim, S.; Schramm, S. *et al*. Lysine specific demethylase 1 is strongly expressed in poorly differentiated neuroblastoma: implication for therapy. *Cancer Res.* 2009, *69*, 2065-2071.

[272] Pajtler, K.W.; Weingarten, C.; Thor, T. *et al*. The KDM1A histone demethylase is a promising new target for the epigenetic therapy of medulloblastoma. *Acta Neuropathologica Communications* 2013, *1*, 19.

[273] Lokken, A.A.; Zeleznik-Le, N.J. Breaking the LSD1/KDM1A addiction: therapeutic targeting of the epigenetic modifier in AML. *Cancer Cell* 2012, *21,* 451–453.

[274] Harris, W.J.; Huang, X. *et al*. The histone demethylase KDM1A sustains the oncogenic potential of MLL-AF9 leukemia stem cells. *Cancer Cell* 2012, *21,* 473–487.

[275] Yatim, A.; Benne, C.; Sobhian, B. *et al*. NOTCH1 nuclear interactome reveals key regulators of its transcriptional activity and oncogenic function. *Mol. Cell* 2012, *48*, 445–458.

[276] Zhou, J.; Schmid, T.; S. Schnitzer, B. Brune, Tumor hypoxia and cancer progression. *Cancer Lett.* 2006, *237*, 10–21.

[277] Gort, E.H.; Groot, A.J. *et al*. Hypoxic regulation of metastasis via hypoxia-inducible factors. *Curr. Mol. Med.* 2008, *8*, 60–67.

[278] Schmidt, D. M.; McCafferty, D. G. trans-2-Phenylcyclopropylamine is a mechanism-based inactivator of the histone demethylase LSD1. *Biochemistry* 2007, *46*, 4408–4416.

[279] Humphrey, G. W.; Wang, Y.; Russanova, V. R *et al*. Stable histone deacetylase complexes distinguished by the presence of SANT domain proteins CoREST/kiaa0071 and Mta-L1. *J. Biol. Chem.* 2001, *276*, 6817–6824.

[280] Lee, M.G.; Wynder, C.; Schmidt, D.M. *et al*. Histone H3 lysine 4 demethylation is a target of non selective antidepressive medications. *Chem. Biol.* 2006, *13*, 563-567.

[281] Culhane, J. C.; Wang, D.; Yen, P. M.; Cole, P. A. Comparative analysis of small molecules and histone substrate analogues as LSD1 lysine demethylase inhibitors. *J. Am. Chem. Soc*. 2010, *132*, 3164–3176

[282] Schmidt, D. M.; McCafferty, D. G. trans-2-Phenylcyclopropylamine is a mechanism-based inactivator of the histone demethylase LSD1. *Biochemistry* 2007, *46*, 4408–4416.

[283] Yang, M.; Culhane, J. C.; Szewczuk, L. M. *et al*. Structural basis for the inhibition of the LSD1 histone demethylase by the antidepressant trans-2-phenylcyclopropylamine. *Biochemistry* 2007, *46*, 8058–8065.

[284] Mimasu, S.; Sengoku, T.; Fukuzawa, S.; Umehara, T.; Yokoyama, S. Crystal structure of histone demethylase LSD1 and tranylcypromine at 2.25 Å. *Biochem. Biophys. Res. Commun*. 2008, *366*, 15–22.

[285] Binda, C.; Valente, S.; Romanenghi, M. *et al*. Biochemical, structural, and biological evaluation of tranylcypromine derivatives as inhibitors of histone demethylases LSD1 and LSD2. *J. Am. Chem. Soc*. 2010, *132*, 6827–6833.

[286] Schulte, J. H.; Lim, S. *et al*. Lysine-specific demethylase 1 is strongly expressed in poorly differentiated neuroblastoma: implications for therapy. *Cancer Res*. 2009, *69*, 2065–2071.

[287] Gooden, D. M.; Schmidt, D. M.; Pollock, J. A. *et al*. Facile synthesis of substituted trans-2-arylcyclopropylamine inhibitors of the human histone demethylase LSD1 and monoamine oxidases A and B. *Bioorg. Med. Chem. Lett.* 2008, *18*, 3047–3051.

[288] Benelkebir, H.; Hodgkinson, C. *et al*. . Enantioselective synthesis of tranylcypromine analogues as lysine demethylase (LSD1) inhibitors. *Bioorg. Med. Chem*. 2011, *19*, 3709–3716.

[289] Ueda, R.; Suzuki, T.; Mino, K. e*t al*. Identification of cellactive lysine specific demethylase 1-selective inhibitors. *J. Am. Chem. Soc*. 2009, *131*, 17536–17537.

[290] Binda, C.; Valente, S.; Romanenghi, M. *et al*. . Biochemical, structural, and biological evaluation of tranylcypromine derivatives as inhibitors of histone demethylases LSD1 and LSD2. *J. Am. Chem. Soc*. 2010, *132*, 6827–6833

[291] Ortega, M. A.; Castro-Palomino, L. J.; Fyfe, M. C. T. Paten Appl. WO 2011035941, 2011.

[292] Culhane, J.C.; Szewczuk,L.M. *et al*. A mechanism-based inactivator for histone demethylase LSD1. *J Am Chem Soc* 2006, *128*, 4536-4537.

[293] Culhane, J.C.; Wang, D.; Yen, P.M.; Cole, P.A. Comparative analysis of small molecole and histone substrate analogues as LSD1 lysine demethylase inhibitors. *J Am Chem Soc* 2010, *132*, 3164-3176.

[294] Takeuchi, T.; Yamazaki, Y.; Katoh-Fukui, Y.; Tsuchiya, R.; Kondo, S.; Motoyama, J.; Higashinakagawa, T. Gene trap capture of a novel mouse gene, jumonji, required for neural tube formation. *Genes Dev*. 1995, *9*, 1211-1222.

[295] J. J. Hutton, Jr., A. Kaplan and S. Udenfriend, *Arch. Biochem. Biophys*. 1967, *121*, 384.

[296] Rose, N.R.; McDonough, M.A., *et al*. Inhibition of 2-oxoglutarate dependent oxygenases. *Chem. Soc. Rev*. 2010, DOI: 10.1039/c0cs00203h

[297] Ng, S.S.; Kavanagh, K.L.; McDonough, M.A.; Butler, D.; Pilka, E.S.; Lienard, B.M.R.; Bray, J.E.; Savitsky, P.; Gileadi, O.; von Delft, F.; Oppermann, U. Crystal structures of histone demethylase JMJD2A reveal basis for substrate specificity. *Nature* 2007, *448*, 87-91.

[298] Valegard, K, van Scheltinga, A.C.; Lloyd, M.D. *et al. Nature*, 1998, *394*, 805.

[299] Zhang, Z.; Ren, J.; Harlos, K.; McKinnon, C.H.; Clifton I.J; Schofield C.J. *FEBS Lett.*, 2002, *7*, 517.

[300] Chen, Z.; Zang, J.; Whetstine, J. *et al.* Structural insights into histone demethylation by JMJD2 family members. *Cell* 2006, *125*, 691-702.

[301] Couture, J.F.; Collazo, E.; Ortiz-Tello, P. A.; Brunzelle, J. S.; Trievel, R. C. Specificity and mechanism of JMJD2A, a trimethyllysine-specific histone demethylase. *Nature Struct. Mol. Biol.* 2007, *14*, 689-695.

[302] Arrowsmith, C.H.; Bountra, C.; Fish, P.V.; Lee, K.; Schapira, M.. Epigenetic protein families: a new frontier for drug discovery. *Nat. Rev. Drug Discov.* 2012, *11*, 384-400.

[303] Frescas, D.; Guardavaccaro, D.; Bassermann, F.; Koyama-Nasu, R.; Pagano, M. JHDM1B/FBXL10 is a nucleolar protein that represses transcription of ribosomal RNA genes. *Nature* 2007, *450*, 309-313.

[304] Wu, X.; Johansen, J. V.; Helin, K. Fbxl10/Kdm2b recruits Polycomb repressive complex 1 to CpG islands and regulates H2A ubiquitylation. *Mol. Cell* 2013, *49*, 1134-1146.

[305] Farcas, A. M.; Blackledge, N. P.; Sudbery, I.; Long, H. K.; McGouran, J. F.; Rose, N. R.; Klose, R. J. KDM2B links the Polycomb Repressive Complex 1 (PRC1) to recognition of CpG islands. *Elife* 2012, *1*, e00205.

[306] Suzuki, T., Minehata, K. I., Akagi, K., Jenkins, N. A., Copeland, N. G. Tumor suppressor gene identification using retroviral insertional mutagenesis in Blm-deficient mice. *EMBO l* 2006, *25*, 3422-3431

[307] Frescas, D.; Guardavaccaro, D.; Kuchay, S. M.; Kato, H.; Poleshko, A.; Basrur, V.; Pagano, M.. KDM2A represses transcription of centromeric satellite repeats and maintains the heterochromatic state. *Cell Cycle* 2008, *7*, 3539-3547.

[308] Yamane, K.; Toumazou, C.; Tsukada, Y. I.; Erdjument-Bromage, H.; Tempst, P.; Wong, J.; Zhang, Y. JHDM2A, a JmjC-containing H3K9 demethylase, facilitates transcription activation by androgen receptor. *Cell* 2006, *125*, 483-495.

[309] Inagaki, T., Tachibana, M., Magoori, K., Kudo, H., Tanaka, T., Okamura, M., Sakai, J. Obesity and metabolic syndrome in histone demethylase JHDM2a-deficient mice. *Genes to Cells* 2009, *14*, 991-1001.

[310] Liu, Z.; Zhou, S.; Liao, L.; Chen, X.; Meistrich, M.; Xu, J. Jmjd1a demethylase-regulated histone modification is essential for cAMP-response element modulator-regulated gene expression and spermatogenesis. *Journal of Biological Chemistry* 2010, *285*, 2758-2770.

[311] Krieg, A. J.; Rankin, E. B.; Chan, D.; Razorenova, O.; Fernandez, S.; Giaccia, A. J. Regulation of the histone demethylase JMJD1A by hypoxia-inducible factor 1α enhances hypoxic gene expression and tumor growth. *Molecular and cellular biology* 2010, *30*, 344-353.

[312] Park, S. J.; Kim, J. G.; Son, T. G.; Yi, J. M.; Kim, N. D.; Yang, K.; Heo, K. The histone demethylase JMJD1A regulates adrenomedullin-mediated cell proliferation in hepatocellular carcinoma under hypoxia. *Biochemical and biophysical research communications* 2013, *434*, 722-727.

[313] Brauchle, M.; Yao, Z.; Arora, R.; Thigale, S.; Clay, I.; Inverardi, B.; Ruffner, H. Protein complex interactor analysis and differential activity of KDM3 subfamily members towards H3K9 methylation. *PloS one* 2013, *8*, e60549.

[314] Couture, J. F.; Collazo, E.; Ortiz-Tello, P. A.; Brunzelle, J. S.; Trievel, R. C. Specificity and mechanism of JMJD2A, a trimethyllysine-specific histone demethylase. *Nature Struct. Mol. Biol.* 2007, *14*, 689-695.

[315] Cloos, P. A.; Christensen, J.; Agger, K.; Maiolica, A.; Rappsilber, J.; Antal, T.; Helin, K. The putative oncogene *GASC1* demethylates tri- and dimethylated lysine 9 on histone H3. *Nature* 2006, *442*, 307-311.

[316] Wissmann, M.; Yin, N.; Müller, J. M.; Greschik, H.; Fodor, B. D.; Jenuwein, T.; Schüle, R. Cooperative demethylation by JMJD2C and LSD1 promotes androgen receptor-dependent gene expression. *Nature cell biology* 2007, *9*, 347-353.

[317] Liu, G.; Bollig-Fischer, A.; Kreike, B.; van de Vijver, M. J.; Abrams, J.; Ethier, S. P.; Yang, Z. Q. Genomic amplification and oncogenic properties of the GASC1 histone demethylase gene in breast cancer. *Oncogene* 2009, *28*, 4491-4500.

[318] Rui, L.; Emre, N. C.; Kruhlak, M. J.; Chung, H. J.; Steidl, C.; Slack, G.; Staudt, L. M. Cooperative epigenetic modulation by cancer amplicon genes. *Cancer Cell* 2010, *18*, 590-605.

[319] Di Tacchio, L.; Le, H. D.; Vollmers, C.; Hatori, M.; Witcher, M.; Secombe, J.; Panda, S. Histone lysine demethylase JARID1a activates CLOCK-BMAL1 and influences the circadian clock. *Science* 2011, *333*, 1881-1885.

[320] Benevolenskaya, E.V., Murray, H.L., Branton, P., Young, R.A., Kaelin, W.G., Binding of pRB to the PHD protein RBP2 promotes cellular differentiation. *Mol Cell* 2005, *18*, 623-635.

[321] Zeng, J., Ge, Z., Wang, L., Li, Q., Wang, N., Björkholm, M., Xu, D. The histone demethylase RBP2 Is overexpressed in gastric cancer and its inhibition triggers senescence of cancer cells. *Gastroenterology* 2010, *138*, 981-992.

[322] Sharma, S. V.; Lee, D. Y.; Li, B.; Quinlan, M. P.; Takahashi, F.; Maheswaran, S.; Settleman, J. A chromatin-mediated reversible drug-tolerant state in cancer cell subpopulations. *Cell* 2010, *141*, 69-80.

[323] Schmitz, S. U.; Albert, M.; Malatesta, M.; Morey, L.; Johansen, J. V.; Bak, M.; Helin, K. Jarid1b targets genes regulating development and is involved in neural differentiation. *EMBO J.* 2011, *30*, 4586-4600.

[324] Lu, P. J.; Sundquist, K.; Baeckstrom, D.; Poulsom, R.; Hanby, A.; Meier-Ewert, S.; Taylor-Papadimitriou, J. A novel gene (PLU-1) containing highly conserved putative DNA/chromatin binding motifs is specifically up-regulated in breast cancer. *Journal of Biological Chemistry* 1999, *274*, 15633-15645

[325] Hayami, S.; Yoshimatsu, M.; Veerakumarasivam, A.; Unoki, M.; Iwai, Y.; Tsunoda, T.; Hamamoto, R. Overexpression of the JmjC histone demethylase KDM5B in human carcinogenesis: involvement in the proliferation of cancer cells through the E2F/RB pathway. *Mol Cancer* 2010, *9*, 59.

[326] Xiang, Y.; Zhu, Z.; Han, G.; Ye, X.; Xu, B.; Peng, Z.; Chen, C. D. JARID1B is a histone H3 lysine 4 demethylase up-regulated in prostate cancer. *Proceedings of the National Academy of Sciences* 2007, *104*, 19226-19231.

[327] M. Tahiliani, P. Mei, R. Fang, T. Leonor, M. Rutenberg, F. Shimizu, J. Li, A. Rao, Y. Shi, The histone H3K4 demethylase SMCX links REST target genes to X-linked mental retardation. *Nature* 2007, *447*, 601-605.

[328] De Santa, F.; Totaro, M. G.; Prosperini, E.; Notarbartolo, S.; Testa, G.; Natoli, G. The histone H3 lysine-27 demethylase Jmjd3 links inflammation to inhibition of polycomb-mediated gene silencing. *Cell* 2007, *130*, 1083-1094.

[329] Ishii, M. *et al*. Epigenetive regulation of the alternatively activated macrophage phenotype. *Blood* 2009, *114*, 3244-3254.

[330] De Santa, F.; *et al*. JMJD3 contributes to the control of gene expression in LPS activated macrophages. *EMBO J.* 2009, *28*, 3341-3352.

[331] Issaeva, I.; Zonis, Y.; Rozovskaia, T.; Orlovsky, K.; Croce, C. M.; Nakamura, T.; Canaani, E. Knockdown of ALR (MLL2) reveals ALR target genes and leads to alterations in cell adhesion and growth. *Molecular and cellular biology* 2007, *27*, 1889-1903.

[332] van Haaften, G.; Dalgliesh, G. L.; Davies, H.; Chen, L.; Bignell, G.; Greenman, C.; Wong, J. Somatic mutations of the histone H3K27 demethylase gene UTX in human cancer. *Nature genetics* 2009, *41*, 521-523.

[333] Yokoyama, A.; Okuno, Y.; Chikanishi, T.; Hashiba, W.; Sekine, H.; Fujiki, R.; Kato, S. KIAA1718 is a histone demethylase that erases repressive histone methyl marks. *Genes to Cells* 2010, *15*, 867-873.

[334] Lagarou, A.; Mohd-Sarip, A.; Moshkin, Y. M.; Chalkley, G. E.; Bezstarosti, K.; Demmers, J. A.; Verrijzer, C. P. dKDM2 couples histone H2A ubiquitylation to histone H3 demethylation during Polycomb group silencing. *Genes & development* 2008, *22*, 2799-2810.

[335] Kooistra, S. M.; Helin, K. Molecular mechanisms and potential functions of histone demethylases. *Nature reviews Molecular cell biology* 2012, *13*, 297-311.

[336] Huang, C.; Xiang, Y.; Wang, Y.; Li, X.; Xu, L.; Zhu, Z.; Chen, C. D. Dual-specificity histone demethylase KIAA1718 (KDM7A) regulates neural differentiation through FGF4. *Cell research* 2010, *20*, 154-165.

[337] Qi, H. H.; Sarkissian, M.; Hu, G. Q.; Wang, Z.; Bhattacharjee, A.; Gordon, D. B.; Shi, Y. Histone H4K20/H3K9 demethylase PHF8 regulates zebrafish brain and craniofacial development. *Nature* 2010, *466*, 503-507.

[338] Smith, E. H.; Janknecht, R.; Maher, L. J., III. Succinate inhibition of α-ketoglutarate-dependent enzymes in yeast model of paraganglioma. *Hum. Mol. Genet*. 2007, *16*, 3136–3148.

[339] Chen, H.; Kluz, T.; Zhang, R.; Costa, M. Hypoxia and nickel inhibit histone demethylase JMJD1A and repress Spry2 expression in human bronchial epithelial BEAS-2B cells. *Carcinogenesis* 2010, *31*, 2136–2144.

[340] Chowdhury, R.; Yeoh, K. K.; Tian, Y. M.; Hillringhaus, L.; Bagg, E. A.; Rose, N. R.; Leung, I. K.; Li, X. S.; Woon, E. C.; Yang, M.; McDonough, M. A.; King, O. N.; Clifton, I. J.; Klose, R. J.; Claridge, T. D.; Ratcliffe, P. J.; Schofield, C. J.; Kawamura, A. The oncometabolite 2-hydroxyglutarate inhibits histone lysine demethylases. *EMBO Rep*. 2011, *12*, 463–469.

[341] Hamada, S.; Kim, T. D.; Suzuki, T.; Itoh, Y.; Tsumoto, H.; Nakagawa, H.; Janknecht, R.; Miyata, N. Synthesis and activity of Noxalylglycine and its derivatives as Jumonji C-domain-containing histone lysine demethylase inhibitors. *Bioorg. Med. Chem. Lett*. 2009, *19*, 2852–2855.

[342] Ng, S. S.; Kavanagh, K. L.; McDonough, M. A.; Butler, D.; Pilka, E. S.; Lienard, B. M.; Bray, J. E.; Savitsky, P.; Gileadi, O.; von Delft, F.; Rose, N. R.; Offer, J.; Scheinost, J. C.; Borowski, T.; Sundstrom, M.; Schofield, C. J.; Oppermann, U. Crystal structures of histone demethylase JMJD2A reveal basis for substrate specificity. *Nature* 2007, *448*, 87–91

[343] Rose, N. R.; Woon, E. C. Y.; Kingham, G. L.; King, O. N. F.; Mecinovi_c, J.; Clifton, I. J.; Ng, S. S.; Talib-Hardy, J.; Oppermann, U.; McDonough, M. A.; Schofield, C. J. Selective inhibitors of the JMJD2 histone demethylases: combined nondenaturing mass spectrometric screening and crystallographic approaches. *J. Med. Chem*. 2010, *53*, 1810–1818.

[344] Rose, N. R.; Ng, S. S.; Mecinovic, J.; Li_enard, B.M. R.; Bello, S.H.; Sun, Z.; McDonough, M. A.; Oppermann, U.; Schofield, C. J. Inhibitor scaffolds for 2-oxoglutarate-dependent histone lysine demethylases. *J. Med. Chem*. 2008, *51*, 7053–7056.

[345] Thalhammer, A.; Mecinovi_c, J.; Loenarz, C.; Tumber, A.; Rose, N. R.; Heightman, T. D.; Schofield, C. J. Inhibition of the histone demethylase JMJD2E by 3-substituted pyridine 2,4-dicarboxylates. *Org. Biomol. Chem*. 2011, *9*, 27–35.

[346] King, O. N.; Li, X. S.; Sakurai, M.; Kawamura, A.; Rose, N. R.; Ng, S. S.; Quinn, A. M.; Rai, G.; Mott, B. T.; Beswick, P.; Klose, R. J.; Oppermann, U.; Jadhav, A.; Heightman, T. D.; Maloney, D. J.; Schofield, C. J.; Simeonov, A. Quantitative high-throughput screening identifies 8-hydroxyquinolines as cell-active histone demethylase inhibitors. *PLoS One* 2010, *5*, No. e15535.

[347] Chang,K.H.;King,O.N.;Tumber,A.;Woon, E.C.;Heightman, T.D.;McDonough,M. A.; Schofield, C. J.; Rose,N. R. Inhibition of histone demethylases by 4-carboxy-2,20-bipyridyl compounds. *ChemMedChem* 2011, *6*, 759–764.

[348] Hamada, S.; Suzuki, T.; Mino, K.; Koseki, K.; Oehme, F.; Flamme, I.; Ozasa, H.; Itoh, Y.; Ogasawara, D.; Komaarashi, H.; Kato, A.; Tsumoto, H.; Nakagawa, H.; Hasegawa, M.; Sasaki, R.; Mizukami, T.; Miyata, N. Design, synthesis, enzyme-inhibitory activity, and effect on human cancer cells of a novel series of jumonji domain-containing protein 2 histone demethylase inhibitors. *J. Med. Chem.* 2010, *53*, 5629–5638.

[349] H.; Podoll, J.; Heightman, T. D.; Oppermann, U.; Schreiber, S. L.; Wang, X. A selective inhibitor and probe of the cellular functions of Jumonji C domain-containing histone demethylases. *J. Am. Chem. Soc*. 2011, *133*, 9451–9456.

[350] Sekirnik, R.; Rose, N. R.; Thalhammer, A.; Seden, P. T.; Mecinovi_c, J.; Schofield, C. J. Inhibition of the histone lysine demethylase JMJD2A by ejection of structural Zn(II). *Chem. Commun*. 2009, 6376–6378.

[351] Hamada, S.; Suzuki, T.; Mino, K.; Koseki, K.; Oehme, F.; Flamme, I.; Ozasa, H.; Itoh, Y.; Ogasawara, D.; Komaarashi, H.; Kato, A.; Tsumoto, H. Nakagawa, M. Hasegawa, R. Sasaki, T. Mizukami, N. Miyata, H. Design, synthesis, enzyme-inhibitory activity, and effect on human cancer cells of a novel series of jumonji domain-containing protein 2 histone demethylase inhibitors. *J. Med. Chem*. 2010, *53*, 5629-5638.

[352] Sams-Dodd, F. Target-based drug discovery: is something wrong? *Drug Discov. Today* 2005, *10*, 139-147.

[353] Keith, C. T.; Borisy, A. A.; Stockwell, B. R. Multicomponent therapeutics for networked systems. *Nat. Rev. Drug Discov.* 2005, *4*, 461-467.

[354] Kamb, A.; Wee, S.; Lengauer, C. Why is cancer drug discovery so difficult? *Nat. Rev. Drug Discov.* 2007, *6*, 115-120.

[355] Daub, H.; Specht, K.; Ullrich, A. Strategies to overcome resistance to targeted protein kinase inhibitors. *Nat. Rev. Drug Discov*. 2004, *3*, 1001-1010.

[356] Rather, M. A.; Bhat, B. A.; Qurishi, M. A. Multicomponent phytotherapeutic approach gaining momentum: is the "one drug to fit all" model breaking down? *Phytomedicine* 2013, http://dx.doi.org/10.1016/j.phymed.2013.07.015

[357] Morphy, R.; Rankovic, Z. Designed Multiple Ligands. An Emerging Drug Discovery Paradigm. *J. Med. Chem.* 2005, *48*, 6523-6543.

[358] Zimmerman, G. R.; Lehar, J.; Keith, C. T. Multi-target therapeutics: when the whole is greater than the sum of the parts. *Drug Discov. Today* 2007, *12*, 34-42.

[359] Fortin, S.; Berube, G. Advances in the development of hybrid anticancer drugs. *Expert Opin. Drug Discov.* 2013, *8*, 1029-1047.

[360] Mai, A.; Cheng, D.; Bedford, M. T.; Valente, S.; Nebbioso, A.; Perrone, A.; Brosch, G.; Sbardella, G.; De Bellis, F.; Miceli, M.; Altucci, L. Epigenetic multiple ligands: mixed histone/protein methyltransferase, acetyltransferase, and class III deacetylase (sirtuin) inhibitors. *J. Med. Chem.* 2008, *51*, 2279-2290.

[361] Upadhyay, K.; Rotili, D.; Han, J. W.; Hu, R.; Chang, Y.; Labella, D.; Zhang, X.; Yoon, Y. S.; Mai, A.; Cheng, X. An analog of BIX-01294 selectively inhibits a family of histone H3 lysine 9 Jumonji demethylases. *J. Mol. Biol.* 2012, *416*, 319-327

[362] Rotili, D.; Altun, M.; Kawamura, A.; Wolf, A.; Fischer, R.; Leung, I. K.; Mackeen, M. M.; Tian, Y. M.; Ratcliffe, P. J.; Mai, A.; Kessler, B. M.; Schofield, C. J. A photoreactive small-molecule probe for 2-oxoglutarate oxygenases. *Chem. Biol.* 2011, *18*, 642-654.

[363] Binda, C.; Valente, S.; Romanenghi, M.; Pilotto, S.; Cirilli, R.; Karytinos, A.; Ciossani, G.; Botrugno, O. A.; Forneris, F.; Tardugno, M.; Edmondson, D. E.; Minucci, S.; Mattevi, A.; Mai, A. Biochemical, structural, and biological evaluation of tranylcypromine derivatives as inhibitors of histone demethylases LSD1 and LSD2. *J. Am. Chem. Soc*. 2010, *132*, 6827-6833.

[364] Rose, N. R.; Ng, S. S.; Mecinovic, J.; Lienard, B. M. R.; Bello, S. H.; Sun, Z.; McDonough, M. A.; Opperman, U.; Schofield, C. J. Inhibitor scaffolds for 2-oxoglutarate-dependent histone lysine demethylases. *J. Med. Chem.* 2008, *51*, 7053-7056.

[365] Hopkinson, R. J.; Tumber, A.; Yapp, C.; Chowdhury, R.; Aik, W.; Che, K. H.; Li, X. S.; Kristensen, J. B. L.; King,, O. N. F.; Chan, M. C.; Yeoh, K. K.; Choi, H.; Walport, L. J.; Thinnes, C. C.; Bush, J. T.; Lejeune, C.; Rydzik, A. M.; Rose, N. R.; Bagg, E. A.; McDonough, M. A.; Krojer, T. J.; Yue, W. W.; Ng, S. S.; Olsen, L.; Butler, E. S.; Opperman, U.; Muller, S.; Klose, R. J.; Ratcliffe, P. J.; Schofield, C. J.; Kawamura, A. 5-Carboxy-8-hydroxyquinoline is a broad spectrum 2-oxoglutarate oxygenase inhibitor which causes iron translocation. *Chem. Sci.* 2013, *4*, 3110-3117.

[366] Ng, S. S.; Kavanagh, K. L.; McDonough, M. A.; Butler, D.; Pilka, E. S.; Lienard, B. M.; Bray, J. E.; Savitsky, P.; Gileadi, C.; Von Delft, F.; Rose, N. R.; Offer, J.; Scheinost, J. C.; Borowski, T.; Sundstrom, M.; Schofield, C. J.; Oppermann, U. Crystal structures of histone demethylase JMJD2A reveal basis for substrate specificity. *Nature*, 2007, *448*, 87-91.

[367] Chang, K. H.; King, O. N.; Tumber, A.; Woon, E. C.; Heightman, T. D.; McDonough, M. A.; Schofield, C. J.; Rose, N. R. Inhibition of histone demethylases by 4-carboxy-2,2'-bipyridyl compounds. *ChemMedChem* 2011, *6*, 759-764.

[368] Gros, L.; Lorente, S. O.; Jimenez, C. J.; Yardley, V.; Rattray, L.; Wharton, H.; Little, S.; Croft, S. L.; Ruiz-Perez, L. M.; Gonzalez-Pacanowska, D.; Gilbert, I. H. Evaluation of azasterols as antiparasitics. *J. Med. Chem.* 2006, *49*, 6094-6103

[369] Rose, N. R.; McDonough, M. A.; King, O. N.; Kawamura, A.; Schofield, C. J. Inhibition of 2- oxoglutarate dependent oxygenases. *Chem. Soc. Rev.* 2011, *40*, 4364-4397.

[370] Harris, W. J.; Huang, X.; Lynch, J. T.; Spencer, G. J.; Hitchin, J. R.; Li, Y.; Ciceri, F.; Blaser, J. G.; Greystoke, B. F.; Jordan, A. M.; Miller, C. J.; Ogilvie, D. J.; Somervaille, T. C. The histone demethylase KDM1A sustains the oncogenic potential of MLL-AF9 leukemia stem cells. *Cancer Cell* 2012, *21*, 473-487.

[371] Schenk, T.; Chen, W. C.; Gollner, S.; Howell, L.; Jin, L.; Hebestreit, K.; Klein, H. U.; Popescu, A. C.; Burnett, A.; Mills, K.; Casero, R. A. Jr.; Marton, L.; Woster, P.; Minden, M. D.; Dugas, M.; Wang, J. C.; Dick, J. E.; Muller-Tidow, C.; Petrie, K.; Zelent, A. Inhibition of the LSD1 (KDM1A) demethylase reactivates the all-trans-retinoic acid differentiation pathway in acute myeloid leukemia. *Nat. Med.* 2012, *18*, 605-611.

[372] Miceli, M.; Franci, G.; Dell'Aversana, C.; Ricciardiello, F.; Petraglia, F.; Carissimo, A.; Perone, L.; Maruotti, G. M.; Savarese, M.; Martinelli, P.; Cancemi, M.; Altucci, L. MePR: a novel human mesenchymal progenitor model with characteristics of pluripotency. *Stem Cells Dev.* 2013, *22*, 2368-2383.

[373] Kalgutkar, A. S.; Dalvie, D. K. Drug discovery for a new generation of covalent drugs. *Expert Opin. Drug Discov.* 2012, *7*, 561-581.

[374] Marks, P. A.; Breslow, R. Dimethyl sulfoxide to vorinostat: development of this histone deacetylase inhibitor as an anticancer drug. *Nat Biotechnol.* 2007, *25*, 84-90.

[375] Rose, N. R.; Woon, E. C.; Tumber, A.; Walport, L. J.; Chowdhury, R.; Li, X. S.; King, O. N.; Lejeune, C.; Ng, S. S.; Krojer, T.; Chan, M. C.; Rydzik, A. M.; Hopkinson, R. J.; Che, K. H.; Daniel, M.; Strain-Damerell, C.; Gileadi, C.; Kochan, G.; Leung, I. K.; Dunford, J.; Yeoh, K. K.; Ratcliffe, P. J.; Burgess-Brown, N.; von Delft, F.; Muller, S.; Marsden, B.; Brennan, P. E.; McDonough, M. A.; Oppermann, U.; Klose, R. J.; Schofield, C. J.; Kawamura, A. *J. Med. Chem.* 2012, *55*, 6639-6643.